

**Chiral Phosphoric Acid-Catalyzed Stereoselective
Transformations of Vinyl Ethers and Acetals**

by

Grace A. Winschel

**A dissertation submitted in partial fulfillment
of the requirements for the degree of
Doctor of Philosophy
(Chemistry)
in the University of Michigan
2015**

Doctoral Committee:

**Assistant Professor Pavel Nagorny, Chair
Professor John Montgomery
Professor Matthew B. Soellner
Professor John P. Wolfe**

Dedication

For PT, who made every day better.

Acknowledgements

First and foremost thanks are due to my advisor, Dr. Pavel Nagorny. I knew when I began graduate school that I wanted to work for someone who would work me hard and teach me a lot. I knew Pavel was just that person during our first meeting together, and I am grateful for him allowing me to work in his lab for a double rotation and then continue on to finish my Ph.D. Pavel taught me how to run a TLC, how to purify things on column, how to handle azides and how to work with *t*-BuLi all within my first rotation. I have been learning from him ever since.

I am also deeply indebted to Dr. Paul Zimmerman, who agreed to let me work with him on computational analyses of my reactions despite starting with a very limited computational background. He introduced me to both computational chemistry and his graduate students, both of which now have a soft spot in my heart.

I'd also like to thank my committee members Dr. John Wolfe, Dr. John Montgomery and Dr. Matt Soellner for their guidance, as well the members of the Nagorny group. You have helped shape my graduate career in such positive ways.

To my family, I know growing up I said I wanted to be an entomologist or perform in the circus, but chemistry is a close third. Thank you for encouraging me to go into science rather than the circus (though I know you'd be proud of me either way). Thank you for telling me to focus and keep writing when I got off track. And thank you for allowing me to miss out on a significant amount of family time so that I could focus on completing my Ph.D.

To my friends, thank you for never talking to me about chemistry. To those near, thank you for driving with me down to Kentucky to climb rocks, for flying with me to Vegas to jump out of planes, for coming with me to hang from ceilings and to slack line out in the Diag. When I started graduate school I didn't have any hobbies. Now I have too many and it's thanks to you. To those far, though there's not much time to visit with old friends during grad school, we'll always have the Internet. Thank you for being a constant source of positivity and encouragement.

Table of Contents

Dedication	ii
Acknowledgements	iii
List of Figures	vi
List of Schemes	viii
List of Tables	xi
List of Abbreviations	xii
Chapter 1: Introduction: Chiral Phosphoric Acids and Spiroketal	1
1.1 Introduction to Asymmetric Organocatalysis	1
1.2 Asymmetric Organocatalysis through Hydrogen Bonding	3
1.3 Chiral Phosphoric Acid Catalysts	5
1.4 Utilization of CPAs to Promote Asymmetric Acetylation Reactions	7
1.5 Introduction to Spiroketal	8
1.6 The Anomeric Effect	11
1.7 Synthesis of Spiroketal	12
1.8 Summary	18
1.9 References	19
Chapter 2: Development of Stereoselective Chiral Phosphoric Acid-Catalyzed Spiroketalization Reactions	23
2.1 Introduction	23
2.2 Optimization the Chiral Phosphoric Acid-Catalyzed Enantioselective Spiroketalization Reaction	23
2.3 Substrate Scope of the Enantioselective Spiroketalization Reaction	26
2.4 Development of a Diastereoselective Approach to Kinetic Spiroketal	31
2.5 Conclusions	34
2.6 Experimental	35

2.7 References	48
----------------	----

Chapter 3: Computational and Experimental Investigations of the Stereoselective Spiroketalization Reaction Mechanism	49
3.1 Introduction	49
3.2 Synthesis of Hammett Study Substrates	61
3.3 Hammett Study	62
3.4 Synthesis of Deuterium Labeled Substrates	66
3.5 Deuterium Labeling Study	70
3.6 Computational Analysis of the Spiroketalization Mechanism	72
3.7 Conclusions	80
3.8 Experimental	81
3.9 References	99

Chapter 4: Computing the Mechanism and Source of Enantioselectivity in the Synthesis of Chiral Piperidines through the Formation of Chiral Mixed Phosphoric Acid Acetals	103
4.1 Introduction	103
4.2 Optimization of CPA-Catalyzed Stereoselective Aza-Michael Reaction	108
4.3 Reaction Scope	110
4.4 Introduction to a Computational Investigation of the Mechanism of Reaction	111
4.5 Preliminary Computational Studies with a Model System	113
4.6 Computational Studies on the Full Reactive System	113
4.7 Conclusions	120
4.8 Experimental	121
4.9 References	144

List of Figures

Chapter 1

Figure 1.1 Depictions of various types of chirality	1
Figure 1.2 Acid catalysis types	4
Figure 1.3 Simple spiroketal structures found in nature	9
Figure 1.4 Structurally complex, biologically active natural products containing spiroketals	10
Figure 1.5 Ivermectin	11
Figure 1.6 Orbital alignment in configurations of 6,6-spiroketals	12
Figure 1.7 Truncated structure of aplysiatoxin	13

Chapter 2

Figure 2.1 X-ray crystal structures of spiroketals 56b and 87	34
--	----

Chapter 3

Figure 3.1 Hammett analysis of the CPA-catalyzed spirocyclization	64
Figure 3.2 Spiroketalization of 71a to 71b	68
Figure 3.3 Flowchart depicting the steps followed for the generation of isomers and low barrier transition states	73
Figure 3.4 Plausible reaction pathways for the formation of 50	77
Figure 3.5 Tracking electron density and C-O bond distance in the formation of 61b	78
Figure 3.6 Direct dynamic calculations measuring collapse of the transition state of 49 to 50 over time	79
Figure 3.7 Hammett plot following removal of 132e	89
Figure 3.8 Hammett plot against σ values	89
Figure 3.9 Geometry of enol ether 61a	94

Figure 3.10 Geometry of transition state 152	96
Figure 3.11 Final geometry of 61b	97

Chapter 4

Figure 4.1 Chiral piperidine moieties present in pharmaceutical agents	106
Figure 4.2 Calculated most favored reaction pathway	115
Figure 4.3 Reaction energy diagram for S _N 2'-like pathway to form the minor piperidine stereoisomer	117
Figure 4.4 Hydrogen bond between N-H of 173a and P-O of 51 in TS _{173a} – II of the reaction is visible.	119
Figure 4.5 Additional distance and poor angle between N-H of 185 and P-O of 51 in TS ₁₈₅ – II of the reaction is visible.	120
Figure 4.6 Transition state geometry for full system prior to chiral phosphate formation, TS _{173a} - I	123
Figure 4.7 Geometry of chiral phosphate acetal intermediate 182	125
Figure 4.8 Transition state geometry TS _{173a} – II of the full system	127
Figure 4.9 Geometry of full system 174a_{boat} following cyclization	129
Figure 4.10 Geometry of full system 174a following conformational change	130
Figure 4.11 Geometry of free catalyst system 51 following regeneration of the catalyst after the reaction	132
Figure 4.12 Transition state geometry TS _{173a} – III of the full system prior to concerted cyclization	133
Figure 4.13 Geometry of 185 , prior to forming minor enantiomer	135
Figure 4.14: Transition state geometry for full system prior to reaction forming minor enantiomer phosphate intermediate, TS ₁₈₅ - I	137
Figure 4.15: Geometry for 186 , the chiral phosphate acetal intermediate full system prior to cyclizing to form the minor enantiomer	139
Figure 4.16: Geometry TS ₁₈₅ - II following MeOH departure for full system prior to cyclization to form the minor enantiomer	140
Figure 4.17: Geometry for the minor enantiomer product, 187	142

List of Schemes

Chapter 1

Scheme 1.1 Organocatalysis from MacMillan and List from 2000	3
Scheme 1.2 Akiyama's CPA-catalyzed Mannich-type reaction	5
Scheme 1.3 Terada's use of CPAs to catalyze a Mannich reaction	5
Scheme 1.4 Synthesis of BINOL-derived CPAs	7
Scheme 1.5 List's CPA-catalyzed asymmetric transacetylation	7
Scheme 1.6 Evan's synthesis of the CD spiroketal of Spongistatin 1	14
Scheme 1.7 Iwata's utilization of a pyramidal sulfoxide moiety to direct spirocyclization reactions	15
Scheme 1.8 Deslongchamps spiroketalization to different conformers	15
Scheme 1.9 Direct kinetic formation of non-anomeric spiroketals	16
Scheme 1.10 Enantioselective synthesis of the core of γ -rubromycin	16
Scheme 1.11 Stereo-controlled synthesis of glycal-based spiroketals from Tan	17
Scheme 1.12 Rychnovsky's synthesis of the spiroketal of Pectenotoxin	18
Scheme 1.13 Hypothetical stereoselective transformation of enol ethers	19

Chapter 2

Scheme 2.1 Synthesis of 49 for use in the optimization of CPA-catalyzed spiroketalizations	24
Scheme 2.2 Synthesis of 6,6-dibenzyl and 6,7-dibenzyl precursors 61a and 62a	27
Scheme 2.3 Synthesis of a 6,5-dibenzylated spiroketalization precursor	28
Scheme 2.4 Synthesis of 71a , a diphenylated dihydrobenzoisopyran scaffold	29
Scheme 2.5 Synthesis of 75a , a spiroketalization precursor with a dihydrobenzoisopyran scaffold	29
Scheme 2.6 Initial synthetic route to glycal-derived enol ethers	32
Scheme 2.7 Revised synthesis of glycal-derived enol ethers	33
Scheme 2.8 An example of the diastereoselective spiroketalization	33

Chapter 3

Scheme 3.1 Brønsted acid catalysis	50
Scheme 3.2 Various types of oxocarbenia observed spectroscopically	52
Scheme 3.3 Generation of an alkoxy-carbenium ion pool	52
Scheme 3.4 Deslongchamps' proposed early transition state for the formation of 102 from exposure of 98 to acid.	53
Scheme 3.5 Yoshida's preparation of a glycosyl oxocarbenium ion	54
Scheme 3.6 Modes of addition to a 2-deoxyglucose-derived oxocarbenium ion	55
Scheme 3.7 Crich-proposed intermediates in glycosylation	56
Scheme 3.8 Crich use of molecular cationic clocks	56
Scheme 3.9 Fairbanks' application of CPA to stereoselective glycosylation	57
Scheme 3.10 Tan's stereoselective spiroketalizations	58
Scheme 3.11 Schmidt's use of thiourea and strong, achiral Brønsted acids	59
Scheme 3.12 Alternate modes of activation	60
Scheme 3.13 Synthesis of panel of substrates for rate analysis	61
Scheme 3.14 Frank's glycal deuterium-labeling study	66
Scheme 3.15 Selective <i>cis</i> delivery of acidic proton	66
Scheme 3.16 Differentiating between an ionic and concerted pathway	67
Scheme 3.17 Various synthetic approaches to install a D-label	69
Scheme 3.18 Substrates used in the deuterium-labeling study	70
Scheme 3.19 Selected systems to investigate the presence of oxocarbenia	75
Scheme 3.20 Possible configurations of the spiroketal product	76

Chapter 4

Scheme 4.1 Activation modes of α,β -unsaturated acetals and carbonyls	104
Scheme 4.2 Gassman's TfOH-promoted Diels-Alder	104
Scheme 4.3 Sammakia's asymmetric Diels-Alder reaction	104
Scheme 4.4 Chiral 162 for application in an asymmetric Diels-Alder	105
Scheme 4.5 162 -catalyzed ionic Diels-Alder reaction	105
Scheme 4.6 Proline-catalyzed Michael addition to yield chiral piperidines	107

Scheme 4.7 Synthesis of chiral piperidines	107
Scheme 4.8 Chiral phosphoric acid-mediated aza-Michael reaction of unsaturated acetals for the stereoselective formation of chiral piperidines	107
Scheme 4.9 Enantioenrichment of racemic piperidine 174	110
Scheme 4.10 Potential reaction mechanisms	112
Scheme 4.11 Model reaction for initiation of computational studies	113
Scheme 4.12 Depiction of alternative, concerted, ionic pathway	116

List of Tables

Chapter 2

Table 2.1 Optimization of conditions for enantioselective spiroketalization	25
Table 2.2 Enantioselective spiroketalizations	27
Table 2.3 Expanded scope of enantioselective spiroketalization	30

Chapter 3

Table 3.1 Acid-catalyzed spirocyclizations of D-labeled 142	71
Table 3.2 Acid-catalyzed spirocyclization of D-labeled 144	72
Table 3.3 Sample of kinetic data for spiroketal formation	87
Table 3.4 Observed average rates for spirocyclizations	88
Table 3.5 Data for Hammett plot analysis	88

Chapter 4

Table 4.1 Initial reaction optimization	109
Table 4.2 Reaction scope	111
Table 4.3: Calculated values for geometries of starting materials, transition states, intermediates and products for the pathways investigated for the formation of the major piperidine enantiomer	116
Table 4.4: Calculated values for geometries of starting materials, transition states, intermediates and products for the pathways investigated for the formation of the minor piperidine enantiomer	118

List of Abbreviations

Å	angstrom
Ac	acetyl
acac	acetylacetone
Ac ₂ O	acetic anhydride
anhyd	anhydrous
aq	aqueous
Ar	aryl
BINOL	1,1'-Bi(2-naphthol)
br	broad
Bu	butyl
°C	degrees Celsius
<i>c</i>	concentration
C ₆ D ₆	deuterated benzene
CAM	cerium ammonium molybdate
CD ₃ OD	deuterated methanol
CDCl ₃	deuterated chloroform
CD ₂ Cl ₂	deuterated methylene chloride
CF ₃ CO ₂ H	trifluoroacetic acid
CH ₂ Cl ₂	methylene chloride
CH ₃ CN	acetonitrile
COSY	correlation spectroscopy
CPA	chiral phosphoric acid
CSA	camphor sulfonic acid
d	days
DIBAL-H	diisobutylaluminum hydride
DMAP	<i>N,N</i> -dimethyl-4-aminopyridine
dr	diastereomeric ratio
ee	enantiomeric excess
equiv	equivalents
ESI-MS	electrospray ionization-mass spectrometry
Et	ethyl
Et ₂ O	diethyl ether
Et ₃ N	triethyl amine
EtOAc	ethyl acetate
FDA	Food and Drug Administration
g	grams
h	hours
HCl	hydrochloric acid

HSQC	heteronuclear single quantum coherence
Hz	hertz
imid	imidazole
<i>i</i> Pr	isopropyl
IR	infrared
<i>J</i>	coupling constant
<i>k</i> _{obs}	observed rate
<i>k</i> ₀	rate of unsubstituted (reference) substrate
kcal	kilocalorie
kD	kiloDalton
LC	liquid chromatography
M	molarity
Me	methyl
MeOH	methanol
mg	milligrams
min	minutes
mL	milliliters
mmol	millimoles
mol	moles
MS	molecular sieve or mass spectrometry
MW	molecular weight
N.D.	not determined
NIH	National Institute of Health
NMR	nuclear magnetic resonance spectroscopy
NOE	nuclear Overhauser effect
NOESY	nuclear Overhauser effect spectroscopy
Np	naphthyl
o/n	overnight
Ph	phenyl
PhMe	toluene
ppm	parts per million
pyr	pyridine
R	alkyl group (generic)
<i>r</i> ²	coefficient of determination
rac	racemic
rel int	relative intensity
R _f	retention factor
RDS	rate determining step
rt	room temperature
satd	saturated
S _N 1	unimolecular nucleophilic substitution
S _N 2	bimolecular nucleophilic substitution
t	time
T	temperature
TBAF	tetrabutylammonium fluoride
TBDPS	<i>tert</i> -butyldiphenylsilyl

TBS	<i>tert</i> -butylmethylsilyl
Tf	trifluoromethanesulfonyl
TFA	trifluoroacetic acid
THF	tetrahydrofuran
TIPS	triisopropylsilyl
TLC	thin layer chromatography
TMS	trimethylsilyl
TsOH	para-toluene sulfonic acid
US NCI	United States National Cancer Institute
UV	ultraviolet
δ	chemical shift (parts per million)
σ	sigma - Hammett constant
σ^*	sigma * - Hammett constant
ρ	rho - slope of Hammett plot

Chapter 1:
Introduction: Chiral Phosphoric Acids and Spiroketal

1.1 Introduction to Asymmetric Organocatalysis

Asymmetric organocatalysis involves the utilization of a chiral organic compound to catalyze a reaction. Though asymmetric catalysis began by employing compounds with chiral centers such as that present on proline, chirality extends far beyond the traditional sp^3 hybridized carbon with four distinct substituents, commonly referred to as “point chirality” or chirality derived from stereogenic centers (Figure 1.1).¹ Inherent chirality can also be expressed as planar chirality or axial chirality. In these two sources of stereochemistry, no true stereogenic center is present in the molecule, yet stereoisomerism is still possible through non-superimposable mirror images structures with axial or planar chirality.

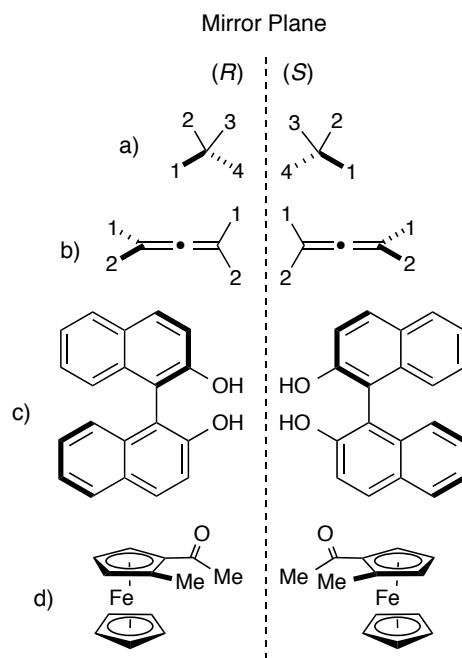


Figure 1.1: Depictions of various types of chirality. a) Point chirality. b) Axial chirality as seen in allenes. c) Axial chirality as seen in BINOL. d) Planar chirality in a ferrocene metallocene.

In planar chirality, two subunits of a molecule exist in different planes, but cannot rotate due to steric or rotational strain in the molecule. This inability to rotate through the plane causes an inability to freely interconvert between conformations and leads to a source of stereochemistry. This type of chirality is often observed in metallocenes like ferrocenes or compounds like cyclooctene. Though rarely observed in nature, planar chirality does occasionally occur as observed in the natural product cavicularin, which can be isolated from *Calvicularia densa*, a type of non-vascular bryophyte found in Japan.²

Axial chirality is similar to the planar variety in that the compound in question does not possess a classical stereogenic center. Instead, two substituents are placed around an axis such that they are non-superimposable upon their mirror image and have restricted rotation around the axis connecting the two substituents.¹ This type of chirality can be observed in allenes, as well as in biaryl compounds such as 1,1'-bi-2-naphthol (BINOL).

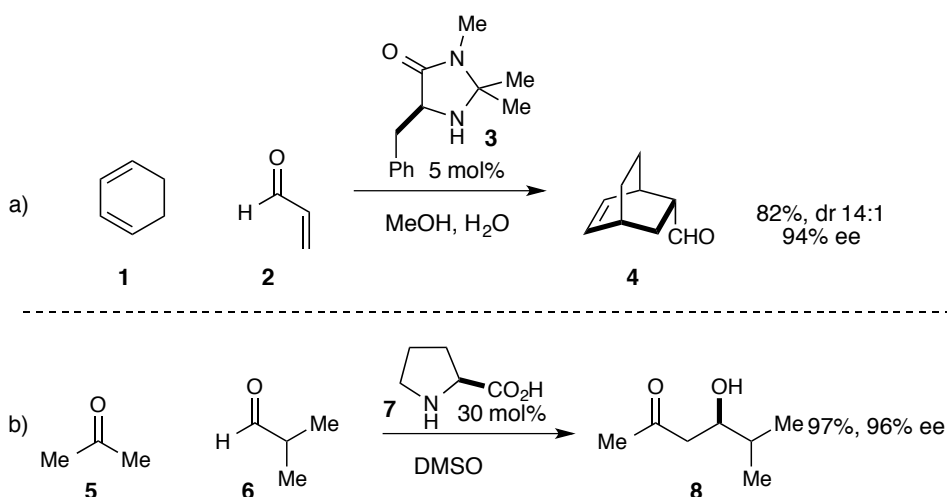
The field of organocatalysis underwent a marked growth period in the early 2000's and over the past fifteen years has blossomed into a very large and diverse field.³ While the field found its beginnings in organic catalysis with point chirality, modern asymmetric catalysis has utilized all four types of chirality presented in Figure 1.1. Organocatalysis boasts some obvious advantages over organometallic, metallic or enzymatic catalysis in that they usually operate under much milder reaction conditions, do not require the use of expensive or toxic metals and are usually straightforward to synthesize in an enantiomeric fashion. In addition, modes of activation can be varied, as well as the structural features of the catalyst.

Though asymmetric organocatalysis did not observe large scientific interest until the early 2000's, evidence of the use of organocatalysis in the literature dates back to 1912, during which a cinchona alkaloid was utilized to activate benzaldehyde to accelerate the addition of hydrogen cyanide and give the resulting addition product in low enantioselectivities.^{4,5} Decades later, in 1960, another cinchona alkaloid was utilized by Pracejus to accelerate the addition of methanol to various ketenes.⁶ Hajos and Parish,^{7,8} of Hajos-Parish ketone-fame, and Eder, Sauer and Wiechert^{9,10} independently reported a proline-catalyzed Aldol reaction in 1971, however these four publications did not garner the large interest in organocatalysis that was soon to come.

In the year 2000, MacMillan and List with Barbas both independently disclosed the application of amines for asymmetric organocatalysis (Scheme 1.1). The MacMillan group utilized a chiral imidazolidinone **3** to activate dienophile **2** in a Diels Alder reaction.¹¹ By

condensing the imidazolidinone onto the α,β -unsaturated aldehyde **2**, a drop in energy of the lowest unoccupied molecular orbital (LUMO) is observed, creating a more reactive electrophile, and accelerating the reaction with diene **1**. By utilizing a chiral imidazolidinone with a bulky benzyl substituent, MacMillan was able to block one face of the dienophile, resulting in reactions carried out in 82% yield with **4** formed in 14:1 dr and 94% ee.

That same year, List published an *L*-proline-catalyzed Aldol addition reaction, which, as in MacMillan's work, involved the condensation of the chiral secondary amine onto carbonyl **5**.¹² In this case, however, the iminium ion directly yielded an enamine, which, rather than lowering the LUMO, raises the highest occupied molecular orbital (HOMO), producing a more reactive nucleophile reacting with **6**, and the Aldol product **8** could be obtained in 97% yield and 96% ee.



Scheme 1.1: Simultaneous accounts of organocatalysis from MacMillan and List from 2000. a) MacMillan's imidazolidinone-catalyzed Diels-Alder reaction produced cyclohexene **4** in 94% ee. b) List's **7**-catalyzed Aldol, which delivered **8** in 96% ee.

Following these two publications, interest in organocatalysis skyrocketed, with thousands of papers on the subject currently being published each year.

1.2 Asymmetric Organocatalysis through Hydrogen Bonding

Since 2000, many different types of organocatalysts have emerged, each operating through their own mode of activation. In addition to the previously discussed variations in chirality source, asymmetric catalysis can be further broken down into modes of activation. Acid catalysis makes up

one of several classifications of organocatalysis and can even be divided further into specific acid catalysis, in which an electrophile is reversibly protonated in a pre-equilibrium step prior to nucleophilic attack, or general acid catalysis, in which a hydrogen bond is donated from the catalyst to the electrophile, but a full proton transfer has not occurred (Figure 1.2).^{13,14}

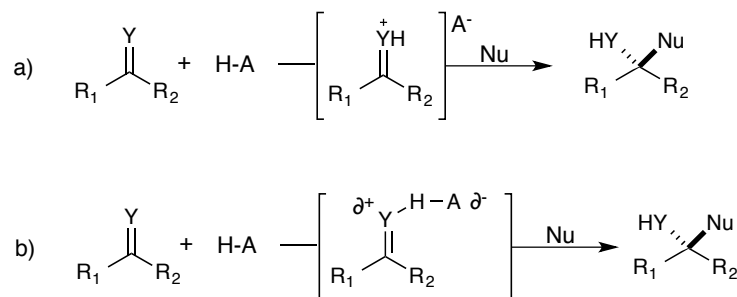


Figure 1.2: Acid catalysis types. a) Specific acid catalysis. b) General acid catalysis.

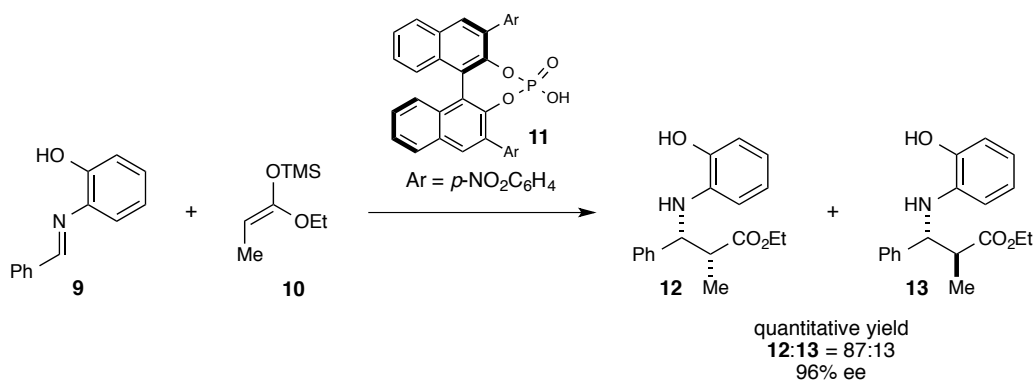
Though hydrogen bonds are generally thought to be weak interactions as compared to sigma bonds of a covalent nature, the thermodynamic favorability of forming a hydrogen bond is more than enough to drive a reaction forward, and the ability to form a hydrogen bond in one of two diastereomeric transition states can yield extremely high enantioselectivities. A weak, electrostatic hydrogen bond typically has a bond energy lower than 4 kcal/mol, and is anywhere from 2.2-3.2 angstroms (Å) in length.¹³ Though a 4 kcal/mol difference in energy is enough to supply high ees, catalysts have been modified to be even more efficient at promoting reactions by increasing the number of hydrogen bonds possible, as in urea and thiourea-based catalysis. Notably, chiral thioureas were utilized in 1998 by Jacobsen and Sigman to catalyze Strecker reactions,¹⁵ however neither proposed hydrogen bonding was the root cause of activation of the substrates until several years later.

Also popular in asymmetric organocatalysts is to place a Brønsted basic site in close proximity to the Brønsted acidic site, such as in cinchona alkaloids and phosphoric acids. This bifunctionality of the catalyst can activate both the nucleophile and electrophile and results in very active hydrogen bond catalysts due to lowered catalyst loadings and increased reaction rates.

1.3 Chiral Phosphoric Acid Catalysts

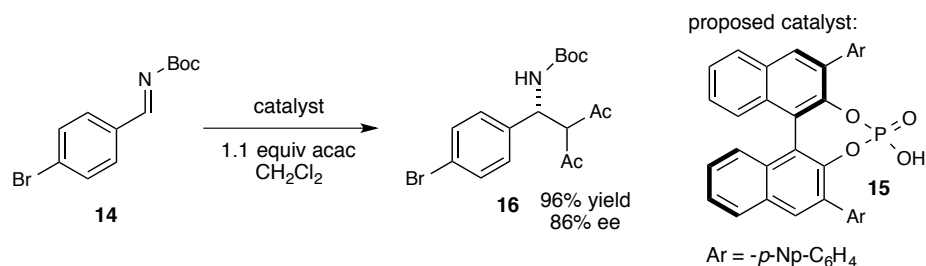
In 2004, Terada and Akiyama independently published the first examples of BINOL-based chiral phosphoric acid (CPA) catalysis.^{16,17} These catalysts, with conformationally rigid BINOL backbones can be tuned by *ortho*-functionalization of each naphthalene ring to exhibit a range of electron densities and steric bulk. In functionalizing BINOL, *ortho*-substituents extend the axial chirality of the BINOL scaffold, creating a chiral pocket, which contains both the acidic proton and the basic phosphoryl oxygen in which the substrates can react.¹⁸

In Akiyama's enantioselective Mannich-type reaction, the BINOL-based CPA **11** was functionalized with *para*-nitro benzene rings to increase the acidity of the single acidic proton in the catalyst. Akiyama observed reaction of aldimines **9** with silyl enolates **10** with mostly quantitative yields and enantioselectivities of **12** and **13** from 81-96% yield (Scheme 1.2).



Scheme 1.2: Akiyama's CPA-catalyzed Mannich-type reaction. Products isolated in 96% ee.

In Terada's paper, a *para*- β -naphthyl-phenyl ligand was utilized to increase steric bulk on **15**, which he utilized to catalyze a Mannich reaction between Boc-protected imines **14** and acetyl acetone with yields and enantioselectivities of **16** in the mid 80's and 90's (Scheme 1.3).

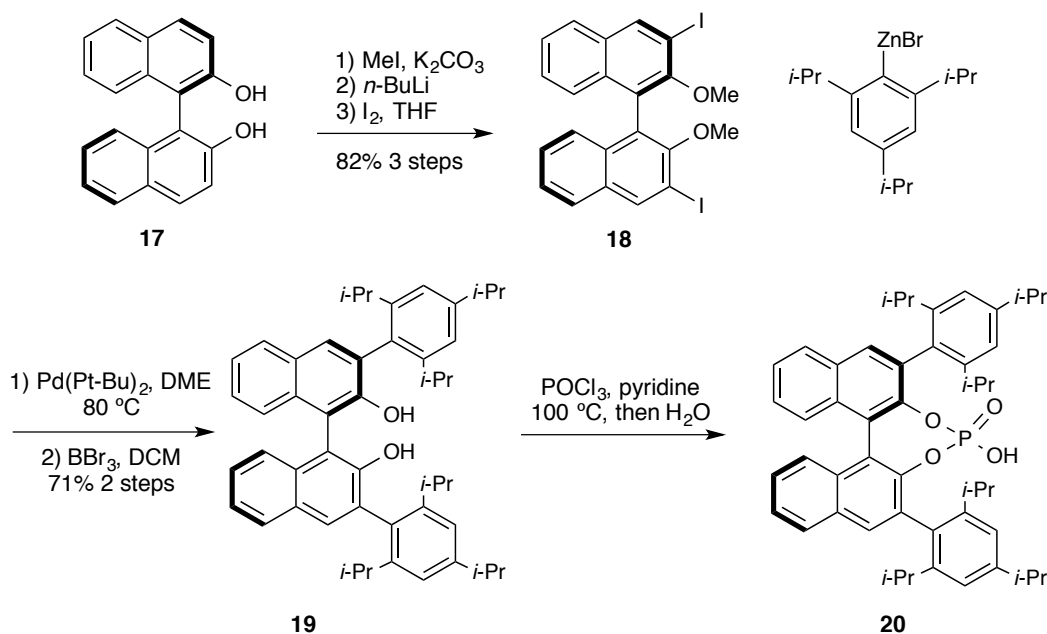


Scheme 1.3: Terada's use of CPAs to catalyze a Mannich reaction between Boc-protected imines and acetyl acetone resulted in adducts in over 90% yield and high enantioselectivities.

Interestingly, Ishihara issued a follow-up paper revising the originally proposed structure of the catalyst used to promote these Mannich reactions.¹⁹ Though billed as a CPA-catalyzed Mannich reaction, in actuality it was a metal salt of the phosphate that was being used in the reactions, as the group did not wash the acids with HCl post-column chromatography and on column the phosphate tends to pick up metal ions like calcium and magnesium. Despite this, both papers marked the beginning of the field of CPA-catalyzed reactions, which has now expanded greatly to include hydrocyanations,²⁰⁻²³ Aldol-type reactions,²⁴⁻²⁶ Mannich reactions,^{27,28} Friedel-Crafts reactions,²⁹⁻³² cycloadditions,³³⁻³⁶ various rearrangements^{37,38} and multi-component/cascade reactions.³⁹⁻⁴¹

As the amount of reactions catalyzed by CPAs has expanded, so have the structural variations of the original BINOL scaffold. Though the most popular scaffolds still retain the BINOL backbone, with a bulky 2,4,6-(*i*-Pr₃)C₆H₂ *ortho*-substituent, often referred to as TRIP, or an electron withdrawing 3,5-(CF₃)C₆H₄ *ortho*-substituent, alternate structures are also available. By hydrogenating the far phenyl rings of the BINOL core, one can access H8-BINOLS,⁴² a more sterically bulky backbone with slightly different solubility properties. VAPOL-derived acids extend the phenyl backbone further towards the reactive site of the catalyst and have shown to perform better in the synthesis of amins.⁴³ In addition, *bis*-BINOL-based scaffolds,⁴⁴ SPINOL-derived acids⁴⁵ as well as thiophosphoramides,⁴⁶ dithiophosphoric acids⁴⁷ and many other variations have also been employed in the literature.

BINOL-derived acids still remain a field favorite, however, due to the relatively cheap starting materials needed and the comparatively shorter synthesis. Synthesis of a CPA such as TRIP begins with methylating the diol, followed by *ortho*-lithiation and iodination of the naphthalene rings (Scheme 1.4). The resulting diiodide can undergo cross-coupling with a magnesium or zinc bromide, after which the diol can be deprotected with BBr₃ and phosphorylated by refluxing with POCl₃.

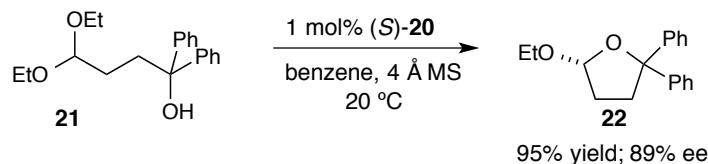


Scheme 1.4: Synthesis of commonly-used chiral phosphoric acid, TRIP.

By varying the bromide, a library of CPAs can be developed with relative ease, though the multiple steps and sterically demanding cross coupling leave room for improvement.⁴⁸

1.4 Utilization of CPAs to Asymmetric Acetylation Reactions

In 2010, the List group published a seminal paper on the use of CPAs as promoters of asymmetric transacetylation reactions (Scheme 1.5). Prior to this paper, a very limited number of enantioselective acetylation reactions had been reported with most relying on chiral starting materials or reagents.^{23,49-51} There existed only one other catalytic asymmetric approach to the formation of acetals, which involved a metal-catalyzed hydroetherification reaction of enol ethers.⁵² The List paper demonstrated that CPAs could control the addition of nucleophiles to the less-explored oxygen variant, the oxocarbenium ion.



Scheme 1.5: List's CPA-catalyzed asymmetric transacetylation.

By employing a bulky CPA such as (*S*)-**20** (TRIP) in a nonpolar solvent such as benzene, List was able to achieve transacetalization products with enantioselectivities in the high 80's at room temperature upon the first optimization screen.

While substituents could be varied to include both aromatic and aliphatic substituents, as well as electron donating and electron withdrawing groups, the highest enantioselectivities were observed by increasing the steric bulk; substituting the alcohol nucleophile with isopropyl or *tert*-butyl groups resulted in the stereoselective formation acetals in 90-93% yield and 96% ee.

Given the successful application of chiral phosphoric acids to asymmetric nucleophilic additions to reactive centers and with the publishing of the CPA-catalyzed asymmetric transacetylation reaction, it was clear that chiral phosphoric acids could control the stereoselective synthesis of *O,O*-acetals. Thus, the application of CPAs as catalysts for the formation of *O,O*-ketals such as spiroketals could yield a general, direct method for the synthesis of these important, but hard-to-access subunits. Driven by these advances, our lab began investigating spiroketals as potential products of CPA-catalyzed cyclizations.

1.5 Introduction to Spiroketals

Spiroketals are a common scaffold present in many natural products extracted from marine life, insects and bacteria.⁵³⁻⁵⁵ The spiroketal moiety is comprised of two rings, each of which has an oxygen atom connected to the same sp³-hybridized carbon atom. Though simple in structure, the spiroketals present in natural products are often directly implicated in a molecule's medicinal properties and have been shown to exhibit a broad range of biological activities.⁵⁶⁻⁵⁸ The olive fruit fly *Bactrocera oleae* sex pheromone olean is one of the simplest spiroketals present in nature (Figure 1.3) and serves as an excellent example of how spiroketals can serve as potent pharmacophores.⁵⁹ Though present as a racemate in the female flies, the two isolated enantiomers exhibit remarkable selective activity for each gender of the fly, with the (*R*)-enantiomer active on male flies and the (*S*)-enantiomer active on female flies.⁶⁰ Of similar structural simplicity are conophthorin, a methylated 6,5-spiroketal and chalcogran, an ethylated 5,5-spiroketal (Figure 1.8).

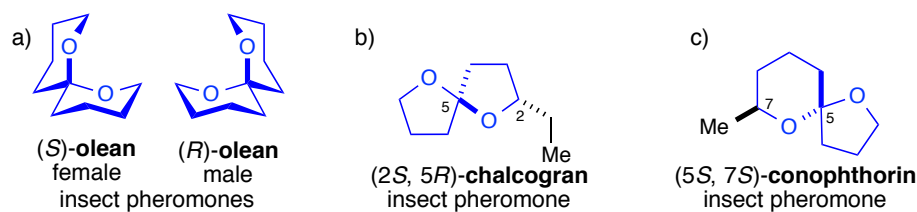


Figure 1.3: Simple spiroketal structures found in nature. a) 6,6 Spiroketal from (*R*) and (*S*) enantiomers of olean, found to be active in the olive fruit fly *Bactrocera oleae*. b) The active epimer of chalcogran, a pheromone produced as a racemate in the European spruce bark beetle. c) An enantiomer of the structurally simplistic navel orangeworm moth pheromone.

Despite their simplistic structure, both have been implicated in numerous plant and insect systems, particularly the navel orangeworm moth and the European spruce bark beetle, respectively.⁶¹ Similarly to olean, the stereochemistries of these spiroketals play an important role in their use in chemical communication systems in nature. The European spruce bark beetle again produces the spiroketals as a racemate, yet only the (*2S,5R*)-epimer has been shown to be biologically active.

Though there are many examples of simple spiroketal structures in nature, there are many more examples of more complex structures of biological interest, which contain a spiroketal moiety (Figure 1.4). Spongistatins, first identified independently in 1993 by three different research groups,⁶²⁻⁶⁴ contain spiroketals and have demonstrated notable growth inhibition against a panel of 60 human cancer cell lines from the US National Cancer Institute. Spongistatin 1, the most potent member of the family, has been shown to be active against highly chemoresistant tumors, with GI_{50} values of $2.5-3.5 \times 10^{-1}$ M.^{65,66} Pectenotoxin 1, isolated from the scallop *Patinopecten yessoensis* was first isolated in 1985 by Yasumoto, and has demonstrated high cytotoxicity against lung, colon and breast cancer cell lines.^{67,68} The acortatarins have been shown to be active in high glucose-stressed kidney cells, decreasing the reactive oxygen species present and thus becoming targets for potential diabetes-oriented pharmaceuticals.⁶⁹

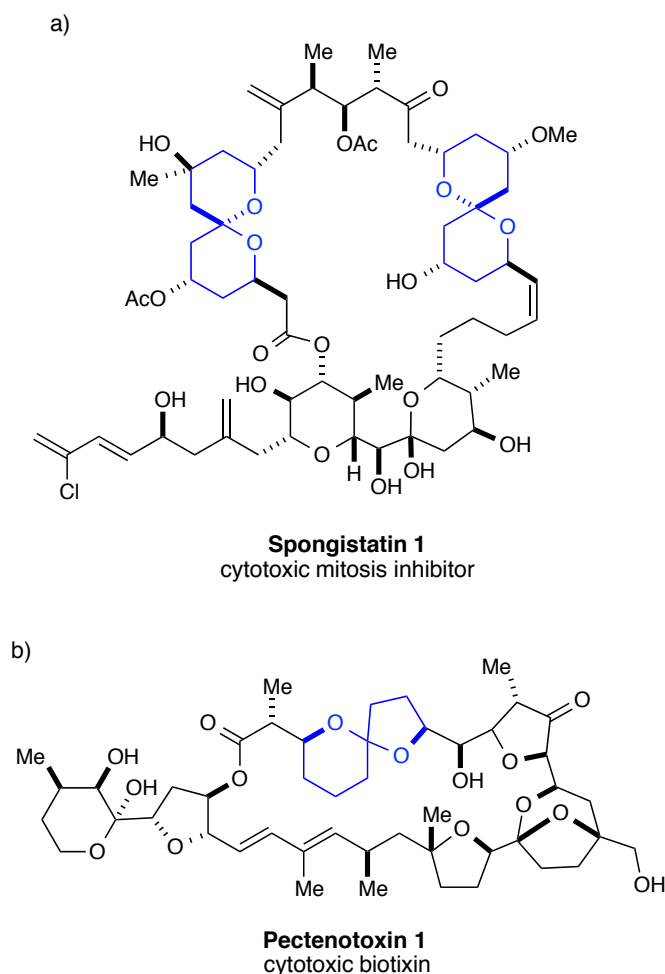


Figure 1.4: Structurally complex, biologically active natural products containing spiroketals. a) Spongistatin 1, which has shown inhibition against all 60 human cancer cell lines from the US NCI. b) Pectenotoxin 1, though highly active against various cancers has never been synthesized.

Avermectin, a potent antiparasitic contains a spiroketal moiety which has been implicated in the direct binding interactions with the glutamate-gated chloride channel through which avermectin is suggested to operate.^{70,71}

In possessing such a broad range of biological activity, it is clear that spiroketals are useful structural motifs in designing pharmaceuticals. However, as of March 2015, only a single FDA-approved drug contains a spiroketal moiety (Figure 1.5), though several are currently in the experimental phase. Though the past few years have seen many groups making progress on developing spiroketal libraries, the motif is strikingly lacking in most screening libraries commercially available through the NIH.

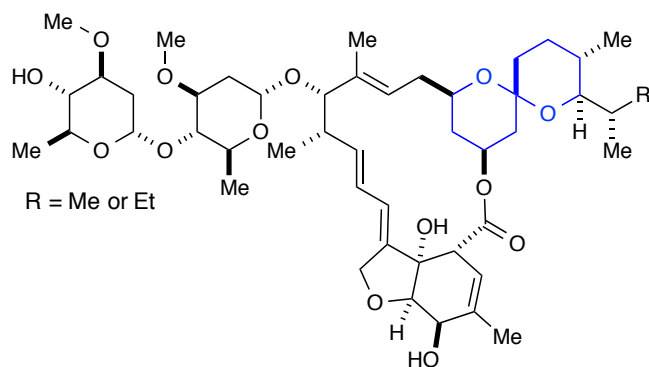


Figure 1.5: Ivermectin, a broad-spectrum antiparasitic dispensed as a mixture of the methylated and ethylated structures, is the only FDA-approved drug, which contains a spiroketal moiety.

The most prominent small molecule repository located at the NIH contains 405,853 compounds, however a search of this database reveals it contains just 110 compounds include a spiroketal motif. Nature has demonstrated that the chirality of spiroketals is extremely important in the context of biological activity; however, it is synthetically difficult to control the stereochemistry present at the central sp^3 -hybridized carbon of the spiro motif. This is in part due to the lability of the oxygens connected to the carbon, as well as the stereoelectronic-based thermodynamics of the anomeric effect.

1.6 The Anomeric Effect

In 1955, Edward first described what has become known as the anomeric effect.⁷² Named by Lemieux,⁷³ the anomeric system affects rings such as that of a pyranose-based system, in which the thermodynamics of substitution at the C1 position place an electronegative substituent like the second oxygen of a spiroketal system in the axial position.⁷⁴ This thermodynamic preference is due to a confluence of factors. Most often, a favorable hyperconjugative orbital overlap is thought to be the dominating cause. When an electronegative substituent off of C1 is axial, the non-bonding orbital associated with the lone pair of electrons on the oxygen within the ring system has strong overlap with the unoccupied anti-bonding σ^*_{C-O} orbital of the C1 substituent (Figure 1.6).

In addition to orbital orientations, dipole moments seem to have an effect. In a system with an equatorial C1 oxygen, the dipole due to the ring oxygen and the dipole due to the C1 oxygen are oriented in the same direction on the same plane, creating a source of destabilization in

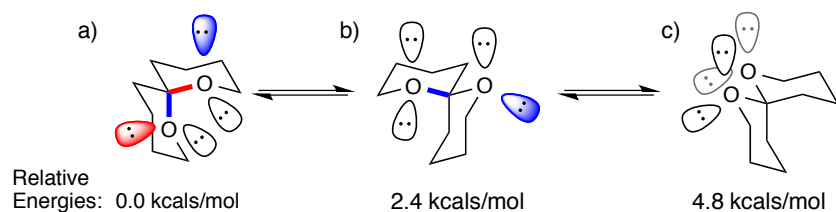


Figure 1.6: Orbital alignment in configurations of 6,6-spiroketal. a) Two anomeric effects are present in this system. Orbital overlap is present between the non-bonding orbital of the electrons present on the oxygens and the adjacent anti-bonding orbital of the axially oriented oxygens. b) Only one anomeric effect is present. c) No anomeric effects are present in this configuration.

the molecule. When in an axial position, the C1 oxygen dipole is pointing away from the ring oxygen dipole, which does not provide the same destabilization as its epimer. A third source of instability of an equatorial C1 oxygen in a spiroketal is the resulting gauche effects that increase the energy of the rings' conformations. Combining these factors in the olefin system results in the mono-anomeric substrate being 1.4-2.4 kcal/mol less stable and the non-anomeric substrate being as much as 4.8 kcal/mol less stable than the double anomeric configuration.^{75,76}

1.7 Synthesis of Spiroketal

The strong thermodynamic preference for the double-anomeric spiroketal configuration makes the directed synthesis of other spiroketal conformations quite challenging, while the synthesis of doubly axial spiroketals has been carried out in countless syntheses via acid-catalyzed cyclizations. Often, these cyclizations proceed from dihydroxyketone-based substrates, which can undergo two condensations to yield a thermodynamic spiroketal product. This equilibrating acid-mediated approach can also be employed to access non-doubly anomeric spiroketals, providing that the desired configuration of the spirocenter is still thermodynamic. For example, aplysiatoxin, isolated from the sea hare *Stylocheilus longicauda* contains a spiroketal in a nonanomeric configuration (Figure 1.7). Despite this, Ireland showed that the spiroketal subunit can still be readily accessed via acid catalysis as 1,3-diaxial interactions between the C4 and C6 methyl groups of the system destabilize the doubly anomeric configuration.⁷⁷

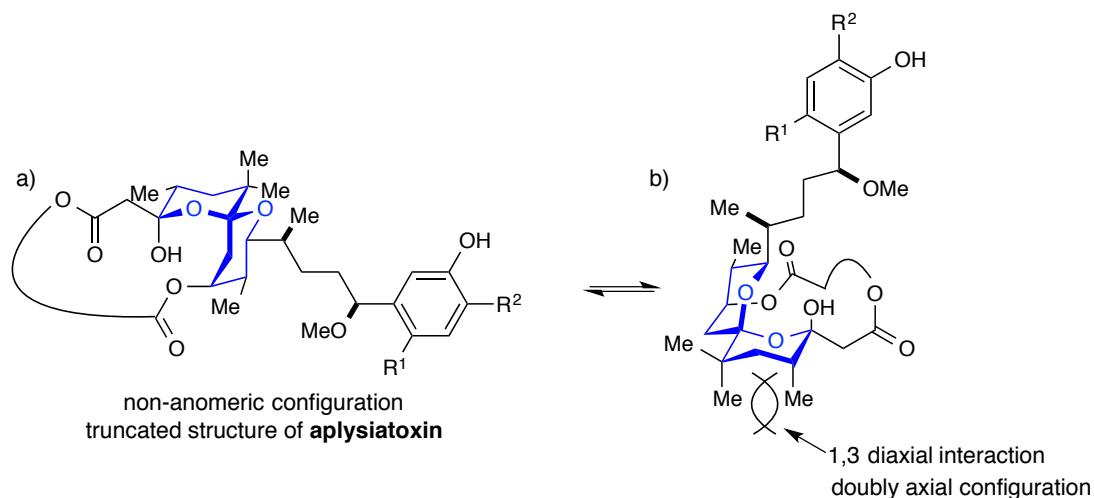
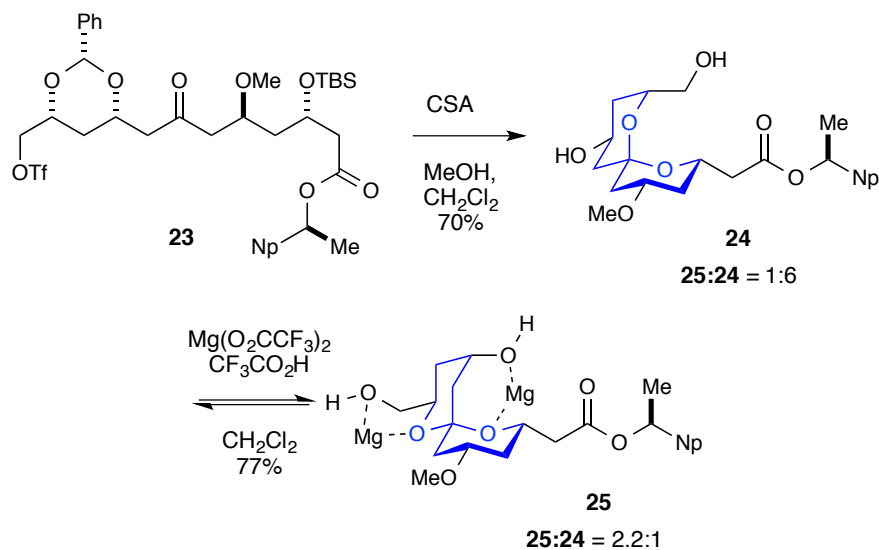


Figure 1.7: Truncated structure of aplysiatoxin. a) The thermodynamic configuration is non-anomeric. b) The doubly axial configuration of the spiroketal moiety in aplysiatoxin, which results in unfavorable 1,3 diaxial interactions of the methyl groups present on the spiroketal.

While contrathermodynamic spiroketals are not as easily accessed, several inventive strategies have been executed to achieve such configurations. While the overall configuration of an isolated spiroketal-containing natural product may be contrathermodynamic, the overall energy of the system may be lowered by an internal metal chelate or an intramolecular hydrogen bond. For example, an intramolecular hydrogen bond, as well as conformational constraints imposed by the 42-membered macrolactone of Spongistatin 1 made the C,D spiroketal more accessible than it otherwise would be; the first total synthesis of Spongistatin 1 was completed by Evans in 1997 and involved spiroketalization of **23** using CSA, followed by equilibration of a 6:1 ratio of fully anomeric spiroketal **24** to a 1:2.2 ratio favoring the monoanomeric configuration **25** using an internal $\text{Mg}(\text{O}_2\text{CCF}_3)_2$ chelate (Scheme 1.6).⁷⁸⁻⁸⁰

In cases in which intramolecular hydrogen bonding and metal chelates do not provide the desired stereoisomer, forming a nonanomeric spiroketal becomes far more challenging. Such is the case with Pectenotoxin 1. Due to a lack of stabilizing features within the molecule, the total synthesis of Pectenotoxin 1 has never been accomplished, despite many fragment-based formal attempts. A notable amount of progress, however, was published by the Pihko group, in which they demonstrated an approach to the synthesis of both anomers of the spiroketalization fragment of Pectenotoxin 1.⁸¹ The nonanomeric spiroketal was accessed in 49% yield through mild, kinetic cyclization of the appropriate precursor by employing chloroacetic acid.

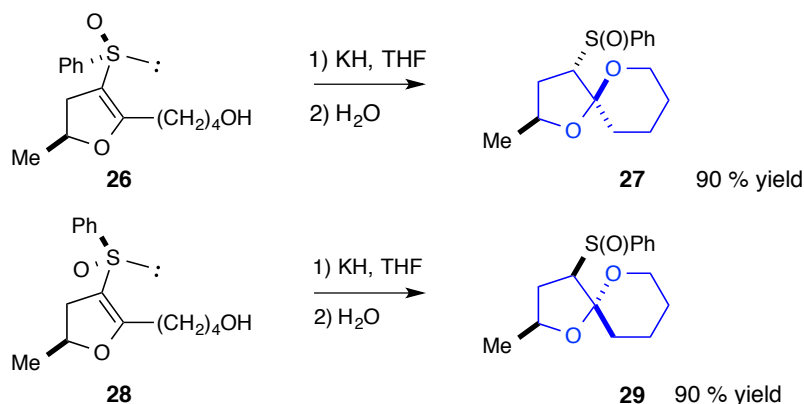


Scheme 1.6: Evan's synthesis of the CD spiroketal moiety of Spongistatin 1, utilizing internal chelation of magnesium to favor the formation of the monoanomeric spiroketal. Np = 2-naphthyl.

Most completed syntheses of natural products containing nonanomeric spiroketals rely on unique structural features of the molecule of interest. These substrate-based approaches have allowed access to several natural products, however current synthetic methods are lacking a general approach to nonanomeric spiroketals. Of the methods available today, only a few grant access to nonanomeric spiroketals.

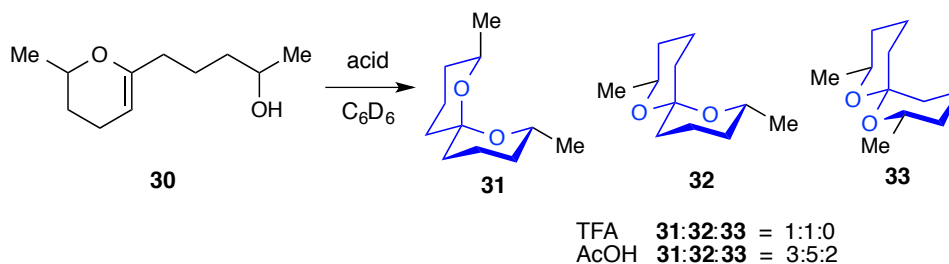
Initial efforts towards the stereoselective formation of spiroketalizations began with adding chiral directing groups such as sulfoxides and selenoxides. Iwata first published a direct route to spiroketals by performing an intramolecular Michael addition to α,β -unsaturated sulfoxides (Scheme 1.7).⁸² In this instance, the resulting configuration of spiroketals **27** and **29** was apparently a direct result of the configuration of the pyramidal sulfoxide handles in **26** and **28**, which could then be readily cleaved upon exposure to Raney nickel.

In a similar approach, the Ohta group took advantage of an asymmetric oxyselenenylation of a derivatized DHP substrate with triethylamine to yield mixtures of spiroketals with chiral selenoxide handles. The axial selenoxide substituent could be readily epimerized to the equatorial position and upon an AIBN-mediated radical reduction of the selenoxides with tributyltin hydride, both enantiomers of olean were accessible.⁸³



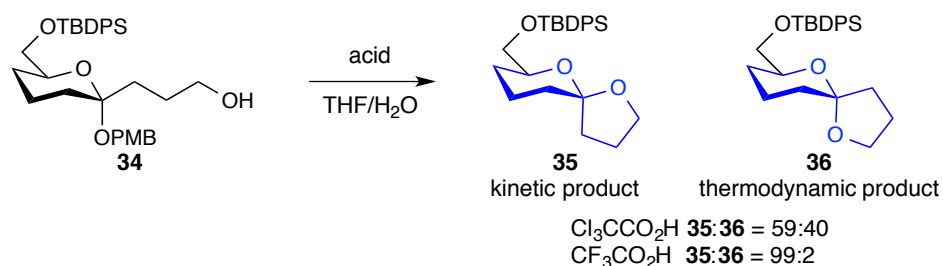
Scheme 1.7: Iwata's utilization of a pyramidal sulfoxide moiety to direct spirocyclizations.

Direct formation of nonthermodynamic spiroketals through acid-catalyzed cyclization, however, is a two-part challenge.⁵⁴ The acid catalyst must be acidic enough to promote spiroketalization in a kinetic manner, but not acidic enough to racemize the resulting acid-labile ketal stereocenter. Deslongchamps was the first to illustrate that different acids can result in the formation of either thermodynamic or kinetic spiroketals (Scheme 1.8). Exposure of enol ethers **30** to strong acids such as TFA resulted in a 1:1 ratio of the doubly anomeric **31** and mono anomeric **32**. However, exposure to acetic acid resulted in a 3:5:2 mixture of **31**:**32**:**33**. Deslongchamps rationalized formation of **32** via an early transition state, in which favorable electronics from anomeric effects were not yet developed to yield the thermodynamic spiroketal.⁸⁴



Scheme 1.8: Deslongchamps' spiroketalization to different conformers using different acids.

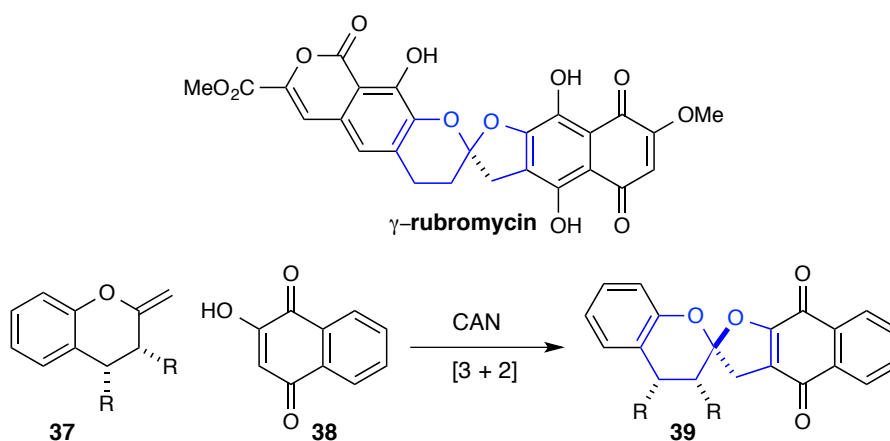
A large amount of progress towards understanding the acid-catalyzed kinetic spirocyclization and solving the synthetic challenge of direct formation of nonanomeric spiroketals **35** from **34** was made by the Pihko group in 2007 (Scheme 1.9).⁸⁵ Pihko screened achiral Brønsted acids in an attempt to identify a kinetic spiroketalization protocol that did not result in thermodynamic equilibration or epimerization of the spiroketal stereocenter to **36**.



Scheme 1.9: Direct kinetic formation of non-anomeric spiroketals using trichloroacetic acid.

Though substitution and the presence of existing stereocenters played a significant role in the success or failure of this kinetic spiroketalization protocol, this publication performed as a notable proof-of-concept paper; chloroacetic acid and trichloroacetic acid proved to have appropriate pKas to accomplish formation of non-doubly anomeric spiroketals in modest yields.

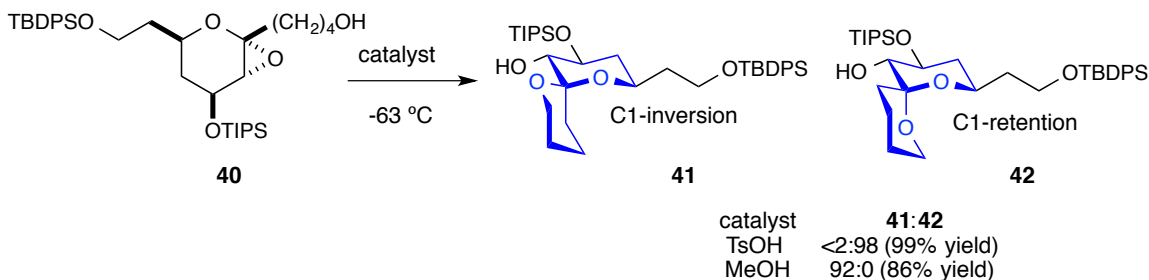
Also in 2007, the Pettus group adapted a [3+2] cyclization approach to synthesize the core of rubromycin **39** from chiral starting material **37** and **38** (Scheme 1.10).



Scheme 1.10: Enantioselective synthesis of the core of γ -rubromycin via a diastereoselective [3+2] cyclization from the Pettus group.

By including chirality in **37**, proximal to the site of spiroketal formation, Pettus was able to direct the stereoselectivity of the cycloaddition to yield the desired stereoisomer. The directing groups could then be cleaved to yield the spiroketal stereocenter as the only chirality present in the molecule.⁸⁶

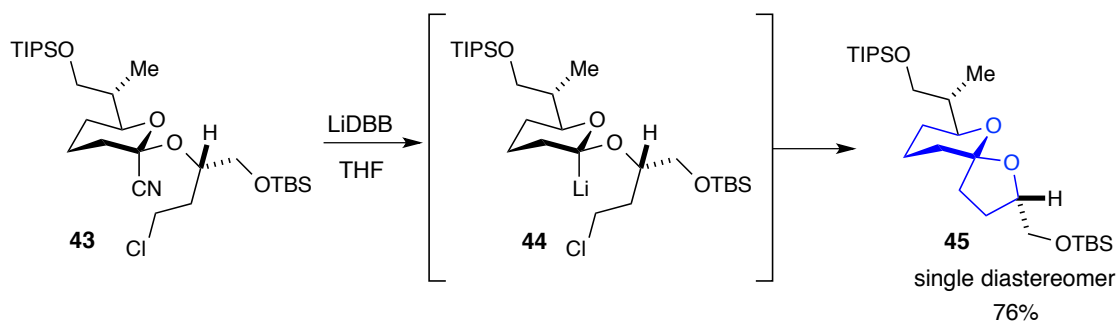
The Tan group recently disclosed a stereoselective, methanol-catalyzed glycal epoxide **40**-opening protocol to give non-anomeric 6,6-spiroketal systems **41** in high dr (Scheme 1.11).^{87, 88}



Scheme 1.11: Stereo-controlled synthesis of glycal-based spiroketals from the Tan group.

Mechanistic investigations revealed that the epoxide opening is S_N2 -like in nature, yielding inversion of configuration at the anomeric center and thus providing the desired nonanomeric spiroketal stereoisomers **41**.⁸⁹ Notably, the reaction displayed second-order dependence on methanol. Tan suggests one of the molecules of methanol participating in the transition state of the rate-determining epoxide-opening step coordinates to the epoxide oxygen, activating it towards attack, and the second coordinates the incoming nucleophile as well as the glycal oxygen. This hydrogen bond formation of the second equivalent of methanol is said to help promote the S_N2 -like nature of the mechanism and disfavor oxocarbenium ion formation. This methanol-catalyzed spirocyclization is the second of three methodologies produced by the Tan group to access spiroketals. The first strategy involved the use of a titanium isopropoxide catalyst,⁹⁰ which activated the same type of glycal epoxide substrates but proceeded with retention of configuration at the anomeric carbon to yield **42**. Most recently, by varying solvent polarity, the Tan group was also able to utilize scandium triflate as either a Lewis acid or Brønsted acid, yielding the kinetic and thermodynamic spiroketalization products respectively.⁹¹

Alternatively, Rychnovsky utilized a reductive decyanation method to deliver contrathermodynamic spiroketals (Scheme 1.12).⁹² This protocol proceeds from **43** through two LiDBB-mediated⁹³ single-electron transfers (SETs) to yield an axial lithium anion **44**, which then reacts with a pendant alkyl chloride to yield the desired nonanomeric configuration of spiroketal **45**.⁹⁴ This methodology was utilized to build the spiroketal fragment of Pectenotoxin 2, which was produced as a single diastereomer from the cyanoglycal in 76% yield.⁹⁵



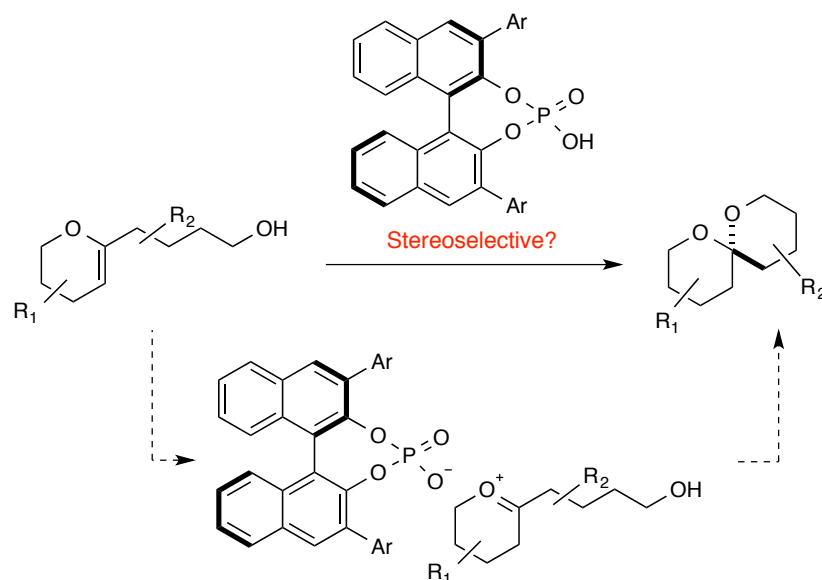
Scheme 1.12: Rychnovsky's synthesis of the spiroketal fragment of Pectenotoxin 1 utilizing the formation of an axial lithium anion to form the desired diastereomer in 76% yield.

A last approach from chiral starting materials is the iodocyclization approach by the Roush group.⁹⁶ In this case, dihydroxyalkenes were derivatized by monoprotecting one of the hydroxy groups and then performing an iodoetherification reaction on the alkene. This monocyclic product then underwent a silver triflate-promoted elimination of the iodide directly followed by spiroketalization to the desired products.

In addition to producing nonanomeric spiroketals by the utilization of chiral starting materials and chiral directing groups, approaches have been developed which utilize achiral starting materials in stereoselective transformations. One such approach is that of the Ding group, which employed an asymmetric hydrogenation reaction using a chiral catalyst to directly precede a diastereoselective spiroketalization to yield aromatic spiroketals in a stereoselective fashion.^{97,98}

1.8 Summary

While several methods exist for accessing nonthermodynamic spiroketals, many of these protocols require chiral starting materials or are substrate-specific. A direct, chiral-catalyst controlled method to form such moieties would greatly simplify the task of synthesizing these nonthermodynamic spiroketal structures. With the publishing of the aforementioned CPA-catalyzed asymmetric transacetylation reaction from the List group (Scheme 1.5), it was clear that CPAs could not only direct asymmetric nucleophilic additions to make *N,N*- and *N,O*-aminals, but also *O,O*-acetals. As this addition could be happening from a chiral ion pair, containing a phosphate anion and oxocarbenium ion, we believe such a transformation could be applied to spiroketals, as presumably the transformation would occur via an analogous mechanism (Scheme 1.13).



Scheme 1.13: Hypothetical stereoselective transformation of enol ethers to spiroketals using chiral phosphoric acids.

In addition, this type of methodology could be applied to related systems such as alpha, beta-unsaturated acetals, which could form unsaturated oxocarbenium ions *in situ*. Coordination with a phosphate anion could result in asymmetric 1,4-nucleophilic addition. Based on literature precedent, we believe applications of CPAs to the synthesis of spiroketals, potentially through the formation of a chiral ion pair, and extension of this methodology to 1,4-conjugate additions to unsaturated oxocarbenia will be a fruitful research avenue.

Described herein are studies conducted towards the development of such methodologies and a combinatorial approach of bench top and computational studies towards understanding the mechanisms of these, and similar transformations.

1.9 References

- (1) Carey, F. A.; Giuliano, R. M. *Organic Chemistry*; 2011.
- (2) Toyota, M.; Yoshida, T.; Kan, Y.; Takaoka, S.; Asakawa, Y. *Tetrahedron Letters* **1996**, 37, 4745.
- (3) Holland, M. C.; Gilmour, R. *Angewandte Chemie* **2015**.
- (4) Bredig, G.; Fiske, P. S. *Durch Katalysatoren bewirkte asymmetrische Synthese*; Biochem. Zeits, 1912.
- (5) Prelog, V.; Wilhelm, M. *Helvetica Chimica Acta* **1954**.
- (6) Pracejus, H. *Justus Liebigs Annalen der Chemie* **1960**, 634, 9.

- (7) Hajos, Z. G.; Parrish, D. R. *Asymmetric synthesis of optically active polycyclic organic compounds*; German patent DE, 1971.
- (8) Hajos, Z. G.; Parrish, D. R. *The Journal of Organic Chemistry* **1974**, *39*, 1615.
- (9) Eder, U.; Sauer, G.; Wiechert, R. *Process for the Manufacture of Optically Active Bicycloalkane Derivatives*; German Patent DE, 1971.
- (10) Eder, U.; Sauer, G.; Wiechert, R. *Angewandte Chemie International Edition in English* **1971**, *10*, 496.
- (11) Ahrendt, K. A.; Borths, C. J.; MacMillan, D. W. C. *J. Am. Chem. Soc.* **2000**, *122*, 4243.
- (12) List, B.; Lerner, R. A.; Barbas, C. F. *J. Am. Chem. Soc.* **2000**, *122*, 2395.
- (13) Taylor, M. S.; Jacobsen, E. N. *Angew. Chem. Int. Ed.* **2006**, *45*, 1520.
- (14) Doyle, A. G.; Jacobsen, E. N. *Chem. Rev.* **2007**, *107*, 5713.
- (15) Sigman, M. S.; Jacobsen, E. N. *Journal of the American Chemical ...* **1998**.
- (16) Uraguchi, D.; Terada, M. *J. Am. Chem. Soc.* **2004**, *126*, 5356.
- (17) Akiyama, T.; Itoh, J.; Yokota, K.; Fuchibe, K. *Angew. Chem. Int. Ed.* **2004**, *43*, 1566.
- (18) Cannon, S. J. *Angew. Chem. Int. Ed.* **2006**, *45*, 3909.
- (19) Hatano, M.; Moriyama, K.; Maki, T.; Ishihara, K. *Angew. Chem. Int. Ed.* **2010**, *49*, 3823.
- (20) Rueping, M.; Sugiono, E.; Moreth, S. A. *Adv. Synth. Catal.* **2007**, *349*, 759.
- (21) Hatano, M.; Ikeno, T.; Matsumura, T.; Torii, S.; Ishihara, K. *Adv. Synth. Catal.* **2008**, *350*, 1776.
- (22) Shen, K.; Liu, X.; Cai, Y.; Lin, L.; Feng, X. *Chem. Eur. J.* **2009**, *15*, 6008.
- (23) Zamfir, A.; Tsogoeva, S. B. *Org. Lett.* **2010**, *12*, 188.
- (24) Rueping, M.; Antonchick, A. P. *Org. Lett.* **2008**, *10*, 1731.
- (25) Akiyama, T.; Katoh, T.; Mori, K. *Angew. Chem. Int. Ed.* **2009**, *48*, 4226.
- (26) Terada, M.; Tanaka, H.; Sorimachi, K. *J. Am. Chem. Soc.* **2009**, *131*, 3430.
- (27) Sickert, M.; Abels, F.; Lang, M.; Sieler, J.; Birkemeyer, C.; Schneider, C. *Chem. Eur. J.* **2010**, *16*, 2806.
- (28) Giera, D.; Sickert, M.; Schneider, C. *Synthesis* **2009**, *2009*, 3797.
- (29) Kang, Q.; Zhao, Z.-A.; You, S.-L. *J. Am. Chem. Soc.* **2007**, *129*, 1484.
- (30) Tang, H.-Y.; Lu, A.-D.; Zhou, Z.-H.; Zhao, G.-F.; He, L.-N.; Tang, C.-C. *Eur. J. Org. Chem.* **2008**, *2008*, 1406.
- (31) Terada, M.; Sorimachi, K. *J. Am. Chem. Soc.* **2007**, *129*, 292.
- (32) Itoh, J.; Fuchibe, K.; Akiyama, T. *Angewandte Chemie International Edition in English* **2008**, *47*, 4016.
- (33) Akiyama, T.; Morita, H.; Fuchibe, K. *J. Am. Chem. Soc.* **2006**, *128*, 13070.
- (34) Akiyama, T.; Tamura, Y.; Itoh, J.; Morita, H.; Fuchibe, K. *Synlett* **2006**, 0141.
- (35) Müller, S.; List, B. *Angew. Chem. Int. Ed.* **2009**, *48*, 9975.
- (36) Momiyama, N.; Tabuse, H.; Terada, M. *J. Am. Chem. Soc.* **2009**, *131*, 12882.
- (37) Rueping, M.; Antonchick, A. P. *Angew. Chem. Int. Ed.* **2008**, *47*, 10090.
- (38) Terada, M.; Toda, Y. *J. Am. Chem. Soc.* **2009**, *131*, 6354.
- (39) Gong, L.-Z.; Chen, X.-H.; Xu, X.-Y. *Chem. Eur. J.* **2007**, *13*, 8920.
- (40) Guo, Q.-X.; Liu, H.; Guo, C.; Luo, S.-W.; Gu, Y.; Gong, L.-Z. *J. Am. Chem. Soc.* **2007**, *129*, 3790.
- (41) Rueping, M.; Antonchick, A. P. *Angew. Chem. Int. Ed.* **2008**, *47*, 5836.
- (42) Chen, X.-H.; Xu, X.-Y.; Liu, H.; Cun, L.-F.; Gong, L.-Z. *J. Am. Chem. Soc.* **2006**, *128*, 14802.
- (43) Rowland, G. B.; Zhang, H.; Rowland, E. B.; Chennamadhavuni, S.; Wang, Y.; Antilla, J.

- C. J. Am. Chem. Soc.* **2005**, *127*, 15696.
- (44) Guo, Q.-S.; Du, D.-M.; Xu, J. *Angew. Chem. Int. Ed.* **2008**, *47*, 759.
- (45) Xu, F.; Huang, D.; Han, C.; Shen, W.; Lin, X.; Wang, Y. *J. Org. Chem.* **2010**, *75*, 8677.
- (46) Cheon, C. H.; Yamamoto, H. *J. Am. Chem. Soc.* **2008**, *130*, 9246.
- (47) Pousse, G.; Devineau, A.; Dalla, V.; Humphreys, L.; Lasne, M.-C.; Rouden, J.; Blanchet, J. *Tetrahedron* **2009**, *65*, 10617.
- (48) Klusmann, M.; Ratjen, L.; Hoffmann, S.; Wakchaure, V.; Goddard, R.; List, B. *Synlett* **2010**, *2010*, 2189.
- (49) Yaruva, J.; Kusumoto, T.; Hiyama, T. *Journal of the ...* **1997**, *119*, 4541.
- (50) Lu'ys, M. *Chemical Communications* **1996**, 1803.
- (51) Rychnovsky, S. D.; Bax, B. M. *Tetrahedron Letters* **2000**, *41*, 3593.
- (52) Nagano, H.; Katsuki, T. *Chem. Lett.* **2002**.
- (53) Perron, F.; Albizati, K. F. *Chem. Rev.* **1989**, *89*, 1617.
- (54) Aho, J. E.; Pihko, P. M.; Rissa, T. K. *Chem. Rev.* **2005**, *105*, 4406.
- (55) Sperry, J.; Wilson, Z. E.; Rathwell, D. C. K.; Brimble, M. A. *Nat Prod Rep* **2010**, *27*, 1117.
- (56) Uckun, F. M.; Mao, C.; Vassilev, A. O.; Huang, H.; Jan, S. T. *Bioorg. Med. Chem. Lett.* **2000**, *10*, 541.
- (57) Mitsunashi, S.; Shima, H.; Kawamura, T.; Kikuchi, K.; Oikawa, M.; Ichihara, A.; Oikawa, H. *Bioorg. Med. Chem. Lett.* **1999**, *9*, 2007.
- (58) **2000**, *41*, 1699.
- (59) Baker, R.; Herbert, R.; Howse, P. E.; Jones, O. T. *J. Chem. Soc.* **1980**.
- (60) Haniotakis, G.; Francke, W.; Mori, K.; Redlich, H.; Schurig, V. *J Chem Ecol* **1986**, *12*, 1559.
- (61) Francke, W.; Kitching, W. *Current Organic Chemistry* **2001**, *5*, 233.
- (62) Pettit, G. R.; Chicacz, Z. A.; Gao, F.; Herald, C. L. *J. Org. Chem.* **1993**, *58*, 1302.
- (63) Fusetani, N.; Shinoda, K. *J. Am. Chem. Soc.* **1993**, *115*, 3977.
- (64) Kobayashi, M.; Aoki, S.; Sakai, H.; Kawazoe, K.; Kihara, N. *Tetrahedron Letters* **1993**, *34*, 2795.
- (65) Bai, R.; Cichacz, Z. A.; Herald, C. L.; Pettit, G. R.; Hamel, E. *Mol. Pharmacol.* **1993**, *44*, 757.
- (66) Bai, R.; Taylor, G. F.; Cichacz, Z. A.; Herald, C. L.; Kepler, J. A.; Pettit, G. R.; Hamel, E. *Biochemistry* **1995**, *34*, 9714.
- (67) Yasumoto, T.; Murata, M.; Oshima, Y.; Sano, M. *Tetrahedron* **1985**, *41*, 1019.
- (68) Leira, F.; Cabado, A. G.; Vieytes, M. R.; Roman, Y.; Alfonso, A.; Botana, L. M.; Yasumoto, T.; Malaguti, C.; Rossini, G. P. *Biochem. Pharmacol.* **2002**, *63*, 1979.
- (69) Tong, X.-G.; Zhou, L.-L.; Wang, Y.-H.; Xia, C.; Wang, Y.; Liang, M.; Hou, F.-F.; Cheng, Y.-X. *Org. Lett.* **2010**, *12*, 1844.
- (70) Banks, B. J.; Bishop, B. F.; Evans, N. A.; Gibson, S. P.; Goudie, A. C.; Gratton, K. A.; Pacey, M. S.; Perry, D. A.; Witty, M. J. *Bioorg. Med. Chem.* **2000**, *8*, 2017.
- (71) Wolstenholme, A. J.; Rogers, A. T. *Parasitology* **2006**, *131*, S85.
- (72) Edward, J. T. *Stability of glycosides to acid hydrolysis-A conformational analysis*; Chemistry & Industry, 1955; pp 1102–1104.
- (73) Lemieux, R. U. *Pure and Applied Chemistry* **1971**, *25*, 527.
- (74) Juaristi, E.; Cuevas, G. *Tetrahedron* **1992**, *48*, 5019.
- (75) Pothier, N.; Goldstein, S.; Deslongchamps, P. *Helvetica Chimica Acta* **1992**, *75*, 604.

- (76) Franck, R. W. *Tetrahedron* **1983**, *39*, 3251.
- (77) Ireland, R. E.; Thaisrivongs, S. *J. Am. Chem. Soc.* **1988**, *110*, 5768.
- (78) Evans, D. A.; Coleman, P. J.; Dias, L. C. *Angew Chem Int Ed Engl* **1997**, *36*, 2738.
- (79) Evans, D. A.; Trotter, B.; Côté, B. *Angew Chem Int Ed Engl* **1997**, *36*, 2741.
- (80) Evans, D. A.; Trotter, B. W.; Côté, B.; Coleman, P. J.; Dias, L. C.; Tyler, A. N. *Angewandte Chemie International Edition in English* **1997**, *36*, 2744.
- (81) Pihko, P. M.; Aho, J. E. *Org. Lett.* **2004**, *6*, 3849.
- (82) Iwata, C.; Hattori, K.; Uchida, S.; Imanishi, T. *Tetrahedron Letters* **1984**, *25*, 2995.
- (83) Uchiyama, M.; Oka, M.; Harai, S.; Ohta, A. *Tetrahedron Letters* **2001**, *42*, 1931.
- (84) Deslongchamps, P.; Dory, Y. L. *Canadian Journal of ...* **1994**, *72*, 2021.
- (85) Castagnolo, D.; Breuer, I.; Pihko, P. M. *J. Org. Chem.* **2007**, *72*, 10081.
- (86) Wu, K.-L.; Wilkinson, S.; Reich, N. O.; Pettus, T. R. R. *Org. Lett.* **2007**, *9*, 5537.
- (87) Potuzak, J. S.; Moilanen, S. B.; Tan, D. S. *J. Am. Chem. Soc.* **2005**, *127*, 13796.
- (88) Liu, G.; Wurst, J. M.; Tan, D. S. *Org. Lett.* **2009**, *11*, 3670.
- (89) Wurst, J. M.; Liu, G.; Tan, D. S. *J. Am. Chem. Soc.* **2011**, *133*, 7916.
- (90) Moilanen, S. B.; Potuzak, J. S.; Tan, D. S. *J. Am. Chem. Soc.* **2006**, *128*, 1792.
- (91) Sharma, I.; Wurst, J. M.; Tan, D. S. *Org. Lett.* **2014**, *16*, 2474.
- (92) Takaoka, L. R.; Buckmelter, A. J.; LaCruz, T. E.; Rychnovsky, S. D. *J. Am. Chem. Soc.* **2005**, *127*, 528.
- (93) Rychnovsky, S. D.; Powers, J. P.; LePage, T. J. *J. Am. Chem. Soc.* **1992**, *114*, 8375.
- (94) La Cruz, T. E.; Rychnovsky, S. D. *Org. Lett.* **2005**, *7*, 1873.
- (95) Vellucci, D.; Rychnovsky, S. D. *Org. Lett.* **2007**, *9*, 711.
- (96) Tony, K. A.; Li, X.; Dabideen, D.; Li, J.; Mootoo, D. R. *Org. Biomol. Chem.* **2008**, *6*, 1165.
- (97) Wang, X.; Han, Z.; Wang, Z.; Ding, K. *Angewandte Chemie International Edition in English* **2012**, *51*, 936.
- (98) Wang, X.; Han, Z.; Wang, Z.; Ding, K. *Angewandte Chemie* **2012**.

Chapter 2:
Development of Stereoselective
Chiral Phosphoric Acid-Catalyzed Spiroketalization Reactions

2.1 Introduction

With the publishing of the aforementioned CPA-catalyzed asymmetric transacetalization reaction from the List group,¹ it was clear chiral phosphoric acids could control the stereoselective synthesis of *O,O*-acetals through a reactive, oxocarbenium-like intermediate. Thus, the application of CPAs as catalysts for spiroketalization could yield a general, direct method for the synthesis of these important, but hard-to-access subunits. Driven by these advances, our lab began the optimization of a stereoselective, chiral phosphoric acid-catalyzed spiroketalization reaction.

Our results demonstrate that nonthermodynamic spiroketals can be synthesized in high yields and enantioselectivities with the employment of a TRIP-based CPA in nonpolar solvents. This chapter details the development of a CPA-catalyzed stereoselective spiroketalization reaction and an exploration of the reaction's substrate scope.¹

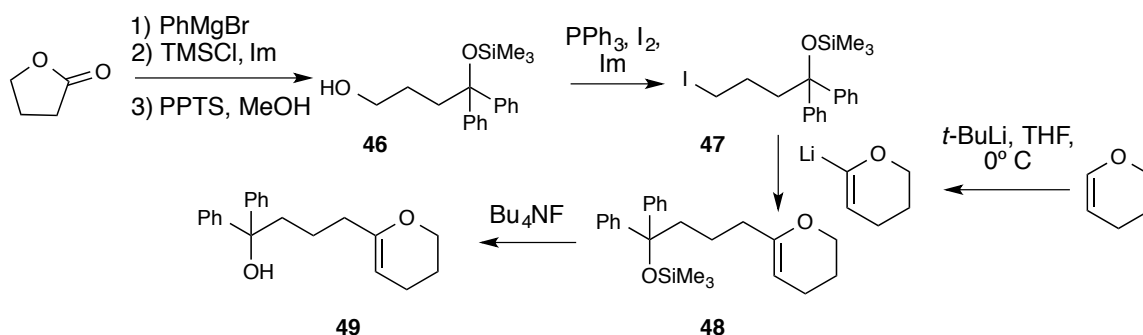
2.2 Optimization of the Chiral Phosphoric Acid-Catalyzed Enantioselective Spiroketalization Reaction

We envisioned that a stereospecific spiroketalization could be carried out with the employment of chiral phosphoric acids, however the specific characteristics of the best performing catalyst as well as optimal solvent, temperature and potential additives had to be investigated.² To initiate optimization studies, enol ether **49** was prepared as illustrated in Scheme 2.1. Synthesis

¹ Adapted with permission from Sun, Z.; Winschel, G. A.; Borovika, A.; Nagorny, P. "Chiral Phosphoric Acid-Catalyzed Enantioselective and Diastereoselective Spiroketalizations." *J. Am. Chem. Soc.* **2012**, *134*, 8074.²
Copyright © **2012** American Chemical Society.

² Initial optimization studies for this reaction described in Scheme 2.9 and Tables 2.1 and 2.2 were performed by Dr. Zhankui Sun.

began with the opening of *gamma*-butyrolactone by double addition of phenyl magnesium bromide.

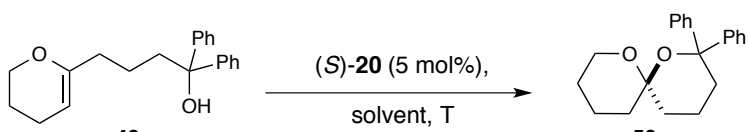


Scheme 2.1: Synthesis of **49** for use in the optimization of CPA-catalyzed spiroketalizations.

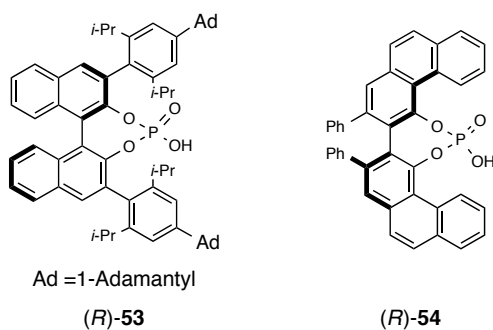
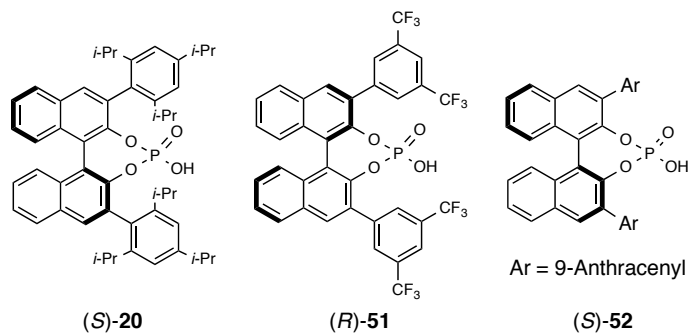
The resulting diol was *bis*-protected using trimethylsilyl chloride. *Mono*-deprotection was carried out by gentle exposure to pyridinium *p*-toluenesulfonate to yield primary alcohol **46**. This alcohol was subsequently subjected to an Appel reaction with triphenylphosphine, iodine and imidazole to give iodide **47**. Simultaneous conversion of dihydropyran to its lithiated form via exposure to *tert*-butyl lithium allowed for conversion of iodide **47** to protected precursor **48**, which was promptly deprotected by exposure to tetrabutylammonium fluoride to give enol ether **49** in overall 43% yield.

With **49** in hand, optimization began with a solvent screen as depicted in Table 2.1. Spiroketalization catalyzed by (*S*)-**20** (TRIP) proceeded extremely quickly in highly polar acetonitrile reaching completion after only 30 minutes, however observed enantioselectivities were only 7%. Similarly low enantioselectivities were observed in other polar solvents, with the reaction in tetrahydrofuran producing spiroketals in 10% ee and that in ethyl acetate at 16%. Though these enantioselectivities were low, they did produce a notable trend: enantioselectivities increased with a decreasing dielectric constant. Accordingly, more nonpolar solvents were explored. Benzene, toluene and carbon tetrachloride gave similar results, reaching 21%, 25% and 24% ee, respectively. A large jump in stereoselectivity was observed in slightly less polar solvents; upon exposure to (*S*)-**20** in hexanes, enol ether **49** underwent spiroketalization to **50** in 63% ee. Cyclohexane and pentane gave similarly promising results, with pentane supplying the desired spiroketal in 69% ee.

Table 2.1: Optimization of conditions for enantioselective spiroketalization.



entry	solvent	T, °C	time, h	ee, %
1	CH ₃ CN	rt	0.5	7
2	THF	rt	12	10
3	EtOAc	rt	12	16
4	PhH	rt	1	24
5	Toluene	rt	1	25
6	CCl ₄	rt	1	40
7	Hexanes	rt	0.5	63
8	Cyclohexane	rt	1	60
9	Pentane	rt	4	69
10	Pentane	0	4	73
11	Pentane	-35	40	66
12	Pentane, 4Å MS	0	14	84
13	Pentane, 4Å MS	-35	40	92



With an optimal solvent identified, the reaction was then cooled in an attempt to reach higher stereospecificity. Upon cooling the reaction to 0 °C, ee's of 73% were observed, while cooling to -35 °C gave **50** in only 66% ee. Though temperature did not illicit a large increase in reaction stereospecificity, the addition of 4 Å MS proved to be beneficial. With sieves, the **20**-catalyzed reaction proceeded with 92% enantioselectivity at -35 °C in pentane. Though the exact role of the sieves in the reaction flask has yet to be formally identified, it is reasonable to presume that the presence of water may promote the formation of anomeric hemiketals, and the molecular sieves are necessary to suppress these potential racemic pathways.

In addition to exploring solvent and temperature, a variety of other chiral phosphoric acids were also explored. The 3,5-bistrifluoromethylphenylated CPA (*R*)-**51** boasts higher acidity than (*S*)-**20**, however (*R*)-**51** only gave 16% ee of **50** in pentane at room temperature.

The 9-anthryl (*S*)-**52** and adamantylated (*R*)-**53** provided vastly different steric environments, yet only gave 1% ee and 43% ee, respectively. Finally, (*R*)-**54** was screened to determine if the BINOL background of the phosphoric acid catalyst was optimal, however VAPOL only produced **50** in 23% ee. Though all of the chiral phosphoric acids screened were able to catalyze the reaction in pentane, the initially chosen (*S*)-**20** catalyst was determined to illicit the highest level of stereocontrol during spiroketalization.

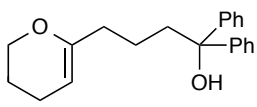
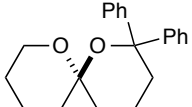
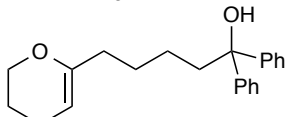
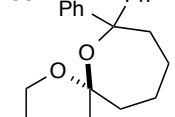
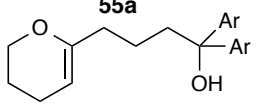
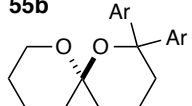
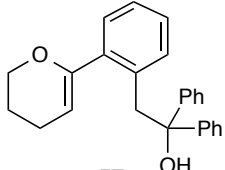
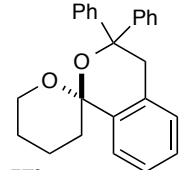
2.3 Substrate Scope of the Enantioselective Spiroketalization Reaction

Following identification of the optimal conditions, the scope of the reaction was explored. Dr. Sun observed enantioselectivities were unaffected by tether length; spiroketalization precursor **55a** was cyclized to **55b** in 94% ee. The reaction also proved to be amendable to alterations of electron density within the substrate as evidenced by the spiroketalization of **56a** to **56b**. Substitution along the alcohol tether was also shown to be well tolerated by the reaction, **57a** to **57b** (Table 2.2).³ In all of these cases, reactions were observed to be high yielding and to proceed with enantioselectivities above 90%.

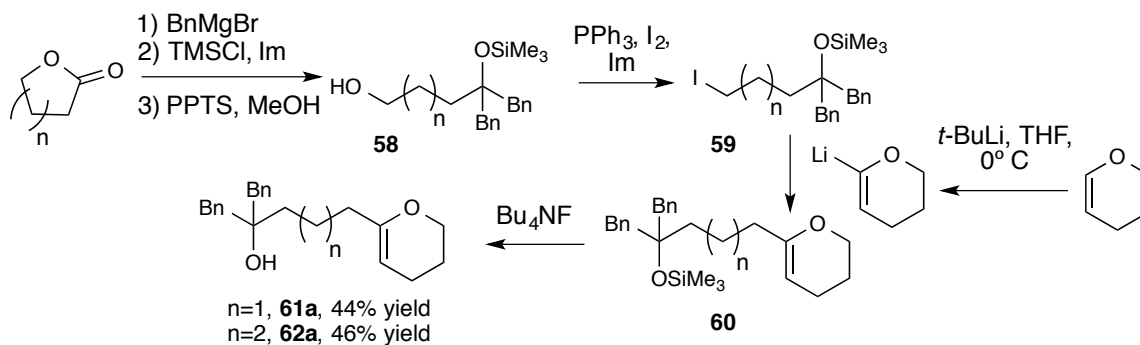
Concomitantly with the spiroketalizations carried out by Dr. Sun, additional substrates of interest were synthesized to explore further structural modifications. Primarily, these substrates were designed to illustrate how substitution on the hydroxy nucleophile affects the stereospecificity of the spiroketalization reaction.

³ The spiroketalizations in Table 2.2 were performed by Dr. Zhankui Sun and Alina Borovika (**56a** to **56b**).

Table 2.2: Enantioselective spiroketalizations.

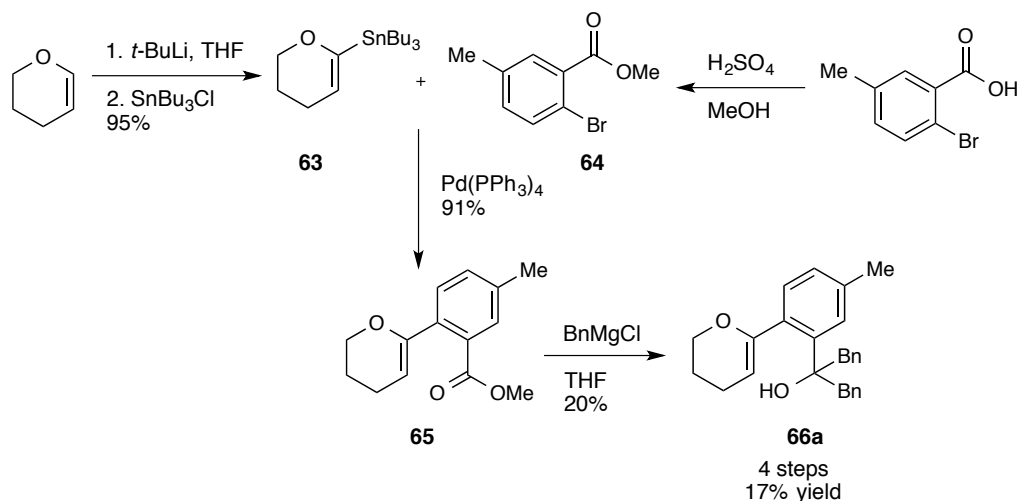
precursor	product	T, °C	time, h	yield, %	ee, %
 49	 50	-35	40	96	92
 55a	 55b	-35	48	96	94
 56a Ar = 4-(MeS)Ph	 56b	-30	22	81	93
 57a	 57b	0	24	93	96

These investigations began with the synthesis of **61a** and **62a**, which were synthesized in 44% and 46% yield, respectively, following a similar synthetic route detailed in Scheme 2.2. Primary alcohol **58** was prepared in a similar fashion to previously described spiroketalization precursors, followed by preparation and subsequent coupling of iodide **59** to lithiated dihydropyran to yield **60**. A simple deprotection using tetrabutylammonium fluoride lead to spiroketalization precursors **61a** and **62a**.³



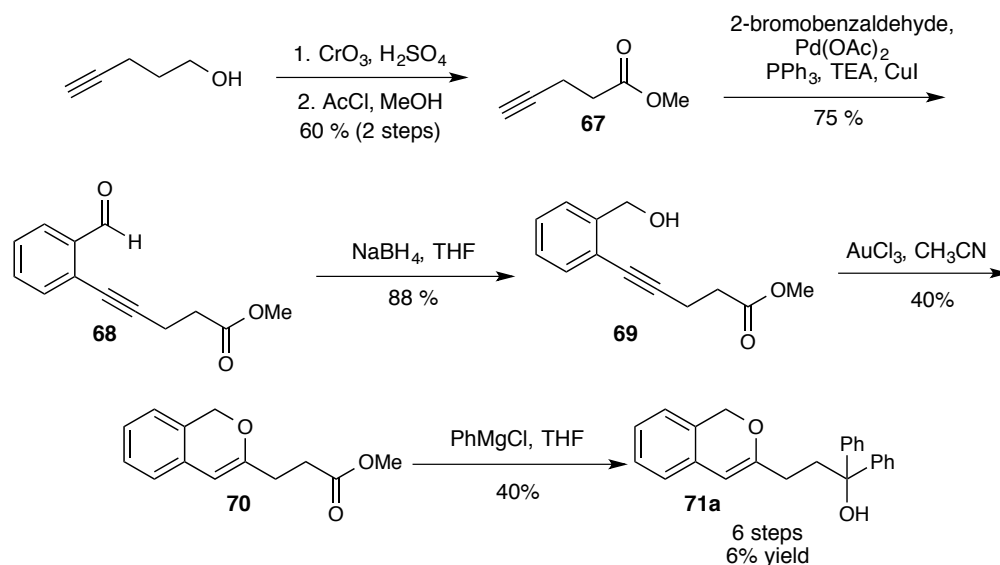
Scheme 2.2: Synthesis of 6,6-dibenzyl and 6,7-dibenzyl precursors **61a** and **62a**.

To determine whether the spiroketalization reaction would proceed with the same selectivity with additional substitution on the tether of the hydroxy nucleophile, **66a** containing a fused phenyl ring was synthesized as depicted in Scheme 2.3. Synthesis of **66a** began by converting dihydropyran to stannane **63**⁴ by lithiating with *tert*-butyl lithium and then stannylating with tributyltin chloride. Readily available 2-bromo-5-methyl benzoic acid was converted to **64** via a simple esterification reaction with H₂SO₄ and methanol.⁵ Proceeding without purification, **63** was coupled to **64** using a standard Stille coupling. A Grignard reaction of **65** with benzyl magnesium chloride completed the synthesis of **66a**, which was obtained in four steps in 17% overall yield.



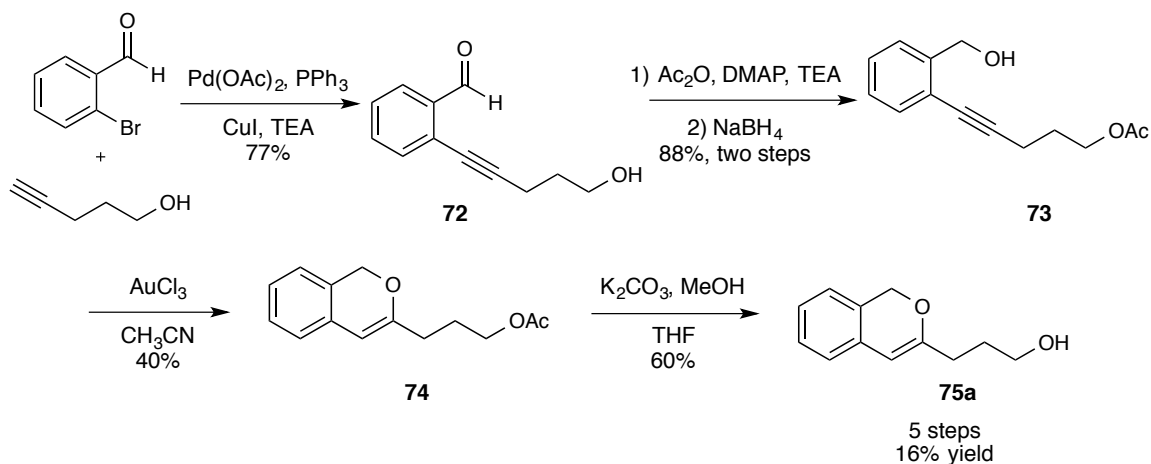
Scheme 2.3: Synthesis of a 6,5-dibenzylated spiroketalization precursor.

A dihydrobenzoisopyran scaffold was synthesized from 4-pentyn-1-ol and 2-bromobenzaldehyde (Scheme 2.4). A Jones oxidation, followed by acetylation afforded **67**, which was reacted with 2-bromobenzaldehyde via a Sonogashira coupling to give **68** in 75% yield. Reduction gave alcohol **69**. To access the desired enol ether scaffold, a 6-endo-*dig* cyclization was explored. Gold (III) chloride proved to be the most promising catalyst, giving clean conversion to **70** in dilute acetonitrile, despite modest yields.⁶ Phenyl groups were installed via a Grignard reaction to give **71a** in a 6% overall yield.



Scheme 2.4: Synthesis of **71a**, a diphenylated dihydrobenzoisopyran precursor scaffold.

In addition to the diphenylated scaffold, a primary version of this type of substrate was synthesized via a similar synthetic route (Scheme 2.5). Work on this substrate began with acetylation of the alcohol with acetic anhydride, however the subsequent Sonogashira coupling was low yielding.



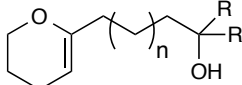
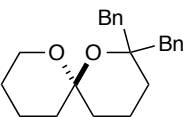
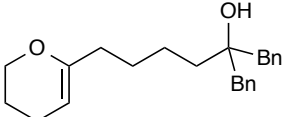
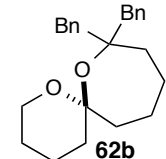
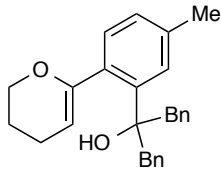
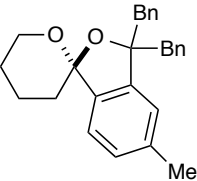
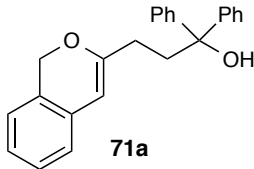
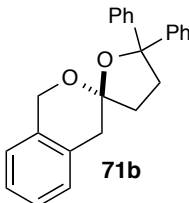
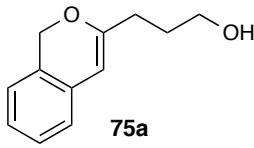
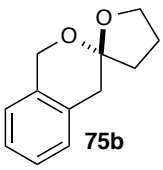
Scheme 2.5: Synthesis of **75a**, a precursor with a dihydrobenzoisopyran scaffold.

Optimization of the synthesis lead to the free alcohol being coupled to 2-bromobenzaldehyde to give **72** in 77% yield, followed by protection of the primary alcohol and

subsequent reduction of the aldehyde to give **73** in 88% yield. Gold (III) chloride afforded **74**, followed by deprotection of the primary alcohol to provide precursor **75a** in overall 16% yield.

With precursors in hand, the extended scope of the enantioselective spiroketalization reaction was evaluated (Table 2.3). Cyclization of **61a** to **61b** proceeded in 75% ee, which is in contrast to related **50**, which was cyclized from **49** with 92% ee. The dibenzylated 6,7-spiroketal **62b** was accessed in 66% ee, as compared to the 94% ee observed for the diphenylated **55b**. This reduction in enantioselectivity continued to be observed for the benzylated substrates, suggesting a decrease in steric bulk near the hydroxy nucleophile results diminished stereoselectivities.

Table 2.3: Expanded scope of the enantioselective spiroketalization.

precursor	product	T, °C	time, h	yield, %	ee, %
 61a	 61b	-35	40	82	75
 62a	 62b	-40	24	91	66
 66a	 66b	0	24	88	74
 71a	 71b	0	24	89	90
 75a	 75b	0	24	72	54

While cyclization of **66a** proceeded with moderate stereoselectivity, giving **66b** in 74% ee, consistency of this value as compared to that for **61b** suggests that though benzyl substitution results in diminished stereospecificity, the presence of the phenyl ring fused to the tether does not negatively affect the stereochemical control of the reaction. This is notable, as the spiroketalizations of **66a**, as well as **57a**, were expected to be complicated by a competing epimerization pathway. Both products, however, were obtained with ees high enough that epimerization did not seem to adversely effect the substrates.

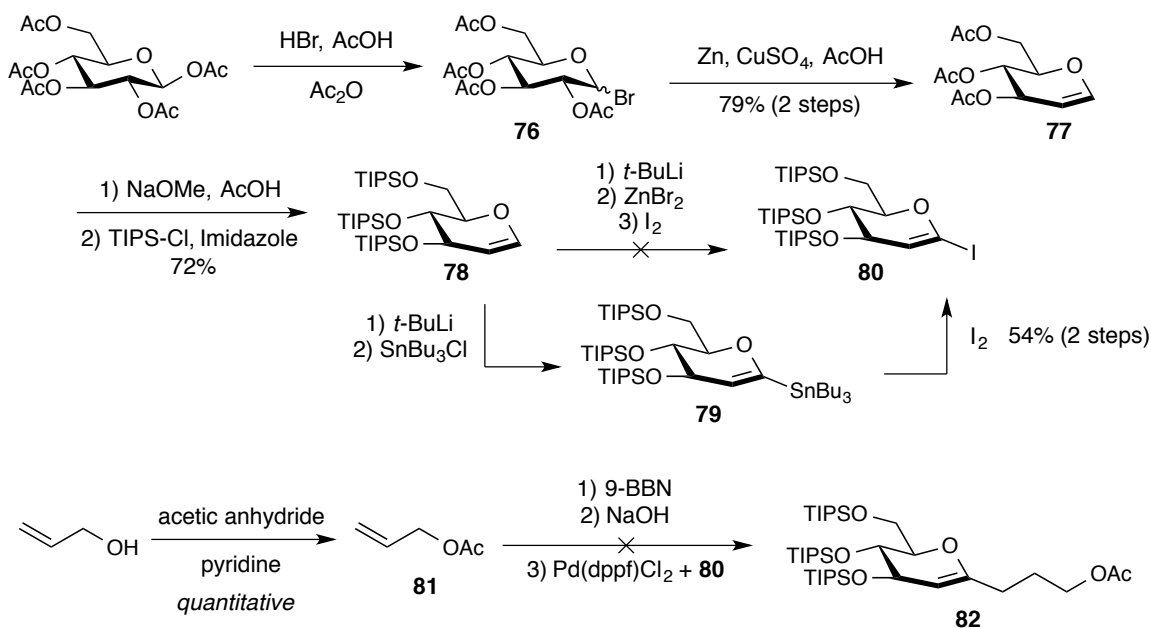
In the context of the dihydrobenzoisopyran scaffold, **71b** was produced in 90% ee, suggesting that substitution on the backbone of the DHP ring has very little effect on the stereospecificity of the reaction. However, a complete lack of substitution on the hydroxy nucleophile resulted in significantly diminished enantioselectivities, with primary alcohol **75a** spiroketalizing with only 54% ee.

Despite the reduction in enantioselectivities as compared to the diphenylated substrates, the less-rigid dibenzylated spiroketals synthesized were readily accessed in moderate enantioselectivities and respectable yields. Notably, though the reaction proved sensitive to a decrease in steric bulk on the hydroxy nucleophile, substitution on the tether, as well as on the dihydropyran moiety did not appear to adversely effect the level of stereocontrol for the CPA-catalyzed enantioselective spiroketalization reaction.

2.4 Development of a Diastereoselective Approach to Kinetic Spiroketal

While we have demonstrated that spiroketals could be obtained in an enantioselective manner from achiral starting materials, we were also interested in determining whether the inherent chirality of a molecule could override the stereoselectivity of the established spiroketalization reaction. In this vein, the synthesis of glycal-derived enol ethers was investigated (Scheme 2.6).

Devising a route to grant synthetic access to the glycal enol ethers began with functionalization of the C1 position of peracetylated glucose to the bromide with HBr to give **76**, which then underwent a zinc-mediated elimination to form glucal **77** in 79% yield.⁷ Conversion of the acetyl groups to TIPS groups proceeded via a deprotection with sodium methoxide and reprotection with TIPS-Cl, which gave **78** in 72% yield.



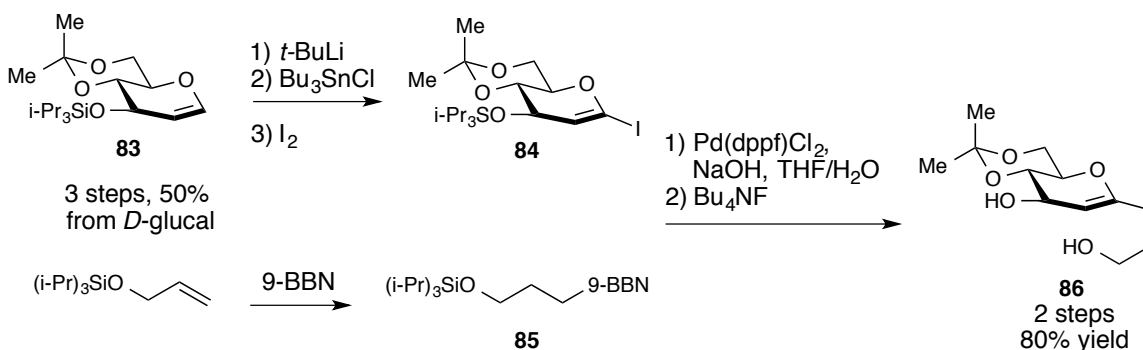
Scheme 2.6: Initial synthetic route to glycal-derived enol ethers.

First attempts at synthesizing the iodide using *tert*-butyl lithium, zinc (II) bromide and iodine did not allow access to **80** in synthetically useful yields. Revision of the synthetic route led to the synthesis of stannane **79** first,⁸ followed by conversion to the iodide. Though this protocol allowed for access to **80**, both the stannane and the iodide proved to be extremely unstable, thus both protocols had to be carried out in the dark and intermediates had to be subjected to the next step immediately due to their propensities to decompose.

Thus, concomitantly with the execution of the stannane/iodide synthetic sequence, allyl alcohol was protected to give **81**, which was boronated with 9-BBN and subjected to a Suzuki coupling with iodide **80** using Pd(dppf)Cl₂.⁹ Unfortunately, enol ether **82** was only observed in trace amounts, likely due to the instability of the iodide to the reaction conditions. In order to carry out the desired Suzuki coupling, a final synthetic revision was made to grant a higher level of stability to the iodide to prevent decomposition prior to the formation of the desired glycal enol ether (Scheme 2.7).

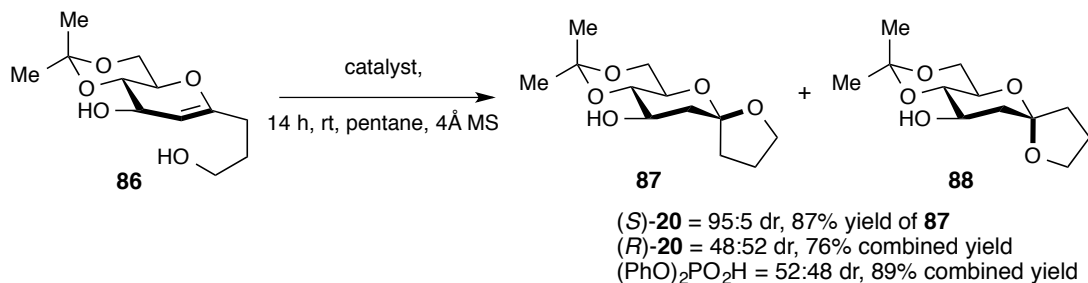
In the fully revised synthesis, the C4 and C6 oxygens of the glycal were tied back into an acetonide, providing additional structural rigidity to the system, **83**. The previously used acetyl-protected allyl alcohol was exchanged for a TIPS variant, which underwent borylation with 9-BBN to give boronate **85** prior to the coupling reaction. These small synthetic revisions allowed for iodide **84** to be synthesized in almost quantitative yields, though the iodination, as well as the

subsequent Suzuki coupling, again had to be carried out in the dark to prevent iodide decomposition. Despite this inherent instability, the presence of the acetonide allowed for glycal-derived enol ether **86** to be prepared in synthetically useful yields, allowing for the study of a diastereoselective spiroketalization reaction.⁴



Scheme 2.7: Revised synthesis of glycal-derived enol ethers.

These enol ethers were exposed to both (*S*)- and (*R*)-**20**, as well as diphenyl phosphoric acid to give spiroketals **87** and **88** (Scheme 2.8). Though these spiroketalizations were performed by Dr. Sun, an example is given to illustrate the utility of the stereoselective spiroketalization reaction discussed in this chapter. Upon exposure to (*S*)-**20**, enol ether **86** underwent a highly diastereoselective spirocyclization, yielding nonthermodynamic spiroketal **87** in 87% yield and in 95:5 dr. Exposure of **86** to (*R*)-**20** gave a 48:52 mixture of **87** to **88** with a combined yield of 76%, while diphenyl phosphoric acid produced a 52:48 mixture of **87** to **88** with a yield of 89%. Prolonged exposure to diphenyl phosphoric acid resulted in complete isomerization of **87** to **88**.



Scheme 2.8: An example of the diastereoselective spiroketalization reaction.

⁴ The studies summarized in Schemes 2.7 and 2.8 were performed by Dr. Sun.

Modifications to the structure of **86**, including lengthening of the tether, installation of a chiral center on the tether, as well as acetylation and methylation of the C3 hydroxyl group were performed, and with the methylated C3-hydroxyl substrate as an exception, the nonthermodynamic spiroketal was able to be obtained in high diastereoselectivity for each structural modification. Although it is unclear why the methylated substrate was unable to selectively cyclize to give the desired nonthermodynamic spiroketal configuration, a higher propensity for this substrate to epimerize was not observed. It is therefore possible that the free C3 hydroxyl group, as well as the acetylated variant are somehow involved in the transition state of the reaction, resulting in the overall favorability of the cyclization to proceed through to the nonthermodynamic spiroketal.

The absolute configuration of **87**, as well as that of spiroketal **56b** were confirmed via X-ray crystallography (Figure 2.1). Both spiroketals exhibited stereochemistry that could be correlated with the stereochemistry of the CPA utilized.



Figure 2.1: X-ray crystal structures of spiroketals **56b** and **87**.

Consequently, employment of (*R*)-**20** promoted nucleophilic attack directed to give the (*S*)-enantiomer of **56a**, (*S*)-**20** promoted attack from the *Si* face of **87**. Though these reactions are often proposed to involve the intermediacy of a reactive oxocarbenium ion intermediate,¹⁰⁻¹⁸ this type of directed attack seems to suggest that the phosphoric acid catalysts are acting in a bifunctional nature, coordinating the hydroxy nucleophile and delivering the acidic proton from the same face of the molecule. A more in depth investigation of the mechanism of this reaction follows.

2.5 Conclusions

We have developed a general, chiral phosphoric acid-mediated spiroketalization reaction yielding spiroketals with high levels of stereocontrol. The optimized protocol described has been demonstrated to be effective on a range of achiral starting materials to give spiroketals in which

the spirocenter is the only source of chirality as well as glycal-derived spiroketals, in which the chirality present in the starting material must be overridden to produce spiroketals of a nonthermodynamic nature.

While (*S*)-**20** proved to be an effective catalyst for the intramolecular addition of bulky hydroxy nucleophiles to the molecules' electrophilic centers, lower levels of stereocontrol were observed when the amount of steric bulk around the nucleophile was decreased. In addition, the installation of a methyl group on the C3 position of a glycal-derived substrate lead to a mixture spiroketals with lower dr than that of related substrates.

A contemporaneous study from the List group confirms that bulkier phosphoric acid catalysts may be utilized to access spiroketals with low steric bulk in higher selectivities than are achievable by the herein described methodology.¹⁹

In order to understand the lack of selectivity observed for these less rigid structures, as well as to understand the source of enantioselectivity and the mechanism of reaction additional studies, both experimental and computational investigations were undertaken. The results of this more in depth mechanistic investigation are outlined in the following chapter.

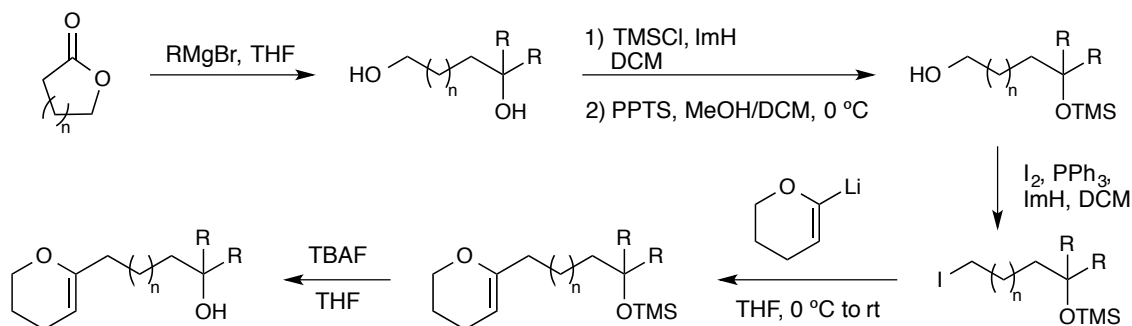
2.6 Experimental

General Methods:

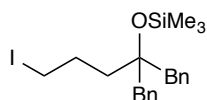
All reactions were carried out under an atmosphere of nitrogen in flame- or oven- dried glassware with magnetic stirring, unless otherwise noted. Air-sensitive reagents and solutions were transferred via syringe or cannula and were introduced to the apparatus through rubber septa. Reactions were cooled via external cooling baths: ice water (0 °C), dry ice-acetone (-78 °C), or Neslab CB 80 immersion cooler (-20 to -60 °C). Heating was achieved by use of a silicone bath with heating controlled by electronic contact thermometer. Deionized water was used in the preparation of all aqueous solutions and for all aqueous extractions. Solvents used for extraction and column chromatography were ACS or HPLC grade. Reagents were purified prior to use following the guidelines of Armarego.²⁰ Tetrahydrofuran (THF), dichloromethane (CH₂Cl₂), toluene and diethyl ether (Et₂O) were filtered through a column (Innovative Technologies) of activated alumina under nitrogen atmosphere. Purification of the reactions mixtures was performed by flash chromatography using SiliCycleSiliaFlash P60 (230-400 mesh) silica gel. Powdered 4 Å molecular sieves were pre-activated before the use. ¹H NMR spectra

were recorded on Varian vnmrs 500 (500 MHz), Varian INOVA 500 (500 MHz) or Varian MR400 (400 MHz) spectrometers and chemical shifts (δ) are reported in parts per million (ppm) with solvent resonance as the internal standard (CDCl_3 at δ 7.26, C_6D_6 at δ 7.15). Data are reported as (br = broad, s = singlet, d = doublet, t = triplet, q = quartet, qn = quintet, sext = sextet, m = multiplet; coupling constant(s) in Hz; integration). Proton-decoupled ^{13}C NMR spectra were recorded on Varian vnmrs 500 (500 MHz), Varian INOVA 500 (500 MHz) or Varian MR400 (400 MHz) spectrometers and chemical shifts (δ) are reported in ppm with solvent resonance as the internal standard (CDCl_3 at δ 77.0, C_6D_6 at δ 127.683). High resolution mass spectra (HRMS) were recorded on MicromassAutoSpecUltima or VG (Micromass) 70-250-S Magnetic sector mass spectrometers in the University of Michigan mass spectrometry laboratory. Infrared (IR) spectra were recorded as thin films on NaCl plates on a Perkin Elmer Spectrum BX FT-IR spectrometer. Absorption peaks were reported in wavenumbers (cm^{-1}). Optical rotations were measured in a solvent of choice on a JASCO P-2000 or Autopol III digital polarimeter at 589 nm (D-line) and reported as follows: $[\alpha]_{\text{D}}^{24}$ (c g/100 mL, solvent).

Synthesis of Enantioselective Spiroketalization Precursors:



Synthesis of Iodide Fragments:



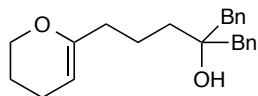
((2-benzyl-5-iodo-1-phenylpentan-2-yl)oxy)trimethylsilane (59a). γ -Butyrolactone (0.55 g, 6.4 mmol) was dissolved in THF (13 mL) and cooled to 0 °C under nitrogen. BnMgBr (6.4 mL, 3 M in Et_2O , 19.0 mmol) was added slowly. The mixture was stirred at 0 °C for 1 h and then warmed

to room temperature. The reaction was monitored by TLC and quenched with $\text{NH}_4\text{Cl}_{(\text{sat.})}$ once complete conversion was observed. The resultant mixture was extracted with EtOAc. The combined organic layers were washed with brine, dried over MgSO_4 , and then concentrated *in vacuo* to provide the crude diol as a white solid. This compound was subjected to the next step without further purification.

TMSCl (1.74 g, 16 mmol) was dissolved in DCM (13 mL) and imidazole (1.01 g, 16 mmol) was added to this solution. The resultant mixture was stirred for 2 min before the solution of the diol from the previous step in DCM (30 mL) was added. The reaction mixture was left overnight. Next morning, TLC indicated complete conversion, and the mixture was washed with brine and water, dried over MgSO_4 , and then concentrated *in vacuo* to provide colorless oil. This product was dissolved in DCM (50 mL) and methanol (10 mL), and the resultant mixture was cooled to 0 °C before catalytic quantities of PPTS (25 mg, 0.1 mmol) was added. The reaction was typically stirred for 0.5–1.5 h before being quenched by the addition of triethylamine (50 μL) followed by brine. The product was extracted with EtOAc. The organic layer was washed with brine, dried over MgSO_4 , and then concentrated *in vacuo*. The resultant product **58** was stored under reduced pressure (overnight) before being used in the next step without further purification.

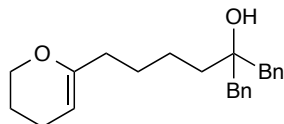
The alcohol **58** from above was dissolved in DCM (32 mL) and cooled to 0 °C. Iodine (1.95 g, 7.7 mmol) and imidazole (0.52 g, 7.7 mmol) were added. PPh_3 (2 g, 7.7 mmol) were added slowly. The mixture was then stirred at room temperature for 30 min. Saturated solutions of sodium thiosulfate (50 mL) and sodium bicarbonate (50 mL) were added to the reaction mixture. The organic phase was separated and the aqueous phase was extracted with methylene chloride. The combined organic layers were washed with brine, dried over MgSO_4 , and then concentrated *in vacuo*. The mixture was purified by column chromatography (1% EtOAc/hexanes) to provide the desired iodide **59a** (1.05 g, 2.3 mmol) in 36% yield (4 steps, unoptimized) from γ -butyrolatone (0.55 g, 6.4 mmol). ^1H NMR (400 MHz, CDCl_3) δ 7.32-7.22 (m, 10H), 3.14 (t, J = 7.2 Hz, 2H), 2.79 (d, J = 2.8 Hz, 4H), 2.07-2.01 (m, 2H), 1.53-1.49 (m, 2H), 0.06 (s, 9H); ^{13}C NMR (100 MHz, C_6D_6) δ 137.7, 130.9, 127.8, 126.3, 78.5, 45.7, 39.5, 29.0, 6.9, 2.7. HRMS (ES) m/z calcd for $\text{C}_{20}\text{H}_{26}\text{IOSi}^+$ $[\text{M}-\text{CH}_3]^+$ 437.0798, found 437.0801. IR (thin film, cm^{-1}) 2952, 1495, 1453, 1249, 1091.

Synthesis of Spiroketalization Precursors:



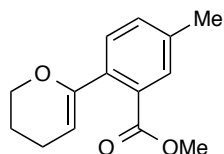
2-benzyl-5-(3,4-dihydro-2H-pyran-6-yl)-1-phenylpentan-2-ol (61a). 3,4-Dihydropyran (84 mg, 1.0 mmol) was dissolved in THF (5 mL) and cooled to $-78\text{ }^{\circ}\text{C}$ under nitrogen. *Tert*-butyl lithium (0.6 mL, 1.7 M in pentane, 1.02 mmol) was added. The mixture was warmed up to $0\text{ }^{\circ}\text{C}$ and stirred for 1 h. To this, the solution of iodide **59** (141 mg, 0.3 mmol) in THF (2 mL) was added. The mixture was warmed up to the room temperature. The reaction was stirred until the complete conversion was detected by TLC (typically 3–4 h) and was quenched with saturated NH_4Cl solution. The resultant mixture was extracted with EtOAc. The organic layer was separated and washed with brine, dried over MgSO_4 , and concentrated *in vacuo* to provide the product as colorless oil.³

The crude product was dissolved in THF (10 mL) and the resultant solution was cooled to $0\text{ }^{\circ}\text{C}$. To this, TBAF (0.5 mL, 1 M in THF) was added. The reaction mixture was stirred for 0.5 h until complete conversion was achieved. The reaction mixture was diluted with brine (10 mL) and EtOAc (50 mL). The organic layer was washed with a mixture of brine and water (1:1) (20 mL x 3), dried over MgSO_4 , and concentrated *in vacuo* to provide crude **61a**. The resultant mixture was purified by column chromatography. The column chromatography was performed as follows: silica was pre-neutralized with 1% solution of triethylamine in 9% EtOAc/hexanes and wet-loaded to the column. Same solution was used to load and elute **61a**. This procedure provided pure **61a** (208 mg, 0.62 mmol) in 62% (2 steps) from the iodide as a colorless oil. ^1H NMR (500 MHz, C_6D_6) δ 7.17-7.04 (m, 10H), 4.36 (t, $J = 3.5\text{ Hz}$, 1H), 3.73 (t, $J = 5.0\text{ Hz}$, 2H), 2.66 (d, $J = 2.5\text{ Hz}$, 4H), 1.95 (t, $J = 7.0\text{ Hz}$, 2H), 1.78-1.75 (m, 2H), 1.70-1.64 (m, 2H), 1.46-1.41 (m, 2H), 1.29-1.25 (m, 2H); ^{13}C NMR (125 MHz, C_6D_6) δ 154.1, 137.7, 130.8, 126.1, 95.2, 73.9, 65.6, 45.5, 37.5, 34.7, 22.4, 21.6, 20.3. HRMS (ES) m/z calcd for $\text{C}_{23}\text{H}_{29}\text{O}_2^+$ $[\text{M}+\text{H}]^+$ 337.2162, found 337.2159. IR (thin film, cm^{-1}) 2927, 1674, 1496, 1454, 1084.

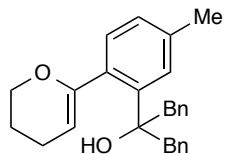


2-benzyl-6-(3,4-dihydro-2H-pyran-6-yl)-1-phenylhexan-2-ol (62a). Following the general procedure provided above, **62a** (208 mg, 0.62 mmol) was obtained in 83% (2 steps) from the iodide as a colorless oil. ^1H NMR (400 MHz, C_6D_6) δ 7.14-7.01 (m, 10H), 4.39 (t, $J = 3.7$ Hz, 1H), 3.73 (m, 2H), 2.64 (d, $J = 2.5$ Hz, 4H), 2.01 (t, $J = 6.7$ Hz, 2H), 1.80-1.76 (m, 2H), 1.50-1.29 (m, 6H), 1.28-1.15 (m, 2H); ^{13}C NMR (125 MHz, C_6D_6) δ 154.7, 137.7, 130.9, 126.3, 95.2, 75.8, 65.7, 45.7, 39.5, 34.7, 27.6, 22.2, 21.6, 20.3. HRMS (ES) m/z calcd for $\text{C}_{24}\text{H}_{30}\text{O}_2^+$ $[\text{M}+\text{H}]^+$ 350.2246, found 350.2243. IR (thin film, cm^{-1}) 2924, 1674, 1492, 1452.

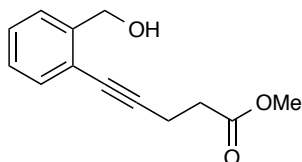
Synthesis of Structurally Diverse Substrates



Methyl 2-(3,4-dihydro-2H-pyran-6-yl)-5-methylbenzoate (65). The stannane derivative **63** (310 mg, 0.825 mmol) and ester **64** (171 mg, 0.75 mmol) were combined in solution of $\text{Pd}(\text{PPh}_3)_4$ (173 mg, 0.15 mmol) in toluene (7.5 mL) and the resultant solution was heated to reflux. After 16 h, the reaction was judged complete by TLC analysis, cooled to room temperature and the solvent was removed *in vacuo*. Purification of the crude reaction mixture by column chromatography (1% triethylamine, 13 % EtOAc/hexanes) provided **65** (158 mg, 91% yield) as a clear oil. ^1H NMR (500 MHz, C_6D_6) δ 7.49 (s, 1H), 7.28 (d, $J = 7.82$ Hz, 1H), 6.86 (d, $J = 7.82$ Hz, 1H), 5.00 (t, $J = 8.81$ Hz, 1H), 3.89 (t, $J = 5.14$ Hz, 2H), 3.61 (s, 3H), 1.91-1.98 (m, 5H), 1.52-1.62 (m, 2H); ^{13}C NMR (125 MHz, C_6D_6) δ 168.9, 153.6, 137.5, 134.8, 131.5, 131.0, 129.7, 128.6, 127.9, 99.1, 66.2, 51.2, 22.2, 20.8. HRMS (ES) m/z calcd for $\text{C}_{14}\text{H}_{17}\text{O}_3^+$ $[\text{M}+\text{H}]^+$ 233.1172; found 233.1167. IR (thin film, cm^{-1}) 2952, 2926, 2872, 2852, 1731, 1660, 1435, 1295, 1204, 1098, 1067.



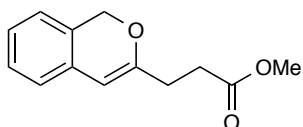
2-(2-(3,4-Dihydro-2H-pyran-6-yl)-5-methylphenyl)-1,3-diphenylpropan-2-ol (66a). Benzyl chloride (0.64 mL, 5.59 mmol) was added drop-wise to a dry flask containing Mg turnings (93 mg, 3.88 mmol), I₂ (ca. 2 mg) and freshly distilled THF (3.3 mL). After 1 h, the ester **65** (76 mg, 0.33 mmol) was added to the reaction flask. After 4 h the reaction was quenched with NH₄Cl_(sat.). The product was extracted with EtOAc, dried over MgSO₄, filtered, and concentrated *in vacuo*. Purification of the crude mixture by column chromatography (1% triethylamine in 11% EtOAc/hexanes) resulted in **66a** (25 mg, 20% yield) as a clear oil. ¹H NMR (500 MHz, C₆D₆) δ 7.14-7.20 (m, 6H), 7.05-7.09 (m, 4H), 7.00-7.03 (m, 2H), 6.78 (d, *J* = 7.68 Hz, 1H), 4.32 (t, *J* = 3.65 Hz, 1H), 3.73 (t, *J* = 5.14 Hz, 2H), 3.55 (d, *J* = 13.4 Hz, 2H), 3.29 (d, *J* = 13.4 Hz, 2H), 2.05 (s, 3H), 1.75 (td, *J* = 3.84, 6.38 Hz, 2H), 1.55 (s, 1H), 1.42-1.47 (m, 2H); ¹³C NMR (125 MHz, C₆D₆) δ 156.1, 144.3, 138.1, 133.6, 132.8, 131.4, 129.0, 127.9, 127.2, 126.4, 100.1, 79.0, 66.3, 48.9, 22.0, 21.3, 20.8; HRMS (ES) *m/z* calcd for C₂₇H₂₉O₂⁺ [M+H]⁺ 385.2162; found 385.2162. IR (thin film, cm⁻¹) 3584, 2926, 1496, 1453, 1286, 1061, 915, 826, 744, 699.



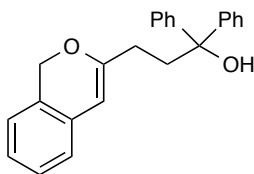
Methyl 5-(2-(hydroxymethyl)phenyl)pent-4-ynoate (69). To a solution of Pd(PPh₃)₄ (57 mg, 0.05 mmol) and CuI (19.0 mg, 0.10 mmol) in triethylamine (10 mL) 2-bromobenzaldehyde (925 mg, 5 mmol) was added. The mixture was cooled to 0 °C and stirred for 5 min. Methyl pent-4-ynoate (448 mg, 4.0 mmol) was slowly added. The mixture was warmed up to 50 °C and stirred for 6 h. The resulting mixture was filtered through a short pad of Celite and filtrate was concentrated *in vacuo* to remove triethylamine.

The residue was dissolved in MeOH (10 mL) and to this, NaBH₄ (304 mg, 8.0 mmol) was added in small portions. The reaction was stirred for 0.5 h, quenched with NH₄Cl_(sat.), and the resultant mixture was extracted with EtOAc. The organic layers were combined, washed with brine, dried over MgSO₄, and concentrated *in vacuo*. The residue was purified by column chromatography

(20% EtOAc/hexanes) to provide **69** (652 mg, 74% yield). ^1H NMR (500 MHz, C_6D_6) δ 7.44 (d, $J = 8.0$ Hz, 1H), 7.35 (d, $J = 7.5$ Hz 1H), 7.05 (t, $J = 8.0$ Hz, 1H), 6.92 (t, $J = 8.0$ Hz, 1H), 4.81 (d, $J = 5.5$ Hz, 2H), 3.49 (br, 1H), 3.30 (s, 3H), 2.41 (t, $J = 7.5$ Hz, 2H), 2.20 (t, $J = 7.0$ Hz, 2H); ^{13}C NMR (100 MHz, C_6D_6) δ 172.0, 143.5, 131.7, 126.7, 126.7, 121.4, 93.1, 79.0, 63.1, 51.1, 33.0, 15.2. HRMS (ES) m/z calcd for $\text{C}_{13}\text{H}_{15}\text{O}_3^+$ $[\text{M}+\text{H}]^+$ 219.1016, found 219.1018. IR (thin film, cm^{-1}) 2948, 1732, 1488, 1224, 1057.

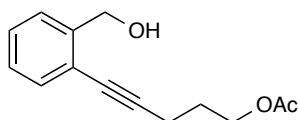


Methyl 3-(1H-isochromen-3-yl)propanoate (70). Compound **69** (545 mg, 2.50 mmol) was dissolved in CH_3CN (25 mL). To this solution, AuCl_3 (38.0 mg, 0.125 mmol) was added, and the resultant mixture was stirred at rt for 6 h. The solvent was removed *in vacuo* and the mixture was loaded on the column directly (1% of triethylamine in 9% EtOAc/hexanes) to provide pure **70** (245 mg, 45% yield). ^1H NMR (400 MHz, C_6D_6) δ 6.97 (t, $J = 7.2$ Hz, 1H), 6.86 (t, $J = 7.6$ Hz 1H), 6.71 (d, $J = 7.6$ Hz, 1H), 6.54 (d, $J = 7.2$ Hz, 1H), 5.45 (s, 1H), 4.71 (s, 2H), 3.26 (s, 3H) 2.39-2.35 (m, 2H), 2.33-2.29 (m, 2H); ^{13}C NMR (100 MHz, C_6D_6) δ 172.0, 156.6, 131.7, 125.7, 123.5, 122.5, 101.4, 68.4, 50.7, 31.3, 28.9. HRMS (ES) m/z calcd for $\text{C}_{13}\text{H}_{15}\text{O}_3^+$ $[\text{M}+\text{H}]^+$ 219.1016, found 219.1018. IR (thin film, cm^{-1}) 3364, 1734, 1163, 1069.



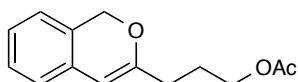
3-(1H-isochromen-3-yl)-1,1-diphenylpropan-1-ol (71a). Ester **70** (109 mg, 0.50 mmol) was dissolved in dry THF (5 mL) and cooled to 0 °C. To this, PhMgBr (0.5 mL, 3 M in Et_2O , 1.5 mmol) was added slowly. The resultant mixture was stirred at 0 °C for 1 h and then warmed to room temperature. The reaction was stirred for 2 h before being quenched with $\text{NH}_4\text{Cl}_{(\text{sat.})}$ and extracted with EtOAc. The organic layer was washed with brine, dried over MgSO_4 , and then concentrated *in vacuo*. The mixture was purified by column chromatography (1% of triethylamine in 10% EtOAc/hexanes) to provide pure **71a** (154 mg, 90 % yield). ^1H NMR (500 MHz, C_6D_6) δ 7.37-7.35 (m, 4H), 7.13-7.03 (m, 4H), 7.02-6.97 (m, 3H), 6.92-6.91 (m, 1H), 6.77

(d, $J = 7.5$ Hz, 1H), 6.61 (d, $J = 7.5$ Hz, 1H), 5.45 (s, 1H), 4.78 (s, 2H), 2.46-2.43 (m, 2H), 2.26-2.22 (m, 2H), 1.65 (s, 1H); ^{13}C NMR (125 MHz, C_6D_6) δ 158.7, 147.0, 132.1, 128.0, 127.9, 127.8, 127.7, 127.6, 127.5, 127.4, 127.1, 126.6, 126.1, 125.5, 123.5, 122.3, 101.0, 77.3, 68.5, 39.4, 28.5. HRMS (ES) m/z calcd for $\text{C}_{24}\text{H}_{23}\text{O}_2^+$ $[\text{M}+\text{H}]^+$ 343.1693, found 343.1691. IR (thin film, cm^{-1}) 2944, 1713, 1494, 1220, 1053, 1017.

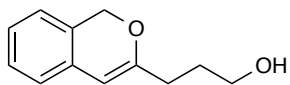


5-(2-(hydroxymethyl)phenyl)pent-4-yn-1-yl acetate (73). To a solution of $\text{Pd}(\text{OAc})_2$ (10.1 mg, 0.45 mmol), PPh_3 (23.6 mg, 0.9 mmol) and CuI (17.1 mg, 0.9 mmol) in triethylamine (10 mL) 2-bromobenzaldehyde (0.53 mL, 4.5 mmol) was added. The mixture was cooled to 0°C and stirred for 5 min. 4-Pentyn-1-ol (0.5 mL, 5.4 mmol) was slowly added. The mixture was warmed up to 80°C and stirred for 12 h. The resulting mixture was filtered through a short pad of Celite and redissolved in DCM (34 mL) and cooled to 0°C . Triethylamine (0.96 mL, 6.89 mmol), DMAP (84.2 mg, 0.69 mmol) and acetic anhydride (0.64 mL, 6.89 mmol) were added and the reaction was run for 30 minutes at 0°C and then at room temperature for 2.5 hours. The reaction was quenched with NaHCO_3 , extracted with ether, washed with water and brine, dried over MgSO_4 , filtered and concentrated *in vacuo*.

The residue was dissolved in THF (6 mL) and water (3 mL) and to this, NaBH_4 (61 mg, 1.62 mmol) was added in small portions. The reaction was stirred for 10 minutes, after which 3 mL of H_2O was added and stirred for an additional 5 minutes. The reaction was extracted with DCM, dried over MgSO_4 , and concentrated *in vacuo*. The residue was purified by column chromatography (20% EtOAc/hexanes) to provide **73** (700 mg, 67% yield). ^1H NMR (500 MHz, CDCl_3) δ 7.41 (dd, $J = 1.48, 6.19$ Hz, 2H), 7.30 (td, $J = 7.5, 1.25$ Hz 1H), 7.24-7.20 (m, 1H), 4.74 (d, $J = 6.36$ Hz, 2H), 4.25 (t, $J = 6.36$ Hz, 1H), 2.56 (t, $J = 7.0$ Hz, 2H), 2.07 (s, 3H), 1.98-1.89 (m, 2H).



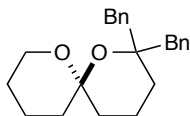
Methyl 3-(1H-isochromen-3-yl)propanoate (74). Compound **73** (194 mg, 0.84 mmol) was dissolved in CH₃CN (6.7 mL). To this solution, AuCl₃ (12.7 mg, 0.04 mmol) was added, and the resultant mixture was stirred at rt for 12 h. The solvent was removed *in vacuo* and the mixture was loaded on the column directly (1% of triethylamine in 9% EtOAc/hexanes) to provide pure **74** (76 mg, 40% yield). ¹H NMR (400 MHz, CDCl₃) δ 7.20-7.17 (m, 1H), 7.10 (t, *J* = 7.5 Hz, 1H), 6.98 (d, *J* = 7.4 Hz, 1H), 6.92 (d, *J* = 7.5 Hz, 1H), 5.67 (s, 1H), 4.13 (s, 2H), 2.28 (t, *J* = 7.4, 2H), 2.04 (s, 3H), 1.94-1.88 (m, 2H); ¹³C NMR (100 MHz, CDCl₃) δ 171.1, 157.3, 131.7, 128.1, 127.1, 125.9, 123.7, 122.4, 101.5, 68.7, 63.8, 30.2, 26.1, 20.9. HRMS (ES) *m/z* calcd for C₁₄H₁₆O₃⁺ [M+H]⁺ 232.1099, found 232.1096.



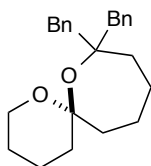
3-(1H-isochromen-3-yl)propan-1-ol (75a). Ester **74** (76 mg, 0.33 mmol) was dissolved in dry THF (2 mL) and MeOH (2 mL). To this, K₂CO₃ (90.6 mg, 0.66 mmol) was added slowly. The resultant mixture was stirred 4 h and then diluted with ether, filtered through celite, dried over MgSO₄, and then concentrated *in vacuo*. The mixture was purified by column chromatography (1% of triethylamine in 10% EtOAc/hexanes) to provide pure **75a** (36.4 mg, 58 % yield). ¹H NMR (500 MHz, C₆D₆) δ 7.16-7.05 (m, 1H), 6.97-6.83 (m, 1H), 6.77 (d, *J* = 7.47 Hz, 1H), 6.59 (d, *J* = 7.35 Hz, 1H), 5.49 (s, 1H), 4.76 (s, 2H), 3.31 (t, *J* = 6.21 Hz, 2H), 2.13 (t, *J* = 7.37 Hz, 2H), 1.59-1.46 (m, 2H); ¹³C NMR (125 MHz, C₆D₆) δ 158.2, 132.1, 125.6, 123.5, 122.3, 121.3, 110.0, 101.3, 68.4, 61.5, 59.7, 30.0. HRMS (ES) *m/z* calcd for C₁₂H₁₄O₂⁺ [M+H]⁺ 190.0994, found 190.0091.

General Procedure for Enantioselective Spiroketalization.

The starting material (0.1 mmol), 4 Å molecular sieves (100 mg) and (*S*)-**20** (0.005 mmol) were added to a 10 mL round bottom flask. The mixture was cooled to -78 °C and stirred for 5 min before 5 mL of pentane was added. The mixture was stirred for 5 min before it was warmed up to -35 °C. The mixture was stirred for certain time and triethylamine was added to quench the reaction. The mixture was loaded on the column (which was pre-saturated with triethylamine) directly and purified.

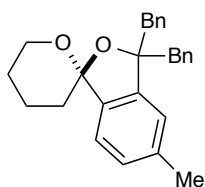


2,2-dibenzyl-1,7-dioxaspiro[5.5]undecane (61b). Compound **61a** (21.0 mg, 0.063 mmol), (*R*)-**20** (2.3 mg, 0.0031 mmol) and 4 Å molecular sieves (100 mg) were added to a 10 mL round bottom flask. The mixture was cooled to $-78\text{ }^{\circ}\text{C}$ and stirred for 5 min before 5 mL of pentane was added. The mixture was stirred for 5 min before it was warmed up to $-35\text{ }^{\circ}\text{C}$. The mixture was stirred for 44 h, quenched with triethylamine and warmed up to rt. The mixture was loaded on the column (pre-equilibrated with 1% of triethylamine in 10% EtOAc/hexanes) and purified to provide spiroketal **61b** as a white crystalline product. (17.4 mg, 82% yield, 75% ee). $[\alpha]_{\text{D}}^{24} = +5.5$ (c 0.65, DCM). $^1\text{H NMR}$ (400 MHz, C_6D_6) δ 7.15-7.02 (m, 10H), 4.00 (d, $J = 13.0$ Hz, 1H), 3.93 (t, $J = 11.5$ Hz, 1H), 3.51 (dd, $J = 4.0, 9.0$ Hz, 1H), 2.93 (d, $J = 13.5$ Hz, 1H), 2.87 (d, $J = 13.0$ Hz, 1H), 2.59 (d, $J = 13.5$ Hz, 1H), 2.23-2.20 (m, 1H), 2.07-2.03 (m, 1H), 1.64 (d, $J = 13.5$ Hz, 1H), 1.57 (t, $J = 14.5$ Hz, 2H), 1.46-1.41 (m, 2H), 1.33-1.25 (m, 2H), 1.22-1.18 (m, 1H), 1.07 (dt, $J = 4.0, 13.5$ Hz, 1H), 0.87 (dt, $J = 4.0$ Hz, 13.0 Hz, 1H); $^{13}\text{C NMR}$ (125 MHz, C_6D_6) δ 139.1, 138.2, 131.4, 130.8, 127.9, 127.9, 127.3, 126.0, 125.8, 95.8, 77.6, 60.7, 46.3, 43.9, 37.5, 36.0, 27.6, 25.7, 19.1, 15.1. HRMS (ES) m/z calcd for $\text{C}_{23}\text{H}_{29}\text{O}_2^+$ $[\text{M}+\text{H}]^+$ 337.2162, found 337.2159. HPLC DAICEL CHIRALPAK AD-H, hexane/2-propanol = 100/0, flow rate: 1 mL/min, $t(\text{major}) = 8.3$ min, $t(\text{minor}) = 9.7$ min, ee = 75%. IR (thin film, cm^{-1}), 2939, 1495, 1453, 1047, 991.



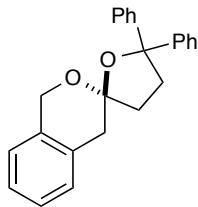
2,2-dibenzyl-1,7-dioxaspiro[5.5]undecane (62b). Compound **62a** (23.6 mg, 0.067 mmol), (*R*)-**20** (2.5 mg, 0.003 mmol) and 4 Å molecular sieves (100 mg) were added to a 10 mL round bottom flask. The mixture was cooled to $-78\text{ }^{\circ}\text{C}$ and stirred for 5 min before 5 mL of pentane was added. The mixture was stirred for 5 min before it was warmed up to $-40\text{ }^{\circ}\text{C}$. The mixture was stirred for 48 h, quenched with triethylamine and warmed up to rt. The mixture was loaded on the column (pre-equilibrated with 1% of triethylamine in 10% EtOAc/hexanes) and purified to provide spiroketal **62b** as a white crystalline product. (21.3 mg, 91% yield, 66% ee). $^1\text{H NMR}$

(500 MHz, C₆D₆) δ 7.25-7.06 (m, 10H), 3.50 (d, *J* = 13.5 Hz, 1H), 3.05 (t, *J* = 13.5 Hz, 1H), 2.90 (d, *J* = 13.5 Hz, 1H), 2.72 (d, *J* = 13.5 Hz, 1H), 2.07 (m, 1H), 1.97 (m, 1H), 1.85-1.79 (m, 1H), 1.696 (m, 1H), 1.49-1.43 (m, 3H), 1.36-1.30 (m, 3H), 1.30-1.17 (m, 4H), 0.94-0.89 (m, 1H), 0.88-0.81 (m, 1H); ¹³C NMR (125 MHz, C₆D₆) δ 139.0, 138.1, 131.4, 130.6, 130.6, 130.6, 127.4, 126.2, 125.8, 95.6, 77.4, 60.4, 46.2, 43.8, 37.3, 35.8, 32.1, 27.7, 25.6, 19.1, 15.0. HRMS (ES) *m/z* calcd for C₂₄H₃₀O₂⁺ [M+H]⁺ 350.2246, found 350.2243. HPLC DAICEL CHIRALPAK OD-H, hexane/2-propanol =100/0, flow rate: 1 mL/min, *t*(major) = 17.64 min, *t*(minor) = 11.12 min, ee = 66%.

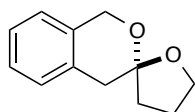


3,3-dibenzyl-5-methyl-3',4',5',6'-tetrahydro-3H-spiro[isobenzofuran-1,2'-pyran] (66b).

Compound **66a** (18.2 mg, 0.047 mmol), (*R*)-**20** (1.8 mg, 0.0024 mmol) and 4 Å molecular sieves (100 mg) were added to a 10 mL round bottom flask. The mixture was cooled to -78 °C and stirred for 5 min before 5 mL of pentane was added. The mixture was stirred for 5 min before it was warmed up to 0 °C. The mixture was stirred for 24 h, quenched with triethylamine and warmed up to rt. The mixture was loaded on the column (pre-equilibrated with 1% of triethylamine in 9% EtOAc/hexanes) and purified to provide spiroketal **66b** (16.0 mg, 88% yield, 74% ee). [α]_D²³ = +2° (*c* 0.197, CHCl₃). ¹H NMR (500 MHz, C₆D₆) δ 7.28-7.29 (m, 2H), 7.19-7.22 (m, 2H), 7.12-7.16 (m, 2H), 6.99-7.01 (m, 1H), 6.89-6.97 (m, 4H), 6.81-6.83 (m, 1H), 6.64 (m, 1H), 4.28 (ddd, *J* = 2.23, 10.87, 12.88 Hz, 1H), 3.70-3.73 (m, 1H), 3.41 (d, *J* = 13.5 Hz, 1H), 3.19 (dd, *J* = 13.6, 21.5 Hz, 2H), 3.01 (d, *J* = 13.6 Hz, 1H), 2.15 (s, 3H), 1.97-2.06 (m, 1H), 1.50-1.67 (m, 4H), 0.84 (d, *J* = 13.0 Hz, 1H); ¹³C NMR (125 MHz, C₆D₆) δ 144.7, 138.0, 137.8, 137.8, 131.5, 131.5, 129.0, 128.6, 128.5, 128.4, 126.3, 122.9, 122.3, 90.2, 63.0, 50.0, 45.0, 34.9, 25.9, 21.5, 20.0. HRMS (ES) *m/z* calcd for C₂₇H₂₉O₂⁺ [M+H]⁺ 385.2162; found 385.2160. HPLC DAICEL CHIRALPAK OJH two columns connected together, hexane/2-propanol =99/1, 1 mL/min, 210.2 nm; *t*(major) = 10.8, *t*(minor) = 14.73; 74 % ee. IR (thin film, cm⁻¹) 3027, 2919, 2838.



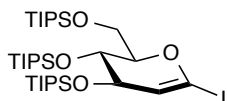
5,5-diphenyl-4,5-dihydro-3H-spiro[furan-2,3'-isochroman] (71b). Compound **71a** (34.2 mg, 0.10 mmol), (*R*)-**20** (3.8 mg, 0.005 mmol) and 4 Å molecular sieves (100 mg) were added to a 10 mL round bottom flask. The mixture was cooled to $-78\text{ }^{\circ}\text{C}$ and stirred for 5 min before 5 mL of pentane was added. The mixture was stirred for 5 min before it was warmed up to $0\text{ }^{\circ}\text{C}$. The mixture was stirred for 24 h, quenched with triethylamine and warmed up to rt. The mixture was loaded on the column (pre-equilibrated with 1% of triethylamine in 9% EtOAc/hexanes) and purified to provide spiroketal **71b**. (30.5 mg, 89% yield, 90% ee). $[\alpha]_{24\text{ D}} = -23.0$ (c 0.60, benzene). $^1\text{H NMR}$ (400 MHz, C_6D_6) δ 7.38-7.35 (m, 4H), 7.09-7.00 (m, 5H), 6.96-6.91 (m, 4H), 6.63(d, $J = 7.2$ Hz, 1H), 5.03 (d, $J = 14.8$ Hz, 1H), 4.50 (d, $J = 15.2$ Hz, 1H), 2.98 (d, $J = 16.8$ Hz, 1H), 2.94-2.88 (m, 1H), 2.81 (d, $J = 16.4$ Hz, 1H), 2.40-2.37 (m, 1H), 2.06-2.03 (m, 1H), 1.72-1.64 (m, 1H). $^{13}\text{C NMR}$ (125 MHz, C_6D_6) δ 147.6, 147.0, 134.3, 132.0, 128.5, 127.9, 127.8, 127.6, 127.5, 127.4, 126.5, 126.4, 126.2, 126.1, 125.8, 125.6, 123.9, 105.5, 89.8, 62.7, 37.6, 37.4, 36.8. HRMS (ES) m/z calcd for $\text{C}_{24}\text{H}_{23}\text{O}_2^+$ $[\text{M}+\text{H}]^+$ 343.1693, found 343.1691. HPLC DAICEL CHIRALPAK OD-H, hexane/2-propanol = 99/1, flow rate: 1 mL/min, $t(\text{major}) = 8.15$ min, $t(\text{minor}) = 12.50$ min, ee = 90%. IR (thin film, cm^{-1}) 2916, 1728, 1447, 1156, 1074, 1046, 1030.



(*R*)-4,5-dihydro-3H-spiro[furan-2,3'-isochromane] (75b). Compound **75a** (12.2 mg, 0.06 mmol), (*R*)-**20** (2.4 mg, 0.002 mmol) and 4 Å molecular sieves (100 mg) were added to a 10 mL round bottom flask. The mixture was cooled to $-78\text{ }^{\circ}\text{C}$ and stirred for 5 min before 4 mL of pentane was added. The mixture was stirred for 5 min before it was warmed up to $0\text{ }^{\circ}\text{C}$. The mixture was stirred for 24 h, quenched with triethylamine and warmed up to rt. The mixture was loaded on the column (pre-equilibrated with 1% of triethylamine in 9% EtOAc/hexanes) and purified to provide spiroketal **75b**. (8.8 mg, 72% yield, 54% ee). $^1\text{H NMR}$ (500 MHz, C_6D_6) δ 7.02-6.95 (m, 2H), 6.89-6.86 (m, 1H), 6.71-6.90 (m, 1H), 4.91 (d, $J = 14.6$ Hz, 1H), 4.56 (d, $J = 14.6$ Hz, 1H), 3.85-3.77 (m, 1H), 3.73-3.67 (m, 1H), 3.00-2.96 (m, 1H), 2.63 (d, $J = 16.3$ Hz,

1H), 2.02-1.94 (m, 1H), 1.92-1.83 (m, 1H), 1.55-1.43 (m, 2H). ¹³C NMR (125 MHz, C₆D₆) δ 135.4, 134.8, 128.0, 127.6, 125.8, 124.2, 121.5, 69.6, 64.6, 39.8, 38.9. HRMS (ES) m/z calcd for C₁₂H₁₄O₂⁺ [M+H]⁺ 190.0994, found 190.0991. HPLC DAICEL CHIRALPAK AD-H, hexane/2-propanol =100/0, flow rate: 1 mL/min, t(major) = 16.51 min, t(minor) = 10.84 min, ee = 54%.

Diastereoselective Spiroketalizations



(((2R,3R,4S)-6-iodo-2-(((triisopropylsilyloxy)methyl)-3,4-dihydro-2H-pyran-3,4-diyl)bis(oxy))bis(triisopropylsilane) (80). In the dark, stannane **79**⁸ (1.19 g, 1.32 mmol) was dissolved in methylene chloride (13.2 mL), which was pre-purged with N₂. To this, iodine (6.6 mL, 0.4 M in DCM, 2.64 mmol) was added. The mixture was stirred for 5 min before it was quenched with Na₂S₂O₃ and extracted with DCM. The combined organic layers were dried with MgSO₄ and filtered. The product was loaded on a short column (pre-equilibrated with 1% triethylamine in 9% EtOAc/hexanes) and eluted with 9% EtOAc/hexanes to afford the title compound **80**. ¹H NMR (500 MHz, C₆D₆) δ 5.62-5.57 (m, 1H), 4.71-4.64 (m, 1H), 4.44-4.34 (m, 1H), 4.33-4.29 (m, 1H), 4.20-4.11 (m, 1H), 4.11-4.04 (m, 1H), 1.19-1.15 (m, 9H) 1.11-1.05 (m, 54H).



3-((2R,3R,4S)-3,4-bis(((triisopropylsilyloxy)methyl)-3,4-dihydro-2H-pyran-6-yl)propyl acetate (82).⁹ Allyl alcohol (1 mL, 14.7 mmol) was dissolved in pyridine (4 mL) and reacted with acetic anhydride (2 mL) overnight. The reaction mixture was diluted with ethyl acetate and washed with copper sulfate. Combined organic layers were concentrated. A portion of the acetylated alcohol (1.98 mmol, 198 mg) was then dissolved in THF (15 mL). 9-BBN (10.56 mL, 0.5 M in THF, 5.28 mmol) was added and allowed to react for 3 h. 1 M NaOH (5.28 mL) was added and allowed to react for 30 minutes. Then 16 mL of this reaction mixture was added to **80** (476 mg, 0.65 mmol) in THF (4.78 mL) and H₂O (1.89 mL). To this, Pd(dppf)Cl₂ (94.3 mg, 0.13 mmol) was added. This mixture was stirred for 1 h 20 min before

being quenched with diluted with diethyl ether. The organic layer was washed with NaOH, H₂O and brine, dried over MgSO₄, and then concentrated *in vacuo*. The mixture was filtered through a short silica column (pre-equilibrated with 1% triethylamine in 9% EtOAc/hexanes), however crude **82** was not observed.

2.7 References

- (1) Corić, I.; Vellalath, S.; List, B. *J. Am. Chem. Soc.* **2010**, *132*, 8536–8537.
- (2) Sun, Z.; Winschel, G. A.; Borovika, A.; Nagorny, P. *J. Am. Chem. Soc.* **2012**, *134*, 8074–8077.
- (3) Li, G.; Kaplan, M. J.; Wojtas, L.; Antilla, J. C. *Org. Lett.* **2010**, *12*, 1960–1963.
- (4) Ghosal, S.; Luke, G. P.; Kyler, K. S. *The Journal of Organic Chemistry* **1987**, *52*, 4296–4298.
- (5) Bashore, C. G.; Samardjiev, I. J.; Bordner, J. *J. Am. Chem. Soc.* **2003**, *125*, 3268–3272.
- (6) Zhang, L.; Kozmin, S. A. *J. Am. Chem. Soc.* **2005**, *127*, 6962–6963.
- (7) Bag, B. C.; Kaushik, M. P.; Sai, M.; Vijayaraghavan, R.; Sekhar, K. An Improved Process for Production of 2-Deoxy-D-Glucose. 2004DE02075, June 19, 2009.
- (8) Dötz, K. H.; Otto, F.; Nieger, M. *Journal of Organometallic Chemistry* **2001**, *621*, 77–88.
- (9) Potuzak, J. S.; Moilanen, S. B.; Tan, D. S. *J. Am. Chem. Soc.* **2005**, *127*, 13796–13797.
- (10) Cox, D. J.; Smith, M. D.; Fairbanks, A. *J. Org. Lett.* **2010**, *12*, 1452–1455.
- (11) Corić, I.; Müller, S.; List, B. *J. Am. Chem. Soc.* **2010**, *132*, 17370–17373.
- (12) Han, Z.-Y.; Guo, R.; Wang, P.-S.; Chen, D.-F.; Xiao, H.; Gong, L.-Z. *Tetrahedron Letters* **2011**, *52*, 5963–5967.
- (13) Kim, J. H.; Corić, I.; Vellalath, S.; List, B. *Angew. Chem. Int. Ed.* **2013**, *52*, 4474–4477.
- (14) Mensah, E.; Camasso, N.; Kaplan, W.; Nagorny, P. *Angew. Chem. Int. Ed.* **2013**, *52*, 12932–12936.
- (15) Kimura, T.; Sekine, M.; Takahashi, D.; Toshima, K. *Angew. Chem. Int. Ed.* **2013**, *52*, 12131–12134.
- (16) Chen, Z.; Sun, J. *Angew. Chem. Int. Ed.* **2013**, *52*, 13593–13596.
- (17) Quach, R.; Furkert, D. P.; Brimble, M. A. *Tetrahedron Letters* **2013**, *54*, 5865–5868.
- (18) Lu, C.; Su, X.; Floreancig, P. E. *J. Org. Chem.* **2013**, *78*, 9366–9376.
- (19) Corić, I.; List, B. *Nature* **2012**, *483*, 315–319.
- (20) Armarego, W. L. F.; Chai, C. L. L. *Purification of Laboratory Chemicals*; Butterworth-Heinemann, 2013.

Chapter 3:

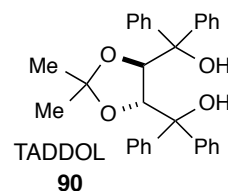
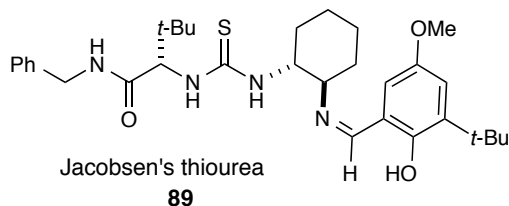
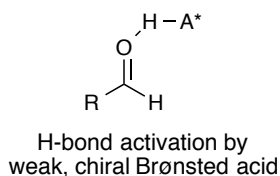
Computational and Experimental Investigations of the Stereoselective Spiroketalization Reaction Mechanism

In order to probe the mechanism of the chiral phosphoric acid-catalyzed enantioselective spiroketalization reaction discussed in Chapter 2, a joint experimental and computational venture was undertaken. Utilizing a panel of electronically diverse enol ether substrates, a Hammett study was performed to identify the amount of charge build-up in the transition state of the reaction. In addition to this, a novel deuterium-labeling study allowed for a unique view into the installation of the acidic proton from the catalyst and the internal hydroxy nucleophile addition to the enol ether. In addition to the experimental studies, a computational study was employed utilizing an automated chemical reaction methodology to compute the mechanistic pathway, as well as determine the lifetime of any oxocarbenium ion that may form within the course of the reaction. Together, these studies suggest the spiroketalization reaction to be undergoing a concerted, asynchronous cyclization, rather than operating through a stable oxocarbenium ion or chiral phosphate acetal intermediate.

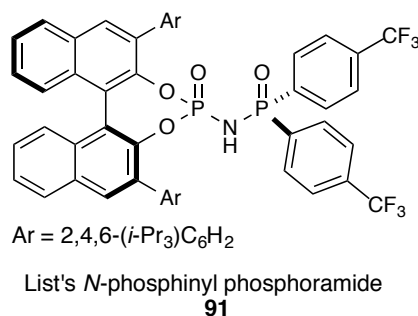
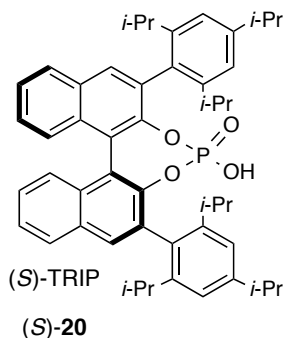
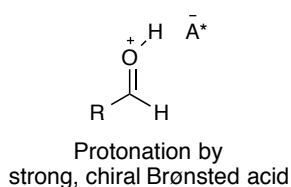
3.1 Introduction

Within the field of asymmetric Brønsted acid catalysis, a distinction can be made between weak Brønsted acids and strong Brønsted acids. Hydrogen-bonding catalysts tend to be weak Brønsted acids, which bind electrostatically through a hydrogen bond rather than operating through full proton transfer.^{1,2} Examples of this type of mode of activation are well documented, and include organocatalysts such as chiral thioureas and diols, inspired by the early observation of polar protic solvents accelerating Diels-Alder reactions. Today, weak, chiral Brønsted acids such as TADDOL **90** and Jacobsen's thiourea **89** have been utilized to carry out various asymmetric organic transformations which involve activation of electrophiles towards nucleophilic attack, Scheme 3.1a.

1a:



1b:



Scheme 3.1: Brønsted acid catalysis. 1a) Weak Brønsted acid catalysts activating through the formation of hydrogen bonds, as in, Jacobsen's thiourea and TADDOL. 1b) Strong Brønsted acid catalysts like TRIP and *N*-phosphinyl phosphoramidates fully protonate the electrophile to activate.

In contrast to weak hydrogen bond donors, strong Brønsted acids lend their acidic protons directly to the electrophile of the reaction. A fully protonated intermediate is usually either observed or proposed, followed by swift nucleophilic attack to form a chiral adduct (Scheme 3.1b). Chiral phosphoric acids **20** and **51-54**, the catalysts employed for the stereoselective spiroketalization reaction discussed in Chapter 2, fall under this category of Brønsted acid catalysts, as do more elaborate versions such as List's *N*-phosphinyl phosphoramidate **91**.³ The mechanism for this type of transformation is taught early on in an organic chemist's career. Indeed undergraduates learn the mechanism of strong Brønsted acid catalyst acetylation and spirocyclization reactions as involving full proton transfer from the acid catalyst to yield an oxocarbenium ion as a reactive, electrophilic intermediate, which then undergoes nucleophilic attack to form the desired product.

Though commonly proposed as an intermediate in many synthetic transformations,³⁻²⁰ oxocarbenium ions remain relatively unexplored for asymmetric transformations and mechanistic studies due to their high rate of reactivity and their inability to form a strong interactions with chiral catalysts. Despite these challenges, the development of stereoselective

transformations that involve additions to oxocarbenium ions is essential, as this chemistry is directly implicated in the synthesis of spiroketals and acetals, as well as glycosides and heterocyclic compounds such as tetrahydropyrans.

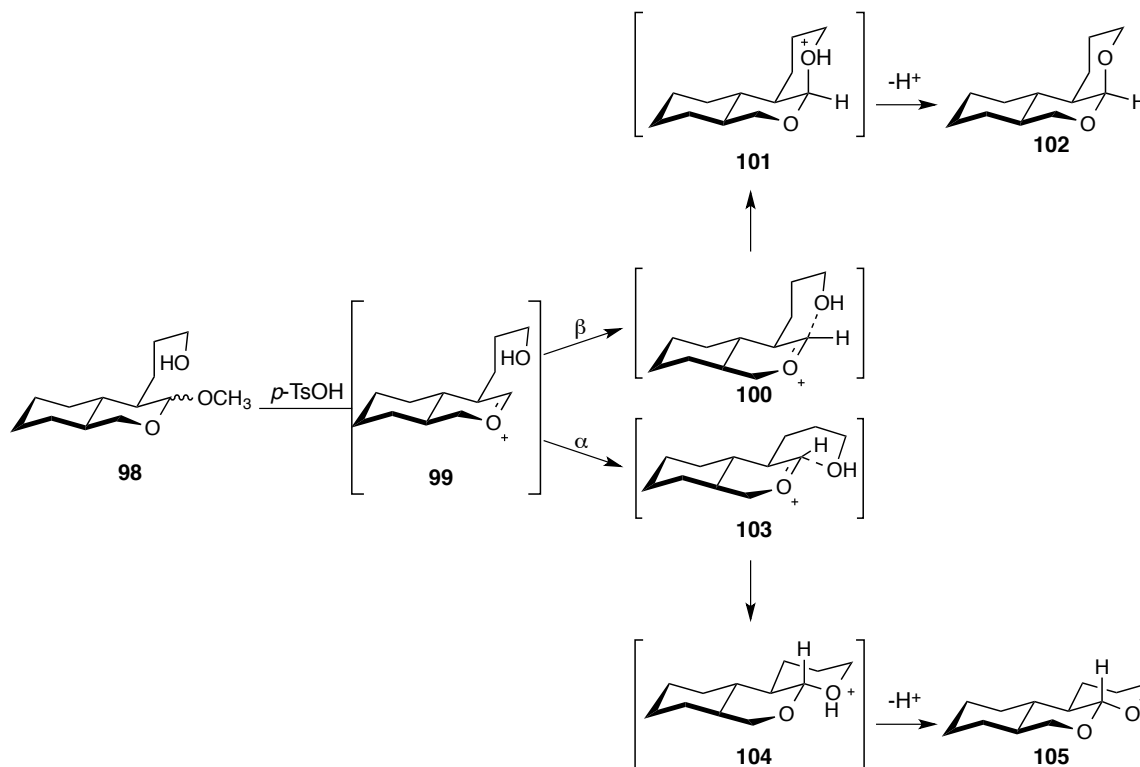
In depth studies are starting to alter the assumption that oxocarbenium species are common, stable intermediates, despite the fact that they are very commonly proposed in mechanistic musings. A thorough combing of recent literature suggests these types of reactions exist on a mechanistic continuum with a set of representative examples of the various types of mechanistic possibilities and variables herein presented.

Carbocationic organic species first sprang into discussion in the late 1800's, with the first experimental discovery of a carbocation dating back to 1891, when Merling exposed cycloheptatriene to bromine to obtain cycloheptatrienylium bromide, an aromatic ionic system. Despite the salt-like nature of the product, a cationic structure was not proposed and the first earnest discussion of a cationic species did not emerge until several years later, when Stieglitz addressed the synthetic community²¹ in 1899 with the following:

In terms of the theory of ionization chemists have accepted the positive ammonium ions R_4N^+ , whose existence is beyond any doubt, but the possibility of the existence of the positive carbon ions R_3C^+ has as yet hardly been considered or, when considered, rejected off-hand ... It would not dispose of the possibility that under certain favorable conditions we can have positive carbon ions, salts of carbon bases which are capable of stronger electrolytic dissociation. We have sulphur, phosphorus, iodine bases, etc. why not carbon bases?

In the many decades that have passed, carbocations have now come to be understood as common intermediates and transition states of organic transformations, no longer the subject of outright rejection. Discussions and preparation of oxocarbenium ions, the related ionic species in which a neighboring oxygen can donate a lone pair to a carbocationic center adding overall stability to the carbocation through resonance was not formally defined until the 1960's. While the first alkoxy-carbenium ions were generated by Meerwin in 1960,²² direct observation of these species was sparingly reported by a handful of groups that decade, and long-lived alkoxy-carbenium ions generated in acidic media from species such as **92** were not reported until the end of the decade by Olah (Scheme 3.2).²³⁻²⁵ Unlike carbocations, oxocarbenia like **93** and **94** were readily accepted into the mindsets of organic chemists and have been integrated into our

proposes a late transition state, with a geometry closer to the protonated form **101**, rather than an oxocarbenium ion, and he noted no barrier exists following protonation to suggest oxocarbenium ion formation.³⁰



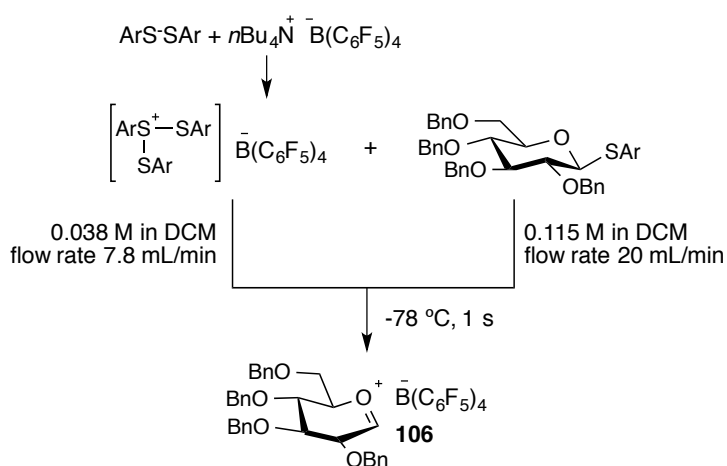
Scheme 3.4: Deslongchamps' proposed early transition state for formation of **102** from exposure of **98** to acid. Late transition state presented for formation of **105**.

Additional, related reports emerged from the Woerpel group on the conformational preferences of polysubstituted dioxocarbenium ions as explanations for stereochemical outcomes of nucleophilic additions to such species.³¹

In the few years that followed, the stability of glycosyl cations was regarded as fleeting and such species were regarded as of "borderline existence," leading Sinnott to claim, "If intimate ion pairs of glycosyl cations and anions are too unstable to exist in water, *a fortiori* they have no real existence in organic solvents and mechanistic proposals, which invoke them are simply in error."³² It seems, however, that such strong declarations questioning glycosyl oxocarbenia were overlooked and oxocarbenia of glycosyl origins have continued to be drawn in most every glycosylation mechanism since, with little regard for solvent or counter ion. A similar disregard has been paid to oxocarbenium ions of a non-glycosyl nature, however since

2010 many groups have sought to reassess the possibility of glycosyl carbocations and the prevalence of non-glycosyl-derived oxocarbenia. This work is limited to a small subset of groups within the expansive set of chemists working in the field of organic chemistry. Many continue to exploit oxocarbenia as intermediates, with glycosyl carbocations and related oxocarbenia invoked in countless mechanistic proposals without strong experimental or computational evidence for them.^{33,34}

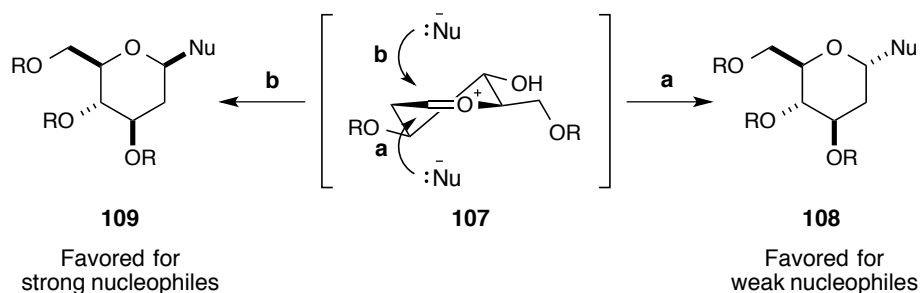
For the former case, to our knowledge, only one publication exists which provides spectroscopic data which confirms the formation of a true glycosyl oxocarbenium ion in an organic solvent. In 2011, Yoshida *et al.* utilized the formation of a tris(4-fluorophenyl)trisulfoniumtetrakis(pentafluorophenyl)borate at low temperatures to activate a thioglucofuranoside, which was then trapped with methanol to give a methyl glucopyranoside.³⁵ By utilizing flow chemistry, and cooling the reaction down to -78 °C, Yoshida was able to measure the lifetime of the tetra-*O*-benzylglucopyranoside-oxocarbenium ion **106** to be on the order of one second (Scheme 3.5).



Scheme 3.5: Yoshida's preparation of a glycosyl oxocarbenium ion **106** in super acidic media, visible on a time scale of 1 second at -78 °C. Ar = *p*-FC₆H₄.

In a less harsh reaction environment, the theorized heightened reactivity of an oxocarbenium ion makes its presence difficult to assess spectroscopically and so other measures are invoked to understand its role in organic transformations. In 2009, Woerpel published a notable lack of stereoselectivity in glycosylation reactions with common oxygen nucleophiles such as ethanol, attributing the low stereocontrol to reaction rates approaching the diffusion limit (Scheme

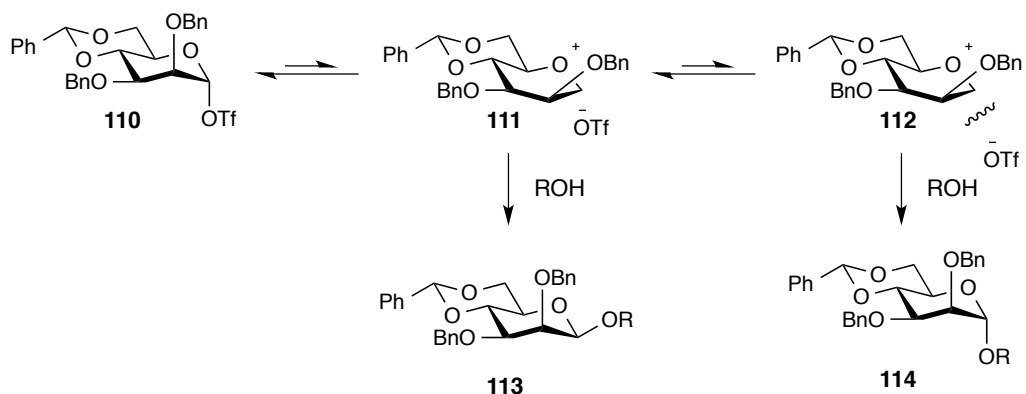
3.6).³⁶ Slowing reaction rates with less active nucleophiles like trifluoroethanol lead to higher stereocontrol, favoring formation of α -addition product **108** from proposed reactive intermediate **107**, a result of the nucleophile following the previously identified preferred trajectory to give the alpha product.^{31,37-40}



Scheme 3.6: Modes of addition to a 2-deoxyglucose-derived oxocarbenium ion **107**, invoked to explain the erosion of stereocontrol with increasing nucleophilicity.

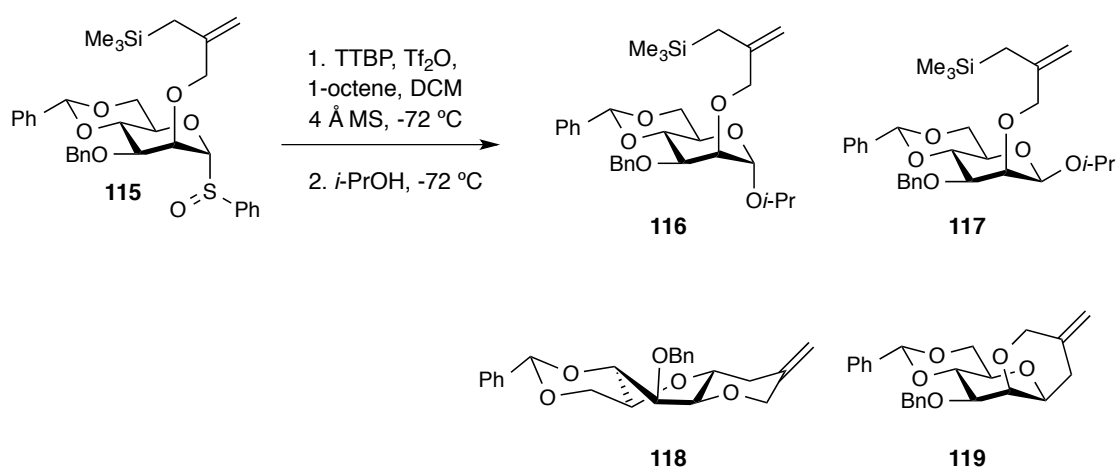
As a nearly 1:1 mixture of **108:109** was observed for nucleophiles like ethanol, Woerpel concluded the statistical mixture was a result of rates approaching the diffusion limit, allowing little regard for facial selectivity in the presence of **107**.

Also in 2010, in an attempt to consolidate experimental observations of selectivity in various glycosylation pathways, Crich demonstrated the existence of a previously proposed equilibrium between the easily observable covalency in an α -glycosyl triflate **110** and a set of contact and solvent-separated ion pairs **111** and **112**, respectively, the formation of which was nominally dependent on glycosyl substitution (Scheme 3.7).⁴¹ Crich went on to suggest that high β -selectivity in **113** was the result of a destabilized oxocarbenium ion **111**, decreasing the concentration of otherwise α -selective solvent-separated ion pair **112**, as were purportedly observed in the glycosylations performed by Woerpel.³⁶ Conversely, Crich suggested electron donating substituents on glycosyl systems such as **110** could stabilize the formation of a longer-lived oxocarbenium ion lead to an increase in α -selectivity.



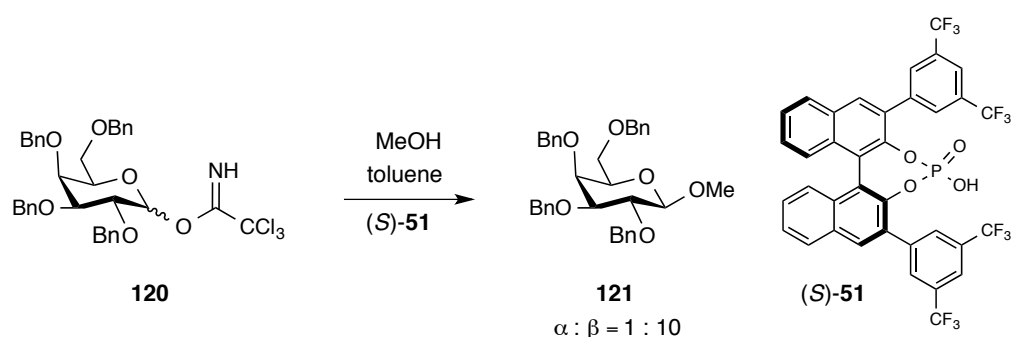
Scheme 3.7: Crich-proposed intermediates **111** and **112** in glycosylation leading to α and β selectivity. ROH = 2,3,6-tri-*O*-benzyl- α -*D*-mannopyranoside.

In addition, the Crich group investigated glycosylation mechanisms that could potentially involve oxocarbenium ion intermediates and have disclosed several studies detailing the many variables which may support one pathway over another.⁴²⁻⁴⁴ In an investigation on the molecularity of an intramolecular glycosylation reaction of **115**, Crich utilized molecular cationic clocks to demonstrate that benzylidene-directed formation of β -mannosides **117** is dependent on the concentration of the acceptor, and is thus S_N2 -like, with little formation of clock products **118** and **119** observed, while the formation of beta-mannosides is far less dependent on concentration and leads to **118** and **119** formation, suggesting it is more S_N1 -like in mechanism.⁴⁵



Scheme 3.8: Crich use of molecular cationic clocks to determine mechanism of glycosylation. TTBP = 2,4,6-tri-*tert*-butylpyrimidine.

While the Crich group, along with several others, have invested a significant amount of effort towards exploring and understanding the continuum of mechanistic possibilities for glycosylations over the past few years, far less effort has been made to understand the formation of non-glycosyl oxocarbenium ions in asymmetric organic transformations. Fairbanks presented the first application of a chiral Brønsted acid catalyst (*S*)-**51** for activation of trichloroacetimidate glycosyl donors **120** towards β -selective glycosylation to **121** in 2010 (Scheme 3.9). In his mechanistic proposal, Fairbanks invokes the presence of an oxocarbenium ion paired with the resulting chiral phosphate as the source of stereocontrol in this reaction.⁴⁶

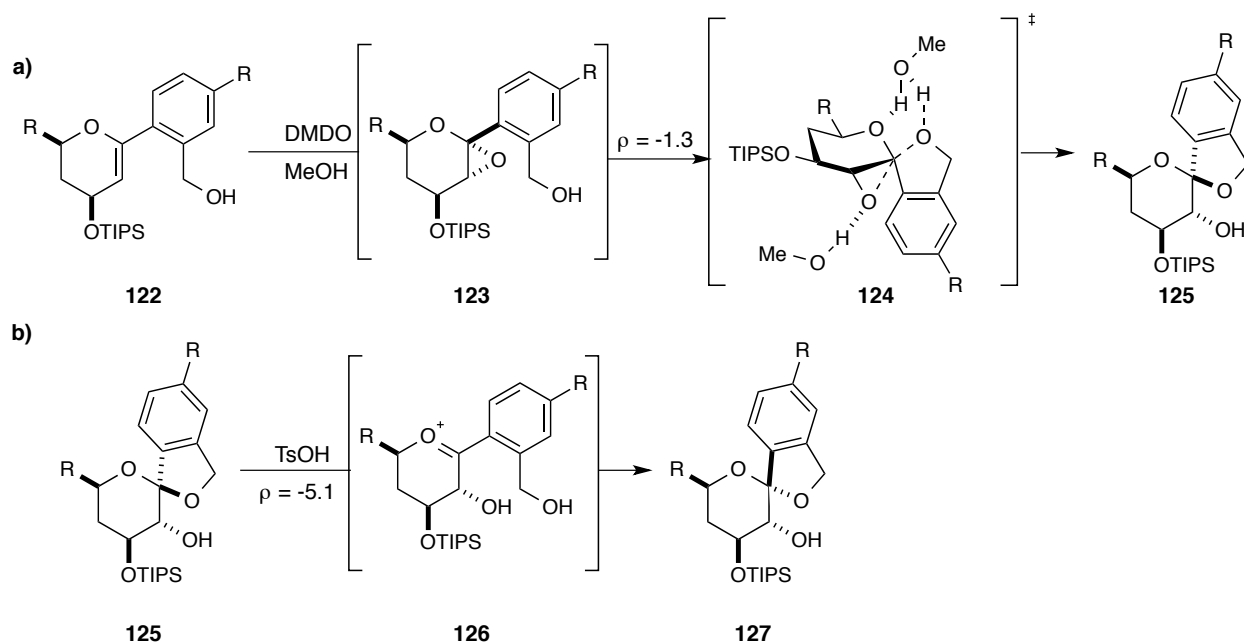


Scheme 3.9: Fairbanks' application of CPA to stereoselective glycosylation.

Several months later, a similar acid, (*S*)-**20**, was utilized in a catalytic asymmetric transacetalization by the List group as was depicted in Figure 1.7.⁶ Here, List proposed the same type of oxocarbenium ion intermediate, to which the phosphate anion grants a chiral reaction environment, as well as a coordination pathway, utilizing the bifunctional nature of the phosphoric acid to direct proton transfer through binding to a hydroxyl group through the phosphoric acid's Brønsted basic site. Despite these mechanistic proposals, no dialogue nor experimental evidence follows to compare the likelihood of one pathway over the other.

The timely release of an in depth mechanistic study of spiroketalization of glycol epoxides from the Tan group provided experimental evidence for reaction conditions which allow for oxocarbenium formation. Due to their reactive nature, *in situ* oxocarbenium ions can be difficult to probe, however, utilization of a Hammett study can help. By assessing the rate of reaction of a panel of electronically-diverse substrates and plotting the observed rate constants against reported *sigma* values, one can deduce the over-all charge build-up in the transition state of the rate determining step of the reaction. The charge build-up, ρ , is typically reported within the range of -5

to +5, the former suggesting positive charge development and the later, negative charge in the transition state.^{47,48} A study of the methanol-catalyzed spirocyclization of glycol epoxides **123** from **122** by the Tan group involved the completion of a Hammett study,⁴⁹ producing a ρ value of -1.3, which strongly suggests that the reaction did not proceed through the development of an oxocarbenium ion as a high level of positive charge in the transition state **124** was not observed (Scheme 3.10a). A Hammett study of the related tosic acid catalyzed epimerization of **125** to give thermodynamic spiroketals **127** gave a ρ value of -5.1, indicating a distinctly positive transition state **126**, and suggesting oxocarbenium formation in the transition state (Scheme 3.10b).

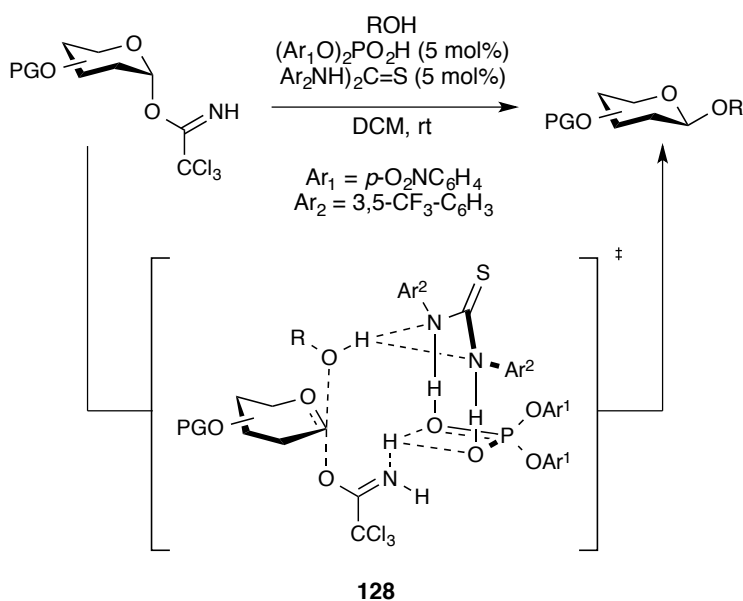


Scheme 3.10: Tan's stereoselective spiroketalizations. a) Methanol-catalyzed glycol epoxide opening reaction to form spiroketals operates with a Hammett ρ value of -1.3, suggesting a relatively uncharged transition state. b) TsOH-catalyzed spiroketalization epimerization operates with a ρ value of -5.1, suggesting a fully charged, oxocarbenium ion transition state.

Utilization of complex Brønsted acids and hydrogen bond donors only makes the picture more complicated. The phosphoric acids utilized in the aforementioned spiroketalization studies have both a Brønsted acidic and Brønsted basic site. Though phosphoric acids are considered strong Brønsted acids, rather than just donating a proton and remaining electrostatically bound to the substrate to provide a chiral scaffold in which asymmetric transformations can occur, chiral phosphoric acids retain the ability to

simultaneously activate the electrophile through protonation and the nucleophile through associate with a phosphate oxygen.

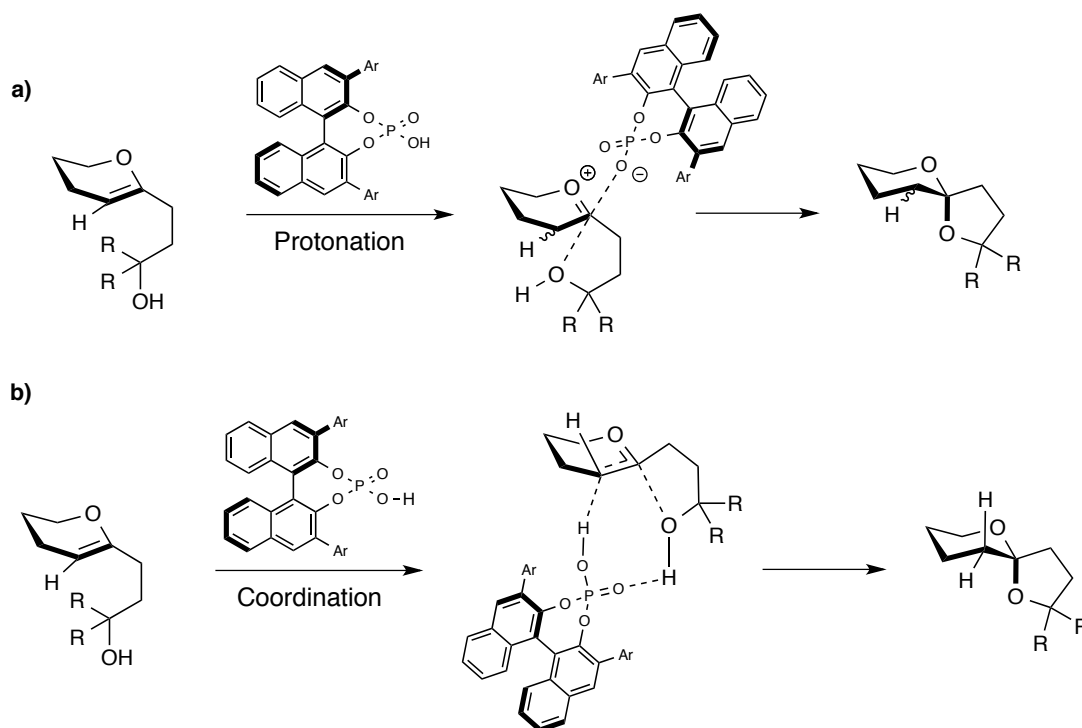
Cooperative catalysis also lends itself to more complex modes of catalyst binding and has lead to some interesting proposals of activation. For example, a recent Schmidt paper utilized both thiourea and phosphoric acid catalysts to co-catalyze a beta-selective glycosylation of armed trichloroacetimidates.⁵⁰ The proposed transition state for this reaction was a seemingly impossibly organized, but simultaneously intriguing four-component scaffold **128** (Scheme 3.11). Importantly, proposed transition states in many recent publications are just that – proposals, and the exact nature of these transition states remains to be fully investigated.



Scheme 3.11: Schmidt’s use of thiourea and achiral, strong Brønsted acids in the co-operative catalysis of beta-selective glycosylations through proposed transition state **128**.

Many recent publications employing chiral phosphoric acids recognize that reactions could thus operate through a concerted mechanism which relies on the bifunctional nature of the CPA and does not involve the intermediacy of an oxocarbenium ion, or through the more common oxocarbenium-based pathway. Such is the case of our recently developed CPA-catalyzed stereoselective spiroketalization reaction discussed in Chapter 2.^{51,52} In this spiroketalization, the DHP ring may be fully protonated by the strong Brønsted activity of the CPA, as in Scheme 3.12a. In this pathway, a full oxocarbenium ion is generated, after which cyclization occurs. This two step mechanism is the more commonly accepted pathway, and is

the one we teach budding organic chemists in their undergraduate studies. However, an alternative concerted pathway harnessing the bifunctional nature of the catalyst may also be at work, Scheme 3.12b. In this pathway, no oxocarbenium ion forms. Instead, a concerted protonation event occurs along with cyclization and deprotonation of the hydroxy nucleophile.



Scheme 3.12: Alternate modes of activation in the stereoselective spiroketalization reaction by the strong Brønsted act bifunctional chiral phosphate.

While together, these two pathways make up the strong majority of mechanistic proposals for these types of systems, alternative mechanisms could still be possible. Addition of the phosphate into the C1 position of the DHP ring upon protonation could lead to a chiral phosphate acetal intermediate, as can be observed in chiral dithiophosphoric acid catalysis.⁵³

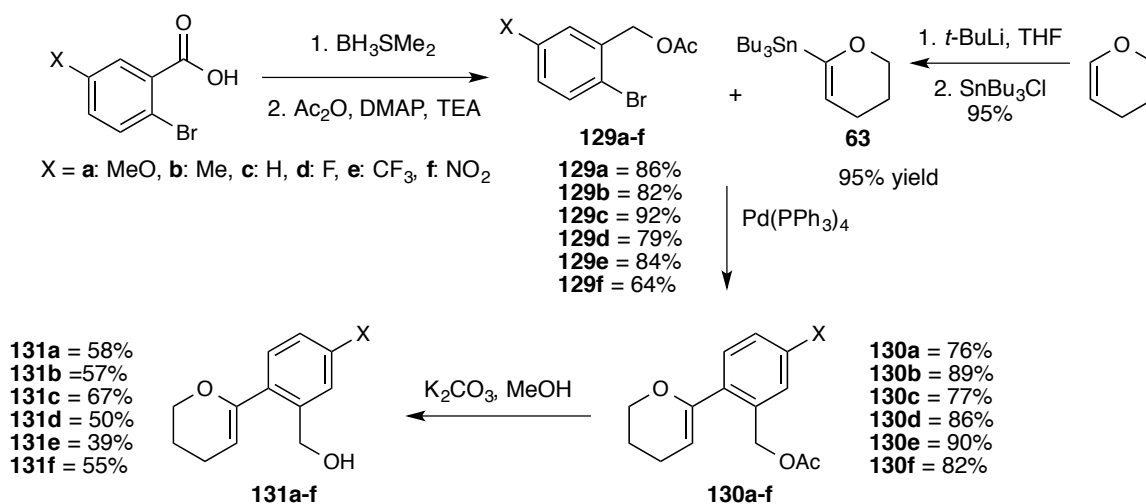
Counterions, protecting groups, hydrogen bonding and configurations have all been shown to effect whether or not an oxocarbenium ion can and will form and both experimental and computational studies experience challenges when it comes to mapping these types of reactions. While a handful of publications have recently emerged demonstrating the wide breadth of mechanistic possibilities for glycosylation reactions^{36,54-68} and solvolysis reactions,^{36,64-73} at both benzylic sites⁷⁴⁻⁸⁴ and at acetals,^{37-39,85-88} most of these studies are of intermolecular

reactions and the cumulative results of these studies have yet to paint a coherent picture of oxocarbenium formation and reactivity. To our knowledge, no thorough investigation of an CPA-catalyzed asymmetric reactions of intramolecular spirocyclizations have been undertaken. As the approach to this type of chemistry becomes more rigorous and with the cloudy understanding of the mechanism of glycosylation becoming more clear, we saw a strong need for an in depth analysis of the stereoselective formation of spiroketals using chiral phosphoric acids. By employing a joint computational and experimental approach, we hope to provide a coherent picture of how this transformation proceeds, and hope to set a standard for mechanistic proposals.

3.2 Synthesis of Hammett Study Substrates

In order to probe which of the two mechanisms proposed in Scheme 3.12 is operating in the CPA-controlled spiroketalization reaction discussed in Chapter 2,⁵¹ a Hammett study was undertaken. As pathway **a** proceeds through a fully cationic species, operation of this mechanism should result in a Hammett ρ value close to -5, as in the tosic acid epimerization study performed by Tan.⁴⁹ If instead the reaction capitalizes on the bifunctional nature of the CPA, and undergoes concerted protonation and ring closure, a fully cationic species will never form, and the Hammett study should then produce a ρ value closer to that of 0, as in the methanol catalyzed glycol epoxide opening reaction, also from the Tan group.

To initiate studies, a panel of electronically diverse substrates was synthesized from corresponding commercially available 2-bromobenzoic acids as depicted in Scheme 3.13.



Scheme 3.13: Synthesis of panel of substrates for rate analysis in a Hammett study.

Variation of the electronics of these systems was accomplished by using a range of substituents on the starting bromobenzoic acids. Strong electron donation was accomplished through the inclusion of a *para*-methoxy unit and similar, though lesser electron donation was provided by a *para*-methyl group. With 2-bromobenzaldehyde used as the starting material for the rate standard, a fluorinated derivative was used to provide a mildly deactivating effect. Stronger electron withdrawing substituents trifluoromethyl- and nitro- were also explored. Each of these six versions of the brominated benzaldehydes were subjected to soft reduction with a borane-dimethyl sulfide complex and promptly acetylated to give **129a-f**. Stannane **63** was prepared via lithiation of DHP by *tert*-butyl lithium followed by exposure to tributyltin chloride. Acetylated alcohols **129a-f** were then coupled to **63** in a Stille reaction catalyzed by tetrakis(triphenylphosphine)palladium(0) to give protected enol ethers **130a-f** in good yields.

The final step of the synthesis of these Hammett precursors, simple deacetylation with potassium carbonate to give free alcohols **131a-f**, consistently proceeded with modest yields. In an attempt to optimize the synthesis, alternative protecting groups were investigated, as well as alternative methods to remove the acetate, including alkyl lithium reagents, Grignards and a host of other nucleophilic bases. Unfortunately, yields of this reaction could not be improved. It is presumed that rather than the reaction conditions acting as the source of yield depletion, it is the very nature of the **131a-f** products that are causing the low yields. As crude yields for the deacetylation protocol were measured to be consistently above 70%, presumably the compounds undergo polymerization during column chromatography, despite pre-equilibrating the column with triethylamine. In addition, several of the precursors showed volatility when placed *in vacuo*. Alternative purification attempts such as utilizing different sources of silica, as well as alternatives such replacing silica with basic alumina did not produce pure enough products to utilize in the Hammett study, and vacuum proved to be the most effective way to remove triethylamine from the precursors. Despite the low yields, the potassium carbonate protocol, followed by column chromatography on a buffered silica column reliably produced highly pure **131a-f**, and so the procedure was retained in the synthesis of these substrates.

3.3 Hammett Study

With precursors **131a-f** in hand, the rates of the spiroketalizations of the electronically

diverse enol ethers were investigated. Enol ethers **131a-f** were treated with diphenyl phosphoric acid (5 mol% in pentanes) at 0 °C in the presence of 4 Å MS to induce cyclization to the corresponding spiroketals (Figure 3.1a). Rates of conversion were measured by running parallel reactions, which were quenched at various time points with triethylamine and subsequently filtered, concentrated and then analyzed by ¹H-NMR. The ratio of enol ether to spiroketal products were determined by integration of the triplet signal emanating from the proton of the DHP double bond versus the upfield doublet produced from the benzylic position of the closing ring upon cyclization.

As both mechanistic pathways proceed with protonation of the enol ether in the rate determining step, increased electron density of the substrate was expected to increase the rate of reaction, while substrates with electron withdrawing substituents were expected to cyclize slower. Accordingly, the *para*-methoxy substrate **131a** showed the fastest rate of reaction, with an average k_{obs} of 6.48. Comparatively, methylated **131b** and unsubstituted **131c** were measured to have k_{obs} of 1.95 and 0.50, respectively. Fluorinated **131d** displayed a k_{obs} of 0.506. This slightly higher rate, as compared to the unsubstituted substrate, is consistent with what would be expected if the phenyl ring is in conjugation with the reactive center, and with the use of σ^+ values for the Hammett plot (Figure 3.1b).

Substrates with more harshly electron withdrawing substituents –NO₂ and –CF₃ were expected to show a marked reduction in rate. After twenty four hours, no conversion to spiroketal product was observed for the NO₂ substrate and the **131f** proved to be almost entirely insoluble in pentanes at 0 °C. As the marked difference in solubility of this substrate versus the others included in the study may affect the rate of reaction, this substrate was excluded from the Hammett study. Instead, effort was focused on measuring the rate of the similarly electron withdrawing trifluoromethylated **131e**. The initial run of **131e** reactions displayed a k_{obs} of 0.11. While the experiments in Figure 3.1 have been consistently reproduced, the cyclizations of **131e** exhibited significant variation. This could be attributable to competitive inhibition of the catalyst by water, due to the slower spiroketalization rate.

Rate constants for each of the substrates were determined using the logarithms of $k_{\text{obs}}/k_{\text{H}}$, and were plotted against known σ^+ values⁸⁹ to define the Hammett correlation and obtain a ρ value. As discussed, ρ values typically range from -5 to +5 with the range of -5 to zero

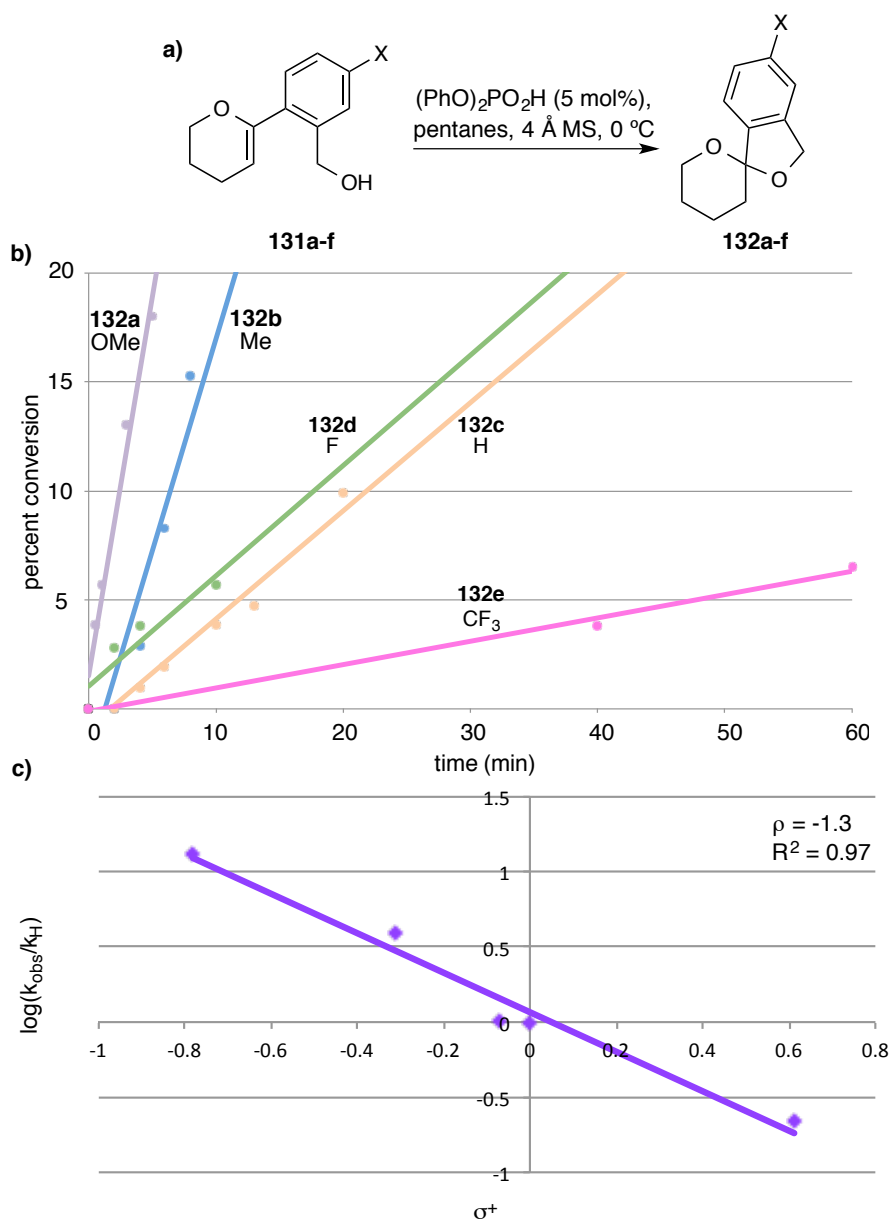


Figure 3.1: Hammett analysis of the phosphoric acid-catalyzed spirocyclization reaction. a) Cyclization of enol ethers to spiroketals investigated. b) Rates of conversion with 5 mol% (PhO)₂PO₂H in pentanes at 0 °C. The *p*-nitro substituted substrate was deemed to be insoluble in the reaction conditions and was excluded from the study. An average of the replicate experiments is shown. c) Hammett plot demonstrates a strong, linear correlation of the panel of electronically diverse substrates and reaction rate, with a shallow negative slope of -1.3, indicating an uncharged transition state.^e

^e Reproductions of cyclizations for substrates **131b-d** in Figure 3.1 were conducted by Dr. Yaroslav Khomutnyk.

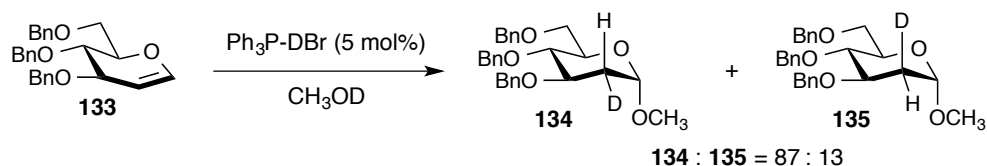
corresponding to reactions which may develop cationic nature in the transition state of the rate determining step of the reaction. The greater the absolute value of ρ , the more developed the positive charge, meaning a ρ value of -5 would suggest a fully formed oxocarbenium ion is present in the rate determining step. The range of 1 to -1 is mostly populated by reactions which proceed through radical intermediates. Accordingly, we anticipated to see a ρ value between -1 and -5. In plotting the logarithm of the relative rates of conversion of **131** to **132** depicted in Figure 3.1a, rate differences between the substrates can be observed, illustrating that electronic donation into the enol ether accelerates the reaction, while the presence of electron withdrawing groups slows the reaction (Figure 3.1b). When these rates of conversions were plotted against the appropriate σ^+ values, a strong, linear correlation was observed, with a ρ of -1.3, indicating a relatively uncharged transition state (Figure 3.1c).

The negative slope in the Hammett plot does in fact identify there is a build-up of positive charge in the transition state, however at a value of -1.3, the nature of the transition state of phosphoric acid-catalyzed spiroketalizations is only slightly positive, in line with a concerted mechanism rather than the formation of an oxocarbenium ion. The linear, negative slope observed also demonstrates that the aryl ring fused to the hydroxy tether is in partial conjugation with the C1 of the DHP ring in the transition state of the reaction. In cases in which the aryl ring exists out of conjugation with reactive site, the left-most portion of the Hammett plot tends to trend downwards, a result of the electron withdrawing effect of *p*-methoxy subunits. As the graph in Figure 3.1c is distinctly linear, with an R^2 value of 0.97, we can conclude the aromatic ring is indeed conjugated to the reactive system.

Also of note are the literature precedents of reactions existing on the spectrum of S_N1 – S_N2 -like reactions at benzylic centers, which present with non-linear Hammett correlations.^{85,90} These graphs appear as bent or U-shaped plots, with the bend indicative of an abrupt change in the polarity of the transition state in the rate determining step of the reaction. Often, this is attributed to a change in mechanism, such as from S_N2 -like, in the case of electron withdrawing substrates, to S_N1 -like, in the case of electron donating substrates, in which case the substituent is able to balance developing charge and promote a more unimolecular transformation. While it could be expected that oxocarbenium ion formation would be more probable with our *p*-methoxy and *p*-methyl-substituted compounds, this type of mechanistic switch has not been observed.

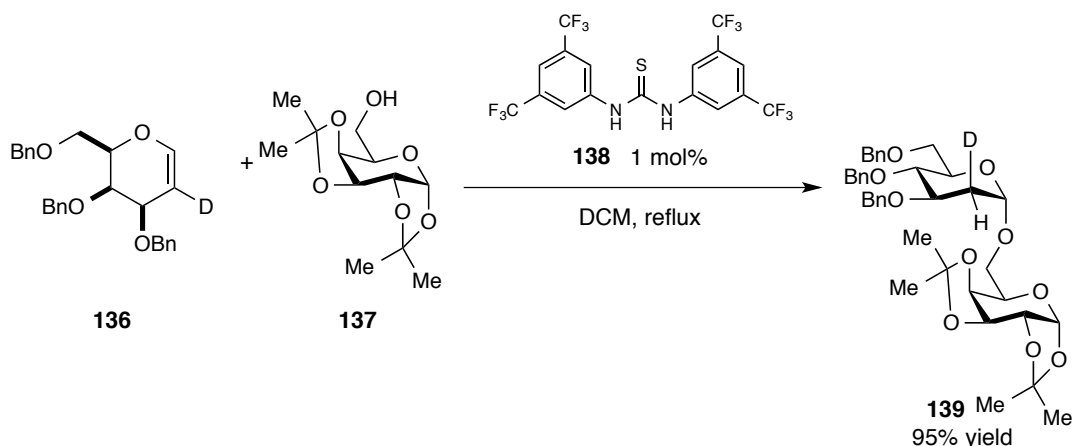
3.4 Synthesis of Deuterium Labeled Substrates

Deuterium labeling of glycols has been used to provide mechanistic insights into glycosylation mechanisms. In 1992, Franck used deuterium labeling to probe the facial selectivity of the protonation of glycols **133** prior to glycosylation and discovered deuterium delivery to mainly occur from the bottom face of the glycols to yield **134** in preference to **135** (Scheme 3.14), concluding that the acid-catalyzed addition of alcohols to glycols does not occur via a *trans* diaxial addition.⁹¹



Scheme 3.14: Franck's glycol deuterium labeling study displaying a preference for *cis* addition.

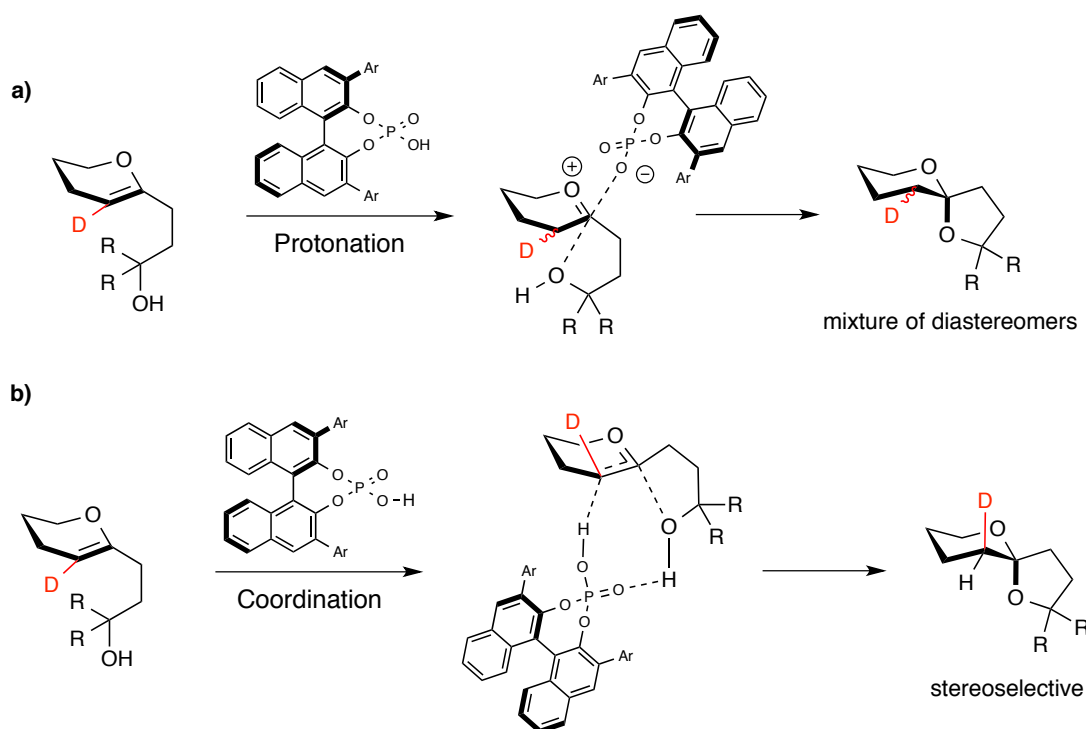
Indeed similar *cis* delivery across a glycol double bond was seen many years later when achiral thiourea **138** was used in the glycosylation of deuterated 2-deoxygalactoside **136** (Scheme 3.15).^{92,93} The proposed mechanism, involving protonation to the less-hindered face of the glycol leading to an ion pair, which collapses to give product **139** is also in line with the mechanism proposed by Schriener for the tetrahydropyranylation of alcohols.⁹⁴



Scheme 3.15: Selective *cis* delivery of acidic proton and alcohol **137** to 2-deoxygalactoside **138**.

Though the Hammett study provided insight into the mechanism of the chiral phosphoric acid-catalyzed spiroketalization reaction, we ventured forward to provide an additional source of experimental evidence in support of the concerted reaction pathway and believed similar deuterium labeling could provide additional insights, as the facial delivery of the acidic proton gave a possible way to discern the two likely operating mechanistic pathways from one another.

The concerted mechanism in Scheme 3.16a begins with a protonation event to yield a fully-formed oxocarbenium ion. As the enol ether starting material for this transformation is achiral, neither face of the molecule should be biased towards protonation, and thus formation of the spiroketal will occur with a racemized C2 stereocenter. In contrast, the concerted mechanism involves a coordination event which allows the phosphoric acid to simultaneously protonate the DHP ring and deprotonate the hydroxy nucleophile for cyclization. In order for this to occur, the



Scheme 3.16: Differentiating between an ionic and a concerted spiroketalization pathway with the use of an installed deuterium label. a) The ionic pathway first proceeds through protonation of the substrate from either face to form an oxocarbenium ion, which can then cyclize to give a spiroketal with a racemic C2 stereocenter. b) The concerted pathway involves coordination of the phosphate catalyst to the substrate from one face. Simultaneous delivery of the acidic proton and deprotonation of the hydroxy nucleophile can only happen from the same face of the molecule if the acid is acting in a bifunctional nature, resulting in sole formation of the deuterium label on the top of the molecule.

acidic proton and the hydroxy nucleophile must be delivered from the same face of the enol ether, thereby resulting in favored formation of the spiroketal stereoisomer with the deuterium label trans to the hydroxy nucleophile.

To probe the delivery of the acidic proton, a non-deuterated substrate was prepared, then analyzed using both one and two-dimensional NMR, as well as NOESY. By examining the NMR spectra of different spiroketals, Tables 2.2 and 2.3, substrate **71b** was identified as an appropriate substrate for this transformation, as the presence of the fused phenyl ring removed some of the upfield signals in the $^1\text{H-NMR}$, making clean identification of enantiotopic protons a far more straight-forward and easy-to-follow task. Enol ether **71a** was prepared as outlined previously in Scheme 2.4, and then cyclized in the presence of TRIP, (*S*)-**20** in pentane to give spiroketal **71b** in high enantiopurity as in Figure 3.2a. The resulting spiroketal was then analyzed to determine which signals in the $^1\text{H-NMR}$ corresponded with protons A and B in Figure 3.2.

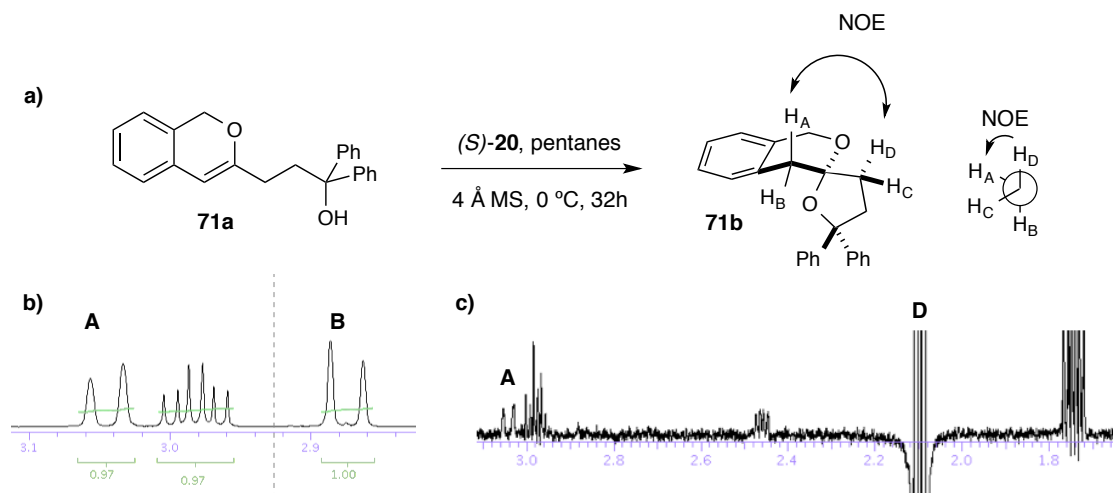
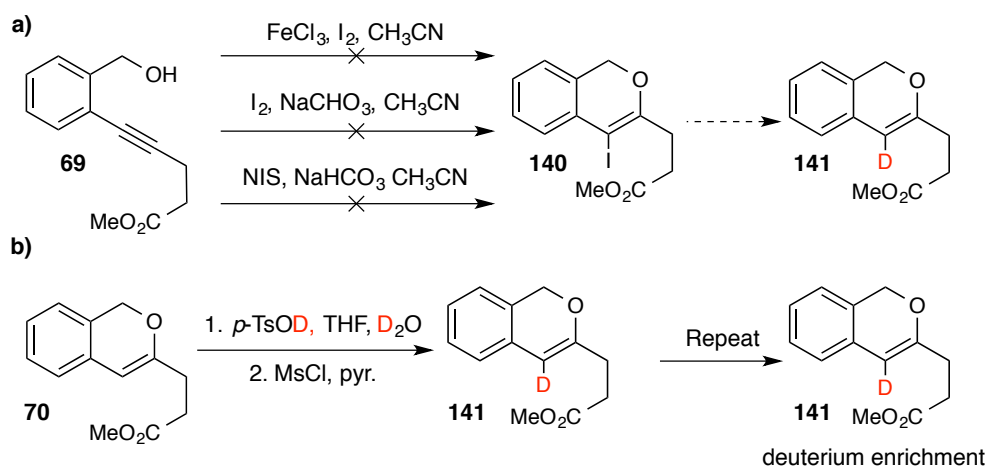


Figure 3.2: a) Spiroketalization of **71a** gave **71b**. b) Truncated $^1\text{H-NMR}$ spectrum of **71b**, showing two doublets arising from the enantiotopic protons present following protonation of the DHP ring. c) As the D proton in **71b** is gauche to A and anti to B in configuration, NOE irradiation of D results in sole excitation of A, identifying the more downfield doublet as belonging to the proton on the top face of the molecule, trans to the hydroxy nucleophile.

Upon spirocyclization, two doublets appear in the 2.8-3.1 ppm region of the $^1\text{H-NMR}$ (Figure 3.2b), which correspond with the geminal protons labeled A and B (Figure 3.2a). As the spiroketal configuration would place proton D gauche to proton A, and anti to proton B, NOE

irradiation of D can excite proton A due to the shorter distance in three-dimensional space between the two protons. As seen in Figure 3.2c, irradiation at D causes excitement of the more downfield doublet, identifying this signal as belonging to the proton on the top face of the molecule, trans to the hydroxy nucleophile. Once an NMR distinction between enantiotopic, geminal protons A and B could be made, the deuterium labeling study could commence.

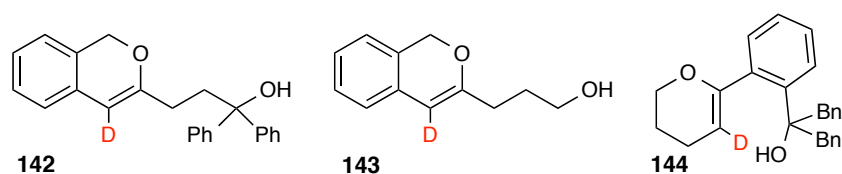
We were hoping that exchange of the catalyst's acidic phosphate proton and substrate's hydroxyl proton with deuterium would allow for the installation of a label *in situ*, however, the presence of sieves in the reaction provided a flood of faster-reacting protons, resulting in low-to-no incorporation of deuterium. Rather than changing reaction conditions to exclude the sieves, which proved to be important in increasing stereocontrol, we investigated methods to install the deuterium label to the enol ether directly. To this end, a variety of synthetic approaches were envisioned and undertaken (Scheme 3.17). Initially, we sought to introduce the label by exchange with an iodide, which could be installed by formation of an iodonium species off of the alkyne, followed by an intramolecular 6-endo-*dig* S_N2-like cyclization, however we were unable to find reaction conditions to efficiently produce **140** in high yields with good regioselectivity (Scheme 3.17a). The use of NIS to provide an electrophilic source of iodide showed the best conversion, but resulted in preferred formation of the 5-*exo* cyclized product. An alternative protocol was then developed, which utilized a deuterated *p*-toluene sulfonic acid to deuterate the enol ether, followed by nucleophilic attack of D₂O to give deuterated acetal **141**.



Scheme 3.17: Various synthetic approaches to install a deuterium label. a) 6-endo-*dig* cyclization to give an iodide handle which could undergo exchange with deuterium to give **141**. b) Acid-catalyzed hydration of the enol ether, followed by mesylation/elimination to give **141**.

Subsequent mesylation of the –OD group, followed by pyridine-promoted elimination, lead to the formation of **141**. Resubjection of **141** to the protocol outlined in 3.11b allowed for levels of over 90% deuterium installation to be achieved. Conversion of **141** to the diphenylated spiroketalization precursor **142** was accomplished with a Grignard reaction.

A similar primary variant of this substrate, **143**, Scheme 3.18, was synthesized for additional deuterium labeling studies. The basic synthesis of this substrate follows that which was outlined in Scheme 2.13, and deuterium installation was again performed following the gold cyclization. Notably, exposure to deuterated tosic acid and D₂O in THF at high temperatures resulted in direct formation of **143**, making the mesylation/elimination step unnecessary. A final substrate, DHP-derived **144** was also prepared.^f



Scheme 3.18: Substrates used in the deuterium labeling study.

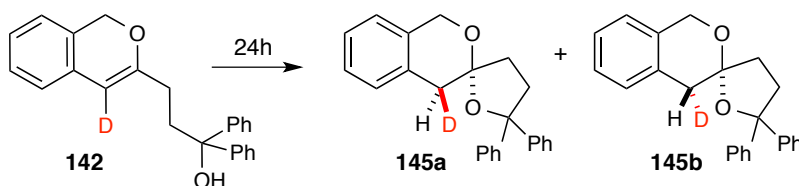
3.5 Deuterium Labeling Study

With deuterium-labeled substrates in hand, we set out to investigate the selectivity of the reaction in a range of solvents and with a variety of acid catalysts. Entries 1 and 6, reaction of substrate **142** in pentane with (*S*)-**20** at both room temperature and 0 °C demonstrated exclusive formation of isomer **145a** (Table 3.1) over isomer **145b**. Indeed, this is in accordance with our belief that the CPA-catalyzed cyclization proceeds in a concerted manner, utilizing the phosphate's bifunctional nature to protonate the substrate and assist in the cyclization of the hydroxy nucleophile all from the same face of the reaction. To probe if different solvents would allow for the alternative ionic pathway and thus a mixture of **A** to **B**, the reaction was repeated again in toluene, ethyl acetate, dichloromethane and diethyl ether (entries 2-4). While diethyl ether gave no conversion to products **145**, all other solvents resulted again in exclusive formation of **145a**, despite their abilities to stabilize an oxocarbenium ion intermediate that may lead to

^f We thank Dr. Yong Guan for help in scaling up the synthesis of **142** and **143**. Substrate **144** in Scheme 3.18 was synthesized by Dr. Yaroslav Khomutnyk.

145b. After collecting these exciting results, we screened several other acids. We anticipated that select formation of **145a** was a phenomenon specific to catalyzation by phosphoric acids, which contain both a Brønsted acidic site and a Brønsted basic site, allowing for bifunctional catalysis from one side of the molecule. To our surprise, however, the *syn* addition of an acidic proton and the oxygen nucleophile proved to be a relatively general phenomenon. Trifluoroacetic acid gave a 77:33 mixture of **145a** to **145b**. TFA was later shown to epimerize pure **145a** to a 1:1 mixture of stereoisomers, suggesting the presence of a competing epimerization pathway causes the lower selectivity observed for entry 7.

Table 3.1: Acid-catalyzed spirocyclizations of deuterium-labeled substrates in various solvents and Brønsted acids.



entry	catalyst	solvent	T, °C	145a : 145b
1	(S)- 20	pentane	25	100 : 1
2	(S)- 20	toluene	25	100 : 1
3	(S)- 20	ethyl acetate	25	100 : 1
4	(S)- 20	dichloromethane	25	100 : 1
5	(S)- 20	diethyl ether	25	-- ^a
6	(S)- 20	pentane	0	100 : 1
7	TFA	pentane	0	77 : 33 ^b
8	ClCH ₂ CO ₂ H	pentane	0	100 : 1 ^c
9	PPTS	pentane	0	100 : 1

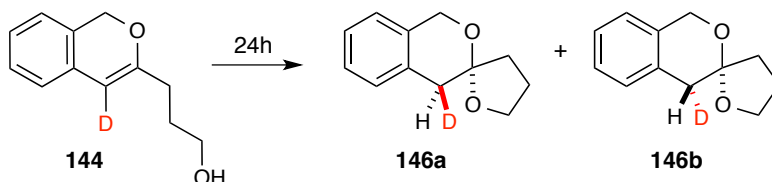
a) No reaction was observed. b) A pure sample of **145a** was subjected to TFA for 12 hours at room temperature in pentane and was shown to completely epimerize, suggesting a competing epimerization pathway is ongoing during the cyclization. c) Low conversion to product observed after 24 hours.

Chloroacetic acid, chosen to mimic the pioneering studies by Pihko, gave selective formation of **145a** over **145b**, though in very low conversions after 24 hours. Pyridinium *p*-

toluene sulfonate also catalyzed the cyclization selectively, giving exclusive formation of the *D/O trans* product.

A similar screen of conditions was performed on substrate **143** (Table 3.2).[§] Though we do observe lower stereocontrol in the cyclizations of less-bulky nucleophiles (Table 2.3), deuterium labeling shows the same propensity of the *D,O-trans* substrate **146a** to be formed both when a CPA such as (*R*)-**20** is used, as well as an achiral acid such as chloroacetic acid is used. In fact, simple exposure to **143** to deuterated chloroform causes swift cyclization to **146a**.

Table 3.2: Acid-catalyzed spirocyclization of deuterium-labeled **144**.



entry	catalyst	solvent	T, °C	146a : 146b
1	(<i>R</i>)- 20	toluene	25	100 : 1
2	(<i>R</i>)- 20	dichloromethane	0	100 : 1
3	ClCH ₂ CO ₂ H	dichloromethane	25	100 : 1
4	--	chloroform- <i>D</i>	25	100 : 1

Thus it appears as though *syn*-delivery of an acidic proton and the oxygen nucleophile is a general phenomenon, rather than a specific observation for chiral phosphoric acid-catalyzed cyclizations in non-polar solvents. Not only does this reinforce the conclusions reached from the Hammett study, suggesting spirocyclization occurs through a concerted mechanism, but it also has broad implications for understanding how simple acid catalysts can interact with achiral substrates to promote stereospecific reactions.

3.6 Computational Analysis of the Spiroketalization Mechanism

While the computational identification of a low-lying mechanistic pathway can be relatively straight forward, identifying it as the sole probable mechanistic pathway can be

[§] Spirocyclizations presented in Table 3.2 were performed by Dr. Yaroslav Khomutnyk.

extremely challenging. In some cases, lower energy conformers are missed, in others, reaction variables are overlooked, systems are truncated, corrections aren't made or the data is simply misinterpreted.^{95,96} In general, calculating the lowest energy pathway of a given organic transformation is demanding both computationally and time-wise, as computation of the entire potential energy surface (PES) of a reaction requires a significant amount of time and cost. Rather than compute entire PESs, we can define intermediates and pathways of interest, focusing computational efforts solely on what we deem as plausible pathways. While this approach no doubt saves many computing hours and produces data faster, it only investigates a small subspace of possible reactions that may occur, and model systems can miss out on key interactions occurring between the full substrate and catalyst of a reaction.

To supplement our experimental studies, we wanted to investigate the mechanism from a computational standpoint. While several computational studies involving chiral phosphoric acids have come out in recent years, many look at pre-identified transition states and pathways to support mechanistic proposals.^{18,94,97,98} We chose to utilize a methodology from Zimmerman lab at the University of Michigan.⁹⁹⁻¹⁰¹ This reaction discovery method provides a systematic approach to identifying low barrier reaction pathways (Figure 3.3).

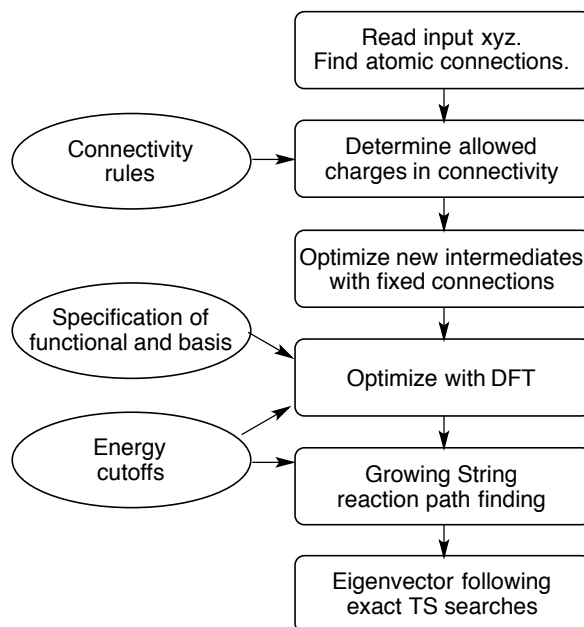


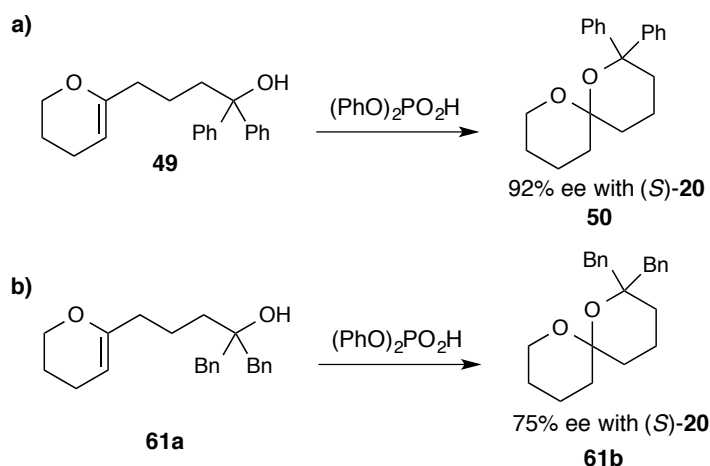
Figure 3.3: Flowchart depicting the steps followed for the generation of isomers and low barrier transition states, right, with required parameters given on left.

To identify key, low-lying transition states within the PES of the reaction, a system is first built in three dimensional space and these coordinates are then submitted and automatically reviewed to ensure if the structure is valid in terms of overall charge and bond connectivity, after which a DFT-optimized structure is generated. Instructions are given, which dictate which bonds to make or break or to specify angles of approach or torsional angles within the molecule. These instructions are then used to optimize new intermediates a single elementary step away from the starting coordinates. If a viable structure is located, its configuration is optimized via DFT, and these two structures can then be used as the starting and ending points of the reaction mechanism. With a specified functional and basis set, structures generated along the path of the reaction, including intermediates are identified as though connecting dots along a string. This process, referred to as Growing String, identifies low lying structures as it builds the reaction path and eventually identifies an exact transition state structure. Structures that are thermodynamically inaccessible are discarded and feasible reaction pathways emerge. Importantly, the process is highly parallel, allowing computations performed via this method to utilize the power of a large computational cluster to accelerate computational times. With the ability to perform these transition state searches over a combinatorial set of possible reactions, this computational approach avoids over-reliance on chemical intuition, which could inadvertently bias the mechanistic outcome by causing important reaction intermediates to be overlooked.

While our experimental chemistry suggests the mechanism of CPA-catalyzed spiroketalization to be concerted, we can not use it to unequivocally deny the presence of an oxocarbenium ion intermediate which does not undergo phosphate detachment prior to cyclization. Reaction intermediate and transition state lifetimes, however, are measurable computationally, and so we set out to investigate if we could utilize a computational approach to not only identify the overall mechanism of the reaction, but also the plausibility and lifetime of any oxocarbenia that may form along the reaction path.

Two similar systems were investigated, shown in Scheme 3.19. Diphenylphosphoric acid was utilized to model the mechanisms of these transformations in order to grant facile insight into the reaction pathways before venturing into computations on the full catalyst system, as well as to reduce atom load for future dynamic calculations utilized to calculate the lifetime of any oxocarbenium ions that may form. Experimentally, substrate **50** in Scheme 3.19a was able to be obtained in very high enantiopurity from **49** in the CPA-catalyzed spiroketalization reaction,

whereas **61b** was prepared with only moderate levels of stereocontrol. Though it is clear a lower amount of steric hindrance present on the hydroxy nucleophile is the direct cause of a reduction in stereoselectivity, we postulated that there may be an observable mechanistic component in the pathways of these reactions that we could model computationally, which would grant a better understanding of the overall reaction. Importantly, we were interested to see if competing pathways had closer barriers in the transformation of **61a** to **61b** that may explain the lower level of stereocontrol, as well as what the lifetime of any oxocarbenia that may form would be.



Scheme 3.19: Selected systems to investigate the presence and lifetime of oxocarbenium ions.^h

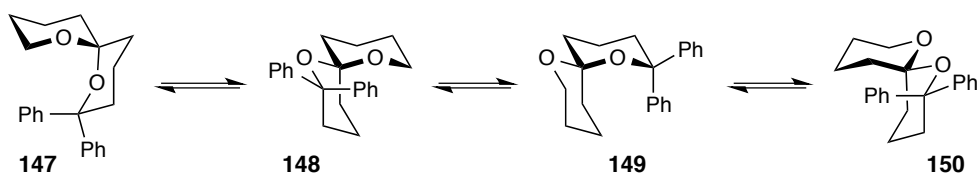
With the exception of solvent computations, all density functional calculations were performed using Q-Chem 4.0.¹⁰² Optimized geometries were evaluated using the ω B97X-D exchange functional using mixed double- ζ -quality basis sets with polarization functions, designated 6-31G* and G-31G**.¹⁰³⁻¹⁰⁶ Images of intermediates were generated in VMD.¹⁰⁷ A single-ended growing string method was primarily used to probe the potential energy profile of the reactions.¹⁰⁰

In all cases, the Gibbs free energies were first computed through single point energies obtained using a ω B97X-D exchange functional with a 6-311+G** basis set for all reported starting geometries, intermediates, transition states and final geometries.^{108,109} Frequency computations were performed using the ω B97X-D density exchange functional with a 6-31G**

^h Computational investigation of the transformation of **49** to **50** as presented in Scheme 3.19 was performed by Alonso Jose Arguelles Delgado.

basis set to account for enthalpic contributions from rotational, translational and vibrational energies as well as entropic energies at 240 K. Solvent corrections for *n*-pentane were performed using the SMD solvent model in GAMESS using a ω B97X-D exchange functional with a 6-311+G** basis set.^{110,111}

Despite the relative simplicity of these substrates, a massive amount of computations must be undertaken to produce an appropriate study of the possible reaction mechanisms. Notably, these spiroketals can exist in four different configurations **147-150**, **147** possessing two anomeric effects, **150** in which no anomeric effects are present and two distinct configurations **148** and **149** which have only one anomeric effect. (Scheme 3.20). As these configurations are interconvertible on the bench, this conformational flexibility is experimentally unimportant, however computationally it matters a great deal, as each conformer arises from a different orientation of the atoms in space, thereby having a unique energy level and transition state.



Scheme 3.20: Possible configurations of the spiroketal product.

As we could not rule out which conformer was formed initially, all four configurations had to be investigated in parallel. The phosphate could also be positioned in several different orientations with respect to the substrate, resulting in installation of either an axial or equatorial proton. In addition, though we propose the catalyst to be operating in a bifunctional mode, we can not rule out that the same oxygen of the phosphate which delivers the acidic proton is not the same proton which deprotonates the hydroxy nucleophile upon cyclization. With these approach and conformational possibilities, each mechanistic investigation required an average of forty computational experiments. To reduce the amount of influence starting configurations of the hydroxy tether may have on the overall energy of the system, mechanistic investigations were run backwards, from the more rigid spiroketal systems to the enol ether starting materials.

Following the systematic protocol outlined in Figure 3.3, and with the aforementioned computationally challenging mechanistic variables, a subset of plausible reaction pathways was identified (Figure 3.4).

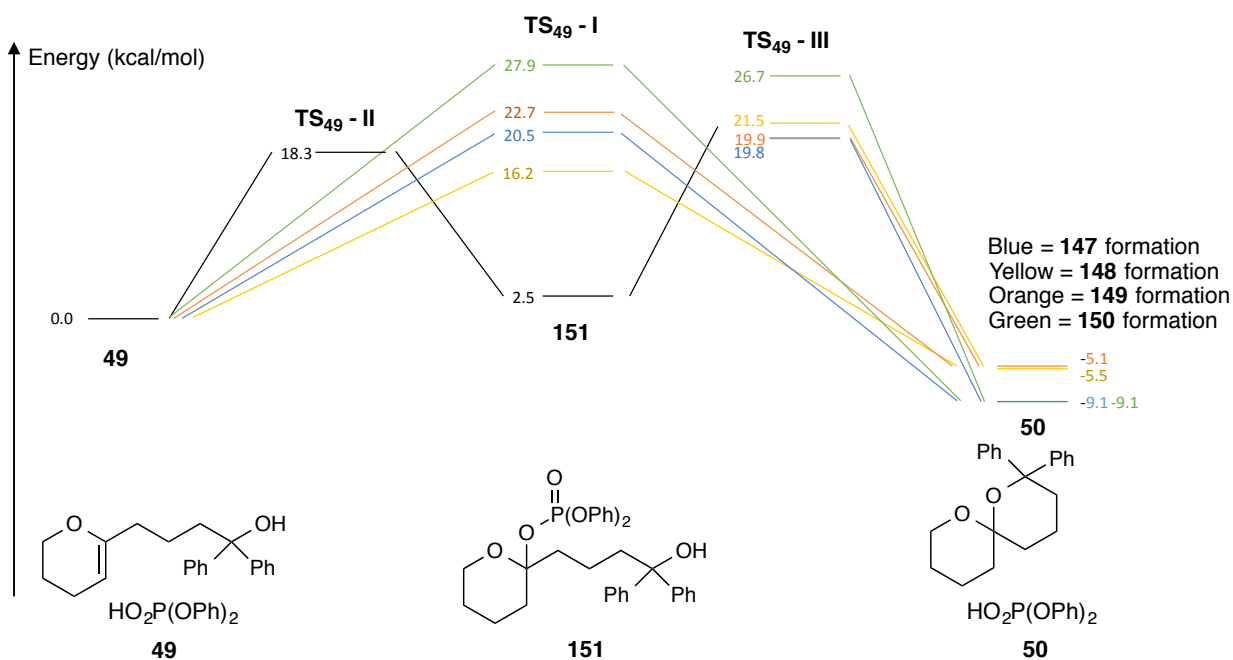


Figure 3.4: Plausible reaction pathways for the formation of **50**. Black pathway formation of a phosphate intermediate. Colored mechanisms represent the four different, lowest lying pathways to access each of **147-150**.ⁱ Calculated values for geometries for the pathways investigated for the formation of **50** at the GAMESS(SMD solvent = *n*-pentane)/ ω B97X-D/6-311+G** level.

While formation of an oxocarbenium ion/ phosphate ion pair had a prohibitively high pathway, two other potential reaction paths emerged. The concerted pathway leading to the formation of a mono-anomeric spiroketal had the lowest reaction barrier at 16.2 kcal/mol. A competing reaction pathway involving the formation of a phosphate acetal intermediate can be observed. While the first step in this pathway appears to be thermodynamically reasonable, collapse of the intermediate to the spiroketal product is too energetically uphill to compete with the concerted cyclization.

The same computational approach was undertaken for the cyclization of **61a** to **61b**, and the same reaction profile was observed. Of note is the particularly low amount of charge development in the transition state of the reaction **152** (Figure 3.5). By tracking the charge on the atoms in the system, we observe a negligible charge difference between the starting material, transition state and product at the site where an oxocarbenium ion may form in the DHP ring. Bond length at this site also remains relatively unchanged, shortening by just 0.05 Å in the

ⁱ Computational data presented in Figure 3.4 was acquired by Alonso Jose Arguelles Delgado.

transition state, suggesting bond order remains consistent, and oxocarbenium formation with significant double bond character is not observed.

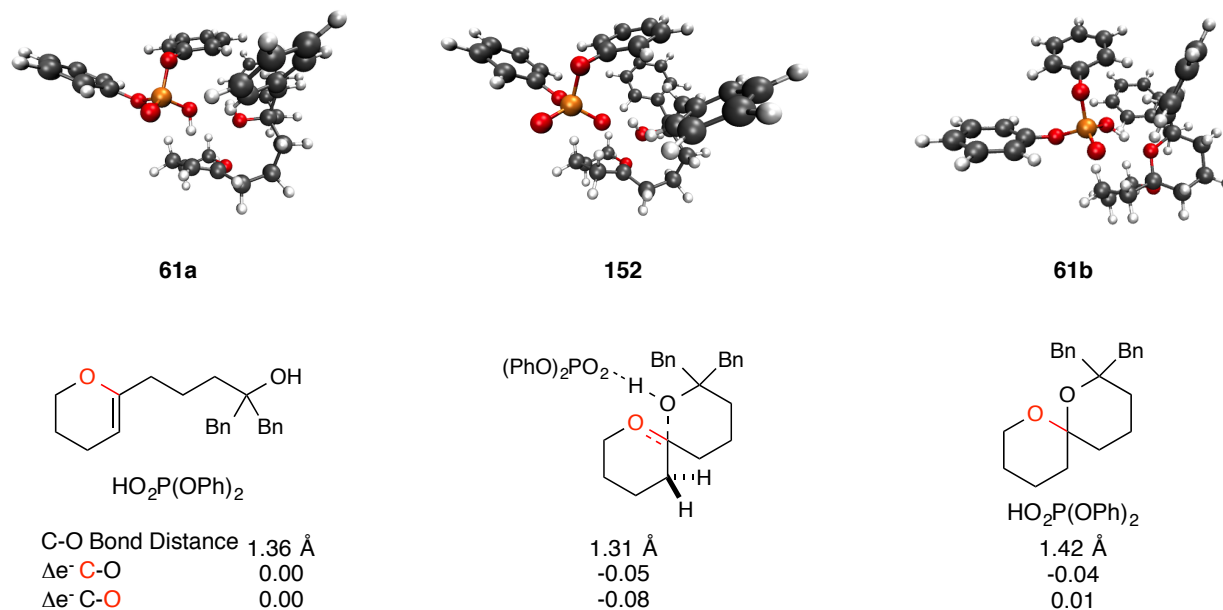


Figure 3.5: Tracking electron density and C-O bond distance in the formation of **61b**. Calculated values for geometries for the pathways investigated for the formation of **61b** at the GAMESS(SMD solvent = *n*-pentane)/ ω B97X-D/6-311+G** level.

It is also worth noting that while the lowest lying pathways for both of these reactions appear to be concerted, they are asynchronous in nature. The reaction begins with the phosphate coordinating to the enol ether. A discrete protonation event occurs, followed by immediate and simultaneous cyclization and deprotonation of the hydroxy nucleophile. Despite these two distinct events, the mechanism is still observed to be concerted and the protonated substrate is not proposed to be a stable structure along the reaction path. Optimization of the geometry of this protonated structure collapses back to the starting materials.

Following the identification of the most reasonable reaction pathway, we sought to measure the amount of time it takes for the transition state to collapse to product by performing direct dynamic calculations. While dynamics computations for the **61a/b** system are still ongoing, those for the **49/50** system have been completed (Figure 3.6). While our computations predict a concerted mechanism is operating, we wanted to continue to probe the system on a time-resolved level to further understand the asynchronous nature of the bond forming events as well as the lifetime of the transition state.

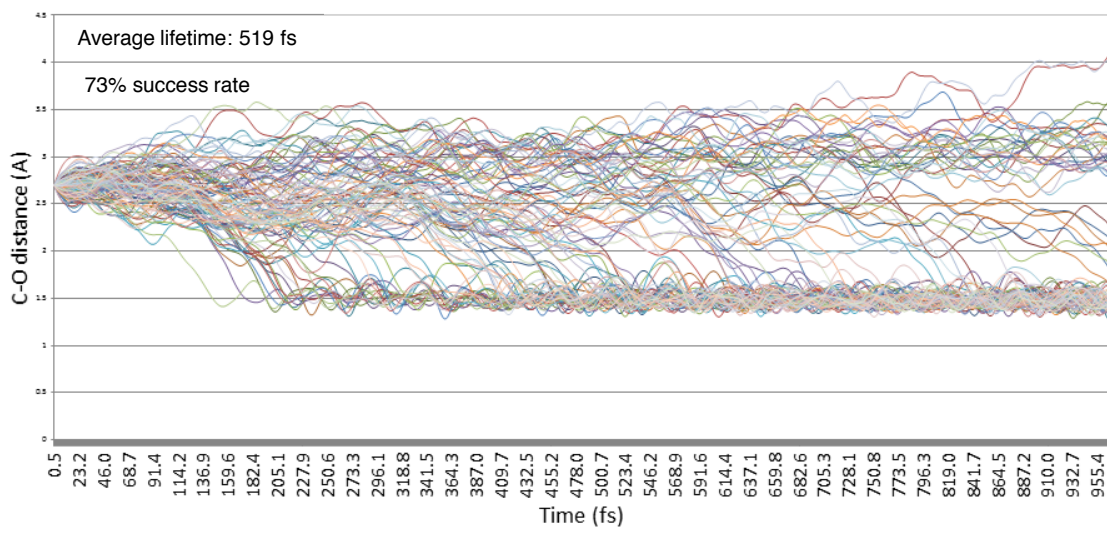


Figure 3.6: Direct dynamic calculations measuring collapse of the transition state of **49** to **50** over time.^j

Though frequency calculations suggest this reaction to proceed through a low-charged transition state, its geometry appears to have tight ion pair geometrical characteristics. By tracking the collapse of the transition state over time, we can estimate lifetime of these oxocarbenium-like geometries in order to better understand the stability of such species. For the cyclization of **49** to **50**, collapse of the transition state geometry was tracked via quasiclassical trajectory calculations. Collapse was measured over a series of 99 runs, with 73% observed to collapse forwards to the desired product. By averaging the amount of time it took for the oxygen cyclization to occur over this combinatorial set of data we can estimate the amount of time it takes for the species present at the reaction transition state to form the spiroketal product with a C-O bond $< 1.5 \text{ \AA}$ to be 519 fs. Quasiclassical trajectory calculations can thus be of great value towards understanding the nuances of a reaction mechanism that are overlooked or not obtained by traditional searching across a PES, however, few direct dynamics investigations have been performed on cationic species and concerted asynchronous reactions and most dynamics studies set different criteria for the beginning and end cutoffs for transition state existence, making lifetime comparisons and assessments challenging.¹¹²⁻¹¹⁴ For comparison, bond stretches usually occur on the magnitude of 10-100 fs, and a bond break encompassing 1 nm of distance occurs on

^j Dynamics computations displayed in Figure 3.6 were performed by Alonso Jose Arguelles Delgado.

the order of 1000 femtoseconds. We can thus conclude that the transition state of these mechanistic pathways are not long lived intermediates.

3.7 Conclusions

We have obtained and presented both experimental and computational mechanistic details involving the chiral phosphoric acid catalyzed stereoselective spiroketalization of enol ethers. Hammett analysis of reaction kinetics are consistent with a concerted mechanism that does not involve a significant amount of charge development in the transition state of the reaction ($\rho = -1.3$). In addition, we have presented a unique and unprecedented deuterium labeling study, which suggests the acidic proton from the catalyst and the hydroxy nucleophile add to the enol ether from the same face of the molecule. This *syn* addition was observed in a range of solvents as well as with a variety of achiral, strong Brønsted acids. These findings raise the possibility that even achiral acids can provide stereocontrol in an underappreciated manner. Finally, we have utilized a new computational methodology to probe the potential mechanistic pathways of this reaction and found agreement with the concerted pathway being lowest in energy. Direct dynamics assist us in concluding oxocarbenium ions are not stable intermediates, nor are they long-lived transition states, with an average lifetime computed to be 519 fs.

While completion of direct dynamics computations for the transformation of **61a** to **61b** will grant additional insight into this mechanism, computing the reaction pathway using the full catalytic system of (*S*)-**20** is also being undertaken and upon identification of reasonable low energy transition states, we hope to explore the dynamics of this full system as well, despite the estimated month-long computational time required for these calculations to run. Together, these computational studies operate in full support of our previously discussed experimental work, clarifying a concerted, asynchronous mechanism is the predominant pathway through which CPA-catalyzed spiroketalization proceeds.

Completion of dynamics studies on additional systems, and finalization of computations on the full reaction pathway will provide fundamental new insights into the source of stereoselectivity in this reaction, and will bring this study to a close. These findings call for a recategorization of the mechanism of strong Brønsted acid-catalyzed spiroketalization reactions from operating through an oxocarbenium ion intermediate to a concerted, asynchronous reaction mechanism.

3.8 Experimental

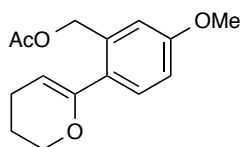
General Methods:

All reagents and solvents were purchased from Sigma-Aldrich or Fisher Scientific and were used as received without further purification unless specified. All reactions were carried out under a positive pressure of nitrogen in flame- or oven-dried glassware with magnetic stirring. Reactions were cooled using external cooling baths: ice water (0 °C) or dry ice/acetone (-78 °C) or Neslab CB 80 immersion cooler (0 °C to -60 °C). Heating was achieved by use of a silicone bath with heating controlled by electronic contact thermometer. Deionized water was used in the preparation of all aqueous solutions and for all aqueous extractions. Solvents used for extraction and chromatography were ACS or HPLC grade. Reagents were purified prior to use following the guidelines of Armarego and Chai.¹ Purification of reactions mixtures was performed by flash chromatography using SiliCycle SiliaFlash P60 (230-400 mesh). The 4 Å molecules sieves were purchased from Sigma-Aldrich. The catalog number is 688363-500g. The molecules sieves were flame-dried under high vacuum for 10 min before use.

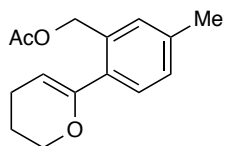
¹H NMR spectra were recorded on Varian vnmrs 700 (700 MHz), Varian vnmrs 500 (500 MHz), Varian INOVA 500 (500 MHz) or Varian MR400 (400 MHz) spectrometers and chemical shifts (δ) are reported in parts per million (ppm) with solvent resonance as the internal standard (CDCl₃ at δ 7.26, C₆D₆ at δ 7.16). Data are reported as (br = broad, s = singlet, d = doublet, t = triplet, q = quartet, m = multiplet; coupling constant(s) in Hz; integration). Proton-decoupled ¹³C NMR spectra were recorded on Varian vnmrs 700 (700 MHz), Varian vnmrs 500 (500 MHz), Varian INOVA 500 (500 MHz) or Varian MR400 (400 MHz) spectrometers and chemical shifts (δ) are reported in ppm with solvent resonance as the internal standard (CDCl₃ at δ 77.0, C₆D₆ at δ 127.683). High resolution mass spectra (HRMS) were recorded on Micromass AutoSpec Ultima or VG (Micromass) 70-250-S Magnetic sector mass spectrometers in the University of Michigan mass spectrometry laboratory. Infrared (IR) spectra were recorded as thin films on NaCl plates on a Perkin Elmer Spectrum BX FT-IR spectrometer. Absorption peaks were reported in wavenumbers (cm⁻¹). Optical rotations were measured in a solvent of choice on a JASCO P-2000 or Autopol III digital polarimeter at 589 nm (D-line) and reported as follows $[\alpha]_D^{24}$ (c g/100 mL, solvent).

Synthesis of Hammett Study Substrates:

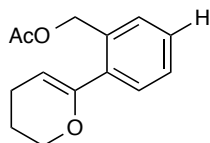
General procedure: Stannane derivative **63** (1.5 mmol) and bromides **129a-f** (1.0 mmol) were dissolved in toluene (10 mL). To this solution, Pd(PPh₃)₄ (0.05 mmol) was added. The mixture was heated to reflux under positive pressure of nitrogen and stirred overnight. The mixture was cooled to room temperature and concentrated *in vacuo*. The obtained residue was purified by column chromatography (1% triethylamine, 10% EtOAc/hexanes) to provide pure **130a-f**.



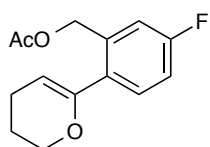
2-(3,4-dihydro-2H-pyran-6-yl)-5-methoxybenzyl acetate (130a). Following the general procedure provided above **130a** (0.49 mmol, 128 mg) was obtained 76%. ¹H NMR (700 MHz, C₆D₆) δ 7.36 (d, J = 8.45 Hz, 1H), 7.11 (d, J = 2.56 Hz, 1H), 6.65 (dd, J = 8.46, 2.71 Hz, 1H) 5.44 (s, 2H), 4.85 (t, J = 3.83 Hz, 1H), 3.84 (m, 2H), 3.29 (s, 3H), 1.89 (m, 2H), 1.69 (s, 3H), 1.50 (m, 2H); ¹³C NMR (175 MHz, C₆D₆) δ 169.6, 159.7, 153.0, 136.1, 130.2, 127.6, 114.2, 112.4, 100.0, 65.9, 64.1, 54.4, 22.1, 20.6, 20.1. HRMS (ES) m/z calcd for C₁₅H₁₈O₄⁺ [M+Na]⁺ 285.1097, found 285.1099.



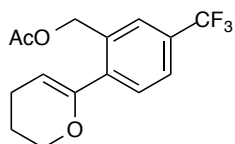
2-(3,4-dihydro-2H-pyran-6-yl)-5-methylbenzyl acetate (130b). Following the general procedure provided above **130b** (0.53 mmol, 141 mg) was obtained 89%. ¹H NMR (700 MHz, C₆D₆) δ 7.48 (s, 1H), 7.28 (d, J = 7.82 Hz, 1H), 6.85 (d, J = 7.82, 1H), 5.00 (t, J = 3.82, 1H), 3.89 (t, J = 5.14 Hz, 2H), 3.61 (s, 3H), 1.95 (s, 3H), 1.56 (m, 2H), 1.27 (m, 2H); ¹³C NMR (175 MHz, C₆D₆) δ 169.6, 153.2, 137.6, 134.5, 129.5, 129.0, 128.2, 127.9, 100.3, 65.9, 64.3, 28.2, 26.6, 22.1, 20.7. HRMS (ES) m/z calcd for C₁₅H₁₈O₃⁺ [M+Na]⁺ 269.1148, found 269.1148.



2-(3,4-dihydro-2H-pyran-6-yl)benzyl acetate (130c). Following the general procedure provided above **130c** (0.43 mmol, 100 mg) was obtained 77%. ^1H NMR (400 MHz, C_6D_6) δ 7.41-7.36 (m, 2H), 7.12-7.03 (m, 2H), 5.49 (s, 2H), 4.84 (t, $J = 3.87$ Hz, 1H), 3.82-3.79 (m, 2H), 1.84 (td, $J = 6.46, 3.92$ Hz, 2H), 1.75-1.63 (m, 2H), 1.49-1.43 (m, 2H); ^{13}C NMR (175 MHz, C_6D_6) δ 169.6, 153.2, 137.1, 132.5, 130.0, 128.7, 127.6, 127.4, 100.5, 65.9, 64.2, 22.0, 20.5, 20.1.



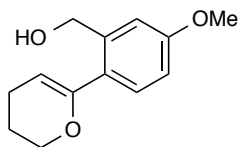
2-(3,4-dihydro-2H-pyran-6-yl)-5-fluorobenzyl acetate (130d). Following the general procedure provided above **130d** (0.23 mmol, 58.3 mg) was obtained 86%. ^1H NMR (700 MHz, C_6D_6) δ 7.14 (m, 2H), 6.69 (m, 1H), 5.29 (s, 2H), 4.71 (t, $J = 3.86$ Hz, 1H), 3.75 (m, 2H), 1.80 (m, 2H), 1.64 (s, 3H), 1.43 (m, 2H); ^{13}C NMR (175 MHz, C_6D_6) δ 169.4, 150.8, 137.3, 133.8, 132.7, 130.6, 127.8, 127.4, 100.8, 65.8, 63.4, 26.7, 21.9, 20.4. HRMS (ES) m/z calcd for $\text{C}_{14}\text{H}_{15}\text{FO}_3^+$ $[\text{M}+\text{Na}]^+$ 273.0899, found 273.0899.



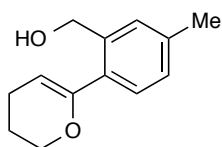
2-(3,4-dihydro-2H-pyran-6-yl)-5-(trifluoromethyl)benzyl acetate (130e). Following the general procedure provided above **130e** (0.5 mmol, 151 mg) was obtained 89%. ^1H NMR (700 MHz, C_6D_6) δ 7.73 (s, 1H), 7.23 (d, $J = 8.1$ Hz, 1H), 7.17 (d, $J = 8.1$ Hz, 1H), 5.25 (s, 2H), 4.73 (t, $J = 3.7$, 1H), 3.73 (t, $J = 5.1$, 2H), 1.62 (s, 3H), 1.60-1.54 (m, 2H), 1.43-1.39 (m, 2H). HRMS (ES) m/z calcd for $\text{C}_{15}\text{H}_{15}\text{F}_3\text{O}_3^+$ $[\text{M}+\text{Na}]^+$ 323.0866, found 323.0868.

General deprotection procedure: Acetates **130a-f** (0.111 mmol) dissolved in a 1:1 mixture of THF (1 mL) and methanol (1 mL). Potassium carbonate (0.222 mmol) was activated in a mortar and pestle and then added to the reaction. When the reaction was deemed complete by thin layer

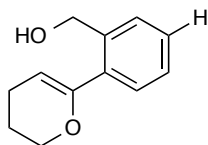
chromatography, the reaction was diluted with diethyl ether, dried over magnesium sulfate, filtered and concentrated in vacuo. The obtained product was purified by column chromatography (6:1 hexanes: ethyl acetate, 1% triethylamine) to provide pure alcohols **131a-f**.



(2-(3,4-dihydro-2H-pyran-6-yl)-5-methoxyphenyl)methanol (131a). Following the general procedure provided above **131a** (0.28 mmol, 61 mg) was obtained 71%. ^1H NMR (700 MHz, C_6D_6) δ 7.35-7.29 (m, 5H), 5.80-5.75 (m, 1H), 5.09 (s, 2H), 4.99 (d, $J=16.8$ Hz, 1H), 4.92 (d, $J=10.0$ Hz, 1H), 4.77 (br, 1H), 3.11 (d, $J=6.4$ Hz, 2H), 2.02-1.94 (m, 2H), 1.45-1.26 (m, 12H); ^{13}C NMR (175 MHz, C_6D_6) δ 156.7, 139.2, 136.7, 128.5, 128.2, 128.1, 114.2, 66.6, 47.1, 36.2, 34.7, 33.4, 27.3, 26.2, 21.4. HRMS (ES) m/z calcd for $\text{C}_{13}\text{H}_{16}\text{DO}_3^+$ $[\text{M}+\text{Na}]^+$ 243.0992, found 243.0992.

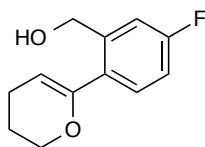


(2-(3,4-dihydro-2H-pyran-6-yl)-5-methylphenyl)methanol (131b). Following the general procedure provided above **131b** (0.12 mmol, 23.6 mg) was obtained 57%. ^1H NMR (700 MHz, C_6D_6) δ 7.35-7.29 (m, 5H), 5.80-5.75 (m, 1H), 5.09 (s, 2H), 4.99 (d, $J=16.8$ Hz, 1H), 4.92 (d, $J=10.0$ Hz, 1H), 4.77 (br, 1H), 3.11 (d, $J=6.4$ Hz, 2H), 2.02-1.94 (m, 2H), 1.45-1.26 (m, 12H); ^{13}C NMR (175 MHz, C_6D_6) δ 156.7, 139.2, 136.7, 128.5, 128.2, 128.1, 114.2, 66.6, 47.1, 36.2, 34.7, 33.4, 27.3, 26.2, 21.4.

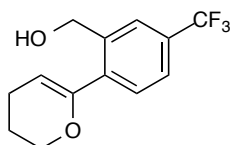


(2-(3,4-dihydro-2H-pyran-6-yl)phenyl)methanol (131c). Following the general procedure provided above **131c** (0.08 mmol, 16.2 mg) was obtained 67%. ^1H NMR (700 MHz, C_6D_6) δ 7.35-7.29 (m, 5H), 5.80-5.75 (m, 1H), 5.09 (s, 2H), 4.99 (d, $J=16.8$ Hz, 1H), 4.92 (d, $J=10.0$ Hz,

1H), 4.77 (br, 1H), 3.11 (d, J =6.4 Hz, 2H), 2.02-1.94 (m, 2H), 1.45-1.26 (m, 12H); ¹³C NMR (175 MHz, C₆D₆) δ 156.7, 139.2, 136.7, 128.5, 128.2, 128.1, 114.2, 66.6, 47.1, 36.2, 34.7, 33.4, 27.3, 26.2, 21.4. HRMS (ES) m/z calcd for C₁₂H₁₄O₂⁺ [M+H]⁺ 191.1065, found 191.1065.



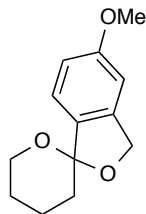
(2-(3,4-dihydro-2H-pyran-6-yl)-5-fluorophenyl)methanol (131d). Following the general procedure provided above **131d** (0.05 mmol, 11.4 mg) was obtained 50%. ¹H NMR (700 MHz, C₆D₆) δ 7.19 (m, 1H), 7.12 (m, 1H), 6.69 (m, 1H), 4.70 (t, J = 3.84, 1H), 4.53 (s, 2H), 3.65 (m, 2H), 1.96 (bs, 1H), 1.79 (m, 2H), 1.41 (m, 2H); ¹³C NMR (175 MHz, C₆D₆) δ 156.7, 139.2, 136.7, 128.5, 128.2, 128.1, 114.2, 66.6, 47.1, 36.2, 34.7, 33.4, 27.3, 26.2, 21.4. HRMS (ES) m/z calcd for C₁₂H₁₃FO₂⁺ [M+Na]⁺ 231.0792, found 231.0794.



(2-(3,4-dihydro-2H-pyran-6-yl)-5-(trifluoromethyl)phenyl)methanol (131e). Following the general procedure provided above **131e** (0.35 mmol, 90 mg) was obtained 39%. ¹H NMR (700 MHz, C₆D₆) δ 7.77 (s, 1H), 7.25 (d, 1H), 7.16 (d, 1H), 4.71 (t, J = 3.4 Hz, 1H), 4.50 (s, 2H), 3.62 (m, 2H), 1.85 (bs, 1H) 1.77 (m, 2H), 1.38 (m, 2H); ¹³C NMR (175 MHz, C₆D₆) δ 152.3, 140.7, 139.4, 120.0, 128.8, 127.9, 125.4, 125.0, 123.8, 123.7, 101.9, 65.9, 627.

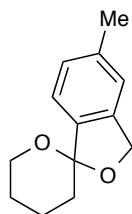
Hammett Study: General Procedure for Spiroketalizations

Each glycol substrate (1 equiv) was dissolved in pentane (0.01 M) and split between 5 vials. 4 Å MS (100 mgs/0.05 mmol) were added to each vial, and then the vials were cooled to 0 °C. The appropriate amount of diphenyl phosphoric acid (5 mol% in a stock solution in DCM) was added. Vials were quenched with triethylamine at each time point, and conversion of the alcohol to the spiroketal was measured by integration of proton signals at the various time intervals.



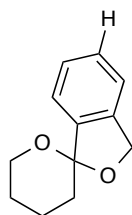
5-methoxy-3',4',5',6'-tetrahydro-3H-spiro[isobenzofuran-1,2'-pyran] (132a).

Following the general procedure provided above **132a** was obtained with a k_{obs} of 6.483. ^1H NMR (700 MHz, C_6D_6) δ 7.32 (d, $J = 8.37$, 1H), 7.20 (d, $J = 8.37$, 1H), 6.76-6.74 (m, 1H), 5.00 (d, $J = 12.47$ Hz, 1H), 4.76 (d, $J = 12.47$ Hz, 1H), 3.79-3.74 (m, 1H) 3.71-3.68 (m, 1H), 3.27 (s, 3H), 2.05-2.03 (m, 1H), 1.88-1.85 (m, 1H), 1.64-1.61 (m, 1H), 1.45-1.43, m 1H), 1.38-1.31 (m, 2H).



5-methyl-3',4',5',6'-tetrahydro-3H-spiro[isobenzofuran-1,2'-pyran] (132b).

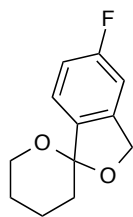
Following the general procedure provided above **132b** was obtained with a k_{obs} of 1.945. ^1H NMR (700 MHz, C_6D_6) δ 7.24-7.17 (m, 3H), 5.016 (d, $J = 12.62$ Hz, 1H), 4.74 (d, $J = 12.62$ Hz, 1H), 4.23-4.17 (m, 1H), 3.61-3.57 (m, 1H), 2.55-2.51 (m, 1H), 2.31 (s, 3H), 2.01-1.96 (m, 1H), 1.76-1.71 (m, 1H), 1.73-1.67 (m, 1H), 1.61-1.54 (m, 2H).



3',4',5',6'-tetrahydro-3H-spiro[isobenzofuran-1,2'-pyran] (132c).

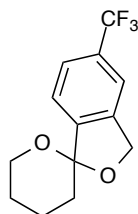
Following the general procedure provided above **132c** was obtained with a k_{obs} of 0.4965. ^1H NMR (700 MHz, C_6D_6) δ 7.37-7.33 (m, 2H), 7.28-7.26 (m, 2H), 5.11 (d, $J = 12.61$ Hz, 1H), 4.98 (d, $J = 12.61$ Hz, 1H), 4.03 (ddd, $J = 12.57$, 11.19, 2.54 Hz, 1H), 3.75-3.72 (m, 1H), 2.16-2.10 (m, 1H), 2.04-1.98 (m, 1H), 1.84-1.80 (m, 2H), 1.80-1.74 (m, 1H), 1.64-1.60 (m, 1H). ^{13}C NMR

(175 MHz, C₆D₆) δ 141.9, 140.0, 128.6, 127.2, 121.6, 121.0, 107.8, 70.7, 63.0, 53.4, 33.8, 25.2, 19.7.



5-fluoro-3',4',5',6'-tetrahydro-3H-spiro[isobenzofuran-1,2'-pyran] (132d).

Following the general procedure provided above **(132d)** was obtained with a k_{obs} of 0.5064. ¹H NMR (700 MHz, C₆D₆) δ 7.07-7.06 (m, 1H), 6.88 (dd, $J = 8.21, 4.92$, 1H), 6.31-6.30 (m, 1H), 4.69 (d, $J = 12.86$ Hz, 1H), 4.44 (d, $J = 12.83$ Hz, 1H), 4.02-3.98 (m, 1H), 3.59-3.56 (m, 1H), 1.96-1.93 (m, 1H), 1.78 (dt, $J = 13.15, 6.62$ Hz, 1H), 1.65-1.63 (m, 1H), 1.47-1.44 (m, 1H), 1.20-1.15 (m, 2H).



5-(trifluoromethyl)-3',4',5',6'-tetrahydro-3H-spiro[isobenzofuran-1,2'-pyran] (132e).

Following the general procedure provided above **132e** was obtained with a k_{obs} of 0.1071. ¹H NMR (700 MHz, C₆D₆) δ 7.28 (d, $J = 8.02$ Hz, 1H), 7.05 (d, $J = 7.95$, 1H), 6.96 (s, 1H), 4.77 (d, $J = 13.06$ Hz, 1H), 4.55 (d, $J = 12.80$ Hz, 1H), 4.09-4.01 (m, 1H), 3.74-3.72 (m, 1H), 2.06-2.04 (m, 1H), 1.88-1.85 (m, 1H), 1.73-1.71 (m, 1H), 1.57-1.54 (m, 1H), 1.32-1.27 (m, 2H).

Table 3.3: Sample of kinetic data collected using NMR for spiroketal formation for substituted alcohols **132a-f**. Time is measured in minutes.

132a (OMe)		132b (Me)		132c (H)		132d (F)		132e (CF ₃)	
Time	% Conv	Time	% Conv	Time	% Conv	Time	% Conv	Time	% Conv
0	0	0	0	0	0	0	0	0	0
0.5	3.85	2	0	2	0	2	2.8	40	3.84
1	5.66	4	2.9	4	0.99	4	3.8	60	6.54

3	13.05	6	8.3	6	1.96	10	5.66		
5	18.03	8	15.3	10	3.85				
				13	4.72				
				20	9.91				

Table 3.4: Observed average $k[A_o]$ for spirocyclization experiments.

132a (OMe)	132b (Me)	132c (H)	132d (F)	132e (CF ₃)
6.483	1.945	0.4965	0.5064	0.1071

Observed rates for the phosphoric acid-induced spirocyclization gave access to a Hammett plot in Figure 3.1 by taking the logarithm of the ratio of observed spirocyclization rate for each alcohol ($k_{\text{obs}}[\text{min}^{-1}]$) divided by the observed rate of spirocyclization for **132c** ($R = \text{H}$; $k_{\text{H}} [\text{min}^{-1}]$) was plotted against known sigma plus values.⁸⁹ As complete conversion to the spiroketals occur over a relatively long time frame, and slower reaction times may be complicated by competing reaction pathways, the observed rates of spiroketalization were calculated based on the method of initial rates, and reactions were monitored until 5-20% conversion was reached.¹¹⁵ In an initial rates assessment, the rate law for a simple first order reaction in which A is converted to P:

$$\frac{d[P]}{dt} = -\frac{d[A]}{dt} = k[A]$$

can be adjusted, as the change in concentration of A is small, meaning $[A]$ can be replaced with $[A]_o$ and approximating $d[P]/dt$ as a constant, equal to $k[A]_o$, and the rate of the reaction can be obtained by dividing the slope of the line by $[A]_o$.

Table 3.5: Data for Hammett plot analysis of phosphoric acid-induced spirocyclization where k_{H} is observed rate for the formation of **132c** (H).

Substrate	σ^+	Average $k_{\text{obs}}[A]_o$	Log ($k_{\text{obs}}/k_{\text{H}}$)
132a (OMe)	-0.78	6.483	1.116
132b (Me)	-0.31	1.945	0.593
132c (H)	0	0.4965	0
132d (F)	-0.07	0.5064	0.008
132e (CF ₃)	0.612	0.1071	-0.666

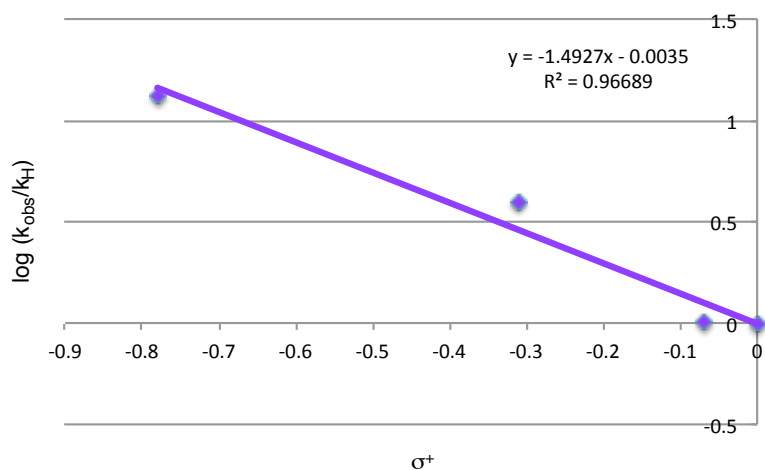


Figure 3.7: Hammett plot following removal of **132e**, $-\text{CF}_3$ data point, resulting in a ρ value of -1.49, consistent with a low-charge transition state.

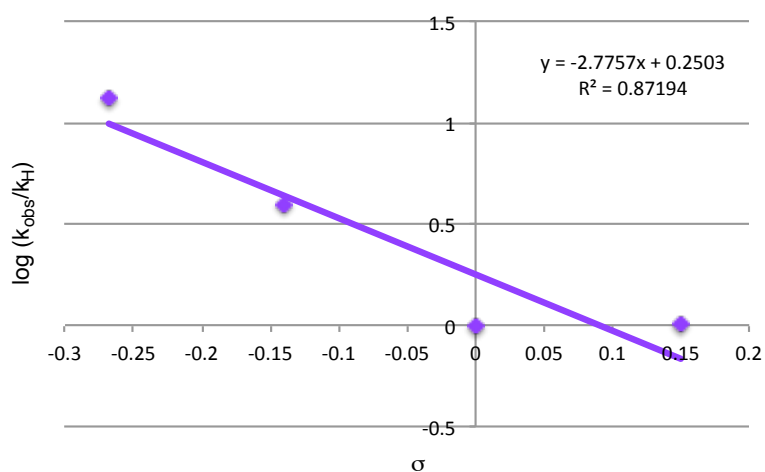


Figure 3.8: Hammett plot against σ values shows a lower correlation with acquired data, indicating σ^+ is more appropriate for the **132** system.

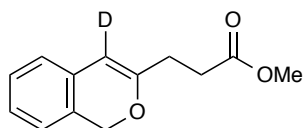
A Hammett plot excluding the **132e** data point results in a consistent conclusion to that made in Figure 3.1 (Figure 3.7), generating a ρ value of -1.49, with a similar correlation factor of 0.97. Though slightly more negative, this ρ again suggests the rate determining step of this reaction proceeds with low charge development in the transition state. As the substituents on the phenyl rings of compounds **131** could be in conjugation with the site of oxocarbenium formation, we believe σ^+ values are more appropriate for this investigation. For comparison, a Hammett plot

using σ values has been included to demonstrate that linear regression of the data presented in Figure 3.8 yields an R^2 of 0.87, supporting the use of σ^+ values for this analysis is appropriate. Linear regression of trend lines ($y=mx+b$) produced in Figures 3.1, 3.7 and 3.8 determined by:

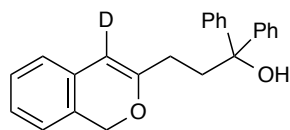
$$r = \frac{n\Sigma(xy) - \Sigma x\Sigma y}{\sqrt{[n\Sigma(x^2) - (\Sigma x)^2][n\Sigma(y^2) - (\Sigma y)^2]}}$$

in which n is the number of data points used to generate the graph. Generation of graphs and linear regression analysis performed with Microsoft Excel.¹¹⁶

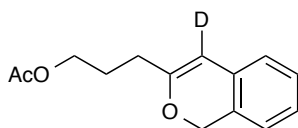
Synthesis of the Deuterium-Labeled Substrates:



Methyl 3-(1H-isochromen-3-yl-4-d)propanoate (141). Methyl 3-(1H-isochromen-3-yl)propanoate **70** (200 mg, 0.92 mmol) was dissolved in THF:D₂O (2.5 mL : 0.75 mL). Deuterated *p*-toluene sulfonic acid (5 mg, 0.028 mmol) was added. The reaction was heated to 70 °C under positive pressure of nitrogen for 12 hours. Reaction quenched with triethyl amine, concentrated *in vacuo*, redissolved in pyridine (0.8 mL), and cooled to 0 °C. MsCl (32 μ L, 1.38 mmol) was added, and the reaction was stirred at 0 °C under positive pressure of nitrogen for 1 hour, and then heated to 90 °C for 1 hour. Reaction cooled to room temperature and partitioned between hexanes and water. The mixture was extracted with hexanes, and the combined organic layers were dried over magnesium sulfate, filtered and concentrated *in vacuo*. Isolated material was then recycled through this procedure two more times to reach 90%+ levels of deuterium label incorporation. Upon sufficient D-label incorporation, the obtained product **141** was purified by column chromatography (3:1 hexanes/ethyl acetate and 1% triethyl amine) to provide the product in 45% yield. ¹H NMR (700 MHz, C₆D₆) δ 7.04-7.02 (m, 1H), 6.93-6.91 (m, 1H), 6.77 (d, $J = 7.5$ Hz, 1H), 6.59 (d, $J = 7.5$ Hz, 1H), 4.77 (s, 2H), 3.31 (s, 3H), 2.45-2.37 (m, 4H); ¹³C NMR (175 MHz, C₆D₆) δ 172.0, 156.5, 131.7, 130.4, 125.8, 123.5, 123.1, 122.5, 68.5, 50.7, 31.4, 28.9. HRMS (ES) m/z calcd for C₁₃H₁₃DO₃⁺ [M+Na]⁺ 242.0898, found 242.0893.

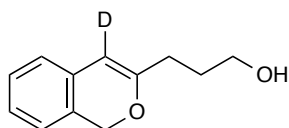


3-(1*H*-Isochromen-3-yl-4-*d*)-1,1-diphenylpropan-1-ol (142). Ester **141** (100 mg, 0.46 mmol) was dissolved in THF (5 mL) and cooled to 0 °C under positive pressure of nitrogen. In a separate flask, Mg (100 mg, 4.1 mmol) was placed in a dry flask in THF (10 mL). To this flask, benzyl bromide (0.7 g, 0.49 mL, 4.1 mmol) was added drop wise, along with a crystal of iodine. After stirring for 3 hours at room temperature, 2 mL was added to the reaction mix, which was stirred at 0 °C for 20 minutes and then warmed to room temperature to stir for two additional hours. The reaction was quenched with saturated ammonium chloride and the product extracted with ethyl acetate. The combined organic layers were dried over magnesium sulfate, filtered and concentrated in vacuo. The obtained product **142** was purified by column chromatography (9:1 hexanes:ethyl acetate, 1% triethylamine) to provide the product in 32% yield. ¹H NMR (700 MHz, C₆D₆) δ 7.41-7.39 (m, 4H), 7.27 (d, J = 7.6 Hz, 1H), 7.13-7.08 (m, 4H), 7.06-7.00 (m, 2H), 6.96-6.92 (m, 1H), 6.79 (d, J = 7.6, 1H), 6.63 (d, J = 7.4, 1H), 5.48 (br, 1H), 4.81 (s, 2H), 2.50-2.46 (m, 2H), 2.29-2.25 (m, 2H); ¹³C NMR (175 MHz, C₆D₆) δ 158.6, 147.1, 128.2, 128.0, 127.6, 127.5, 127.4, 127.1, 126.1, 126.0, 125.6, 123.6, 122.3, 77.4, 68.5, 39.4, 28.4.

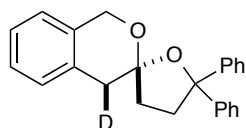


3-(1*H*-isochromen-3-yl-4-*d*)propyl acetate. Compound **74** (200 mgs, 0.86 mmol) was dissolved in THF : D₂O (6.0 mL : 2 mL). Deuterated *p*-toluene sulfonic acid (5 mgs, 0.028 mmol) was added. The reaction was heated to 70 °C under positive pressure of nitrogen for 12 hours. Reaction quenched with triethylamine, concentrated *in vacuo*, redissolved in pyridine (3 mL), and cooled to 0 °C. MsCl (0.066 mL, 0.86 mmol) added, and the reaction was stirred at 0 °C under positive pressure of nitrogen for 1 hour, and then heated to 90 °C for 1 hour. Reaction cooled to room temperature and partitioned between hexanes and water. The mixture was extracted with hexanes, and the combined organic layers were dried over magnesium sulfate, filtered and concentrated *in vacuo*. Isolated material was then recycled through this procedure two more times to reach 90%+ levels of deuterium label incorporation. Upon sufficient D-label

incorporation, the obtained product was purified by column chromatography (6:1 hexanes/ethyl acetate and 1% triethylamine) to provide the product in 42% yield and 92% D label after two cycles of this procedure. ^1H NMR (700 MHz, C_6D_6) δ 7.07-7.03 (m, 1H), 6.94 (td, $J = 7.47, 1.17$ Hz, 1H), 6.80 (d, $J = 7.46$, 1H), 6.62 (d, $J = 7.38$, 1H), 5.49 (s, 0.08 H), 4.79 (s, 2H), 3.99 (t, $J=6.56$, 2H), 2.08 (t, $J = 7.43$, 2H), 1.72 (m, 2H), 1.67 (s, 3H); ^{13}C NMR (175 MHz, C_6D_6) δ 170.0, 157.6, 132.2, 127.6, 126.0, 122.8, 122.75, 122.7, 101.7 (D), 68.8, 63.6, 30.4, 26.4, 20.4. HRMS (ES) m/z calcd for $\text{C}_{14}\text{H}_{15}\text{D}\text{O}_3^+ [\text{M}+\text{Na}]^+$ 256.1060, found 256.1060.

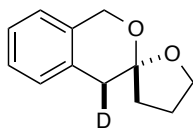


3-(1H-isochromen-3-yl-4-d)propan-1-ol (143). Protected **74** (40 mg, 0.17 mmol) was dissolved in a 1:1 mixture of THF (2 mL) and methanol (2 mL). Potassium carbonate (47.5 mg, 0.34 mmol) was activated in a mortar and pestle and then added to the reaction which was kept dry and under positive pressure of nitrogen. When the reaction was deemed complete by thin layer chromatography, the reaction was diluted with diethyl ether, dried over magnesium sulfate, filtered through elite and concentrated *in vacuo*. The obtained product was purified by column chromatography (6:1 hexanes: ethyl acetate, 1% triethylamine) to provide pure alcohol **143** in 51.8% yield. ^1H NMR (500 MHz, C_6D_6) δ 7.16-7.05 (m, 1H), 6.97-6.83 (m, 1H), 6.77 (d, $J = 7.47$ Hz, 1H), 6.59 (d, $J = 7.35$ Hz, 1H), 4.76 (s, 2H), 3.31 (t, $J = 6.21$ Hz, 2H), 2.13 (t, $J = 7.37$ Hz, 2H), 1.59-1.46 (m, 2H).



(2R,4'S)-5,5-diphenyl-4,5-dihydro-3H-spiro[furan-2,3'-isochromane]-4'-d (145a). Compound **142** (34.2 mg, 0.10 mmol), (*S*)-**20** (3.8 mg, 0.005 mmol) and 4 Å molecular sieves (100 mg) were added to a 10 mL round bottom flask. The mixture was cooled to -78 °C and stirred for 5 min before 5 mL of pentane was added. The mixture was stirred for 5 min before it was warmed up to 0 °C. The mixture was stirred for 24 h, quenched with triethylamine and warmed up to rt. The mixture was loaded on the column (pre-equilibrated with 1% of triethylamine in 9% EtOAc/hexanes) and purified to provide spiroketal **71b**. (30.5 mg, 89%

yield). ^1H NMR (400 MHz, C_6D_6) δ 7.38-7.35 (m, 4H), 7.09-7.00 (m, 5H), 6.96-6.91 (m, 4H), 6.63(d, $J = 7.2$ Hz, 1H), 5.03 (d, $J = 14.8$ Hz, 1H), 4.50 (d, $J = 15.2$ Hz, 1H), 2.94-2.88 (m, 1H), 2.81 (s, 1H), 2.40-2.37 (m, 1H), 2.06-2.03 (m, 1H), 1.72-1.64 (m, 1H).



(2S,4'S)-4,5-dihydro-3H-spiro[furan-2,3'-isochromane]-4'-d (146a). Compound **144** (12.2 mg, 0.06 mmol), (*R*)-**20** (2.4 mg, 0.002 mmol) and 4 Å molecular sieves (100 mg) were added to a 10 mL round bottom flask. The mixture was cooled to -78 °C and stirred for 5 min before 4 mL of pentane was added. The mixture was stirred for 5 min before it was warmed up to 0 °C. The mixture was stirred for 24 h, quenched with triethylamine and warmed up to rt. The mixture was loaded on the column (pre-equilibrated with 1% of triethylamine in 9% EtOAc/hexanes) and purified to provide spiroketal **146a**. (8.8 mg, 72% yield). ^1H NMR (500 MHz, C_6D_6) δ 7.02-6.95 (m, 2H), 6.89-6.86 (m, 1H), 6.71-6.90 (m, 1H), 4.91 (d, $J = 14.6$ Hz, 1H), 4.56 (d, $J = 14.6$ Hz, 1H), 3.85-3.77 (m, 1H), 3.73-3.67 (m, 1H), 2.63 (s, 1H), 2.02-1.94 (m, 1H), 1.92-1.83 (m, 1H), 1.55-1.43 (m, 2H).

Computational Studies:

With the exception of solvent computations, all density functional calculations were performed using Q-Chem 4.0.¹⁰² Optimized geometries were evaluated using the B3LYP density functional using double- ζ -quality basis sets with polarization functions, designated 6-31G**¹⁰³⁻¹⁰⁶. Images of intermediates were generated in VMD.¹⁰⁷ A double-ended growing string method was used to probe the potential energy profile of the reactions.¹⁰⁰

To create the reaction profiles and locate the transition states, 11-15 nodes, including the two fixed end points, were used in the growing string method. The growing string computations proceeded through the addition of new nodes after the perpendicular gradient magnitude on the most recent, frontier node was computed to be less than the 0.15 hartree/Å threshold. A maximum optimization step size of 0.1 was used. A root mean squared (RMS) gradient criterion of <0.0005 hartree/Å was applied to the transition state node to identify complete convergence of a reaction path. Following the convergence of the additive sum of the perpendicular gradient magnitudes over all nodes, F , to $F < 0.3$, the climbing image search was initiated. When $F < 0.1$,

or when highest energy node had a RMS gradient below double the nodal convergence criteria and $F < 0.2$, the exact transition state search was initiated.

In all cases, the Gibbs free energies were first computed through single point energies obtained using a ω B97X-D exchange functional with a 6-311+G** basis set for all reported starting geometries, intermediates, transition states and final geometries.^{108,109} Frequency computations were performed using the B3LYP density exchange functional with a 6-31G** basis set to account for enthalpic contributions from rotational, translational and vibrational energies as well as entropic energies at 298 K. Solvent corrections for *n*-pentane were performed using the SMD solvent model in GAMESS using a ω B97X-D exchange functional with a 6-311+G** basis set.^{110,111}

Cartesian coordinates for the starting geometry, transition states, intermediate and cyclized product of the lowest energy pathway observed are provided below.

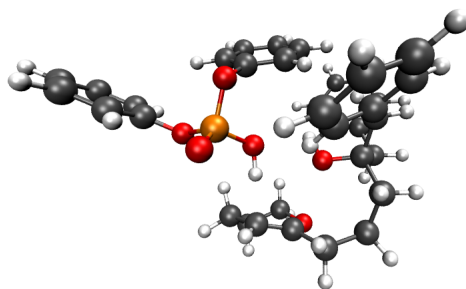


Figure 3.9: Geometry of enol ether **61a**.

61a

81	C 1.884218 -1.222661 0.102882
	C 2.054257 0.316965 -0.011670
	H 1.301364 2.787102 -0.845159
	H -0.543135 2.025343 -1.428002
C 0.930603 1.203706 0.478292	H 0.084760 4.428121 0.563760
C 0.635823 2.424571 -0.058374	H -1.296526 3.418659 0.142562
C -0.307662 3.402286 0.634238	H 0.424020 3.174223 2.677440
C -0.492149 2.972095 2.100769	H -1.325416 3.508334 2.579555
C -0.771307 1.465903 2.134981	H -0.897712 1.084503 3.156567
O 0.330045 0.698935 1.586332	H -1.672176 1.228909 1.544034
O -0.740539 -0.463541 -0.930942	
C 1.164043 -1.933950 -1.064819	

H 1.424818 -1.475985 1.069002
H 2.903616 -1.638501 0.131170
H 2.937517 0.591377 0.592133
H 2.283172 0.596659 -1.050522
C -4.692370 2.129446 -3.299861
C -5.746013 1.364900 -2.761514
H -6.646045 1.868690 -2.407373
C -5.638336 -0.036113 -2.673350
H -6.443824 -0.622349 -2.233117
C -4.479773 -0.684184 -3.145343
H -4.396142 -1.768359 -3.074531
C -3.423166 0.065064 -3.692193
H -2.517449 -0.407820 -4.066613
H -4.754369 3.213305 -3.372621
C -3.541757 1.463779 -3.746586
O -2.457184 2.201112 -4.299711
P -1.365399 2.892439 -3.304340
O -2.165028 4.124355 -2.553580
C -2.702047 5.228924 -3.253956
C -3.879938 5.770850 -2.707458
C -4.470955 6.890157 -3.319622
H -5.383841 7.313269 -2.899202
C -3.889661 7.458909 -4.469711
H -4.351098 8.324187 -4.945810
C -2.708640 6.905154 -4.999843
H -2.250806 7.343012 -5.887367
H -4.311402 5.313094 -1.818225
C -2.098740 5.790224 -4.395089
H -1.178250 5.367782 -4.792125
O -1.287538 1.858603 -2.085895
H -1.396017 -0.162316 -1.578207
O -0.111516 3.265316 -4.009626

C -0.377077 -1.833179 -1.130554
C -0.266506 -1.877730 -3.769867
C -0.109684 -2.769847 -4.848777
H -0.399612 -3.815626 -4.720077
C 0.402184 -2.333179 -6.080450
H 0.513919 -3.043225 -6.902028
C 0.766933 -0.988471 -6.255091
H 1.156156 -0.645320 -7.215087
C 0.628107 -0.089651 -5.185929
H 0.892051 0.962870 -5.296702
C 0.123378 -0.534502 -3.955015
H 0.033821 0.167605 -3.133264
C -2.521337 -2.639458 0.036804
C -3.265297 -3.748655 -0.409526
H -2.737084 -4.652849 -0.720115
C -4.668008 -3.704230 -0.460266
H -5.226642 -4.576196 -0.805428
C -5.348869 -2.543772 -0.059204
H -6.439278 -2.508178 -0.090882
C -4.618132 -1.431140 0.388677
H -5.138338 -0.520882 0.691022
C -3.218115 -1.479304 0.433673
H -2.643632 -0.616230 0.765849
C -1.009333 -2.659368 0.038261
H -0.629736 -2.223210 0.973841
H -0.644483 -3.696097 -0.029071
C -0.909871 -2.376222 -2.484277
H -1.988699 -2.145337 -2.503616
H -0.841907 -3.475104 -2.458787
H 1.411546 -3.007861 -1.018906
H 1.588811 -1.560626 -2.008074

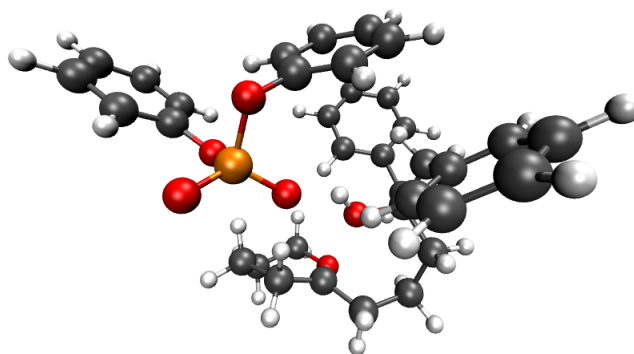


Figure 3.10: Geometry of transition state **152**.

152
81

C 1.079409 0.989953 0.304069
 C 1.000489 2.296265 -0.355072
 C 0.186307 3.397046 0.368228
 C 0.048505 3.091229 1.865854
 C -0.483432 1.673886 2.021519
 O 0.448277 0.699308 1.410757
 O -0.452982 -0.127025 -1.030852
 C 0.902892 -2.126717 -0.971899
 C 1.777270 -1.509340 0.135895
 C 2.129287 -0.015731 -0.072426
 H 2.014835 2.591290 -0.664973
 H 0.451312 2.142738 -1.341891
 H 0.646795 4.378188 0.195587
 H -0.811296 3.428540 -0.093765
 H 1.023178 3.157018 2.377619
 H -0.641895 3.788377 2.362386
 H -0.553586 1.336880 3.061980
 H -1.448624 1.529183 1.517729
 H 1.326668 -1.647546 1.129282
 H 2.731536 -2.056575 0.147552
 H 2.991998 0.236191 0.574466
 H 2.437535 0.183045 -1.107551
 C -4.275784 1.518102 -3.545911
 C -5.099917 0.393095 -3.362655
 H -6.012532 0.486195 -2.776420

C -4.748582 -0.852308 -3.918927
 H -5.382009 -1.723198 -3.748288
 C -3.569737 -0.967047 -4.682922
 H -3.279170 -1.924669 -5.116557
 C -2.739378 0.151865 -4.877025
 H -1.818375 0.081776 -5.449553
 H -4.537078 2.485612 -3.123877
 C -3.090929 1.381106 -4.294246
 O -2.262253 2.489921 -4.534441
 P -1.205241 3.036227 -3.375151
 O -2.250017 3.742937 -2.244880
 C -3.140210 4.773723 -2.557800
 C -4.297026 4.846236 -1.750509
 C -5.242857 5.859997 -1.972257
 H -6.135824 5.908904 -1.347035
 C -5.043280 6.802718 -2.998561
 H -5.779906 7.587355 -3.175336
 C -3.883770 6.721912 -3.796790
 H -3.719415 7.448707 -4.593952
 H -4.436370 4.102433 -0.965865
 C -2.924457 5.717958 -3.582763
 H -2.025520 5.656983 -4.191187
 O -0.684521 1.852953 -2.540751
 H -0.797297 0.390934 -1.809004
 O -0.271865 4.016272 -4.004029
 C -0.530706 -1.556962 -1.110681
 C -0.399654 -1.961339 -3.716249
 C -0.483020 -3.036107 -4.621877
 H -1.086724 -3.907445 -4.355037
 C 0.180940 -3.001672 -5.858774

H 0.091755 -3.845063 -6.546053
 C 0.956095 -1.885441 -6.206391
 H 1.471383 -1.850114 -7.166951
 C 1.058753 -0.812500 -5.307038
 H 1.648989 0.067330 -5.567876
 C 0.388051 -0.847932 -4.074493
 H 0.455990 0.011537 -3.413208
 C -2.865824 -1.635537 0.025884
 C -3.854050 -2.634701 -0.048576
 H -3.547223 -3.683443 -0.044354
 C -5.215898 -2.303605 -0.119211
 H -5.965444 -3.095703 -0.169654
 C -5.611279 -0.956021 -0.123189

H -6.668779 -0.692798 -0.181187
 C -4.635691 0.050509 -0.064934
 H -4.931377 1.100611 -0.091076
 C -3.278082 -0.284075 0.009490
 H -2.524260 0.499473 0.013536
 C -1.399929 -2.020277 0.100933
 H -0.942912 -1.580524 1.000961
 H -1.315847 -3.114599 0.192270
 C -1.201426 -2.023759 -2.427520
 H -2.126032 -1.436402 -2.543683
 H -1.529903 -3.063976 -2.271961
 H 0.820323 -3.208716 -0.782237
 H 1.430224 -2.014144 -1.930168

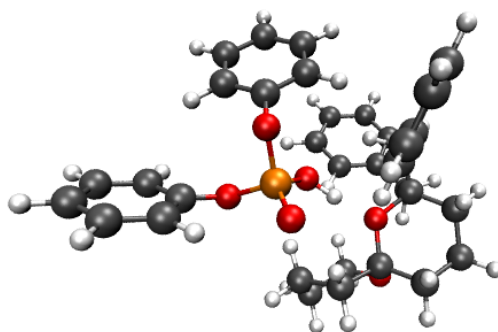


Figure 3.11: Final geometry of **61b**.

61b
 81

C 0.916125 0.676563 0.121421
 C 0.826926 2.177744 -0.206665
 C -0.386585 2.876112 0.435287
 C -0.429501 2.556929 1.937393
 C -0.435804 1.038157 2.129976
 O 0.701672 0.407132 1.499091

O -0.095491 0.022332 -0.731740
 C 1.315198 -2.003415 -1.049545
 C 2.310484 -1.426693 -0.036001
 C 2.306419 0.100998 -0.177190
 H 1.747102 2.630946 0.195206
 H 0.834640 2.317656 -1.295217
 H -0.314248 3.959173 0.260212
 H -1.321753 2.544373 -0.034299
 H 0.456591 2.979405 2.439074
 H -1.325957 2.986225 2.411651

H -0.347791 0.760756 3.189488
H -1.367428 0.601190 1.738262
H 2.039675 -1.701450 0.993484
H 3.316662 -1.823838 -0.235774
H 3.015316 0.577536 0.513487
H 2.580055 0.388277 -1.204622
C -4.912894 1.975597 -4.175412
C -6.094841 1.222847 -4.090348
H -7.054157 1.736965 -4.014343
C -6.046081 -0.180096 -4.100402
H -6.967359 -0.759173 -4.027240
C -4.808720 -0.836514 -4.208284
H -4.764767 -1.926416 -4.216481
C -3.620042 -0.098826 -4.297810
H -2.648519 -0.580864 -4.384180
H -4.925392 3.064274 -4.165415
C -3.692264 1.298735 -4.270429
O -2.497346 2.036944 -4.374570
P -1.692851 2.456804 -3.016092
O -2.657694 3.590272 -2.308090
C -3.001430 4.793484 -2.928208
C -4.297039 5.263790 -2.664462
C -4.709956 6.484849 -3.215594
H -5.716577 6.852480 -3.011698
C -3.836914 7.227098 -4.026949
H -4.160914 8.174504 -4.458707
C -2.543931 6.742383 -4.278085
H -1.858151 7.314779 -4.904359
H -4.955724 4.666971 -2.034184
C -2.110035 5.526789 -3.727388
H -1.106084 5.147020 -3.907265
O -1.948902 1.278636 -1.982363
H -1.138366 0.854150 -1.541779
O -0.297492 2.885242 -3.313068
C -0.119478 -1.454975 -0.888394
C -0.352949 -1.463031 -3.523966
C -0.573325 -2.379532 -4.571394
H -1.101112 -3.312093 -4.358163
C -0.144693 -2.103066 -5.878244
H -0.333393 -2.825346 -6.674177
C 0.518379 -0.898719 -6.160467
H 0.840072 -0.674203 -7.178364
C 0.758156 0.015108 -5.123693
H 1.254103 0.965353 -5.321753
C 0.336035 -0.269979 -3.818023
H 0.531805 0.453424 -3.032996

C -2.346893 -2.035054 0.346434
C -3.083014 -3.234456 0.396708
H -2.546012 -4.181589 0.487977
C -4.484318 -3.232142 0.319611
H -5.030485 -4.176098 0.360640
C -5.177663 -2.021689 0.172885
H -6.265879 -2.016277 0.094947
C -4.458065 -0.818103 0.116522
H -4.979071 0.129854 -0.024395
C -3.060091 -0.825220 0.213210
H -2.524607 0.114966 0.120512
C -0.826839 -2.086677 0.355183
H -0.413360 -1.598561 1.245537
H -0.521250 -3.143655 0.396739
C -0.951437 -1.751852 -2.160441
H -1.905496 -1.214524 -2.071950
H -1.212977 -2.820167 -2.105282
H 1.262561 -3.100802 -0.989440
H 1.671741 -1.752725 -2.058223

3. 9 References

- (1) Rueping, M.; Kuenkel, A.; Atodiresei, I. *Chem. Soc. Rev.* **2011**, *40*, 4539–11.
- (2) MacMillan, D. W. C. *Nature* **2008**, *455*, 304–308.
- (3) Corić, I.; List, B. *Nature* **2012**, *483*, 315–319.
- (4) Cheon, C. H.; Yamamoto, H. *J. Am. Chem. Soc.* **2008**, *130*, 9246–9247.
- (5) Terada, M.; Tanaka, H.; Sorimachi, K. *J. Am. Chem. Soc.* **2009**, *131*, 3430–3431.
- (6) Corić, I.; Vellalath, S.; List, B. *J. Am. Chem. Soc.* **2010**, *132*, 8536–8537.
- (7) Cox, D. J.; Smith, M. D.; Fairbanks, A. J. *Org. Lett.* **2010**, *12*, 1452–1455.
- (8) Han, Z.-Y.; Guo, R.; Wang, P.-S.; Chen, D.-F.; Xiao, H.; Gong, L.-Z. *Tetrahedron Letters* **2011**, *52*, 5963–5967.
- (9) Terada, M.; Toda, Y. *Angew. Chem. Int. Ed.* **2012**, *51*, 2093–2097.
- (10) Wu, H.; He, Y.-P.; Gong, L.-Z. *Org. Lett.* **2013**, *15*, 460–463.
- (11) Kim, J. H.; Corić, I.; Vellalath, S.; List, B. *Angew. Chem. Int. Ed.* **2013**, *52*, 4474–4477.
- (12) Mensah, E.; Camasso, N.; Kaplan, W.; Nagorny, P. *Angew. Chem. Int. Ed.* **2013**, *52*, 12932–12936.
- (13) Kimura, T.; Sekine, M.; Takahashi, D.; Toshima, K. *Angew. Chem. Int. Ed.* **2013**, *52*, 12131–12134.
- (14) Chen, Z.; Sun, J. *Angew. Chem. Int. Ed.* **2013**, *52*, 13593–13596.
- (15) Hsiao, C.-C.; Liao, H.-H.; Sugiono, E.; Atodiresei, I.; Rueping, M. *Chem. Eur. J.* **2013**, *19*, 9775–9779.
- (16) Terada, M.; Yamanaka, T.; Toda, Y. *Chem. Eur. J.* **2013**, *19*, 13658–13662.
- (17) Quach, R.; Furkert, D. P.; Brimble, M. A. *Tetrahedron Letters* **2013**, *54*, 5865–5868.
- (18) Cui, Y.; Villafane, L. A.; Clausen, D. J.; Floreancig, P. E. *Tetrahedron* **2013**, *69*, 7618–7626.
- (19) Lu, C.; Su, X.; Floreancig, P. E. *J. Org. Chem.* **2013**, *78*, 9366–9376.
- (20) Lombardo, V. M.; Thomas, C. D.; Scheidt, K. A. *Angew. Chem. Int. Ed.* **2013**, *52*, 12910–12914.
- (21) Stieglitz, J. *American Chemical Journal* **1899**, *21*, 101–111.
- (22) Meerwein, H.; Bodenbenner, K.; Borner, P.; Kunert, F.; Wunderlich, K. *Justus Liebigs Annalen der Chemie* **1960**, *632*, 38–55.
- (23) Olah, G. A.; White, A. M. *J. Am. Chem. Soc.* **1967**, *89*, 3591–3594.
- (24) Olah, G. A.; Dunne, K.; Mo, Y. K. *J. Am. Chem. Soc.* **1972**, *94*, 4200–4205.
- (25) Olah, G. A.; Berrier, A. L.; Prakash, G. *J. Am. Chem. Soc.* **1982**, *104*, 2373–2376.
- (26) Suzuki, S.; Matsumoto, K.; Kawamura, K.; Suga, S.; Yoshida, J.-I. *Org. Lett.* **2004**, *6*, 3755–3758.
- (27) Suga, S.; Suzuki, S.; Yoshida, J.-I. *Org. Lett.* **2005**, *7*, 4717–4720.
- (28) Suga, S.; Matsumoto, K.; Ueoka, K.; Yoshida, J.-I. *J. Am. Chem. Soc.* **2006**, *128*, 7710–7711.
- (29) Matsumoto, K.; Ueoka, K.; Suzuki, S.; Suga, S.; Yoshida, J.-I. *Tetrahedron* **2009**, *65*, 10901–10907.
- (30) Deslongchamps, P.; Dory, Y. L. *Canadian Journal of ...* **1994**, *72*, 2021–2027.
- (31) Yang, M. T.; Woerpel, K. A. *J. Org. Chem.* **2009**, *74*, 545–553.
- (32) Sinnott, M. *Carbohydrate Chemistry and Biochemistry*; Royal Society of Chemistry: Cambridge, 2007.
- (33) BohÃ, L.; Crich, D. *Comptes rendus - Chimie* **2011**, *14*, 3–16.

- (34) Boháč, L.; Crich, D. *Carbohydrate Research* **2015**, *403*, 48–59.
- (35) Saito, K.; Ueoka, K.; Matsumoto, K.; Suga, S.; Nokami, T.; Yoshida, J.-I. *Angew. Chem. Int. Ed.* **2011**, *50*, 5153–5156.
- (36) Beaver, M. G.; Woerpel, K. A. *J. Org. Chem.* **2010**, *75*, 1107–1118.
- (37) Krumper, J. R.; Salamant, W. A.; Woerpel, K. A. *Org. Lett.* **2008**, *10*, 4907–4910.
- (38) Krumper, J. R.; Salamant, W. A.; Woerpel, K. A. *J. Org. Chem.* **2009**, *74*, 8039–8050.
- (39) Shenoy, S. R.; Woerpel, K. A. *Org. Lett.* **2005**, *7*, 1157–1160.
- (40) Romero, J. A. C.; Tabacco, S. A.; Woerpel, K. A. *J. Am. Chem. Soc.* **2000**, *122*, 168–169.
- (41) Crich, D. *Acc. Chem. Res.* **2010**, *43*, 1144–1153.
- (42) Kancharla, P. K.; Navuluri, C.; Crich, D. *Angew. Chem. Int. Ed.* **2012**, *51*, 11105–11109.
- (43) Crich, D. **2011**, *301*, 141–188.
- (44) Moumé-Pymbock, M.; Furukawa, T.; Mondal, S.; Crich, D. *J. Am. Chem. Soc.* **2013**, *135*, 14249–14255.
- (45) Huang, M.; Retailleau, P.; Bohé, L.; Crich, D. *J. Am. Chem. Soc.* **2012**, *134*, 14746–14749.
- (46) Cox, D. J.; Smith, M. D.; Fairbanks, A. *J. Org. Lett.* **2010**, *12*, 1452–1455.
- (47) Hammett, L. P. *J. Am. Chem. Soc.* **1937**.
- (48) Carpenter, B. K. *Determination of organic reaction mechanisms*; Wiley-Interscience, 1984.
- (49) Wurst, J. M.; Liu, G.; Tan, D. S. *J. Am. Chem. Soc.* **2011**, *133*, 7916–7925.
- (50) Geng, Y.; Kumar, A.; Faidallah, H. M.; Albar, H. A.; Mhkalid, I. A.; Schmidt, R. R. *Angew. Chem. Int. Ed.* **2013**, *52*, 10089–10092.
- (51) Sun, Z.; Winschel, G. A.; Borovika, A.; Nagorny, P. *J. Am. Chem. Soc.* **2012**, *134*, 8074–8077.
- (52) Nagorny, P.; Sun, Z.; Winschel, G. *Synlett* **2013**, *24*, 661–665.
- (53) Shapiro, N. D.; Rauniyar, V.; Hamilton, G. L.; Wu, J.; Toste, F. D. *Nature* **2011**, *470*, 245–249.
- (54) Lemieux, R. U.; Hendriks, K. B.; Stick, R. V. *J. Am. Chem. Soc.* **1975**, *97*, 4056–4062.
- (55) Banait, N. S.; Jencks, W. P. *J. Am. Chem. Soc.* **1991**, *113*, 7951–7958.
- (56) Nukada, T.; Berces, A.; Zgierski, M. Z.; Whitfield, D. M. *J. Am. Chem. Soc.* **1998**, *120*, 13291–13295.
- (57) Jung, K.-H.; Müller, M.; Schmidt, R. R. *Chem. Rev.* **2000**, *100*, 4423–4442.
- (58) Garcia, B. A.; Gin, D. Y. *J. Am. Chem. Soc.* **2000**, *122*, 4269–4279.
- (59) Berces, A.; Enright, G.; Nukada, T.; Whitfield, D. M. *J. Am. Chem. Soc.* **2001**, *123*, 5460–5464.
- (60) Crich, D.; Chandrasekera, N. S. *Angew. Chem. Int. Ed.* **2004**, *43*, 5386–5389.
- (61) Kim, J.-H.; Yang, H.; Park, J.; Boons, G.-J. *J. Am. Chem. Soc.* **2005**, *127*, 12090–12097.
- (62) El-Badri, M. H.; Willenbring, D.; Tantillo, D. J.; Gervay-Hague, J. *J. Org. Chem.* **2007**, *72*, 4663–4672.
- (63) Zhu, X.; Schmidt, R. R. *Angew. Chem. Int. Ed.* **2009**, *48*, 1900–1934.
- (64) Piskiewicz, D.; Bruice, T. C. *Journal of the American Chemical ...* **1967**, *89*, 6237–6243.
- (65) Piskiewicz, D.; Bruice, T. C. *J. Am. Chem. Soc.* **1968**, *90*, 2156–2163.

- (66) Sinnott, M. L.; Jencks, W. P. *Journal of the American Chemical ...* **1980**, *102*, 2026–2032.
- (67) Namchuk, M. N.; McCarter, J. D.; Becalski, A.; Andrews, T.; Withers, S. G. *J. Am. Chem. Soc.* **2000**, *122*, 1270–1277.
- (68) Stubbs, J. M.; Marx, D. *J. Am. Chem. Soc.* **2003**, *125*, 10960–10962.
- (69) Winstein, S.; Grunwald, E.; Jones, H. W. *J. Am. Chem. Soc.* **1951**, *73*, 2700–2707.
- (70) Bentley, T. W.; Schleyer, P. R. *Journal of the American Chemical ...* **1976**, *98*, 7658–7666.
- (71) Frisone, G. J.; Thornton, E. R. *Journal of the American Chemical ...* **1968**.
- (72) Arnett, E. M.; Petro, C.; Schleyer, P. R. ... *the American Chemical Society* **1979**, *101*, 522–526.
- (73) Koo, I. S.; An, S. K.; Yang, K.; Lee, I.; Bentley, T. W. *J. Phys. Org. Chem.* **2002**, *15*, 758–764.
- (74) Baker, J. W. *J. Chem. Soc.* **1933**, 1128–6.
- (75) Baker, J. W.; Nathan, W. S. *J. Chem. Soc.* **1935**, 519–519.
- (76) Baker, J. W.; Nathan, W. S. *J. Chem. Soc.* **1935**, 1840–1845.
- (77) Sugden, S.; Willis, J. B. *J. Chem. Soc.* **1951**, 1360–1364.
- (78) Amyes, T. L.; Richard, J. P. *J. Am. Chem. Soc.* **1990**, *112*, 9507–9512.
- (79) Buckley, N.; Oppenheimer, N. J. *J. Org. Chem.* **1996**, *61*, 7360–7372.
- (80) Toteva, M. M.; Richard, J. P. *J. Am. Chem. Soc.* **2002**, *124*, 9798–9805.
- (81) Richard, J. P. *Simple Relationships Between Carbocation Lifetime and the Mechanism for Nucleophilic Substitution at Saturated Carbon*; ChemInform, 1991.
- (82) Richard, J. P.; Jencks, W. P. *Journal of the American Chemical ...* **1982**, *104*, 4691–4692.
- (83) Lim, C.; Kim, S. H.; Yoh, S. D.; Fujio, M.; Tsuno, Y. *Tetrahedron Letters* **1997**, *38*, 3243–3246.
- (84) Yoh, S. D.; Cheong, D. Y.; Lee, C. H.; Kim, S. H. *Journal of Physical ...* **2001**.
- (85) Young, P. R.; Jencks, W. P. *Journal of the American Chemical ...* **1979**, *101*, 3288–3294.
- (86) Amyes, T. L.; Jencks, W. P. *J. Am. Chem. Soc.* **1989**, *111*, 7900–7909.
- (87) Buckley, N.; Oppenheimer, N. J. *J. Org. Chem.* **1996**, *61*, 8048–8062.
- (88) Liras, J. L.; Lynch, V. M.; Anslyn, E. V. ... *of the American Chemical Society* **1997**, *119*, 8191–8200.
- (89) Hansch, C.; Leo, A.; Taft, R. W. *Chem. Rev.* **1991**, *91*, 165–195.
- (90) Galabov, B.; Nikolova, V.; Wilke, J. J.; Schaefer, H. F.; Allen, W. D. *J. Am. Chem. Soc.* **2008**, *130*, 9887–9896.
- (91) Kaila, N.; Blumenstein, M.; Bielawska, H. *The Journal of Organic ...* **1992**, *57*, 4576–4578.
- (92) Balmond, E.; Galan, M.; McGarrigle, E. *Synlett* **2013**, *24*, 2335–2339.
- (93) Balmond, E. I.; Coe, D. M.; Galan, M. C.; McGarrigle, E. M. *Angew. Chem. Int. Ed.* **2012**, *51*, 9152–9155.
- (94) Kotke, M.; Schreiner, P. *Synthesis* **2007**, *2007*, 779–790.
- (95) Duarte, F.; Geng, T.; Marloie, G.; Hussain, Al, A. O.; Williams, N. H.; Kamerlin, S. C. L. *J. Org. Chem.* **2014**, *79*, 2816–2828.
- (96) Bachrach, S. M. *WIREs Comput Mol Sci* **2014**, *4*, 482–487.
- (97) Mori, K.; Ichikawa, Y.; Kobayashi, M.; Shibata, Y.; Yamanaka, M.; Akiyama, T. *J.*

- Am. Chem. Soc.* **2013**, *135*, 3964–3970.
- (98) Gridnev, I. D.; Kouchi, M.; Sorimachi, K.; Terada, M. *Tetrahedron Letters* **2007**, *48*, 497–500.
- (99) Zimmerman, P. M. *J. Comput. Chem.* **2013**, *34*, 1385–1392.
- (100) Zimmerman, P. *J. Chem. Theory Comput.* **2013**, *9*, 3043–3050.
- (101) Zimmerman, P. M. *J. Chem. Phys.* **2013**, *138*, 184102–184111.
- (102) Fustero, S.; Jiménez, D.; Moscardó, J.; Catalán, S.; del Pozo, C. *Org. Lett.* **2007**, *9*, 5283–5286.
- (103) Becke, A. D. *Physical review A* **1988**, *38*, 3098–3100.
- (104) Lee, C.; Yang, W.; Parr, R. G. *Physical review B* **1988**, *37*, 785–789.
- (105) Becke, A. D. *J. Chem. Phys.* **1993**, *98*, 5648–6.
- (106) Hariharan, P. C.; Pople, J. A. *Theoret. Chim. Acta* **1973**, *28*, 213–222.
- (107) Humphrey, W.; Dalke, A.; Schulten, K. *J Mol Graph* **1996**, *14*, 33–8–27–8.
- (108) Chai, J.-D.; Head-Gordon, M. *Phys. Chem. Chem. Phys.* **2008**, *10*, 6615–6616.
- (109) Clark, T.; Chandrasekhar, J.; Spitznagel, G. W.; Schleyer, P. V. R. *J. Comput. Chem.* **1983**, *4*, 294–301.
- (110) Schmidt, M. W.; Baldridge, K. K.; Boatz, J. A.; Elbert, S. T.; Gordon, M. S.; Jensen, J. H.; Koseki, S.; Matsunaga, N.; Nguyen, K. A.; Su, S.; Windus, T. L.; Dupuis, M.; Montgomery, J. A. *J. Comput. Chem.* **1993**, *14*, 1347–1363.
- (111) Marenich, A. V.; Cramer, C. J.; Truhlar, D. G. *J. Phys. Chem. B* **2009**, *113*, 6378–6396.
- (112) Black, K.; Liu, P.; Xu, L.; Doubleday, C.; Houk, K. N. *Proc. Natl. Acad. Sci. U.S.A.* **2012**, *109*, 12860–12865.
- (113) Zimmerman, P. M.; Tranca, D. C.; Gomes, J.; Lambrecht, D. S.; Head-Gordon, M.; Bell, A. T. *J. Am. Chem. Soc.* **2012**, *134*, 19468–19476.
- (114) Pemberton, R. P.; Tantillo, D. J. *Chem. Sci.* **2014**, *5*, 3301–3308.
- (115) Anslyn, E. V.; Dougherty, D. A. *Modern Physical Organic Chemistry*; University Science Books: Sausalito, California, 2006; Chapter 7; p 389.
- (116) Microsoft. Microsoft Excel. Redmond, Washington: Microsoft, **2011**. Computer Software.

Chapter 4:

Computing the Mechanism and Source of Enantioselectivity in the Synthesis of Chiral Piperidines through the Formation of Chiral Mixed Phosphoric Acid Acetals

CPA's have shown great promise as chiral Brønsted acids, able to catalyze spiroketalization reactions in high yields and selectivities. In a departure from the spiroketalization motif, we turned our attention towards the utilization of chiral phosphoric acids to activate unsaturated acetals towards the nucleophilic attack of a pendant nitrogen nucleophile to give chiral piperidines in an unprecedented transformation.^k In addition to the development of this methodology, a new computational methodology was used to probe the mechanism of this transformation as well as identify the source of enantioselectivity. Interestingly, the computational investigation identified an asynchronous transacetalization/S_N2'-like pathway as the lowest lying pathway.¹

4.1 Introduction

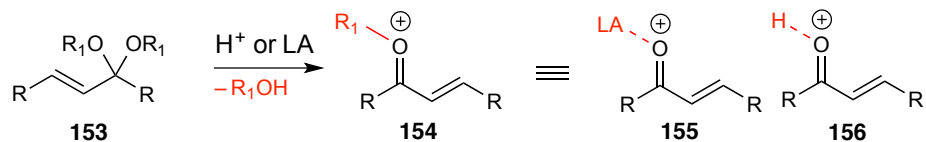
While acetals of carbonyls are often considered protective functionalities, they can also be utilized as a flexible handle for various organic transformations. While many are used as masked acyl anions, they have also been used extensively for a variety of organic transformations, most notably [2+4], [3+4] or [5+2] cyclizations, as well as Nazarov cyclizations and conjugate additions.²

While acetal-derived dienophiles have been shown to be quite reactive, Brønsted acids have previously been utilized to activate unsaturated carbonyl or acetal systems towards functionalization, usually by activating the LUMO of the olefin, resulting in the formation of activated carbonyls of a cationic oxocarbenium-like variety, **155** and **156**.³⁻⁵ An additional

^k Experimental data for the development of the stereoselective aza-Michael reaction was performed by Dr. Zhankui Sun. Computational investigations of this reaction pathway were performed by Grace A. Winschel.

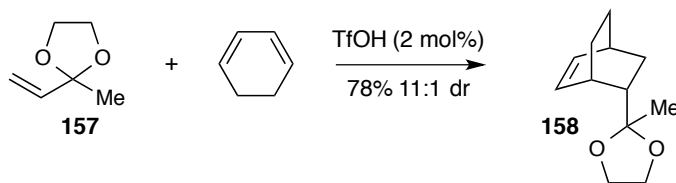
¹ Adapted with permission from Sun, Z.; Winschel, G. A.; Zimmerman, P. A.; Nagorny, P. "Enantioselective Synthesis of Piperidines through the Formation of Chiral Mixed Phosphoric Acid Acetals: Experimental and Theoretical Studies." *Angew. Chemie. Int. Ed.* 53, 11194.¹ Copyright © 2014 Angewandte Chemie International Edition.

approach to activating these types of electrophiles involves Brønsted or Lewis acid coordination to acetals **153** to give reactive intermediates **154** (Scheme 4.1).²



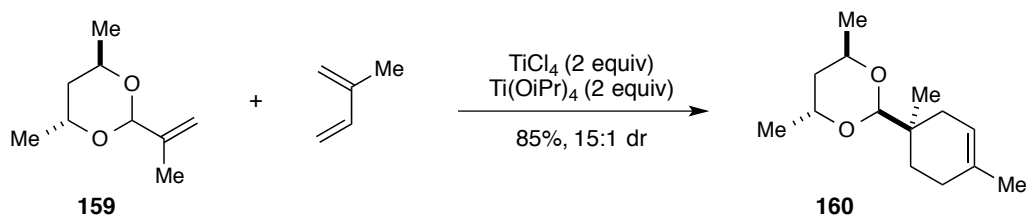
Scheme 4.1: Activation modes of α,β -unsaturated acetals and carbonyls.

The first documented use of α,β -unsaturated acetals in a Diels-Alder reaction was reported in 1987 by Gassman (Scheme 4.2) utilizing LUMO-activation of **157** with triflic acid, for the [4+2] cyclization with cyclohexadiene to yield **158**.⁶ In the years that followed, this type of cycloaddition reaction has been utilized countless times, as the inclusion of an acetal moiety allows for improved stabilities of both the dienophile and the cyclohexene product.



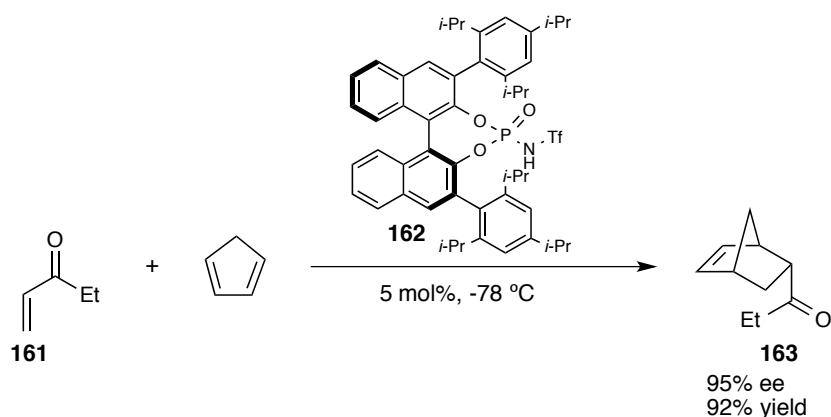
Scheme 4.2: Gassman's TfOH-promoted Diels-Alder of α,β -unsaturated acetals.

An asymmetric variant from the Sammakia group allowed for the diastereoselective formation of Diels-Alder products **160** (Scheme 4.3).⁷ In this example, the source of stereocontrol is derived from the acetal dienophile **159**, in which two stereocenters are installed on the acetal backbone, which can direct the approach and docking of the planar diene.



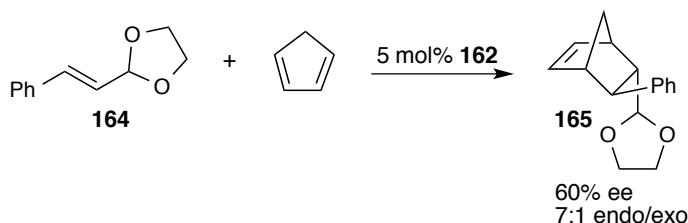
Scheme 4.3: Sammakia's asymmetric Diels-Alder reaction.

Though access to chiral adducts via activation of unsaturated aldehydes and acetals through reactive intermediates **154** are well documented, most approaches, as in the Sammakia example, rely on the installation of auxiliaries to influence stereocenter formation.⁷⁻⁹ Chiral acid-catalyzed transformations of such activated substrates have proven extensively challenging and many groups have had unsuccessful forays into asymmetric ionic Diels-Alder reactions. While condensation of secondary amines to give α,β -unsaturated iminium ions proved to activate the LUMO of the olefin enough towards addition, protonation via phosphoric acids such as (*S*)-**20** to give **156** was not shown to be activating enough to promote a related [2+4] cycloaddition in synthetically useful yields and enantioselectivities. The development of chiral *N*-triflyl phosphoramides **162** by Yamamoto followed to give catalysts with higher acidities, leading to the first chiral phosphoramidate-promoted Diels-Alder being disclosed in 2006 (Scheme 4.4).¹¹



Scheme 4.4: Chiral **162** for application in an asymmetric Diels-Alder reaction to give **163**.

Following these advances, our lab disclosed the first asymmetric chiral *N*-triflylphosphoramidate-catalyzed ionic [2+4] cycloaddition reaction of unsaturated acetals **164** with cyclopentadiene to give **165** (Scheme 4.5).¹²



Scheme 4.5: **162**-catalyzed ionic Diels-Alder reaction of α,β -unsaturated acetals.

With the development of this asymmetric, ionic Diels-Alder reaction, it was made clear that reactions involving the intermediacy of **154** are amenable to asymmetric catalysis and we set out to explore other transformations that could be accomplished through such intermediates. Our group identified CPA-activation of properly designed acetals could be appropriate for the formation of chiral piperidines.

Piperidines are heterocyclic amines, consisting of a nitrogen-containing six membered ring. Piperidines are an important structural moiety seen as the core of a large number of natural products and pharmaceutical agents. Due to their high pharmacological activities, chiral piperidines appear in a wide range of drugs, including desoxypipradrol, a pharmaceutical agent used as a norepinephrine-dopamine reuptake inhibitor, *d*-methylphenidate, a medication used to treat Attention Deficit Hyperactivity Disorder and narcolepsy, under the brand name Concerta and Ritalin and mesoridazine, which, under the brand name Serentil, has been prescribed in the treatment of schizophrenia (Figure 4.1).

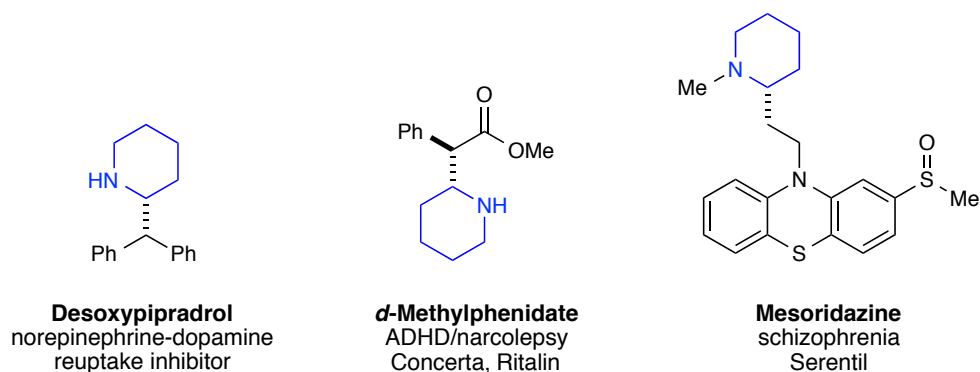
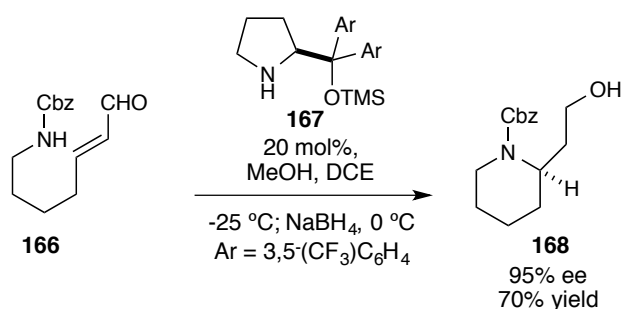


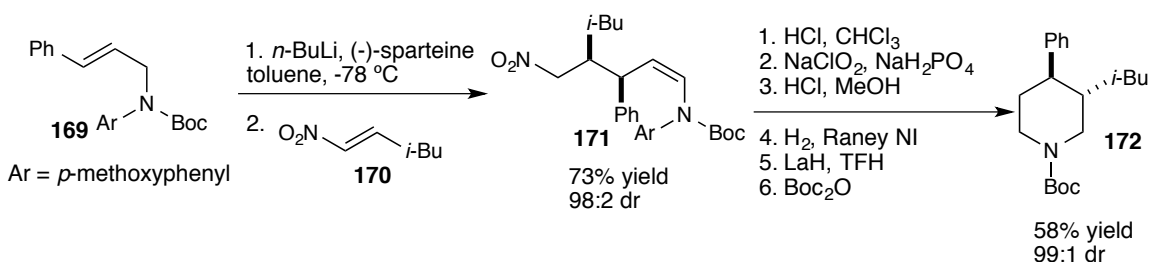
Figure 4.1: Chiral piperidine moieties present in pharmaceutical agents.

Current protocols for the synthesis of chiral piperidines are varied and can involve the use of amino acids and auxiliaries.¹³⁻¹⁶ Most commonly, proline is employed and condenses on the pendant aldehyde to prompt 1,4-addition of the nitrogen nucleophile to form the desired heterocycle by lowering the LUMO of the electrophile (Scheme 4.6).¹⁸⁻²⁶



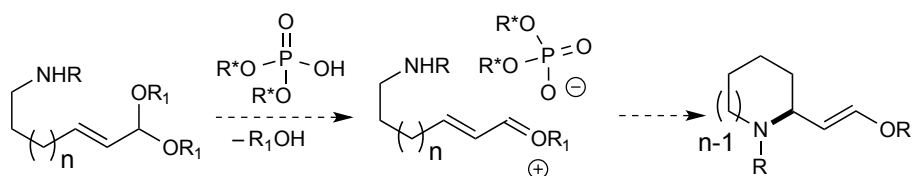
Scheme 4.6: Proline-catalyzed Michael addition to yield chiral piperidines.

In this example, Carter is able to achieve piperidines in 95% ee by employing an TMS-protected proline to catalyze cyclization.²⁰ Another common approach to the stereoselective formation of chiral piperidines involves conjugate additions of lithiated *N*-Boc allylamines **169** to electron-deficient alkenes **170** to give chiral enecarbamates **171**, which can be cyclized to their corresponding lactams and then reduced to the desired piperidines **172** (Scheme 4.7).¹⁷



Scheme 4.7: Synthesis of chiral piperidines through a highly stereoselective conjugate addition of lithated allylamines to nitroalkenes.

We envision a more direct approach to piperidines, in which chiral phosphoric acids are utilized to catalyze cyclization. As the activation of **153** could proceed through the intermediacy of an oxocarbenium ion/chiral phosphate ion pair **154**, the utilization of CPAs for the synthesis of chiral piperidines appeared to be a fruitful avenue for exploration (Scheme 4.8).



Scheme 4.8: Proposed chiral phosphoric acid-mediated aza-Michael reaction of unsaturated acetals for the stereoselective formation of chiral piperidines.

Though several papers document transformations through such an ion pair,²⁷⁻⁴⁵ a more in depth investigation into the mechanism of this type of transformation would also be beneficial to expanding our knowledge of how CPAs activate substrates such as **153** towards nucleophilic attack.

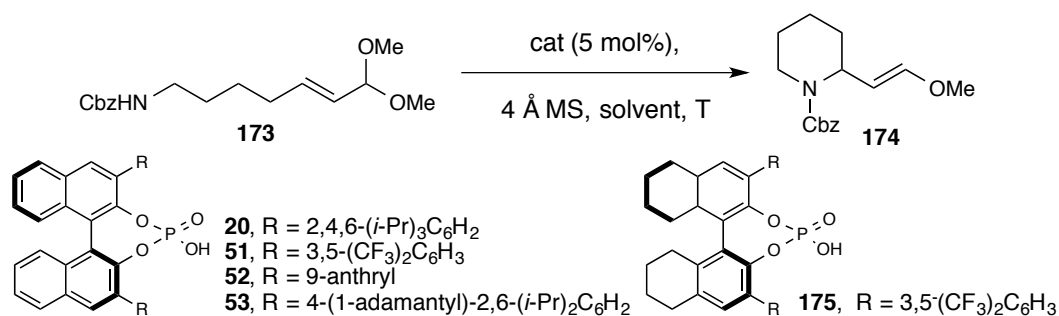
4.2 Optimization of CPA-Catalyzed Stereoselective Aza-Michael Reaction

Optimization began with the cyclization of acetal **173** to chiral piperidine **174** in a variety of polar and non polar solvents (Table 4.1). The cyclization, catalyzed by (*S*)-**20** proved to operate with higher levels of stereocontrol in less polar solvents as was expected; the aza-Michael proceeded with no stereoselectivity in polar solvents like acetonitrile and dichloromethane, however cyclizations in carbon tetrachloride and hexanes gave conversion to chiral piperidines in upwards of 20% ee.

After it was identified that nonpolar solvents gave the best enantioselectivities, an acid screen was conducted. Though (*S*)-**20** was initially chosen for the cyclization reaction, (*S*)-**51** gave piperidine products with over twice the stereocontrol in hexanes at room temperature. Though all of the acids screened showed promising conversion levels after 14 hours, (*S*)-**51** proved to be the most effective for the desired transformation. In addition to hexanes, other nonpolar solvents were rescreened. Toluene, benzene and carbon tetrachloride all resulted in good conversion and higher product enantioselectivities, giving piperidine **174** in 50%, 56% and 57% ee respectively. Carbon tetrachloride was subsequently chosen as the optimal solvent for the transformation.

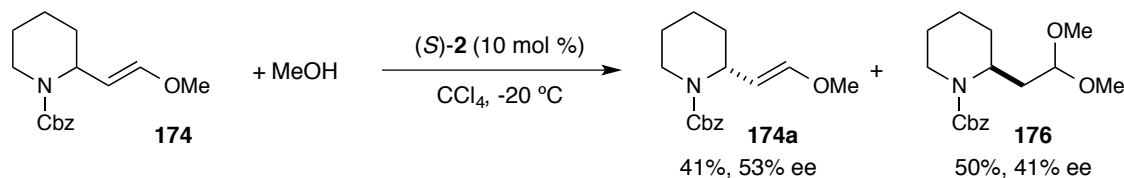
Reduction of the temperature of the reaction to -20 °C from 25 °C resulted in the expected increase of enantioselectivity, boosting ee's to 71% (entry 16). Increasing catalyst loading to 10% gave the only slightly higher stereoselectivity of 75% ee, entry 17, however additional inclusion of 4 Å MS and a lengthening of the reaction time to 24 hours resulted in a noticeable increase to 84% ee, though a slight drop in yield, entry 18. Further elongation of reaction time to 30 hours again boosted enantioselectivity and reduced yield as seen in entries 18-20. This remarkable dependence of stereoselectivities on reaction time, coupled with the observed decrease in yield suggests that (*S*)-**51** catalyzes the reaction of the minor enantiomer of the chiral piperidine product with the methanol by-product of the reaction to give **176**, resulting

Table 4.1: Initial reaction optimization.



entry	catalyst	solvent	T, °C	time, h	yield, %	ee, %
1	(<i>S</i>)- 20	CH ₃ CN	rt	14	78	0
2	(<i>S</i>)- 20	THF	rt	14	20	5
3	(<i>S</i>)- 20	DCM	rt	14	93	0
4	(<i>S</i>)- 20	Et ₂ O	rt	14	15	3
5	(<i>S</i>)- 20	EtOAc	rt	14	20	13
6	(<i>S</i>)- 20	Toluene	rt	14	91	17
7	(<i>S</i>)- 20	CCl ₄	rt	14	95	24
8	(<i>S</i>)- 20	Hexanes	rt	14	86	27
9	(<i>S</i>)- 51	Hexanes	rt	14	96	55
10	(<i>S</i>)- 52	Hexanes	rt	14	78	28
11	(<i>S</i>)- 53	Hexanes	rt	14	83	9
12	(<i>S</i>)- 175	Hexanes	rt	14	95	51
13	(<i>S</i>)- 51	Toluene	rt	14	88	50
14	(<i>S</i>)- 51	Benzene	rt	14	91	56
15	(<i>S</i>)- 51	CCl ₄	rt	14	89	57
16	(<i>S</i>)- 51	CCl ₄	-20 °C	14	86	71
17	(<i>S</i>)- 51	CCl ₄	-20 °C	14	88	75
18	(<i>S</i>)- 51	CCl ₄	-20 °C	24	81	84
19	(<i>S</i>)- 51	CCl ₄	-20 °C	30	75	87
20	(<i>S</i>)- 51	CCl ₄	-20 °C	48	62	95

in effective enantioenrichment of the product **174a**. To confirm that this type of kinetic resolution was operating, racemic piperidine **174** was combined with methanol under the cyclization reaction conditions (Scheme 4.9).



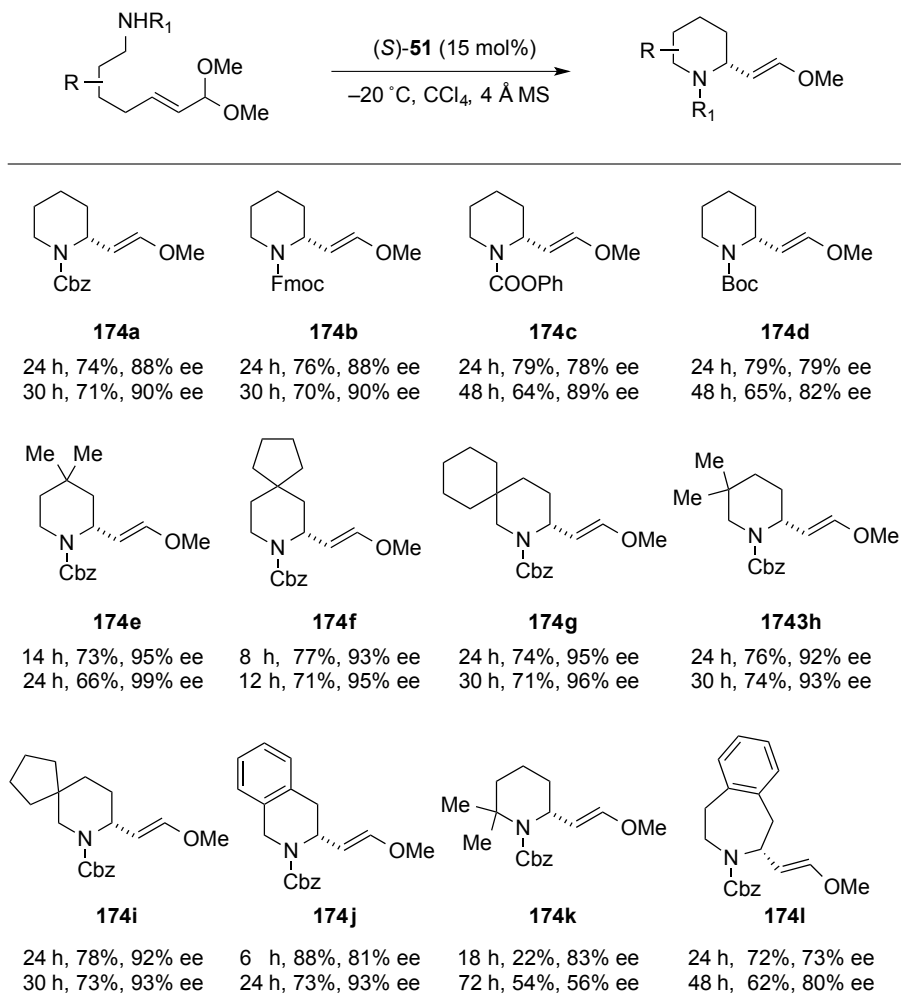
Scheme 4.9: Enantioenrichment of racemic piperidine **174**.

Enantioenrichment was observed; in order to accelerate the kinetic resolution, 15 mol% of the catalyst was subsequently used in the aza-Michael reactions that follow.

4.3 Reaction Scope

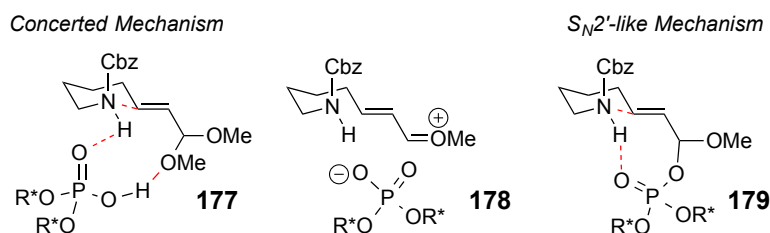
With optimized reaction conditions in hand, Dr. Sun next evaluated the scope of the reaction. In order to illustrate the kinetic resolution pathway, reaction yields and enantioselectivities were monitored at two different time points (Table 4.2). The reaction proved tolerant to a variety of structural modifications of the starting acetal. A variety of nitrogen-protecting groups were evaluated to determine their effect on the stereocontrol of the cyclization, and notably all four piperidine products **174a-174d** were produced in high yields and enantioselectivities, as well as demonstrated involvement of the kinetic resolution pathway.

Next, substitution on the piperidine backbone was investigated. C4 substitution such as geminal dimethyl groups in the case of **174e**, as well as cyclopentane substitution in the case of **174f** proceeded in a highly enantioselective manner. The reaction also proved tolerant to bulky substitution on the C5 position as illustrated by **174g-174i**. Fusion of a phenyl ring to the piperidine back bone resulted in a slight decrease in enantioselectivity, possibly due to increased rigidity in the substrates **174j** and **174l**. Finally, C6 substitution was investigated, and, despite low conversion, piperidine **174k** was produced in good enantioselectivity after 18 hours, however a drop in ee was observed during prolonged reaction times, perhaps due to a competing racemization pathway.

Table 4.2: Reaction scope.

4.4 Introduction to a Computational Investigation of the Mechanism of Reaction

In order to probe the mechanism of the CPA-catalyzed aza-Michael, a computational investigation was initiated. We anticipated the mechanism would either proceed through **177**, in a concerted pathway, utilizing the bifunctional nature of the chiral phosphoric acid catalyst, simultaneously delivering the acidic proton to the methoxy leaving group and deprotonating the nitrogen upon cyclization, or through **178**, an ionic pathway, in which the CPA protonated the methoxy subunit followed by lone pair-assisted ionization, resulting in the formation of an oxocarbenium ion intermediate which could then cyclize and become deprotonated (Scheme 4.10).



Scheme 4.10: Potential reaction mechanisms.

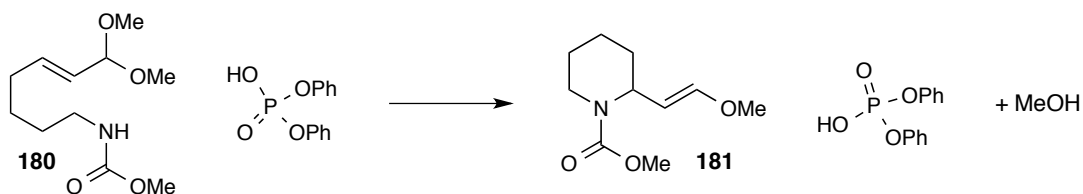
To determine which, if either, of these pathways were operating, a computational study was employed that utilized an automated discovery of chemical reaction steps methodology developed in the Zimmerman group at the University of Michigan (Figure 3.3).⁴⁶⁻⁴⁸ As discussed in the computational analysis of the spiroketalization reaction in Chapter 3, this computational approach investigates a variety of chemically reasonable elementary steps, identifies the energetically most reasonable pathway and then produces internal reaction coordinate-like reaction paths and transition state structures. By utilizing a combinatorial approach, this computational method avoids over-reliance on chemical intuition, which has the possibility of inadvertently biasing the mechanistic outcome by causing key reaction intermediates to be overlooked, while simultaneously saving chemists the trouble of attempting to compute the entire potential energy surface of a reaction.

With the exception of solvent computations, all density functional calculations were performed using Q-Chem 4.0. Optimized geometries were evaluated using the B3LYP density functional using double- ζ -quality basis sets with polarization functions, designated 6-31G**.⁴⁹⁻⁵² A double-ended growing string method was used to probe the potential energy profile of the reactions.⁴⁸

In all cases, the Gibbs free energies were first computed through single point energies obtained using a ω B97X-D exchange functional with a 6-311+G** basis set for all reported starting geometries, intermediates, transition states and final geometries.⁵³⁻⁵⁵ Frequency computations were performed using the B3LYP density exchange functional with a 6-31G** basis set to account for enthalpic contributions from rotational, translational and vibrational energies as well as entropic energies at 298 K. Solvent corrections for carbon tetrachloride were performed using the SMD solvent model in GAMESS using a ω B97X-D exchange functional with a 6-311+G** basis set.^{56,57}

4.5 Preliminary Computational Studies with a Model System

A model system of diphenylphosphoric acid and a truncated variation of **173** were used to search for plausible reaction paths. This model substrate **180** consisted of **173** with a methyl ester protecting group rather than a full Cbz group as shown in Scheme 4.11.



Scheme 4.11: Model reaction for initiation of computational studies.

The Zimmerman methodology⁴⁶⁻⁴⁸ was used to identify potential low energy pathways through which the aza-Michael reaction could be operating. A concerted, ionic mechanism proceeding asynchronously from the starting geometry through an oxocarbenium-like transition state to the cyclized product, as well as an S_N2'-like mechanism invoking the intermediacy of a covalently bound chiral phosphate acetal (**179**, Scheme 4.8) were deemed to have reasonable barriers and these pathways were to be investigated further.

4.6 Computational Studies on the Full Reactive System:

The full (*S*)-**51** catalyst and substrate **173a** were used to probe the reaction path in quantitative detail. After identification of the S_N2'-like pathway, computations involving the full system proceeding through phosphate intermediate **182** were performed.

It is worth noting that the full systems are rather flexible. Due to this flexibility, four different conformations of the catalyst/substrate complex were investigated (*e.g.* directionality of the CBz group, orientation of the fluorinated phenyl rings of the catalyst, orientation and placement of the substrate in the catalytic pocket, cyclization directly through the chair conformation). In addition to conformational changes, the regiochemistry of protonation and departure of either methanol group and addition of either phosphate oxygen into the substrate were investigated. The data presented is for the lowest energy pathway located, as all other geometries and atom combinations gave higher barriers.

An investigation of the reaction pathway depicted in Figure 4.2 below revealed the mechanism to proceed via protonation of the methoxy group closest to the acidic phosphate proton to yield **183** as a transient species. Following protonation, methanol departs from the substrate as the phosphate binds in **TS_{173a} - I**. Although structurally similar carbohydrate-derived anomeric phosphates are known, **182** is energetically uphill from the starting species. As an unstable intermediate, **182** did not prove to be substantially isolable and we could not identify it directly through NMR. It is noteworthy that the proposed mechanism is in line with the studies by Toste and coworkers demonstrating that dithiophosphoric acid-catalyzed asymmetric additions to dienes proceeded through a covalent intermediate similar to **182**.⁵⁸

The activation energy for **TS_{173a} - I** was computed to be 16.9 kcal/mol. As the methanol is liberated, rather than proceeding in a concerted fashion through cyclization (via **178**), the reactive species is trapped by the phosphate to yield energetically favorable intermediate **182**. Following formation of phosphate intermediate **182**, with a PO-C bond distance of 1.50 Å, methanol diffuses away from the catalyst/substrate complex in a free-energy favorable step. This is downhill from **TS_{173a} - I** by 12.7 kcal/mol, relieving the system of the high-energy reorganization process to continue through to the cyclization event. Notably, the ion pair did not prove to be stable at structures near **TS_{173a} - I** for methanol detachment.

The second elementary step begins first with the departure of the phosphate to form species **TS_{173a} - II** which undergoes a nitrogen-carbon bond forming event before immediate deprotonation of **184** to reform the chiral phosphoric acid. This step proceeds with a barrier of 16.6 kcal/mol above the starting species. Overall, this step is seen as a concerted, but asynchronous detachment of the phosphate, ring closure and deprotonation of transitory **184** to yield **174a_{boat}**. As the substrate becomes disengaged from the catalytic pocket, it relaxes without significant barrier from **174a_{boat}** into the lower-energy chair conformation **174a**.

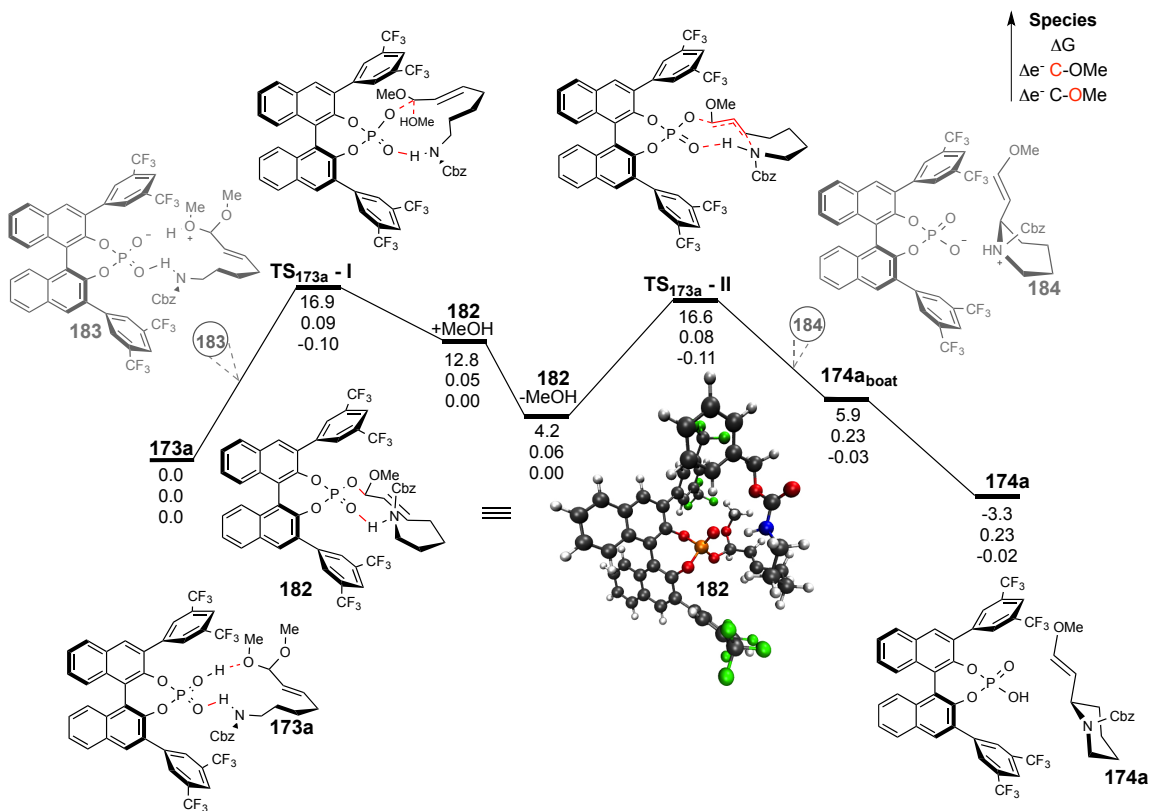
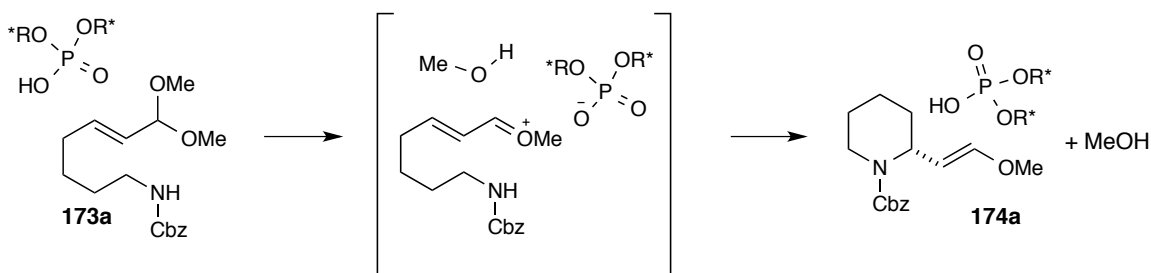


Figure 4.2: Calculated most favored reaction pathway.

While endothermic, the reaction is overall free energy spontaneous. The slight-downhill nature of the reaction is consistent with the observation of chiral resolution. Also of note is the change in electron density of the oxygen in the methoxy group of the substrate. Over the course of the reaction, there is no significant positive charge buildup, with the largest Δe^- observed in **TS_{173a-II}** at $-0.11 e^-$. The carbon to which the methoxy group is attached also does not display significant electron donation from the methoxy oxygen; the largest increase in electron density in a transition state is observed in **TS_{173a-I}**, with an increase of $0.09 e^-$. These numbers are consistent with non-ionic transition states.

Note, PO-C bond distances for the mechanisms proceeding through an **178**-like species and a **179**-like species are different. The oxocarbenium pathway through **178** should show no bond formation between the phosphate oxygen and the oxocarbenium carbon. In addition to the S_N2' -like pathway, growing string was run for the pathway proceeding directly through an ionic intermediate, Scheme 4.12.



Scheme 4.12: Depiction of alternative, concerted, ionic pathway.

The PO-C distance in the transition state remains quite far at 4.29 Å. An investigation of this pathway showed the reaction to be concerted, yet asynchronous, proceeding through three chemical changes in one elementary step. First, protonation of the methoxy leaving group occurs, which prompts the departure of a unit of methanol, leading to transition state **TS_{173a} - III**, which consists of an oxocarbenium ion pair with the chiral phosphate. In this transition state, the nitrogen is poised for cyclization, and following ring closure, the chiral phosphate deprotonates the nitrogen, yielding the piperidine product and regenerating the catalyst. Though chemically reasonable, the barrier for this mechanism was computed to be too high to be a reasonable pathway, at 31.5 kcal/mol. A summary of values including corrections is provided in Table 4.3.

Table 4.3: Calculated values for geometries of starting materials, transition states, intermediates and products for the pathways investigated for the formation of the major piperidine enantiomer at the GAMESS(SMD solvent = carbon tetrachloride)/ ω B97X-D/6-311+G**//B3LYP/6-31G** level.

	E(hartrees)	H (kcal/mol)	S (kcal/mol at 298 K)	Δ G
173a	-4241.100054	587.0	109.6	-
TS_{173a} - I	-4241.072205	586.1	109.3	16.9
182 + MeOH	-4241.081148	587.0	108.7	11.9
182 - MeOH	-4241.071593	586.2	122.5	4.2
TS_{173a} - II	-4241.052486	584.5	120.4	16.6
TS_{173a} - III	-4241.054968	582.7	102.2	31.5
174_{boat}	-4241.077123	584.8	115.9	5.9
174a	-4241.052750	582.9	131.8	-3.3

To confirm the proposed S_N2' -like mechanism, a similar reaction pathway leading to the minor stereoisomer was evaluated using the same methods. The results of the investigation of the stereoisomeric pathway are presented in Figure 4.3. In addition to this pathway, three other conformers (*e.g.* rotated CBz group, ring-flipped chair and repositioned CBz) leading to the minor enantiomer were investigated, though none provided pathways lower in energy than the one reported. While the overall pathway is quite similar to that proposed for the major stereoisomer, in terms of reaction steps, asynchronicity and overall low charge build-up in the transition states of the reaction, the second barrier is notably higher, at 20.1 kcal/mol.

A summary of calculated values including solvent and free-energy corrections is provided in Table 4.4. In support of experimental observations, the reaction pathway to form the minor enantiomer is 3.2 kcal/mol higher in energy than that of the observed major stereoisomer shown in Figure 4.2.

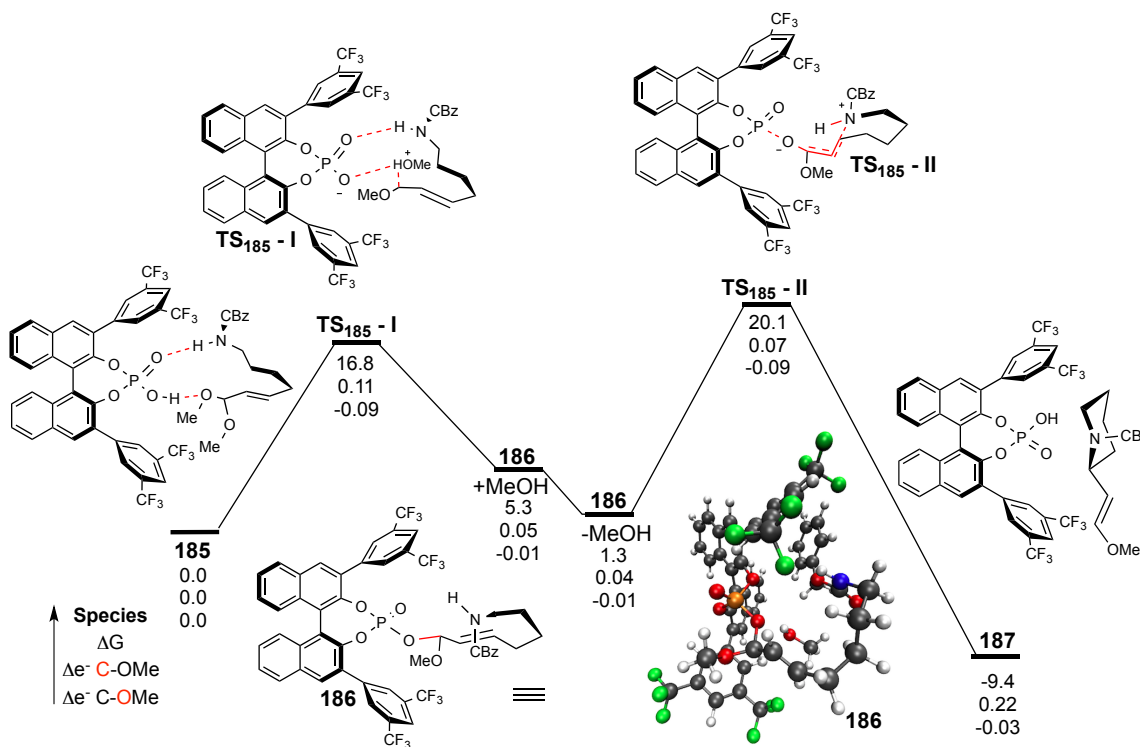


Figure 4.3: Reaction energy diagram for S_N2' -like pathway to form the minor piperidine stereoisomer.

Table 4.4: Calculated values for geometries of starting materials, transition states, intermediates and products for the pathways investigated for the formation of the minor piperidine enantiomer at the GAMESS(SMD solvent = carbontetrachloride)/ ω B97X-D/6-311+G**//B3LYP/6-31G** level.

	E(hartrees)	H (kcal/mol)	S (kcal/mol at 298 K)	ΔG
185	-4241.093595	586.2	105.9	-
TS₁₈₅ - I	-4241.065994	586.3	106.5	16.83
186 + MeOH	-4241.078288	589.4	113.4	5.35
186 - MeOH	-4241.071371	583.7	116.1	1.25
TS₁₈₅ - II	-4241.043858	582.7	113.5	20.08
187	-4241.081485	586.5	123.3	-9.45

By comparing the transition states of the stereoisomeric pathways, the source of stereoselectivity can be identified as stemming from the ability of **173a** to form a hydrogen bond between the N-H and an (*S*)-**51** phosphate oxygen in TS – II. Following the formation of phosphate acetal **182**, the complex leading to the major enantiomer is aligned for hydrogen bond formation (Figure 4.4), while this is not the case for the minor enantiomer, which has the NH bond at a further distance and poor angle for strong H-bond formation with the nearest phosphate oxygen.

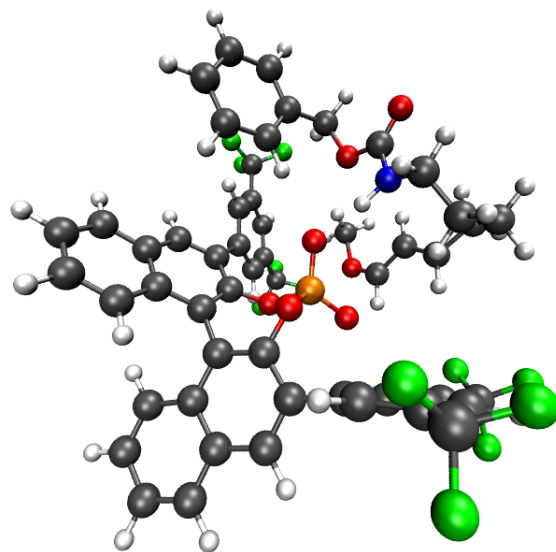


Figure 4.4: Hydrogen bond between N-H of **173a** and P-O of **51** in **TS_{173a} – II** of the reaction is visible.

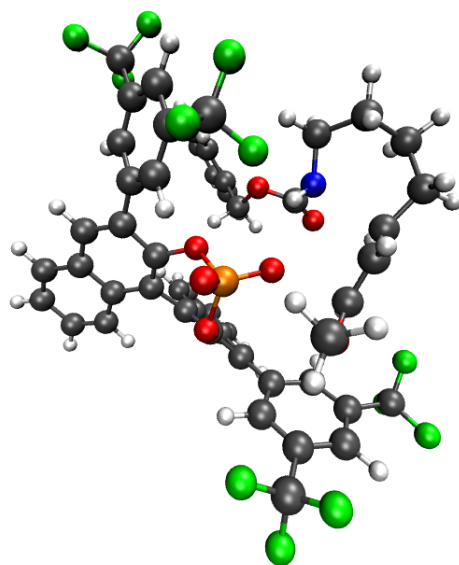


Figure 4.5: Additional distance and poor angle between N-H of **185** and P-O of **51** in **TS₁₈₅ – II** precludes strong H-bond formation in the cyclization to the minor enantiomer.

4.7 Conclusions

We have discovered the first highly enantioselective chiral phosphoric acid-mediated cyclization of unsaturated acetals to chiral piperidines, which are important structural motifs found in the core of many natural products. Direct access to these piperidines was granted by chiral phosphoric acid (*S*)-**51**, which presided over the aza-Michael reaction with high levels of stereocontrol due to its ability to nominally favor one stereoisomeric product as well as an unexpected kinetic resolution, in which the minor enantiomer of the product reacted with the stoichiometric amounts of methanol by-product to yield an unsaturated acetal. By increasing catalyst loading to 15%, we were able to enhance the kinetic resolution step, leading to the acquisition of chiral piperidine products in enriched enantioselectivities within less than 48 hours.

The aza-Michael cyclization reaction developed herein has been demonstrated to be tolerant of a broad range of substitutions on the piperidine core, as well as on the nitrogen nucleophile. A variety of nitrogen protecting groups were examined, including a Cbz- group, Fmoc-, Boc- as well as a phenyl carbamate. Results were relatively consistent for this type of modification, with each alternatively protected substrate providing the desired piperidine product in over 70% yield after 24 hours with high stereocontrol. Notably, all but one substrate demonstrated kinetic resolution, fostering an enantioenriched product after extended reaction times.

Functionalization of the C4 and C5 position with geminal methyl substituents as well as cyclopentyl- and cyclohexyl- subunits provided piperidines with enantioselectivities averaging in the low-to-mid 90%. Unfortunately, geminal substitution on C6 drastically slowed the cyclization reaction and throttled the kinetic resolution; lower yields of the C6 geminally methylated piperidine precursor were observed after prolonged reaction times, perhaps a sign of a competing epimerization pathway.

In our hands, chiral piperidines with a variety of structural scaffolds could now be accessed under very mild conditions. This reaction is thus expected to provide easy access to chiral piperidine cores in the synthesis of a wide array of natural products and other biologically active compounds of interest.

During the development of this aza-Michael cyclization reaction, we undertook a computational investigation of the mechanism of the formation of the chiral piperidines by utilizing an automated discovery of chemical reaction steps methodology developed by the

Zimmerman group. While this computational methodology had shown incredible promise in predicting reasonable elementary mechanistic steps of simple organic reactions, this is the first example of its employment in a highly complex organic environment. Remarkably, rather than confirming the anticipated concerted cyclization, or a stepwise variation involving the intermediacy of an oxocarbenium ion, a new transacetylation/ S_N2' -like pathway was identified as the lowest energy pathway. Indeed the slight down-hill nature of the reaction pathway computed is consistent with the described kinetic resolution.

The validity of this pathway was reinforced upon investigation of the formation of the minor enantiomer of the cyclized product, the pathway for which was 3.2 kcal/mol higher in energy than that of the major stereoisomer. This difference in energy is in agreement with the propensity of the reaction to favor the observed major product, and stems from the ability of the major isomer to form a hydrogen bond between the N-H and a phosphate oxygen present in the catalyst.

4.9 Experimental

To create the reaction profiles and locate the transition states, 11-15 nodes, including the two fixed end points, were used in the growing string method. The growing string computations proceeded through the addition of new nodes after the perpendicular gradient magnitude on the most recent, frontier node was computed to be less than the 0.15 hartree/Å threshold. An initial maximum optimization step size of 0.1 was used. Following the convergence of the additive sum of the perpendicular gradient magnitudes over all nodes, F , to $F < 0.3$, the climbing image search was initiated. When $F < 0.1$, or when highest energy node had a RMS gradient below double the nodal convergence criteria and $F < 0.2$, the exact transition state search was initiated. A root mean squared (RMS) gradient criterion of <0.0005 hartree/Å was applied to the transition state node to identify complete convergence of a reaction path.

Cartesian coordinates for the starting geometry, transition states, intermediate and cyclized product are provided below.

173a	C 1.851870 -4.119916 0.175330
117	C 0.475585 -3.945476 0.531523
	C -0.429706 -5.000036 0.232362
C 2.276631 -5.348571 -0.398886	C 0.008797 -6.169842 -0.346808
C 1.376932 -6.357220 -0.651562	H -0.705430 -6.954507 -0.577027

H 1.709947 -7.289576 -1.096959
H 3.327603 -5.469113 -0.647568
H -1.483180 -4.870737 0.447741
C 2.762647 -3.051758 0.370026
C 2.350192 -1.818848 0.829430
C 0.983246 -1.671919 1.193027
C 0.064350 -2.706387 1.139788
H 3.806134 -3.197820 0.104975
C -1.312006 -2.533604 1.691301
C -1.842095 -3.447930 2.670001
C -2.120360 -1.491045 1.266536
C -3.508962 -1.403042 1.581209
C -4.030214 -2.351781 2.437839
C -3.224162 -3.352550 3.032012
C -4.406738 -0.386118 0.966737
H -5.083823 -2.308206 2.698501
C -1.045556 -4.423570 3.328947
C -1.592404 -5.272291 4.265674
C -2.966179 -5.199154 4.593156
C -3.761771 -4.254394 3.989397
H -3.384843 -5.878999 5.328694
H -4.815016 -4.173194 4.243871
H 0.010586 -4.486907 3.098103
H -0.959457 -6.001559 4.762116
C 3.327764 -0.699209 0.958314
O 0.584295 -0.443134 1.720847
O -1.600051 -0.532364 0.398638
P -0.433047 0.494927 0.868311
O -1.045374 1.362478 2.035379
O 0.127945 1.204468 -0.301782
C -5.599276 -0.801019 0.355106
C -4.119025 0.982509 1.000054
C -6.473401 0.128840 -0.206973
C -6.173881 1.491489 -0.182529
C -4.992522 1.906900 0.426378
C 3.251860 0.425651 0.127034
C 4.210059 1.437009 0.233015
C 5.248771 1.343831 1.158467
C 5.326966 0.220809 1.981299
C 4.375501 -0.794888 1.882291
H 2.461356 0.505328 -0.611128
C 4.096535 2.654309 -0.647655
H 5.989235 2.130803 1.234229
H 4.440843 -1.659587 2.533471
C 6.484162 0.075120 2.933583
H -5.834091 -1.857841 0.297458

H -3.216262 1.328821 1.484737
C -4.607029 3.361357 0.456565
C -7.781301 -0.334824 -0.793551
H -6.845973 2.211987 -0.631496
F -7.693851 -1.584564 -1.296949
F -8.202092 0.479387 -1.784213
F -8.757320 -0.354820 0.143762
F -5.601208 4.168827 0.041937
F -3.533714 3.604606 -0.337521
F -4.256283 3.754097 1.705182
F 3.699741 2.334984 -1.895611
F 5.269121 3.316385 -0.746346
F 3.186307 3.539319 -0.162683
F 6.906659 1.272852 3.392840
F 7.544589 -0.515500 2.336247
F 6.162956 -0.683486 4.004205
H -0.902183 2.360816 2.041852
O -1.048789 3.890686 2.547824
C -1.826402 3.855249 3.754816
C 0.003218 4.871976 2.588368
O 1.015836 4.520022 3.492253
C 1.804511 3.380186 3.142133
C 0.487052 5.153426 1.191265
C -0.225225 4.997906 0.072532
C 0.255626 5.418198 -1.290767
C -0.907739 3.583066 -2.698839
C -0.720224 2.465111 -3.735051
N 0.161509 1.412186 -3.255056
C 1.268272 1.036113 -3.937377
O 1.999382 0.152069 -3.183684
O 1.591980 1.404770 -5.057281
H 1.221292 5.926801 -1.188252
H -0.449486 6.161095 -1.694105
H -1.609211 4.318061 -3.117318
H -1.393212 3.165501 -1.809503
H -1.700247 2.043071 -3.997111
H -0.276766 2.854259 -4.655376
H 0.087584 1.122062 -2.284593
C 3.183733 -0.376843 -3.820462
H -1.220265 4.564203 0.140122
H 1.474868 5.609396 1.153670
H -2.515883 3.016551 3.665234
H -1.180129 3.719017 4.626239
H -2.398713 4.783620 3.856945
H 2.598537 3.322828 3.888722
H 1.217219 2.455734 3.180246

H 2.248666 3.480943 2.146964
 H -0.426504 5.782046 3.030596
 C 0.404532 4.271096 -2.311164
 H 0.872788 4.677662 -3.217391
 H 1.100455 3.530570 -1.907396
 C 2.892729 -1.649455 -4.579643
 C 2.547623 -1.609774 -5.937023
 C 2.263193 -2.787768 -6.628018
 C 2.314474 -4.018503 -5.970606

C 2.650047 -4.066629 -4.616451
 C 2.938727 -2.888090 -3.928965
 H 3.876159 -0.564612 -2.996564
 H 3.600242 0.388695 -4.477159
 H 3.195849 -2.927076 -2.873261
 H 2.093167 -4.935073 -6.510304
 H 2.685268 -5.018973 -4.094763
 H 2.485546 -0.647770 -6.435719
 H 1.999325 -2.744209 -7.680977

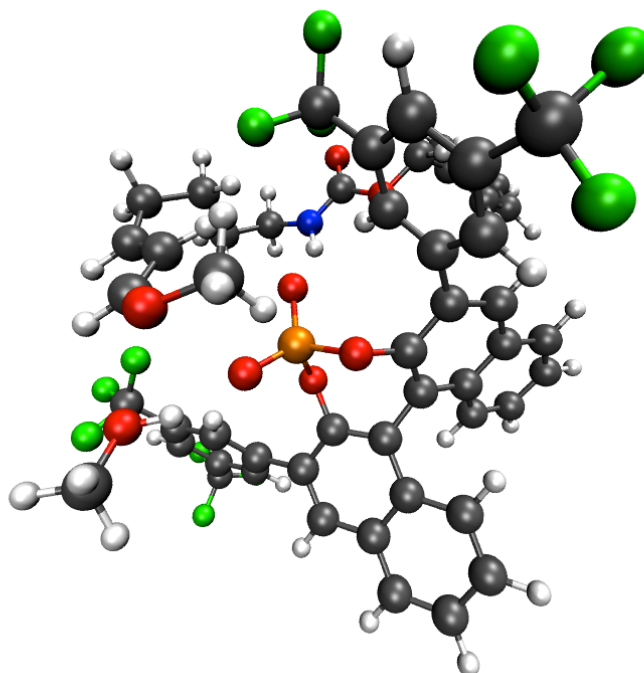


Figure 4.6: Transition state geometry for full system prior to chiral phosphate formation, **TS_{173a} – I**.

TS_{173a} – I
117

C 1.987502 -5.332580 -0.575068
 C 1.034178 -6.303077 -0.774836
 C 1.646019 -4.082686 0.009273
 C 0.296850 -3.846979 0.428964
 C -0.666685 -4.862465 0.181935
 C -0.308723 -6.054782 -0.406492
 H -1.066743 -6.809796 -0.592533
 H 1.304743 -7.252737 -1.226090
 H 3.019429 -5.502614 -0.871164
 H -1.700196 -4.683099 0.451735

C 2.610828 -3.055649 0.170257
 C 2.265411 -1.811669 0.651794
 C 0.922744 -1.592796 1.073513
 C -0.033328 -2.596533 1.058086
 H 3.637337 -3.247244 -0.131056
 C -1.361065 -2.379659 1.699446
 C -1.842222 -3.278877 2.713924
 C -2.155783 -1.304415 1.328520
 C -3.509659 -1.171128 1.763086
 C -3.997495 -2.106226 2.656010
 C -3.189073 -3.144749 3.178598
 C -4.427122 -0.124288 1.230275
 H -5.024326 -2.023736 3.001069

C -1.027365 -4.281562 3.308069
C -1.529246 -5.128085 4.271101
C -2.876335 -5.025148 4.691213
C -3.684291 -4.048600 4.157776
H -3.262920 -5.706939 5.442604
H -4.714563 -3.943077 4.487108
H 0.008571 -4.367307 3.004169
H -0.881978 -5.878848 4.714764
C 3.285011 -0.730445 0.771331
O 0.613094 -0.368027 1.621589
O -1.668038 -0.386421 0.421072
P -0.459102 0.657207 0.860956
O -0.898156 1.576624 1.971694
O 0.117545 1.201032 -0.412687
C -5.673163 -0.520946 0.723180
C -4.113819 1.242327 1.248030
C -6.587278 0.421723 0.254544
C -6.275779 1.780222 0.281434
C -5.036857 2.180867 0.778601
C 3.228804 0.402506 -0.050407
C 4.209976 1.391262 0.056732
C 5.244727 1.278085 0.986126
C 5.296417 0.152332 1.806947
C 4.329159 -0.848076 1.696343
H 2.424347 0.504036 -0.767964
C 4.121598 2.621893 -0.800883
H 5.999821 2.051076 1.066966
H 4.373175 -1.714733 2.346233
C 6.433050 0.003276 2.782562
H -5.917502 -1.575814 0.670165
H -3.156069 1.572360 1.629832
C -4.710741 3.651086 0.850770
C -7.936201 -0.020670 -0.245091
H -6.978953 2.512104 -0.095629
F -7.900732 -1.268693 -0.760972
F -8.410987 0.804702 -1.203773
F -8.854870 -0.033964 0.750246
F -5.503473 4.383471 0.031791
F -3.429364 3.903834 0.477909
F -4.869920 4.148901 2.092002
F 3.587427 2.378058 -2.010623
F 5.321220 3.205776 -0.987135
F 3.323150 3.578458 -0.217981
F 6.778349 1.193949 3.324955
F 7.540873 -0.492043 2.187104
F 6.121107 -0.830494 3.797382

H -1.798977 2.647876 3.067300
O -2.320260 3.436019 3.321960
C -2.402728 3.545774 4.731009
C -0.045245 4.362254 2.056046
O 0.670113 3.937659 3.036717
C 1.795658 3.031432 2.844990
C 0.236042 4.261273 0.676790
C -0.511154 5.046596 -0.149272
C -0.229016 5.332069 -1.587695
C -0.867910 3.237961 -2.914643
C -0.433358 2.142235 -3.895792
N 0.514254 1.206930 -3.316369
C 1.630653 0.816272 -3.977121
O 2.317659 -0.102745 -3.227182
O 2.000039 1.211390 -5.073697
H 0.547248 6.116697 -1.563427
H -1.106543 5.811229 -2.035363
H -1.651074 3.827871 -3.409463
H -1.318807 2.776387 -2.028762
H -1.330614 1.607874 -4.239071
H 0.042895 2.575447 -4.779991
H 0.358630 0.885373 -2.362951
C 3.594609 -0.521972 -3.757783
H -1.350536 5.581199 0.295585
H 1.046137 3.648470 0.305951
H -2.937886 2.704608 5.192923
H -1.413953 3.623569 5.208224
H -2.963295 4.458702 4.954060
H 2.297635 3.010462 3.809898
H 1.381966 2.055242 2.593565
H 2.462292 3.405023 2.068060
H -0.918597 4.908424 2.400244
C 0.265653 4.178080 -2.485169
H 0.719147 4.629508 -3.375818
H 1.061490 3.614438 -1.991285
C 3.501515 -1.734651 -4.655604
C 3.577779 -1.600183 -6.047041
C 3.542096 -2.726480 -6.870619
C 3.413142 -3.999273 -6.312150
C 3.314607 -4.141573 -4.926647
C 3.363612 -3.015701 -4.105476
H 4.186540 -0.753018 -2.867922
H 4.050862 0.315150 -4.289126
H 3.287568 -3.128048 -3.026780
H 3.388580 -4.876370 -6.953064
H 3.205845 -5.129073 -4.486832

H 3.654214 -0.605937 -6.475872

H 3.614893 -2.610835 -7.948456

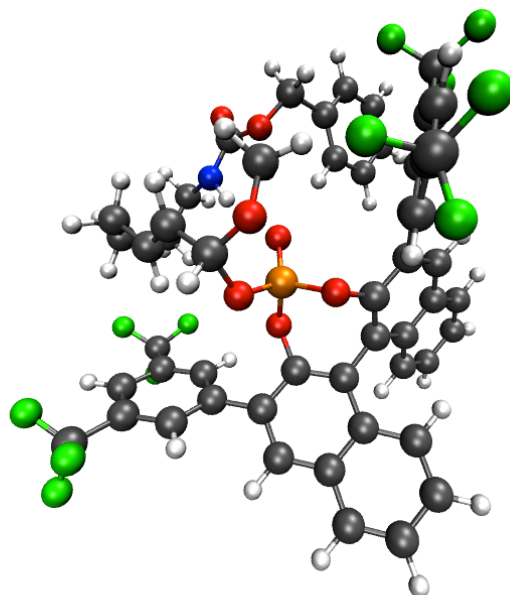


Figure 4.7: Geometry of chiral phosphate acetal intermediate **182**.

182

111

C 2.042857 -5.203119 -1.954301
C 1.134053 -6.031143 -2.570351
C 1.615011 -4.207315 -1.035370
C 0.220638 -4.087057 -0.728977
C -0.692122 -4.949299 -1.394525
C -0.246007 -5.893319 -2.292762
H -0.961761 -6.535194 -2.797451
H 1.470552 -6.783755 -3.276681
H 3.104464 -5.289481 -2.168827
H -1.753367 -4.847659 -1.200490
C 2.545216 -3.341657 -0.408345
C 2.147935 -2.324700 0.437862
C 0.750042 -2.181016 0.668320
C -0.198125 -3.072104 0.197075
H 3.604343 -3.496580 -0.591393
C -1.612669 -2.946462 0.658384
C -2.264865 -4.015238 1.367721
C -2.304883 -1.762522 0.474789
C -3.669393 -1.590238 0.839212
C -4.304876 -2.643020 1.464471

C -3.632765 -3.853323 1.762143
C -4.413228 -0.337246 0.543211
H -5.352345 -2.546228 1.734973
C -1.600045 -5.215341 1.740773
C -2.260589 -6.206788 2.431859
C -3.621865 -6.058815 2.785861
C -4.290189 -4.902944 2.458452
H -4.130373 -6.852271 3.324640
H -5.331023 -4.766661 2.738744
H -0.555129 -5.342550 1.486440
H -1.727962 -7.110437 2.712525
C 3.156752 -1.485739 1.135726
O 0.312411 -1.093411 1.430414
O -1.664905 -0.682289 -0.130039
P -0.444905 0.098393 0.608570
O -1.160350 0.898469 1.773575
O 0.373539 0.837510 -0.377123
C -4.477473 0.175787 -0.760398
C -5.111796 0.321611 1.562375
C -5.238741 1.310960 -1.033040
C -5.933786 1.964804 -0.014328
C -5.862789 1.464811 1.284252
C 4.283761 -1.005837 0.452152

C 5.284943 -0.317555 1.137410
C 5.184028 -0.095198 2.510768
C 4.057935 -0.557608 3.190237
C 3.050134 -1.242030 2.512463
H 4.371231 -1.153151 -0.617801
C 6.477215 0.234416 0.400424
H 5.973849 0.422175 3.043098
H 2.189502 -1.600473 3.062730
C 3.904619 -0.262988 4.659197
H -3.934025 -0.312546 -1.560373
H -5.048959 -0.045793 2.580359
C -6.639823 2.143402 2.382322
C -5.369343 1.809745 -2.448179
H -6.504964 2.860359 -0.229083
F -4.322237 1.441753 -3.216004
F -5.452411 3.161243 -2.493236
F -6.486139 1.331775 -3.039883
F -7.913786 1.692493 2.437495
F -6.702264 3.478824 2.193662
F -6.089367 1.924982 3.595441
F 6.368585 1.575226 0.216170
F 6.634217 -0.324790 -0.812279
F 7.619446 0.037571 1.097248
F 5.097318 -0.264037 5.294257
F 3.112300 -1.166235 5.273259
F 3.353387 0.956062 4.864926
C -0.562443 2.070092 2.496205
O 0.732460 1.813883 2.894446
C 1.835192 2.362275 2.143021
C -0.762486 3.327356 1.696674
C -1.735014 3.546520 0.810532
C -1.889467 4.832552 0.040088
C -1.973233 3.652467 -2.310620
C -0.558899 3.936025 -2.826975

N 0.468806 3.560858 -1.857370
C 1.772416 3.805748 -2.160152
O 2.590449 3.165801 -1.257820
O 2.177255 4.504082 -3.071734
H -0.905525 5.297929 -0.077609
H -2.495835 5.533134 0.633343
H -2.635753 3.609391 -3.181784
H -1.998408 2.641643 -1.881393
H -0.402805 3.388932 -3.767669
H -0.435329 4.997459 -3.066229
H 0.301611 2.739485 -1.281710
C 3.961497 3.045316 -1.655035
H -2.460590 2.757476 0.616679
H -0.052740 4.120992 1.917415
H 2.713029 1.841705 2.520317
H 1.730024 2.197057 1.070184
H 1.951262 3.431647 2.347159
H -1.171246 2.053166 3.405075
C -2.576684 4.670714 -1.328114
H -3.623219 4.388409 -1.162610
H -2.605169 5.654736 -1.813308
C 4.200600 1.846521 -2.551685
C 3.314457 0.762614 -2.578569
C 3.583789 -0.346180 -3.385539
C 4.743341 -0.391424 -4.161008
C 5.630822 0.685977 -4.134483
C 5.356626 1.797942 -3.339331
H 4.518110 2.931065 -0.720665
H 4.281068 3.965389 -2.151002
H 6.046520 2.638654 -3.334080
H 4.950607 -1.254533 -4.787313
H 6.532223 0.665102 -4.740503
H 2.412787 0.788045 -1.974320
H 2.881254 -1.175227 -3.407256

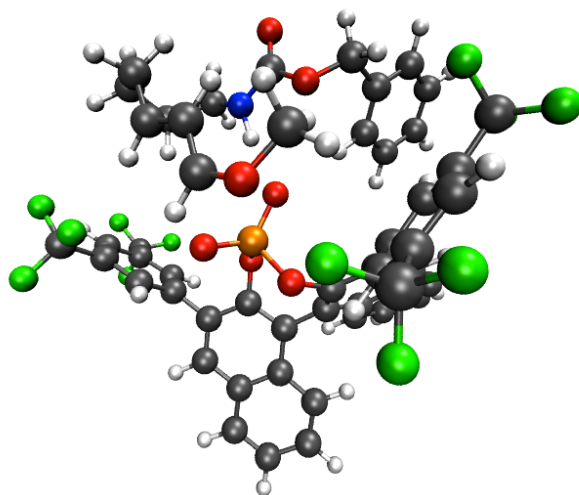


Figure 4.8: Transition state geometry $\text{TS}_{173a} - \text{II}$, the full system prior to cyclization.

$\text{TS}_{173a} - \text{II}$

111

C 2.486382 -4.900710 -1.859633
 C 1.733156 -5.752689 -2.631865
 C 1.867909 -4.038594 -0.917605
 C 0.446979 -4.063610 -0.736512
 C -0.298593 -4.962793 -1.551682
 C 0.327562 -5.774683 -2.473499
 H -0.265560 -6.436892 -3.097168
 H 2.211997 -6.394187 -3.365950
 H 3.566899 -4.851528 -1.969307
 H -1.378346 -4.987975 -1.460114
 C 2.647185 -3.133991 -0.167394
 C 2.078902 -2.198876 0.670436
 C 0.656704 -2.182711 0.794668
 C -0.155605 -3.142519 0.192838
 H 3.727523 -3.177531 -0.265214
 C -1.625948 -3.122966 0.488152
 C -2.332525 -4.221376 1.104626
 C -2.315939 -1.937657 0.270268
 C -3.683411 -1.765587 0.617117
 C -4.339134 -2.794093 1.250754
 C -3.704200 -4.035719 1.489789
 C -4.434046 -0.527574 0.262324

H -5.383240 -2.675820 1.529991
 C -1.749277 -5.490636 1.378535
 C -2.483889 -6.508464 1.952511
 C -3.841680 -6.320579 2.304086
 C -4.430925 -5.100487 2.083814
 H -4.411651 -7.132535 2.745823
 H -5.471964 -4.928925 2.348060
 H -0.711698 -5.663608 1.121496
 H -2.016500 -7.470815 2.137328
 C 2.998037 -1.305546 1.421316
 O 0.089905 -1.166557 1.535493
 O -1.656183 -0.863171 -0.282893
 P -0.660697 0.065283 0.676092
 O -1.438276 0.866038 1.684023
 O 0.304689 0.725479 -0.265421
 C -5.133074 -0.483825 -0.947270
 C -4.527500 0.553246 1.143135
 C -5.965150 0.595910 -1.245263
 C -6.053254 1.678771 -0.372761
 C -5.305633 1.662291 0.805408
 C 4.125338 -0.784144 0.760139
 C 5.132278 -0.134338 1.466739
 C 5.037371 0.026061 2.850182
 C 3.897536 -0.440780 3.503365

C 2.877620 -1.089208 2.801135
H 4.210922 -0.892330 -0.314440
C 6.322537 0.438551 0.745794
H 5.836919 0.500335 3.407548
H 2.011782 -1.463584 3.333031
C 3.740194 -0.205012 4.980594
H -5.060069 -1.316639 -1.638118
H -3.939404 0.548006 2.052605
C -5.347775 2.840890 1.738269
C -6.842775 0.524293 -2.465160
H -6.681392 2.526081 -0.616244
F -6.225794 -0.099556 -3.491625
F -7.219125 1.748435 -2.894993
F -7.976407 -0.170493 -2.211441
F -6.237436 2.675253 2.740477
F -5.681836 3.983313 1.095087
F -4.141159 3.058505 2.327520
F 6.206657 1.788382 0.599837
F 6.476793 -0.077433 -0.485566
F 7.467496 0.229023 1.430521
F 4.917322 0.075673 5.578054
F 3.197725 -1.264913 5.612299
F 2.919992 0.854974 5.219336
C 0.289261 2.849463 2.558261
O 1.362141 2.350935 3.067373
C 2.670400 2.753788 2.561197
C 0.269722 3.904736 1.625081
C -0.909372 4.362505 1.124643
C -0.984361 5.518439 0.192439
C -2.049417 4.057871 -1.692821
C -0.762852 3.682646 -2.440785
N 0.331684 3.262351 -1.567531
C 1.599604 3.662149 -1.858020

O 2.512199 2.961198 -1.092092
O 1.923197 4.537518 -2.643035
H 0.008230 5.722439 -0.219836
H -1.247516 6.392446 0.813512
H -2.852498 4.115514 -2.437564
H -2.327391 3.236205 -1.019528
H -0.998827 2.865691 -3.135492
H -0.396585 4.521127 -3.038562
H 0.250430 2.351121 -1.092571
C 3.802656 2.801898 -1.710869
H -1.835337 3.872936 1.431514
H 1.199027 4.332057 1.268452
H 3.377725 2.186036 3.154054
H 2.728455 2.500144 1.500880
H 2.814136 3.823967 2.724146
H -0.620327 2.366992 2.907222
C -2.039606 5.390670 -0.927953
H -3.035550 5.558823 -0.500477
H -1.860471 6.213138 -1.630706
C 3.852761 1.591303 -2.625831
C 2.923303 0.546294 -2.524457
C 3.016903 -0.557980 -3.377449
C 4.033918 -0.634992 -4.329774
C 4.964510 0.402388 -4.428923
C 4.871575 1.506378 -3.583482
H 4.517777 2.703631 -0.889247
H 4.043350 3.711329 -2.267495
H 5.589787 2.317273 -3.679515
H 4.097712 -1.491795 -4.994978
H 5.755343 0.357038 -5.172530
H 2.125035 0.592664 -1.788889
H 2.285766 -1.357829 -3.295032

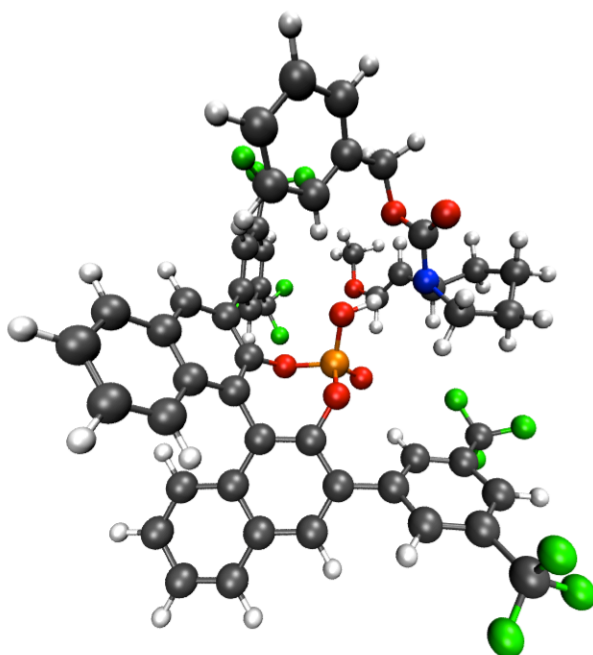


Figure 4.9: Geometry of full system **174a_{boat}** following cyclization.

174a_{boat}

111

C 2.338451 -5.155210 -1.800683
 C 1.547532 -5.965505 -2.580573
 C 1.760257 -4.235514 -0.884272
 C 0.334714 -4.178770 -0.747880
 C -0.451477 -5.017253 -1.584091
 C 0.139482 -5.883310 -2.477109
 H -0.482933 -6.506343 -3.112294
 H 1.998784 -6.658627 -3.283855
 H 3.421293 -5.194443 -1.882260
 H -1.531402 -4.960164 -1.524569
 C 2.572108 -3.363655 -0.116859
 C 2.031023 -2.412910 0.725450
 C 0.611793 -2.363399 0.829519
 C -0.236882 -3.248323 0.188488
 H 3.651910 -3.447216 -0.201483
 C -1.704817 -3.192500 0.452859
 C -2.423681 -4.344773 0.924914
 C -2.402008 -2.008229 0.265667
 C -3.820384 -1.918717 0.368060
 C -4.509887 -3.059806 0.726453
 C -3.848779 -4.271221 1.042830
 C -4.570474 -0.667411 0.067813
 H -5.591616 -3.017441 0.815790

C -1.781785 -5.550232 1.321915
 C -2.511677 -6.626233 1.775825
 C -3.922312 -6.561714 1.856148
 C -4.573783 -5.404327 1.500747
 H -4.484175 -7.420316 2.210800
 H -5.655267 -5.331298 1.576900
 H -0.701258 -5.614811 1.280190
 H -1.997343 -7.531892 2.083040
 C 2.904469 -1.478339 1.482390
 O 0.059070 -1.370276 1.637112
 O -1.703652 -0.871490 -0.131446
 P -0.699264 -0.122633 0.923008
 O -1.365704 0.749493 1.914475
 O 0.364537 0.517484 -0.043679
 C -5.615790 -0.702764 -0.863904
 C -4.298202 0.538211 0.730933
 C -6.374646 0.438563 -1.129074
 C -6.104323 1.634941 -0.468903
 C -5.062576 1.673360 0.458643
 C 3.968807 -0.838114 0.831671
 C 4.808548 0.027006 1.531571
 C 4.618549 0.253348 2.893741
 C 3.554141 -0.369579 3.541838
 C 2.701049 -1.225263 2.846544
 H 4.116579 -0.983901 -0.231836

C	5.853475	0.820532	0.797301	O	0.862360	3.285064	-3.020659
H	5.276092	0.920780	3.436524	H	0.793208	5.838693	-0.162156
H	1.870618	-1.686741	3.366225	H	-0.647765	5.905525	0.837955
C	3.342327	-0.150281	5.017293	H	-2.690127	4.558402	-2.309632
H	-5.832240	-1.625155	-1.391758	H	-2.763553	4.457348	-0.559656
H	-3.494596	0.595768	1.457277	H	-1.972904	2.294851	-0.942618
C	-4.796661	2.942689	1.225054	H	-1.264820	2.713697	-2.509903
C	-7.446232	0.386577	-2.185433	H	0.221437	1.498699	-0.291502
H	-6.693367	2.520422	-0.673801	C	3.370448	3.160936	-2.105796
F	-6.937213	0.593208	-3.421324	H	-0.918160	3.558203	0.903649
F	-8.396001	1.325219	-1.986433	H	2.079229	4.184115	1.048217
F	-8.061196	-0.816890	-2.212119	H	3.826683	3.262516	4.100779
F	-5.467309	2.977645	2.396168	H	3.725707	3.123684	2.321204
F	-5.173545	4.038421	0.522683	H	3.096740	4.582942	3.138618
F	-3.483934	3.087132	1.517979	H	0.108600	2.515114	2.751505
F	5.364422	2.038868	0.426899	C	-1.049089	5.554023	-1.286768
F	6.273150	0.209216	-0.325623	H	-1.550806	6.527004	-1.274952
F	6.936809	1.065253	1.565618	H	-0.406133	5.548597	-2.173766
F	3.867858	1.026831	5.430230	C	3.582072	1.855532	-2.842279
F	3.937922	-1.121405	5.750061	C	3.071713	0.643668	-2.365746
F	2.037105	-0.154876	5.343145	C	3.327385	-0.545629	-3.051486
C	1.025860	3.027005	2.472969	C	4.107793	-0.539551	-4.207942
O	1.974084	2.849932	3.423721	C	4.621708	0.667065	-4.684909
C	3.225483	3.496669	3.222788	C	4.354236	1.856978	-4.008951
C	1.146374	3.708534	1.323352	H	4.207807	3.361225	-1.432382
C	-0.014234	3.902632	0.393298	H	3.271591	3.986875	-2.815205
C	-0.193435	5.384284	-0.012272	H	4.744374	2.795281	-4.396196
C	-2.078054	4.424641	-1.411781	H	4.307103	-1.465793	-4.738844
C	-1.382059	3.042971	-1.479088	H	5.222074	0.684634	-5.589945
N	-0.017521	3.043649	-0.869736	H	2.460325	0.625930	-1.469901
C	1.020269	3.198892	-1.821216	H	2.910829	-1.477091	-2.677969
O	2.228687	3.150559	-1.221324				

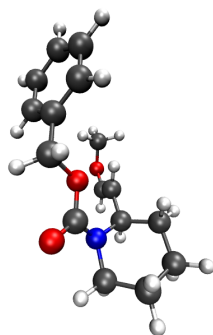


Figure 4.10: Geometry of full system **174a** following conformational change.

174a

41

C 0.51218112 -2.72807115 1.08401933
O -0.61224315 -3.46612078 1.25905002
C -1.74175391 -3.12069304 0.46632264
C 0.71137320 -1.69957787 0.24975053
C 2.06213486 -1.04717043 0.15247428
C 2.62117713 -1.00670287 -1.28680479
C 4.26940121 0.78301398 -0.52182755
C 3.62138047 0.70954303 0.86856266
N 2.20884878 0.31198055 0.75416943
C 1.31702372 1.35139436 0.65444380
O 0.09240432 0.96608490 0.20015872
O 1.56877319 2.50996227 0.95455196
H 1.99310958 -0.33375254 -1.88549386
H 2.54329599 -2.00437087 -1.73387044
H 3.80624750 1.61173674 -1.07216397
H 5.33502523 1.02289105 -0.42299505
H 4.13100272 -0.03735990 1.49071793
H 3.66199409 1.66931017 1.38172685
C -0.89118533 2.02759124 0.15712160

METHANOL BY-PRODUCT:

6

C 0.65522106 -0.03468975 -0.00000169
O -0.75303706 0.12803117 0.00000291
H 1.02396375 -0.56388940 -0.89185815

H 2.75153133 -1.66305677 0.74670152
H -0.07452474 -1.33762936 -0.39854499
H -2.53419203 -3.81700623 0.74452808
H -2.06735508 -2.09237863 0.66189448
H -1.52156076 -3.22574790 -0.60376283
H 1.29509440 -3.09029326 1.74647433
C 4.08454196 -0.53285415 -1.29189377
H 4.70632856 -1.31091924 -0.82622638
H 4.44552762 -0.42561407 -2.32133836
C -2.22307734 1.40941693 -0.17506348
C -2.99932573 0.82054788 0.83207683
C -4.22752876 0.23246683 0.53107717
C -4.69609642 0.22839099 -0.78519998
C -3.93206044 0.81468194 -1.79485819
C -2.70275378 1.40095420 -1.48944424
H -0.58950047 2.76356077 -0.59429979
H -0.90783948 2.53267042 1.12622240
H -2.11018417 1.85861545 -2.27748718
H -5.65503145 -0.22395671 -1.02078282
H -4.29388903 0.81910327 -2.81901800
H -2.63526648 0.82624379 1.85620182
H -4.82215779 -0.21431820 1.32267392

H 1.02396589 -0.56392086 0.89183518
H 1.09112801 0.96770665 0.00001535
H -1.15059349 -0.75134818 -0.00001133

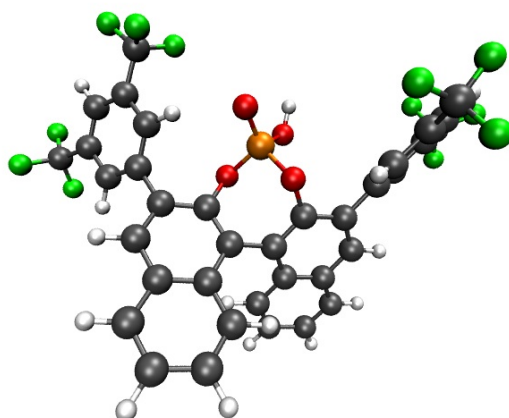


Figure 4.11: Geometry of free catalyst system **51** following regeneration of the catalyst after the reaction.

51

70

C 2.37529637 -4.24112142 -2.96797790
 C 1.42035282 -5.15069750 -3.35599971
 C 2.08199697 -3.24545281 -1.99761116
 C 0.78435861 -3.21179370 -1.39052545
 C -0.18510418 -4.15262301 -1.83372779
 C 0.12506196 -5.09254992 -2.79144824
 H -0.63571194 -5.79437380 -3.11974936
 H 1.65194398 -5.90322394 -4.10336016
 H 3.36826531 -4.25852573 -3.40873436
 H -1.18590595 -4.11808477 -1.42140699
 C 3.04660801 -2.27155708 -1.64165045
 C 2.76737233 -1.25485807 -0.75078150
 C 1.47289339 -1.24237121 -0.16049397
 C 0.50720769 -2.20334843 -0.40196727
 H 4.03401029 -2.32776506 -2.09077105
 C -0.80380624 -2.13588739 0.30866754
 C -1.30333064 -3.24028138 1.08148694
 C -1.57170543 -0.98487928 0.23505452
 C -2.90240544 -0.89842967 0.73496545
 C -3.40534584 -2.00307100 1.39349421
 C -2.62815411 -3.16497915 1.61964108
 C -3.76888347 0.29235165 0.51029815

H -4.41683348 -1.96702902 1.78780369
 C -0.52517513 -4.39341434 1.37418350
 C -1.03957770 -5.42104942 2.13303518
 C -2.36026940 -5.35783711 2.63566141
 C -3.13437635 -4.24949686 2.38555477
 H -2.75400211 -6.17893553 3.22665159
 H -4.14387007 -4.17859030 2.78106489
 H 0.49267706 -4.45306257 1.00760500
 H -0.42251464 -6.28729105 2.35201128
 C 3.78688051 -0.21707413 -0.44459908
 O 1.17898835 -0.20116581 0.72462421
 O -1.05486293 0.12730218 -0.43931108
 P 0.14376381 0.96112584 0.26717834
 O -0.18687284 1.86857890 1.38029909
 O 0.76803677 1.64673595 -1.04234179
 C -5.02957728 0.11022335 -0.07541328
 C -3.38231294 1.58558318 0.88581105
 C -5.88223960 1.19445007 -0.28222028
 C -5.49088154 2.48151721 0.08306658
 C -4.23873005 2.66577373 0.66613098
 C 4.50336675 0.38201076 -1.49096650
 C 5.49415735 1.32652429 -1.22617121
 C 5.79410670 1.69110206 0.08620738
 C 5.08396299 1.10067542 1.12959536
 C 4.08634218 0.15978011 0.87189271

H 4.27545841 0.11827039 -2.51772177
 C 6.19465222 2.00741381 -2.37298431
 H 6.56684021 2.42116411 0.29158821
 H 3.54365428 -0.28189334 1.69918638
 C 5.41184932 1.42907183 2.56397205
 H -5.33732354 -0.88053686 -0.39210738
 H -2.42072823 1.75628797 1.35800729
 C -3.76193114 4.04755015 1.03425705
 C -7.24984793 0.95587592 -0.86503759
 H -6.14788122 3.32485788 -0.08756287
 F -7.22639804 -0.00668282 -1.81398384
 F -7.76150877 2.07083744 -1.42723517

F -8.12812708 0.54895214 0.08086640
 F -4.75893358 4.95803280 0.98383477
 F -2.79126870 4.47103480 0.19205583
 F -3.24430061 4.07843267 2.27912170
 F 6.35361747 1.17509372 -3.42572879
 F 7.41633187 2.45721485 -2.01830972
 F 5.49155711 3.07418965 -2.81833914
 F 6.21686365 2.50705633 2.66756419
 F 6.04137165 0.39603661 3.16907050
 F 4.29519754 1.67886415 3.27896850
 H 0.98511517 2.57333639 -0.86235293

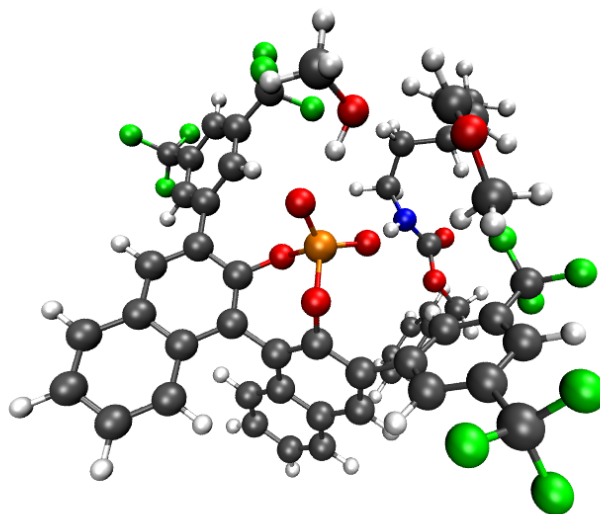


Figure 4.12: Transition state geometry $TS_{173a} - III$, the full system prior to concerted cyclization.

$TS_{173a} - III$

117

C 2.304891 -5.408511 -0.484394
 C 1.432171 -6.432494 -0.768436
 C 1.864806 -4.240713 0.195389
 C 0.499599 -4.143212 0.620134
 C -0.380517 -5.209268 0.282463
 C 0.072987 -6.320487 -0.392131
 H -0.621812 -7.116395 -0.642125
 H 1.778521 -7.320091 -1.289648
 H 3.348218 -5.472172 -0.783373

H -1.426881 -5.134866 0.550994
 C 2.748327 -3.157887 0.437485
 C 2.316869 -1.997306 1.040319
 C 0.962923 -1.915222 1.468758
 C 0.068962 -2.965771 1.324644
 H 3.783752 -3.244861 0.118350
 C -1.321516 -2.825217 1.844671
 C -1.882144 -3.767072 2.774726
 C -2.100309 -1.755169 1.420933
 C -3.499422 -1.677846 1.703364
 C -4.050960 -2.644411 2.521694
 C -3.270871 -3.668793 3.108824

C -4.379812 -0.647034 1.091551
H -5.109939 -2.596161 2.760063
C -1.110848 -4.773235 3.419155
C -1.686125 -5.642773 4.318772
C -3.065450 -5.561415 4.622434
C -3.837607 -4.590705 4.028901
H -3.506766 -6.255430 5.331403
H -4.895090 -4.503667 4.264298
H -0.050494 -4.840509 3.206310
H -1.072614 -6.395271 4.805666
C 3.258551 -0.855525 1.250730
O 0.545052 -0.759543 2.096218
O -1.540801 -0.788361 0.612151
P -0.420959 0.276800 1.230161
O -1.077269 1.165995 2.259432
O 0.317070 0.858558 0.068820
C -5.583813 -1.045154 0.490482
C -4.063579 0.716945 1.109686
C -6.448687 -0.106946 -0.072042
C -6.125168 1.250556 -0.062937
C -4.931348 1.647311 0.533283
C 3.436357 0.118801 0.260819
C 4.351945 1.158194 0.460625
C 5.100333 1.234253 1.634463
C 4.917722 0.265514 2.621560
C 4.002580 -0.770051 2.433038
H 2.858930 0.069165 -0.656137
C 4.493490 2.232496 -0.586292
H 5.814173 2.034261 1.782054
H 3.859381 -1.511610 3.211412
C 5.761503 0.302429 3.867130
H -5.833528 -2.098750 0.439028
H -3.146909 1.051342 1.584417
C -4.503592 3.087957 0.528001
C -7.765908 -0.554394 -0.645301
H -6.787685 1.979645 -0.512321
F -7.706208 -1.812063 -1.134121
F -8.180165 0.253724 -1.645993
F -8.741290 -0.545298 0.294517
F -5.479401 3.929439 0.126856
F -3.448998 3.276672 -0.306568
F -4.105729 3.494910 1.755724
F 4.893925 1.752119 -1.778215
F 5.388532 3.183356 -0.216401
F 3.316077 2.879891 -0.800517
F 6.146049 1.565118 4.172249

F 6.889000 -0.428598 3.726727
F 5.101284 -0.189671 4.935954
H -0.951338 2.720140 2.240090
O -1.040713 3.728289 2.236105
C -1.698952 4.088637 3.443689
C 0.919783 4.955493 1.947797
O 1.777306 4.489027 2.793976
C 2.844423 3.614184 2.326011
C 1.125652 5.047557 0.534733
C 0.100128 5.262358 -0.325997
C 0.260930 5.698540 -1.745795
C -1.234578 3.767414 -2.716045
C -0.985463 2.291227 -3.107089
N 0.243681 1.711951 -2.594432
C 1.227101 1.346876 -3.453809
O 2.123891 0.514001 -2.838410
O 1.333292 1.707681 -4.619581
H 1.268215 6.105616 -1.885818
H -0.445482 6.532472 -1.874686
H -2.042559 4.121363 -3.367930
H -1.633508 3.820488 -1.699807
H -1.833961 1.691376 -2.758083
H -0.940675 2.210016 -4.196067
H 0.262689 1.307779 -1.653237
C 3.177893 -0.002512 -3.688903
H -0.905140 5.121036 0.069295
H 2.147031 4.984816 0.167195
H -2.438467 3.330402 3.716014
H -0.995415 4.195115 4.283474
H -2.222176 5.039400 3.296114
H 3.254877 3.161395 3.225016
H 2.424886 2.858930 1.662325
H 3.607895 4.203919 1.815420
H 0.136713 5.516802 2.430124
C 0.017289 4.647072 -2.863096
H -0.001170 5.200913 -3.807068
H 0.897200 3.999285 -2.901887
C 2.747125 -1.230019 -4.453014
C 2.264931 -1.125626 -5.763689
C 1.870684 -2.266208 -6.464049
C 1.945629 -3.521941 -5.859421
C 2.416279 -3.634356 -4.549775
C 2.817588 -2.493758 -3.854367
H 3.983418 -0.245067 -2.994071
H 3.509533 0.789060 -4.363312
H 3.178105 -2.583558 -2.832400

H 1.636954 -4.408981 -6.405055
H 2.467851 -4.606268 -4.067240

H 2.183227 -0.142712 -6.215722
H 1.500080 -2.173021 -7.481073

Cartesian coordinates for the starting geometry, transition states, intermediate and cyclized enantiomeric product are provided below.

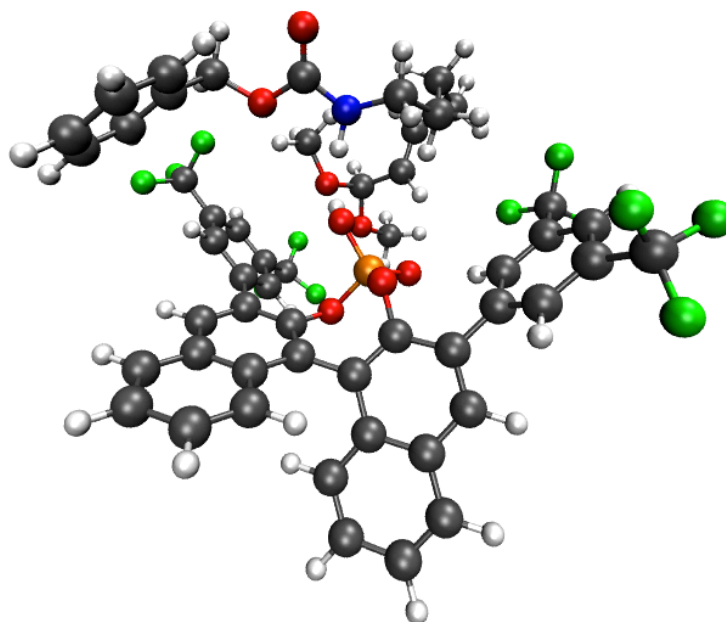


Figure 4.13: Geometry for full system prior to reaction forming minor enantiomer, **185**.

185

117

C -1.697483 -0.590661 5.766138
C -0.795709 -1.177732 6.621269
C -1.659809 -0.857835 4.370795
C -0.695470 -1.782911 3.855302
C 0.238753 -2.349519 4.764844
C 0.190018 -2.052989 6.108785
H 0.920329 -2.492612 6.781442
H -0.826639 -0.960000 7.684388
H -2.444274 0.103851 6.140869
H 1.006464 -3.014575 4.389653
C -2.534423 -0.192038 3.479658
C -2.479295 -0.383549 2.112745
C -1.543405 -1.340785 1.626637
C -0.691305 -2.062737 2.444331
H -3.258585 0.505141 3.890346
C 0.251685 -3.053068 1.846961
C 0.280868 -4.424020 2.277313
C 1.133103 -2.652777 0.853077
C 2.181567 -3.484559 0.365928

C 2.260491 -4.770209 0.864215
C 1.312520 -5.283498 1.781599
C 3.214065 -3.012360 -0.599428
H 3.047471 -5.427161 0.505031
C -0.696170 -4.981701 3.146679
C -0.636606 -6.305155 3.522487
C 0.403847 -7.143182 3.057293
C 1.355522 -6.640342 2.201842
H 0.440002 -8.183206 3.366609
H 2.149731 -7.276432 1.820429
H -1.505942 -4.356710 3.503615
H -1.400746 -6.711344 4.178434
C -3.329871 0.434322 1.209261
O -1.498714 -1.570485 0.252706
O 1.042419 -1.349997 0.357418
P -0.230561 -1.017571 -0.607979
O -0.212780 -1.622135 -1.954895
O -0.215803 0.560105 -0.481756
C 4.564542 -3.156082 -0.261808
C 2.885082 -2.488800 -1.860681
C 5.570407 -2.785419 -1.157943

C 5.244142 -2.269491 -2.407197
C 3.896315 -2.129440 -2.748983
C -3.476847 1.802505 1.474984
C -4.285553 2.603495 0.667439
C -4.946755 2.060670 -0.431439
C -4.791594 0.701981 -0.709951
C -4.001279 -0.108204 0.100862
H -2.935966 2.248636 2.302199
C -4.368637 4.079584 0.943364
H -5.561226 2.686841 -1.067311
H -3.896211 -1.158240 -0.137437
C -5.533565 0.115710 -1.882677
H 4.834909 -3.555535 0.709876
H 1.847070 -2.372493 -2.152156
C 3.558458 -1.629107 -4.128260
C 7.008547 -2.903478 -0.728490
H 6.023786 -1.983253 -3.103251
F 7.229485 -4.057459 -0.058783
F 7.362184 -1.896876 0.102951
F 7.856290 -2.871910 -1.778031
F 3.846862 -2.547223 -5.076572
F 4.275540 -0.517176 -4.438706
F 2.253246 -1.312198 -4.258887
F -4.347311 4.347230 2.270713
F -5.485940 4.632180 0.432836
F -3.316407 4.753230 0.402778
F -5.494449 0.936277 -2.955408
F -6.842996 -0.072464 -1.587476
F -5.038303 -1.080551 -2.259720
C -1.748234 1.478771 -3.413159
O -2.512127 0.316496 -3.305698
C -2.708924 -0.379959 -4.529118
C -0.336623 1.267147 -3.894334
C 1.838608 2.231002 -4.770601
C 2.604170 2.883111 -3.583031
C 3.086429 2.563107 -1.063300
N 1.812881 2.967933 -0.479980
C 0.354720 2.230307 -4.514406
C 1.646258 4.139170 0.188351

O 0.383087 4.180117 0.720125
O 2.465320 5.038971 0.285351
H 2.026900 3.738283 -3.210656
H 3.556098 3.290607 -3.943935
H 3.706976 3.459978 -1.135634
H 3.600074 1.864545 -0.388531
H 1.129193 2.241108 -0.303642
C 0.046764 5.350758 1.504782
H -3.378295 -1.207710 -4.296959
H -3.182025 0.265742 -5.283000
H -1.768272 -0.772288 -4.932431
H -2.262669 2.245896 -4.020850
C 2.881241 1.900159 -2.433003
H 2.054355 1.185757 -2.340017
H 3.765314 1.301992 -2.677632
C 0.101882 5.046450 2.981334
C -1.076061 4.880389 3.717917
C -1.024388 4.586309 5.082149
C 0.208629 4.449688 5.719496
C 1.389256 4.612078 4.989904
C 1.337425 4.912128 3.629876
H -0.968538 5.617389 1.203995
H 0.736468 6.152296 1.232763
H 2.251901 5.044232 3.058389
H 0.251983 4.220804 6.780509
H 2.351210 4.509722 5.484174
H -2.037577 4.984858 3.222100
H -1.946171 4.465766 5.644489
H 2.049413 2.789432 -5.689784
H 2.207497 1.212002 -4.920277
H -0.169091 3.150733 -4.782753
H 0.128416 0.327378 -3.602956
C -1.509904 3.354409 -1.895677
H -0.552961 3.653621 -2.333641
H -2.327690 3.914004 -2.364249
H -1.489012 3.555505 -0.827314
O -1.733573 1.948353 -2.046343
H -0.837273 1.048511 -1.121875

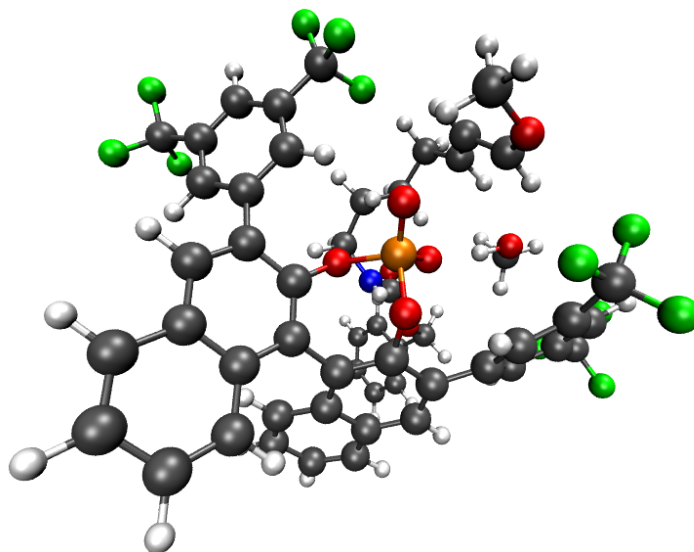


Figure 4.14: Transition state geometry for full system prior to reaction forming minor enantiomer phosphate intermediate, **TS₁₈₅ - I**.

185

117

C 1.098613 4.704489 2.418726
 C -0.060572 5.338761 2.793135
 C 1.147018 3.900210 1.249136
 C -0.024351 3.782946 0.431782
 C -1.205869 4.451403 0.849941
 C -1.224822 5.201477 2.002429
 H -2.146559 5.682625 2.315464
 H -0.091647 5.929427 3.703614
 H 1.991671 4.782015 3.033166
 H -2.109386 4.341978 0.262723
 C 2.310443 3.165747 0.913513
 C 2.347771 2.280696 -0.147769
 C 1.165764 2.177653 -0.949013
 C 0.024821 2.926638 -0.718856
 H 3.187521 3.285075 1.543073
 C -1.168257 2.686418 -1.583198
 C -1.796344 3.720607 -2.356678
 C -1.680470 1.394978 -1.644251
 C -2.915269 1.104529 -2.293039
 C -3.541276 2.113597 -2.994040
 C -2.990740 3.412428 -3.087601

C -3.609074 -0.199696 -2.141319
 H -4.474286 1.901869 -3.509051
 C -1.270039 5.035773 -2.474267
 C -1.890783 5.980857 -3.261774
 C -3.073197 5.670776 -3.975355
 C -3.608945 4.409575 -3.886493
 H -3.549113 6.424598 -4.595066
 H -4.512484 4.148118 -4.431878
 H -0.357298 5.288570 -1.946910
 H -1.464458 6.976026 -3.343762
 C 3.512625 1.389175 -0.384465
 O 1.117753 1.250414 -1.980612
 O -1.035634 0.368392 -0.984875
 P 0.424069 -0.207076 -1.590904
 O 0.199843 -0.967096 -2.854195
 O 1.121182 -0.811978 -0.400018
 C -4.937776 -0.176701 -1.692900
 C -3.024779 -1.432854 -2.458986
 C -5.676308 -1.351400 -1.570270
 C -5.104311 -2.576954 -1.905124
 C -3.782381 -2.602763 -2.349972
 C 4.269508 0.898900 0.690036
 C 5.280712 -0.041231 0.482781

C 5.525489 -0.553022 -0.788840
C 4.789171 -0.058244 -1.862504
C 3.829888 0.931304 -1.673884
H 4.021766 1.192154 1.703943
C 6.104805 -0.536902 1.639437
H 6.243161 -1.351474 -0.930974
H 3.271233 1.289037 -2.524164
C 4.994745 -0.645195 -3.231933
H -5.391226 0.772612 -1.430770
H -1.993972 -1.462929 -2.802683
C -3.148615 -3.913184 -2.709950
C -7.071262 -1.280290 -1.012249
H -5.676047 -3.492070 -1.821946
F -7.716867 -0.169924 -1.434348
F -7.060932 -1.236226 0.339772
F -7.815635 -2.348755 -1.369619
F -2.540176 -3.879026 -3.917039
F -4.026021 -4.932875 -2.721231
F -2.172881 -4.255800 -1.814107
F 5.422203 -0.493550 2.811966
F 7.222192 0.203663 1.819127
F 6.507868 -1.817440 1.461082
F 5.120063 -1.997117 -3.164525
F 6.114297 -0.181680 -3.831193
F 3.961581 -0.384866 -4.059053
C 2.084204 -3.561284 -2.190501
O 2.291246 -3.316418 -3.433783
C 1.199449 -3.414972 -4.399090
C 0.897263 -4.047108 -1.609209
C -0.204510 -4.634908 0.617991
C -0.570289 -3.453133 1.576099
C -1.643244 -1.124904 1.758003
N -0.430990 -0.412036 2.127526
C 0.921237 -4.243382 -0.257621
C 0.177850 -0.683527 3.304399
O 1.183611 0.191249 3.570279
O -0.146419 -1.596026 4.059317
H 0.347945 -2.979669 1.930621
H -1.054210 -3.863829 2.466622
H -2.148624 -1.376797 2.692245
H -2.276439 -0.428280 1.202729
H 0.074010 0.101786 1.413694
C 1.823314 0.005176 4.858732
H 1.666439 -3.228218 -5.362397
H 0.770697 -4.419167 -4.366331
H 0.476815 -2.637771 -4.144500

H 2.954111 -3.366070 -1.562274
C -1.451911 -2.393797 0.911723
H -1.024640 -2.115367 -0.052861
H -2.450276 -2.802482 0.713957
C 1.052875 0.599380 6.019835
C 1.460073 1.814410 6.594814
C 0.790962 2.345130 7.699680
C -0.297209 1.667074 8.250539
C -0.711158 0.454619 7.687257
C -0.052671 -0.071542 6.576972
H 2.790295 0.500273 4.746143
H 1.982337 -1.064894 5.011831
H -0.378148 -1.003179 6.129379
H -0.818905 2.074028 9.112362
H -1.558252 -0.081772 8.106924
H 2.309824 2.352130 6.183598
H 1.123667 3.283873 8.133076
H 0.132227 -5.474922 1.240879
H -1.077497 -4.953673 0.047625
H 1.860957 -4.013117 0.238950
H -0.001659 -4.191459 -2.191090
C 3.358813 -2.720768 1.842261
H 2.463603 -3.184798 2.278124
H 4.190627 -3.424503 1.933762
H 3.597788 -1.836573 2.437741
O 3.207284 -2.421424 0.462134
H 2.439002 -1.828642 0.308619
C -0.500921 -5.297265 1.776361
C -1.072404 -6.348835 2.457662
C -2.347704 -6.215315 3.055037
C -3.016779 -5.016693 2.976996
H -2.788347 -7.055083 3.583530
H -3.988528 -4.893556 3.447361
H 0.481753 -5.412802 1.334244
H -0.535144 -7.288712 2.542121
C 4.031721 -1.341372 -0.153860
O 1.639057 -1.274019 1.383360
O -0.648022 -0.571351 0.503851
P 0.663856 0.022980 1.268331
O 0.434631 0.632796 2.594201
O 1.181865 0.965767 0.088466
C -4.566207 -0.223761 1.116763
C -2.719754 0.935945 2.145865
C -5.297961 0.962299 1.086443
C -4.745062 2.149096 1.569100
C -3.454593 2.122473 2.093646

C 4.447509 -0.492059 -1.183847
 C 5.499880 0.404413 -0.974630
 C 6.159291 0.453796 0.249315
 C 5.744651 -0.397407 1.276528

C 4.687813 -1.282562 1.083566
 H 3.898855 -0.491095 -2.120642
 C 5.849210 1.366253 -2.076167

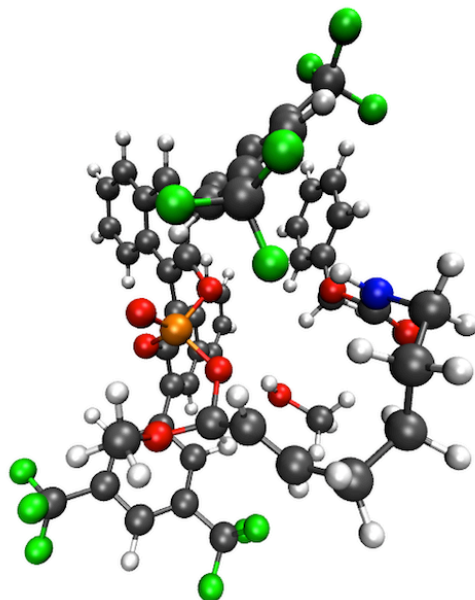


Figure 4.15: Geometry for **186**, the chiral phosphate acetal intermediate full system prior to cyclizing to form the minor enantiomer.

186

117

C 1.961478 -4.949329 -2.840029
 C 0.881094 -5.720769 -3.195980
 C 1.883836 -4.044518 -1.747307
 C 0.673521 -3.955466 -0.985587
 C -0.433310 -4.746162 -1.402028
 C -0.329900 -5.604179 -2.474803
 H -1.190992 -6.195248 -2.772380
 H 0.948194 -6.404886 -4.036222
 H 2.891353 -5.006547 -3.399059
 H -1.375621 -4.657812 -0.877163
 C 2.974162 -3.201995 -1.423617
 C 2.903087 -2.278019 -0.403626
 C 1.700403 -2.213695 0.352043
 C 0.615729 -3.044076 0.127642
 H 3.884579 -3.273841 -2.011469
 C -0.609145 -2.922582 0.969451
 C -1.172479 -4.049984 1.660275
 C -1.246848 -1.697468 1.078603
 C -2.527914 -1.540479 1.681061
 C -3.108985 -2.656211 2.248921

C -2.447095 -3.907029 2.296570
 C -3.268474 -0.250454 1.647547
 H -4.086565 -2.564749 2.713650
 H 6.977999 1.146043 0.403441
 H 4.374952 -1.929801 1.894260
 C 6.414064 -0.297689 2.620858
 H -4.993667 -1.129070 0.702532
 H -1.726020 0.939706 2.581484
 C -2.785131 3.390827 2.542499
 C -6.663661 0.989493 0.455015
 H -5.310921 3.072440 1.542401
 F -7.247993 -0.227803 0.458052
 F -6.607133 1.394340 -0.839420
 F -7.493108 1.844529 1.091482
 F -2.133048 3.246277 3.708294
 F -3.648714 4.417638 2.672571
 F -1.847749 3.781246 1.621640
 F 4.860109 2.293074 -2.247706
 F 5.994191 0.744125 -3.263765
 F 6.983392 2.048738 -1.827176
 F 5.942406 0.754676 3.336449
 F 7.747268 -0.112627 2.499821

F 6.219894 -1.402177 3.369405
C 2.292611 1.978869 0.264085
O 3.065153 1.662140 1.363168
C 2.961354 2.446318 2.565300
C 1.689920 3.345163 0.202495
C 1.467593 5.555005 -1.043135
C 0.201043 5.514814 -1.947534
C -2.300834 4.897657 -1.787563
N -2.251529 3.455230 -1.601575
C 2.010774 4.173991 -0.796771
C -1.963684 2.576409 -2.596658
O -2.004524 1.305211 -2.104191
O -1.712826 2.871366 -3.756473
H 0.200947 4.587350 -2.530060
H 0.240552 6.329467 -2.679243
H -2.340872 5.078400 -2.864626
H -3.237421 5.270460 -1.355205
H -2.343377 3.082546 -0.667706
C -1.859893 0.227867 -3.052268
H 3.731221 2.040274 3.220824
H 3.175688 3.499916 2.360853
H 1.980397 2.330146 3.029926
H 2.896849 1.781476 -0.621316
C -1.108769 5.620486 -1.143932
H -0.973592 5.207928 -0.138417

H -1.365602 6.678132 -1.001429
C -2.975771 -0.774559 -2.876536
C -2.723550 -2.135034 -3.086558
C -3.754357 -3.071420 -2.991510
C -5.048615 -2.660013 -2.670363
C -5.305281 -1.305452 -2.447070
C -4.276413 -0.369263 -2.553477
H -0.882220 -0.235284 -2.889726
H -1.869694 0.659502 -4.057836
H -4.480692 0.679268 -2.365840
H -5.850571 -3.388600 -2.592021
H -6.304757 -0.972537 -2.184379
H -1.714997 -2.465466 -3.321147
H -3.542608 -4.123373 -3.161356
H 2.249329 6.156075 -1.519698
H 1.227658 6.048440 -0.094211
H 2.708823 3.807113 -1.550735
H 0.985085 3.623188 0.982646
C 1.698121 1.218232 -3.760323
H 0.757439 1.769012 -3.884259
H 2.499850 1.925672 -3.505565
H 1.952411 0.756080 -4.717892
O 1.594029 0.163150 -2.805599
H 1.247958 0.525929 -1.976068

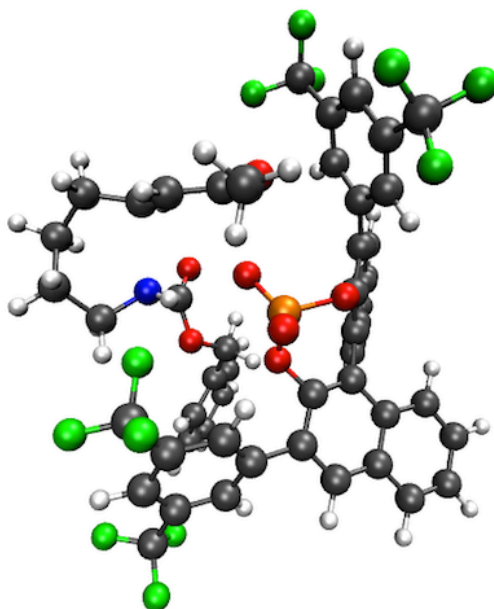


Figure 4.16: Transition state geometry $TS_{185} - II$ following methanol departure for full system prior to cyclization to form the minor enantiomer.

TS₁₈₅ – II**111**

C 2.628513 -4.399851 -2.487097
C 1.685813 -4.975833 -3.304484
C 2.244238 -3.685824 -1.321030
C 0.860395 -3.600559 -0.956954
C -0.086760 -4.195213 -1.837377
C 0.314865 -4.855539 -2.978884
H -0.432085 -5.284066 -3.640443
H 1.988484 -5.505509 -4.202742
H 3.686138 -4.459120 -2.730937
H -1.143012 -4.110257 -1.614012
C 3.212574 -3.018889 -0.536182
C 2.858423 -2.223367 0.532715
C 1.476583 -2.140157 0.884188
C 0.490091 -2.872658 0.232393
H 4.260183 -3.121662 -0.805041
C -0.920656 -2.841742 0.731618
C -1.663053 -4.044205 1.007883
C -1.553349 -1.620157 0.926528
C -2.943559 -1.504222 1.238114
C -3.662361 -2.665440 1.424089
C -3.054514 -3.942016 1.340386
C -3.614760 -0.175980 1.203866
H -4.722854 -2.607642 1.653872
C -1.084210 -5.342747 0.978068
C -1.843847 -6.468362 1.210929
C -3.224863 -6.364045 1.495895
C -3.810707 -5.122574 1.569532
H -3.814050 -7.260237 1.665333
H -4.867138 -5.021252 1.804262
H -0.025898 -5.445480 0.771280
H -1.375134 -7.447479 1.177787
C 3.902611 -1.446123 1.247846
O 1.142622 -1.318138 1.935579
O -0.874018 -0.460295 0.654253
P 0.350540 0.119146 1.626040
O -0.129626 0.622672 2.945064
O 1.111420 1.004716 0.664202
C -4.779040 -0.026446 0.436247
C -3.077999 0.956989 1.834505
C -5.382468 1.222519 0.285080
C -4.821231 2.353819 0.874982
C -3.665781 2.208441 1.642386
C 4.880941 -0.778725 0.501338
C 5.886199 -0.038290 1.128541

C 5.943066 0.042619 2.514869
C 4.971494 -0.622910 3.266979
C 3.960194 -1.354549 2.649570
H 4.837788 -0.810035 -0.582336
C 6.831265 0.749095 0.264848
H 6.710038 0.632759 3.000854
H 3.201624 -1.836678 3.252411
C 5.036682 -0.537812 4.768801
H -5.188933 -0.882281 -0.088220
H -2.181805 0.872764 2.443306
C -2.989595 3.424359 2.217777
C -6.639274 1.346816 -0.531128
H -5.260293 3.330479 0.717796
F -6.661891 0.452921 -1.549678
F -6.770355 2.577925 -1.072651
F -7.748838 1.121741 0.208758
F -2.986838 3.438748 3.563201
F -3.580716 4.569490 1.800396
F -1.686408 3.502668 1.824329
F 6.170838 1.749524 -0.380008
F 7.391985 -0.016984 -0.695888
F 7.828607 1.318906 0.969102
F 5.454721 0.689314 5.171129
F 5.902843 -1.434024 5.290154
F 3.836838 -0.754680 5.344063
C 2.997801 2.379098 1.149054
O 3.241792 1.938739 2.347268
C 2.634002 2.561856 3.506588
C 2.486274 3.635445 0.809765
C 2.139058 5.409625 -0.927648
C 0.919819 5.747094 -1.807164
C -0.964946 4.111032 -1.312991
N 0.090477 3.113118 -1.020313
C 2.325370 3.979355 -0.515143
C 0.174804 1.996201 -1.921698
O -0.971164 1.299875 -1.923394
O 1.162581 1.742753 -2.571516
H 0.940622 5.150842 -2.726825
H 1.016335 6.795498 -2.108082
H -1.256035 4.006334 -2.363142
H -1.860541 3.930720 -0.711067
H -0.001609 2.697343 -0.090084
C -0.954085 -0.043316 -2.479461
H 2.996433 1.983201 4.353880
H 2.954835 3.602839 3.592805
H 1.548341 2.463517 3.427859

H 3.404538 1.728356 0.384394
 C -0.418717 5.523207 -1.077570
 H -0.287334 5.686450 -0.000268
 H -1.168118 6.249087 -1.412946
 C -2.014747 -0.266389 -3.524827
 C -1.701653 -1.062780 -4.631275
 C -2.691287 -1.434107 -5.541766
 C -4.003694 -0.993202 -5.367837
 C -4.321512 -0.179157 -4.277876
 C -3.334393 0.175272 -3.358201
 H -1.130863 -0.684905 -1.615524

H 0.041651 -0.250005 -2.872785
 H -3.594216 0.782525 -2.496419
 H -4.762245 -1.284253 -6.088752
 H -5.340785 0.162812 -4.123213
 H -0.681234 -1.412041 -4.764899
 H -2.437250 -2.065910 -6.387990
 H 3.056577 5.692380 -1.465222
 H 2.104492 6.028391 -0.023333
 H 2.604257 3.262634 -1.283458
 H 2.174911 4.324878 1.587274

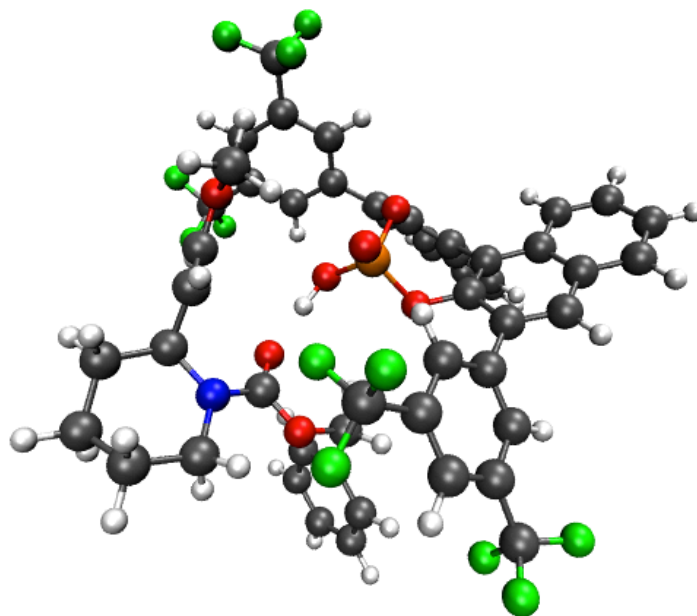


Figure 4.17: Geometry for the minor enantiomer product, **187**.

187

111

C 2.34408811 -5.91246438 -1.89749695
 C 1.34265771 -6.71143172 -2.39620596
 C 2.06228801 -4.89401384 -0.94786354
 C 0.72005183 -4.72301207 -0.47306533
 C -0.29207185 -5.55491283 -1.02562107
 C 0.01109319 -6.51793731 -1.96237197
 H -0.78336149 -7.13030730 -2.37818402
 H 1.56757915 -7.47854141 -3.13082917
 H 3.36937331 -6.03543618 -2.23493674
 H -1.31977688 -5.41710721 -0.71449553
 C 3.08229676 -4.01813749 -0.49819716
 C 2.81786215 -2.98200318 0.37096197

C 1.48367010 -2.83976713 0.84140145
 C 0.44769871 -3.68677281 0.48883713
 H 4.09436831 -4.15755562 -0.86777155
 C -0.92451176 -3.44604496 1.02833752
 C -1.66434033 -4.46660028 1.71983523
 C -1.52000707 -2.20431996 0.85288405
 C -2.88375371 -1.94461488 1.17446149
 C -3.61507393 -2.96659539 1.74454534
 C -3.03321808 -4.21813943 2.06284921
 C -3.53789412 -0.64459269 0.85539839
 H -4.65761048 -2.79580795 1.99775366
 C -1.09070254 -5.70812869 2.11018919
 C -1.83708619 -6.65702878 2.77297214

C -3.19806994 -6.42181884 3.07813662
C -3.77939507 -5.22496350 2.73242261
H -3.77519510 -7.18243826 3.59436189
H -4.81895742 -5.02479414 2.97653170
H -0.04672466 -5.89895925 1.89105954
H -1.37411962 -7.59357331 3.06933644
C 3.86772631 -1.99842102 0.75213833
O 1.21776859 -1.76565955 1.68994812
O -0.79571975 -1.18720020 0.24273927
P 0.44813868 -0.48227129 1.05934527
O 0.02856438 0.47341096 2.10610681
O 1.37359559 -0.00946883 -0.11420134
C -4.70345383 -0.64181358 0.07691556
C -3.03654869 0.57896779 1.32268485
C -5.35190167 0.55512588 -0.23065727
C -4.85388444 1.77035793 0.23738582
C -3.69561988 1.76999968 1.01234766
C 4.54058888 -1.28526757 -0.24794358
C 5.50549118 -0.33597802 0.08695187
C 5.82793509 -0.09260063 1.42096145
C 5.17053168 -0.80986806 2.41723482
C 4.19113200 -1.74907347 2.09075124
H 4.28546175 -1.45345698 -1.28843934
C 6.14048890 0.48529654 -1.00153388
H 6.57786556 0.64326412 1.67965555
H 3.67654572 -2.28830141 2.87870902
C 5.49439951 -0.57595564 3.86825047
H -5.09642524 -1.57830658 -0.30358188
H -2.12966951 0.60694094 1.91885730
C -3.15145225 3.06440818 1.55866590
C -6.53992761 0.54158977 -1.15309266
H -5.35579119 2.69887430 -0.00291834
F -6.15399784 0.57830065 -2.45598548
F -7.34701116 1.60414363 -0.95602876
F -7.28329415 -0.57459890 -1.00180456
F -3.42583849 3.20557545 2.87340965
F -3.68350199 4.14134193 0.92680517
F -1.81094622 3.14345222 1.42415485
F 5.35911013 1.53715413 -1.35497596
F 6.34135229 -0.23880170 -2.12499601
F 7.33311255 0.99237617 -0.62396428
F 6.49575572 0.31194027 4.03352145
F 5.86122367 -1.72301067 4.48446959
F 4.42115422 -0.10389120 4.55044161
C 2.85081876 2.96743451 0.73211180
O 3.34645925 2.31460075 1.80792036

C 2.67229582 2.50011578 3.05360440
C 1.80697805 3.80514742 0.67511506
C 1.61879244 6.04289935 -0.41140599
C 0.70883006 6.91823996 -1.27152777
C -1.07537822 5.14443225 -1.28224059
N 0.01234274 4.17250545 -1.00517980
C 1.41507821 4.52098791 -0.59350095
C -0.18308572 2.89367736 -1.39148420
O -1.46473034 2.63392684 -1.72353685
O 0.72057809 2.04386223 -1.47106526
H 0.87984822 6.74206170 -2.34260833
H 0.92292844 7.97616962 -1.08318541
H -1.29225553 5.10558192 -2.35675553
H -1.97562688 4.81472660 -0.76275995
H 1.11027745 0.84405441 -0.59231653
C -1.78302423 1.30480273 -2.22854803
H 3.21957028 1.89900096 3.77883021
H 2.69490584 3.55609196 3.35262109
H 1.63731664 2.14983732 2.98936665
H 3.43508046 2.72231096 -0.15047776
C -0.73284229 6.58001693 -0.89616493
H -0.85922458 6.72367715 0.18427543
H -1.45453295 7.23933685 -1.39101808
C -1.85702009 1.28885077 -3.73332871
C -0.68621773 1.31311508 -4.50464832
C -0.76092289 1.29221436 -5.89599586
C -2.00437020 1.24177836 -6.53170655
C -3.17282286 1.21262530 -5.77020607
C -3.09862879 1.23801338 -4.37656351
H -2.75187198 1.07120274 -1.78651060
H -1.04210102 0.60008096 -1.85292858
H -4.00886261 1.20570742 -3.78353682
H -2.06086654 1.22149862 -7.61641805
H -4.14179204 1.16961623 -6.25928965
H 0.27756313 1.34678007 -4.00529218
H 0.15057691 1.30700489 -6.48655111
H 2.67846376 6.24761464 -0.59280191
H 1.43615447 6.30176749 0.63925022
H 2.06230424 4.17855207 -1.40918898
H 1.20597036 4.03080180 1.55091310

4.9 References

- (1) Sun, Z.; Winschel, G. A.; Zimmerman, P. M.; Nagorny, P. *Angewandte Chemie International Edition in English* **2014**, *53*, 11194–11198.
- (2) Harmata, M.; Rashatasakhon, P. *Tetrahedron* **2003**, *59*, 2371–2395.
- (3) Corma, A.; García, H. *Chem. Rev.* **2003**, *103*, 4307–4366.
- (4) Doyle, A. G.; Jacobsen, E. N. *Chem. Rev.* **2007**, *107*, 5713–5743.
- (5) Rueping, M.; Kuenkel, A.; Atodiresei, I. *Chem. Soc. Rev.* **2011**, *40*, 4539–11.
- (6) Gassman, P. G.; Singleton, D. A.; Wilwerding, J.J.; Chavan, S. P. *J. Am. Chem. Soc.* **1987**, *109*, 2182–2184.
- (7) Sammakia, T.; Berliner, M. A. *The Journal of Organic Chemistry* **1994**, *59*, 6890–6891.
Sammakia, T.; Berliner, M. A. *The Journal of Organic Chemistry* **1995**, *60*, 6652–6653.
- (8) Haudrechy, A.; Picoul, W.; Langlois, Y. *Tetrahedron: Asymmetry* **1997**, *8*, 139–148.
- (9) Kumareswaran, R.; Vankar, P. S.; Reddy, M.; Pitre, S. V. *Tetrahedron* **1999**, *55*, 1099–1110.
- (10) Northrup, A. B.; MacMillan, D. W. C. *J. Am. Chem. Soc.* **2002**, *124*, 2458–2460.
- (11) Nakashima, D.; Yamamoto, H. *J. Am. Chem. Soc.* **2006**, *128*, 9626–9627.
- (12) Borovika, A.; Nagorny, P. *Tetrahedron* **2013**, *69*, 5719–5725.
- (13) Davis, F. A.; Chao, B. *Org. Lett.* **2000**, *2*, 2623–2625.
- (14) Bailey, P. D.; Millwood, P. A.; Smith, P. D. *Chemical Communications* **1998**, 633–640.
- (15) Wilkinson, T. J.; Stehle, N. W.; Beak, P. *Org. Lett.* **2000**, *2*, 155–158.
- (16) Ma, D.; Sun, H. *Org. Lett.* **2000**, *2*, 2503–2505.
- (17) Johnson, T. A.; Curtis, M. D.; Beak, P. *J. Am. Chem. Soc.* **2001**, *123*, 1004–1005.
- (18) Takasu, K.; Maiti, S.; Ihara, M. *ChemInform* **2003**, *34*, 51.
- (19) Fustero, S.; Jiménez, D.; Moscardó, J.; Catalán, S.; del Pozo, C. *Org. Lett.* **2007**, *9*, 5283–5286.
- (20) Carlson, E. C.; Rathbone, L. K.; Yang, H.; Collett, N. D.; Carter, R. G. *J. Org. Chem.* **2008**, *73*, 5155–5158.
- (21) You, S.-L.; Feng, Z.; Xu, Q.-L.; Dai, L.-X. *Heterocycles* **2010**, *80*, 765.
- (22) Liu, J.-D.; Chen, Y.-C.; Zhang, G.-B.; Li, Z.-Q.; Chen, P.; Du, J.-Y.; Tu, Y.-Q.; Fan, C.-A. *Adv. Synth. Catal.* **2011**, *353*, 2721–2730.
- (23) Cheng, T.; Meng, S.; Huang, Y. *Org. Lett.* **2013**, *15*, 1958–1961.
- (24) Miyaji, R.; Asano, K.; Matsubara, S. *Org. Lett.* **2013**, *15*, 3658–3661.
- (25) Veerasamy, N.; Carlson, E. C.; Collett, N. D.; Saha, M.; Carter, R. G. *J. Org. Chem.* **2013**, *78*, 4779–4800.
- (26) Fukata, Y.; Asano, K.; Matsubara, S. *Chem. Lett.* **2013**, *42*, 355–357.
- (27) Terada, M.; Tanaka, H.; Sorimachi, K. *J. Am. Chem. Soc.* **2009**, *131*, 3430–3431.
- (28) Corić, I.; Vellalath, S.; List, B. *J. Am. Chem. Soc.* **2010**, *132*, 8536–8537.
- (29) Cox, D. J.; Smith, M. D.; Fairbanks, A. J. *Org. Lett.* **2010**, *12*, 1452–1455.
- (30) Corić, I.; Müller, S.; List, B. *J. Am. Chem. Soc.* **2010**, *132*, 17370–17373.
- (31) Han, Z.-Y.; Guo, R.; Wang, P.-S.; Chen, D.-F.; Xiao, H.; Gong, L.-Z. *Tetrahedron Letters* **2011**, *52*, 5963–5967.
- (32) Corić, I.; List, B. *Nature* **2012**, *483*, 315–319.
- (33) Sun, Z.; Winschel, G. A.; Borovika, A.; Nagorny, P. *J. Am. Chem. Soc.* **2012**, *134*, 8074–8077.

- (34) Terada, M.; Toda, Y. *Angew. Chem. Int. Ed.* **2012**, *51*, 2093–2097.
- (35) Kim, J. H.; C̄orić, I.; Vellalath, S.; List, B. *Angew. Chem. Int. Ed.* **2013**, *52*, 4474–4477.
- (36) Mensah, E.; Camasso, N.; Kaplan, W.; Nagorny, P. *Angew. Chem. Int. Ed.* **2013**, *52*, 12932–12936.
- (37) Nagorny, P.; Sun, Z.; Winschel, G. *Synlett* **2013**, *24*, 661–665.
- (38) Kimura, T.; Sekine, M.; Takahashi, D.; Toshima, K. *Angew. Chem. Int. Ed.* **2013**, *52*, 12131–12134.
- (39) Chen, Z.; Sun, J. *Angew. Chem. Int. Ed.* **2013**, *52*, 13593–13596.
- (40) Hsiao, C.-C.; Liao, H.-H.; Sugiono, E.; Atodiresei, I.; Rueping, M. *Chem. Eur. J.* **2013**, *19*, 9775–9779.
- (41) Terada, M.; Yamanaka, T.; Toda, Y. *Chem. Eur. J.* **2013**, *19*, 13658–13662.
- (42) Quach, R.; Furkert, D. P.; Brimble, M. A. *Tetrahedron Letters* **2013**, *54*, 5865–5868.
- (43) Cui, Y.; Villafane, L. A.; Clausen, D. J.; Floreancig, P. E. *Tetrahedron* **2013**, *69*, 7618–7626.
- (44) Lu, C.; Su, X.; Floreancig, P. E. *J. Org. Chem.* **2013**, *78*, 9366–9376.
- (45) Lombardo, V. M.; Thomas, C. D.; Scheidt, K. A. *Angew. Chem. Int. Ed.* **2013**, *52*, 12910–12914.
- (46) Zimmerman, P. M. *J. Comput. Chem.* **2013**, *34*, 1385–1392.
- (47) Zimmerman, P. M. *J. Chem. Phys.* **2013**, *138*, 184102–184111.
- (48) Zimmerman, P. *J. Chem. Theory Comput.* **2013**, *9*, 3043–3050.
- (49) Becke, A. D. *Physical review A* **1988**, *38*, 3098–3100.
- (50) Lee, C.; Yang, W.; Parr, R. G. *Physical review B* **1988**, *37*, 785–789.
- (51) Becke, A. D. *J. Chem. Phys.* **1993**, *98*, 5648–6.
- (52) Hariharan, P. C.; Pople, J. A. *Theoret. Chim. Acta* **1973**, *28*, 213–222.
- (53) Chai, J.-D.; Head-Gordon, M. *Phys. Chem. Chem. Phys.* **2008**, *10*, 6615–6616.
- (54) Clark, T.; Chandrasekhar, J.; Spitznagel, G. W.; Schleyer, P. V. R. *J. Comput. Chem.* **1983**, *4*, 294–301.
- (55) Frisch, M. J.; Pople, J. A.; Binkley, J. S. *J. Chem. Phys.* **1984**, *80*, 3265–3266.
- (56) Marenich, A. V.; Cramer, C. J.; Truhlar, D. G. *J. Phys. Chem. B* **2009**, *113*, 6378–6396.
- (57) Schmidt, M. W.; Baldridge, K. K.; Boatz, J. A.; Elbert, S. T.; Gordon, M. S.; Jensen, J. H.; Koseki, S.; Matsunaga, N.; Nguyen, K. A.; Su, S.; Windus, T. L.; Dupuis, M.; Montgomery, J. A. *J. Comput. Chem.* **1993**, *14*, 1347–1363.
- (58) Shapiro, N. D.; Rauniyar, V.; Hamilton, G. L.; Wu, J.; Toste, F. D. *Nature* **2011**, *470*, 245–249.